THE
PHYSICAL REVIEW
A Journal of Experimental and Theoretical Physics Established by E. L. Nichols in 1893
VOL. 60, NO. 3 AUGUST 1, 1941 SECOND SERIES

The Problem of Energy Production in Red Giants

M. A. GREENFIELD
New York University, New York, New York
(Received May 29, 1941)

Evolutionary changes in stars producing their energy by thermonuclear reactions of light elements are studied by the method of homology transformations. Formulae have been developed for the luminosity and radius of the star as a function of time. Formulae were also developed for the gravitational contraction of the star in the transitional stages between various nuclear reactions. Comparison of these two classes of formulae permits demarcation of the $L-R$ diagram into regions in which either gravitational contraction or various nuclear reactions play the most important role. These regions have been correlated with various known groups of pulsating stars thus permitting a definite nuclear reaction to be ascribed to each group. The observed constancy of period is consistent with the derived rates of evolution in different parts of the $L-R$ diagram.

1. INTRODUCTION

IF one considers the stars plotted (Fig. 1) in a Hertzsprung-Russell (hereafter referred to as H-R) diagram, there is, apart from the main sequence, a large class of stars having very high luminosities but possessing much greater radii than the stars of the main sequence of the same luminosity. The distribution of these so-called red giants is limited from above by a line of pulsating variable stars, whose luminosities change periodically. Very few stars are known that are located between this line (Fig. 1) and the upper part of the main sequence. Red giant stars also do not extend to smaller luminosities as do members of the main sequence.

The periodic changes of the variable stars are usually interpreted[1] as caused by mechanical pulsations of the whole star resulting in periodic luminosity, radius and other changes.

If the number of variables which have periods lying between specified limits are plotted (Fig. 2), one obtains a distribution curve with a number of maxima. The periods are clustered about the values 0.5, 2.0, 4.75, 33 and 300 days. Figure 2a (constructed by Russell[2]) was based on a study of approximately 1000 variable stars. An insufficient number of stars were studied in the region three to eight days. The variables in this region (called Cepheids) were studied by Shapley.[3] An early investigation based on a study of 288 Cepheids in the galactic system (Fig. 2b) revealed a strong maximum at 4.75 days. However, Shapley stated that a definite selection of brighter stars had occurred. A more recent investigation[3] of 295 Cepheids in the small Magellanic Cloud (care was taken to eliminate selection) led to a distribution curve with a maximum at approximately two days (Fig. 2c).

[1] A. S. Eddington, *The Internal Constitution of Stars* (Cambridge University Press, 1926).

[2] Russell, Dugan, and Stewart, *Astronomy*, Vol. II.

[3] H. Shapley and V. McKibben, Proc. Nat. Acad. Sci. (1940).

The energy production in main sequence stars was successfully explained by Bethe[4] in terms of catalytic thermonuclear reactions between hydrogen, nitrogen and carbon going on in the stars' interiors. The energy liberation depends upon the density and sensitively on the temperature. For the sun T (central) is 2×10^7 °K while the density there is 80 g/cm³.

Since their radii are so large, red giants possess low densities and low central temperatures (for some red giants densities are 5×10^{-7} g/cm³, and central temperatures are 1×10^6 °K). The C−N cycle used to explain the energy production in main sequence stars will not produce sufficient energy to explain the observed luminosities of red giants at these low interior temperatures. Calculations[5,6] show that the only reactions taking place with appreciable energy evolution at these comparatively low interior temperatures involve a proton capture by the isotopes of heavy hydrogen, lithium, beryllium and boron as follows:

$$\begin{aligned}
&H^2+H^1\rightarrow He^3+h\nu\\
&Li^6+H^1\rightarrow He^4+He^3\\
&Li^7+H^1\rightarrow 2He^4\\
&Be^9+H^1\rightarrow Li^6+He^4\\
&B^{10}+H^1\rightarrow C^{11}+h\nu\\
&B^{11}+H^1\rightarrow 3He^4.
\end{aligned}\qquad (1)$$

In the N−C cycle occurring in main sequence stars the elements N and C are not destroyed but act as catalysts. However, in the reactions mentioned above, the light elements are permanently removed, which causes a shorter evolutionary span as compared with the evolution of main sequence stars.

Two distinct methods in which energy may be generated in a star should be considered. One is by means of a thermonuclear reaction and the other is by the gravitational contraction of the star. In general both processes will go on in the star at any particular time. However, under appropriate circumstances one or the other of these processes may be predominant. This will be discussed in detail below.

In these calculations the assumptions of a point source model for the nuclear evolution will be made, with a hydrogen content in the star of 35 percent.[7] The state of the star is determined by a number of fundamental equilibrium equations and in addition by the average molecular weight, the opacity and the rate of energy production by stellar material. The amount of light element required to explain red giant evolution is small compared to the hydrogen concentration. It will therefore be assumed that the hydrogen content does not change materially with time. The fundamental equations are then employed in conjunction with the homology transformations.

The equilibrium equations are[1,7] in a standard notation:

$$\begin{aligned}
&dp/dr=-GM_r\rho/r^2;\quad dM_r/dr=4\pi r^2\rho,\\
&p=K\rho T/\beta\mu m_H;\quad p_R=p(1-\beta)=\tfrac{1}{3}aT^4,\\
&\frac{d}{dr}(\tfrac{1}{3}aT^4)=-\frac{1}{c}\kappa\rho\frac{L_r}{4\pi r^2},\quad dL_r/dr=4\pi r^2\rho\epsilon.
\end{aligned}\qquad (2)$$

The energy equations are

$$L_G=\frac{d}{dt}\left(\frac{\gamma GM^2}{r}\right)\qquad (3)$$

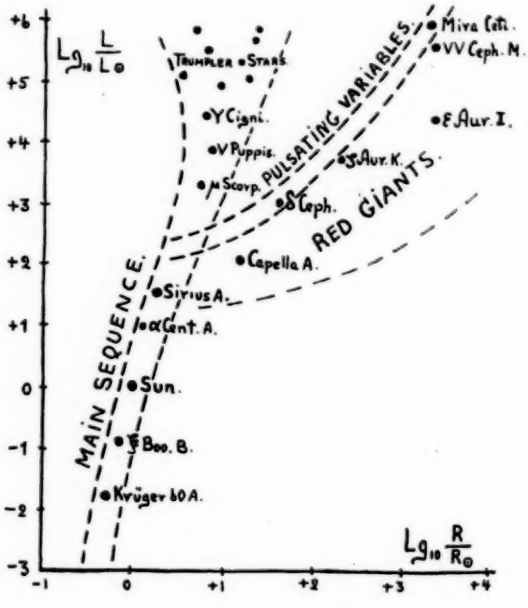

FIG. 1. Luminosity *versus* radius.

[4] H. A. Bethe, Phys. Rev. **55**, 434 (1939).
[5] G. Gamow, Phys. Rev. **55**, 718 (1939).
[6] G. Gamow, Nature **144**, 575 (1939).
[7] B. Strømgren, Ergeb. d. exakt. Naturwiss. **16**, 465 (1937).

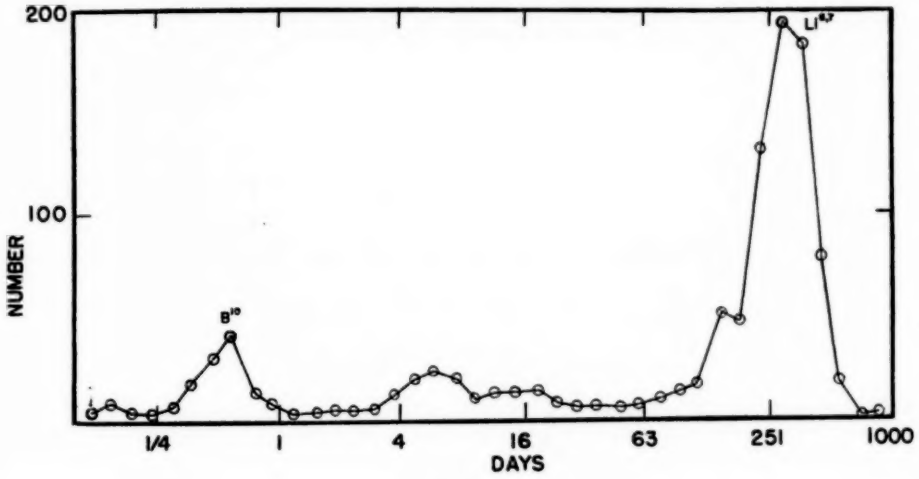

FIG. 2a.

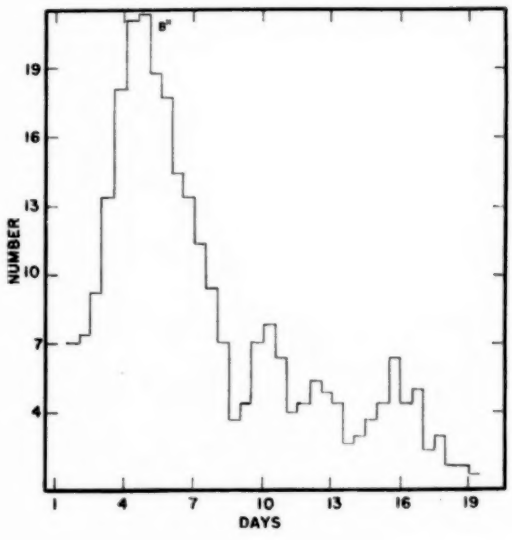

FIG. 2b.

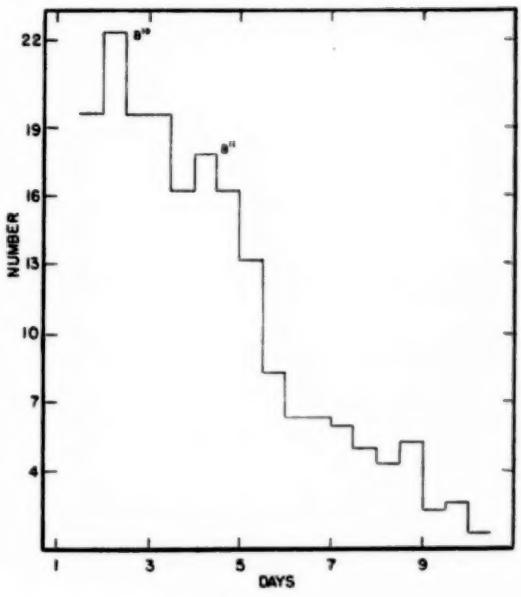

FIG. 2c.

FIG. 2. Number of variable stars *versus* period. (After Russell (2a), Shapley (2b, 2c).)

for gravitational contraction;[8]

$$\epsilon=\frac{4}{3^{5/2}}\rho x_1 x_2\frac{\hbar\Gamma r_0^2 Q}{m_1 m_2 m e^2 z_1 z_2}\times\exp 4\left(\frac{2r_0 m e^2 z_1 z_2}{\hbar^2}\right)^{\frac{1}{3}}\tau^2 e^{-\tau} \quad (4)$$

with

$$\tau=3\left(\frac{\pi^2 m e^4 z_1^2 z_2^2}{2\hbar^2 KT}\right)^{\frac{1}{3}}$$

for nuclear energy production.[9,10]

Chandrasekhar[11] has proved a useful theorem

[8] Where γ is a numerical coefficient of the order of magnitude unity depending on the density distribution within the star.

[9] G. Gamow and E. Teller, Phys. Rev. **53**, 608 (1938).

[10] F. G. Houtermans and R. Atkinson, Zeits. f. Physik **54**, 656 (1929).

[11] S. Chandrasekhar, *Introduction to Study of Stellar Structure* (University of Chicago Press, 1939).

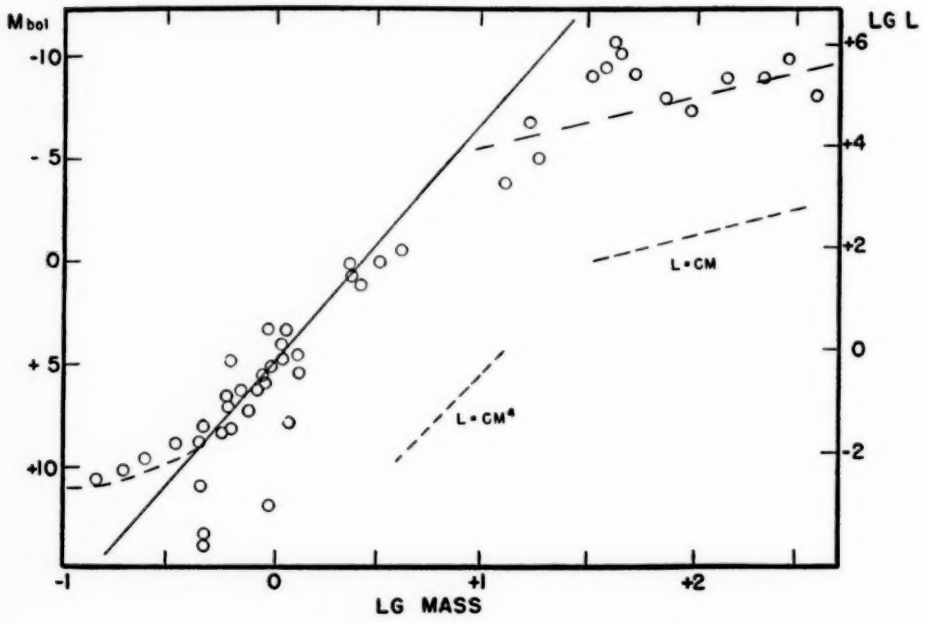

FIG. 3. Empirical mass luminosity curve. (After Kuiper.)

about the ratio, $(1-\beta)$, of radiative to total pressure. From this theorem we infer that $(1-\beta)$ can be appreciable for stars of large mass.

This essential difference between stars of small and large masses is clearly reflected in the empirical mass-luminosity relation (see Fig. 3).[12] There are two distinct groups of stars. In the first group (small masses) the luminosity L varies approximately as M^4 while in the second (large masses) L varies as M. It will be shown later that these relations may be approximated by employing only the ideal gas pressure for the first group, and only the radiative pressure for the second.

For the point source model L_r is constant and is denoted by L.

2. Nuclear and Gravitational Regions in H-R Plane

Equilibrium equations involve the six variables M, r, ρ, p, T and L. It is therefore possible to express the change in four of the variables in terms of arbitrary changes of the remaining two. The expression to be employed for the opacity is

$$\kappa = \kappa_0 \rho^{0.5} T^{-2.75}, \tag{5}$$

obtained by Bethe on the basis of Strømgren's opacity tables. This represents an empirical expression that is good for stars whose central temperatures are comparable with that for the sun. Nevertheless it has been used throughout since some approximation has to be employed. Fortunately the calculations are insensitive to the exact expression for κ. Let M_0, r_0, ρ_0, p_0, T_0 and L_0 refer to some standard known star such as Sirius, while the same quantities without the subscript will describe the red giant star under discussion. Let M and r be the independent variables expressed in terms of the corresponding values for Sirius.

$$M = \varphi M_0$$

If $$r = \delta r_0, \tag{6}$$

then the changes in the other four variables required to keep the equilibrium equations invariant are given by:

$$\begin{aligned} \rho &= \varphi\delta^{-3}\rho_0, & \rho &= \varphi\delta^{-3}\rho_0, \\ p &= \varphi^2\delta^{-4}p_0, & p &= \varphi^2\delta^{-4}p_0, \\ T &= \varphi\delta^{-1}T_0, \quad (7) & T &= \varphi^{\frac{1}{4}}\delta^{-1}T_0, \quad (7') \\ L &= \rho^{5.25}\delta^{-1.25}L_0, & L &= \varphi^{1.875}\delta^{-1.25}L_0, \\ L/L_0 &= \varphi\epsilon/\epsilon_0. & L/L_0 &= \varphi\epsilon/\epsilon_0. \end{aligned}$$

[12] G. P. Kuiper, Astrophys. J. **88**, 472 (1938).

These are the homology relations with κ_0, μ, x assumed constant. Equations (7) were obtained by using the ideal gas pressure while (7′) resulted from employing the expression for radiative pressure. In the ensuing analysis similar dual sets of equations will be developed, and as in the above primed numbers will refer to the "radiative pressure" equations. It may be noted that the dependence on δ is the same in both sets of equations.

By employing the homology relations in conjunction with the energy equations it is possible to relate the element concentration x_2 with the variable δ which defines the radius.

Let (4) be written as

$$\epsilon=(Q/m_2)\rho x_2 P; \quad P=F\tau^2 e^{-\tau}. \tag{8}$$

F includes the constants characterizing the reacting nuclei. P is introduced for computational convenience. x_2 and m_2 refer to the light element reacting with the proton. Henceforth the subscript 2 will be omitted.

Consider the star in a portion of the H-R plane such that its principal energy source is due to nuclear reactions. Then the total energy production L may be replaced by the expression for the nuclear energy production. For some red giant in this region:

$$\epsilon=(Q/m)\rho x P. \tag{9}$$

For some standard star, as Sirius

$$\epsilon_0=(Q_0/m_0)\rho_0 x_0 P_0 \tag{10}$$

with temperature T_0 and nitrogen concentration x_0. Let

$$\tau_n=\tau(T_0)$$

(τ_n refers to light element in red giant at temperature T_0).

From Eqs. (7) and (7′) we have

$$P=P_n e^{\tau_n}(\delta/\varphi)^{2/3}\exp[-(\delta/\varphi)^{1/3}\tau_n], \tag{11}$$

$$P=P_n e^{\tau_n}\varphi^{-1/3}\delta^{2/3}\exp[-\delta^{1/3}/\varphi^{1/6}\tau_n]. \tag{11′}$$

Since

$$L/L_0=\varphi\frac{\epsilon}{\epsilon_0}=\frac{M}{M_0}\frac{Q}{Q_0}\frac{m_0}{m}\frac{\rho}{\rho_0}\frac{x}{x_0}\frac{P}{P_0}, \tag{12}$$

$$x/x_0=\frac{Q_0}{Q}\frac{m}{m_0}\frac{P_0}{P_n e^{\tau_n}}\varphi^{3.92}\delta^{1.08}\exp[(\delta/\varphi)^{1/3}\tau_n], \tag{13}$$

$$x/x_0=\frac{Q_0}{Q}\frac{m}{m_0}\frac{P_0}{P_n e^{\tau_n}}\varphi^{0.21}\delta^{1.08}\exp[\delta^{1/3}\tau_n/\varphi^{1/6}]. \tag{13′}$$

Thus the concentration of the light element x has been obtained as a function of various parameters and the radius δ.

In order to determine in which parts of the H-R plane the nuclear reactions are more important than gravitational contraction or vice versa it is necessary to determine the locus in the H-R plane where gravitational contraction and some nuclear reaction (each process assumed to be acting independently of the other) cause equal rates of contraction. That process will be predominant on either side of this demarcation line for which $d\delta/dt$ has the smaller value. For consider the star to be evolving at some point of the H-R plane with $(d\delta/dt)_N \ll (d\delta/dt)_G$. If the star is living on nuclear reactions then the value of $(d\delta/dt)$ will be given by $(d\delta/dt)_N$. However this value of $(d\delta/dt)$ will only produce a small amount of gravitational energy. Hence the nuclear reaction source of energy will be important.

Now suppose $(d\delta/dt)_G \ll (d\delta/dt)_N$. If the star were living on the nuclear reaction $(d\delta/dt)$ would again be given by $(d\delta/dt)_N$. However this value of $(d\delta/dt)$ greatly exceeds the contraction rate necessary to produce the same amount of energy gravitationally, and the amount of gravitational energy released under these circumstances would be too large. Therefore the gravitational contraction process would be the important energy source.

Thus in general the total energy produced is:

$$L = L_N + L_G; \quad L_N = -Q\frac{d}{dt}\left(\frac{Mx}{m}\right); \quad L_G = \frac{d}{dt}\left(\frac{\gamma GM^2}{r}\right) \tag{14}$$

or

$$L = -\frac{QM}{m}\frac{dx}{dt} - \frac{\gamma GM^2}{r^2}\frac{dr}{dt}. \tag{15}$$

The approximation described above will be made and it will be assumed that either L_N or L_G is to be chosen as the energy expression depending on the region of the H-R plane in which the star is located.

In any event the luminosity L at some point in the H-R plane will be described by

$$L = \varphi^{5.25}\delta^{-1.25}L_0. \tag{16}$$

$$L = \varphi^{1.875}\delta^{-1.25}L_0. \tag{16'}$$

If gravitational contraction be assumed one also writes

$$L = (d/dt)(\gamma GM^2/r). \tag{17}$$

Combining Eqs. (7) and (17) we obtain

$$L = -\frac{\gamma G\varphi^2 M_0^2}{r_0}\frac{1}{\delta^2}\left(\frac{d\delta}{dt}\right)_G. \tag{18}$$

If nuclear reactions be assumed then

$$L = -(QM/m)(dx/dt). \tag{19}$$

By combining Eqs. (19), (13), (13') and (6) we have

$$L = -\frac{x_0Q_0P_0M_0}{m_0P_ne^{\tau_n}}\varphi^{4.92}\exp\left[(\delta/\varphi)^{1/3}\tau_n\right]\delta^{0.08}\left(\frac{\tau_n}{3}\frac{\delta^{1/3}}{\varphi^{1/3}}+1.08\right)\left(\frac{d\delta}{dt}\right)_N, \tag{20}$$

$$L = -\frac{x_0Q_0P_0M_0}{m_0P_ne^{\tau_n}}\varphi^{1.21}\exp\left[\delta^{1/3}\tau_n/\varphi^{1/6}\right]\delta^{0.08}\left(\frac{\tau_n}{3}\frac{\delta^{1/3}}{\varphi^{1/6}}+1.08\right)\left(\frac{d\delta}{dt}\right)_N. \tag{20'}$$

The term 1.08 is omitted since it affects the accuracy of the calculations only slightly and the computational work is thereby reduced.

At some specified point L, R, in the H-R plane the quantities $(d\delta/dt)_G$ and $(d\delta/dt)_N$ are in general not equal. To obtain the above described loci Eqs. (18) and (20) are combined while $(d\delta/dt)_G$ is set equal to $(d\delta/dt)_N$. The loci are then defined by the following:

$$\frac{\gamma GM_0^2}{r_0} = \frac{x_0Q_0P_0M_0}{m_0P_ne^{\tau_n}}\varphi^{2.59}\delta^{1.75}\frac{\tau_n}{3}\exp\left[(\delta/\varphi)^{1/3}\tau_n\right], \tag{21}$$

$$\frac{\gamma GM_0^2}{r_0} = \frac{x_0Q_0P_0M_0}{m_0P_ne^{\tau_n}}\varphi^{-0.95}\delta^{1.75}\frac{\tau_n}{3}\exp\left[\delta^{1/3}\tau_n/\varphi^{1/6}\right]. \tag{21'}$$

Thus for each nuclear reaction there corresponds a locus in the H-R plane defined by Eq. (21) involving φ and δ and the homology expression for L given by Eq. (7). A relation between L and δ finally obtains, thus resulting in a line which roughly parallels the main

sequence. In each of the Eqs. (21) and (21′) the left-hand side is a constant, while the right-hand side is a monotonic exponential function of the radius δ. Therefore for values of δ smaller than the δ defined by Eq. (21) the left-hand side will be greater than the right-hand side. For values of δ greater than the δ defined by the Eq. (21) the right-hand side will be much greater than the left-hand side because of the exponential dependence on δ. These conclusions also apply to $(d\delta/dt)_G$ and $(d\delta/dt)_N$ inversely since the products of these quantities and the left- and right-hand sides of (21) respectively are equal. (The products in fact are equal to L to within a factor of φ^2/δ^2.) Thus to the right of the locus one may expect nuclear reactions to constitute the main source of energy while to the left gravitational contraction will be the predominant energy source.

The "conflict" lines in Fig. 4 represent the loci defined by Eq. (21) for H^2, Li^6, Li^7, Be^9, B^{11} and B^{10}. Each locus consists of two parts with the upper corresponding to the radiative pressure and the lower one to the ideal gas pressure. The dotted line connecting the two parts represents roughly the transitional region where gas and radiative pressure are equally important. The circles represent the positions of the maxima (Fig. 2) of the distribution of variable star periods. It may be noted that each maximum lies approximately 0.1 or 0.2 log units to the *right* of some locus line. Specifically, Table I of correspondence may be made:

Thus the stratification of the pulsating variable stars with regard to their period may be explained by the fact that each group of such stars "lives" on some nuclear reaction. It has been shown that the concentrations of pulsating stars are found to be in those regions where nuclear reactions are the principal source of energy. It has also been shown that these stars are located in regions such that $d\delta/dt$ has a small value (relative to

TABLE I. *Period of star and element supplying energy.*

PERIOD (DAYS)	ELEMENT
0.5	B^{10} (gas pressure, smaller masses)
2	B^{10} (radiative pressure, larger masses)
4.75	B^{11} (radiative pressure, larger masses)
33	Be^9 (radiative pressure, larger masses)
300	$Li^{6,7}$ (radiative pressure, larger masses)

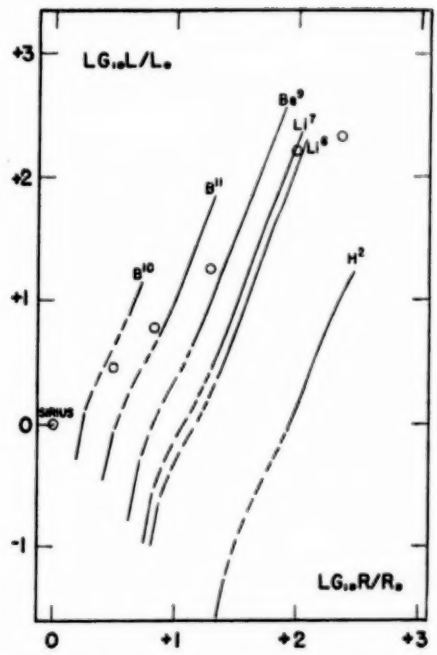

FIG. 4. Pulsating variables and different nuclear reactions

that obtained for gravitational contraction for the same luminosity).

Each maximum in Fig. 2 has been labeled with the element responsible for the energy production.

The two Shapley curves may now be interpreted as arising from two distinct entities. The two-day group corresponds to stars living on B^{10}, while the more massive and brighter stars of the 4.75-day group live on B^{11}. Shapley's two groups of data consist of different admixtures of these two types of stars. This interpretation differs from that made by Gamow and Teller[13] who supposed that the Cepheids lived on B^{11}, Be^9, and $Li^{6,7}$ while the Mira variables lived on H^2. The more precise calculations above have suggested the arrangement of Fig. 4. It may be noted there that H^2 does not account for the evolution of any group of variables. The surface temperatures of stars living on H^2 would be lower than any which have been observed for variables. If it is correct that the 0.5- and 2-day groups both live on B^{10}, it is somewhat surprising that there is a gap between them. One might expect a continuous spread of variables between the two period limits.

[13] G. Gamow and E. Teller, Phys. Rev. **55**, 791 (1939).

3. Light Element Concentrations in the Pulsating Variables

It is now necessary to calculate the values of $d\delta/dt$ or better $d \lg\delta/dt$ (which gives the percent change of radius per unit time) in the nuclear regions as well as those corresponding to gravitational contraction. This is done to see whether the theory is capable of explaining the observed constancy of pulsation periods. The cluster and Cepheid variables particularly possess periods which are nearly constant. The expressions for $d \lg\delta/dt$ will now be obtained.

For the case of gravitational contraction Eqs. (16) and (18) may be combined to give:

$$\left(\frac{dt}{d \lg\delta}\right)_G = -\frac{\gamma G M_0^2}{r_0 L_0}\varphi^{-3.25}\delta^{0.25}, \tag{22}$$

$$\left(\frac{dt}{d \lg\delta}\right)_G = -\frac{\gamma G M_0^2}{r_0 L_0}\varphi^{0.125}\delta^{0.25}. \tag{22'}$$

For the case of nuclear reaction Eqs. (16) and (20) yield:

$$\left(\frac{dt}{d \lg\delta}\right)_N = -\frac{x_0 Q_0 P_0 M_0}{L_0 m_0 P_n e^{\tau_n}}\frac{\tau_n}{3}\varphi^{-2/3}\delta^{8/3}\exp\left[(\delta/\varphi)^{1/3}\tau_n\right], \tag{23}$$

$$\left(\frac{dt}{d \lg\delta}\right)_N = -\frac{x_0 Q_0 P_0 M_0}{L_0 M_0 P_n e^{\tau_n}}\frac{\tau_n}{3}\varphi^{-5/6}\delta^{8/3}\exp\left[\delta^{1/3}\tau_n/\varphi^{1/6}\right]. \tag{23'}$$

The numerical calculation of $dt/d \lg\delta$ from (22) and (23) was made for each group of stars corresponding to a maximum in the period distribution.

Thus if gravitation were providing the energy there would be a change in radius/year equal to 10^{-3} percent. This would result in a corresponding decrease in the period of pulsation. In fact such a rapid decrease in period has not been noted for the cluster and Cepheid variables. For example δ Cephei[14] (period = 5.3 days) has a period which is decreasing at the rate of 10^{-5} percent per year or $\Delta t/\Delta \lg P = 1.85\times10^{14}$ seconds. This may be compared with the rate of the 4.75-day group above. In any event gravitational contraction would cause a systematic decrease in pulsation periods which is not observed. The situation is different in the case of non-pulsating red giants. For the latter one must observe the changes in magnitude and make a comparison with the changes demanded by the gravitational contraction hypothesis. In a paper by Gamow[5] the value of $\Delta R/R$ (based on gravitational contraction) for ζ Aurigae K was incorrectly stated to be 10^{-2} per year. It should be 2×10^{-4} per year. This leads to a secular change of luminosity of 0.05 m per century. Since such a change is below the limit of observation no conclusive statement may be made.

Table II. *Data on red giant stars.*

Element	Period (Days)	$\left(\frac{dt}{d \lg\delta}\right)$ Nucl. (Sec.)	$\left(\frac{dt}{d \lg\delta}\right)$ Grav. (Sec.)
B^{10} (gas)	0.5	2×10^{14}	7×10^{11}
B^{10} (rad.)	2	1×10^{16}	5×10^{12}
B^{11}	4.75	1×10^{15}	7×10^{12}
Be^{9}	33	2×10^{15}	1×10^{13}
Li^{7}	300	2×10^{16}	2×10^{13}
Li^{6}	300	2×10^{15}	2×10^{13}

There are a number of stars such as ζ Geminorum[14] for which the period possesses a periodic variation. There are also a number of variables whose periods are slowly increasing; e.g., T Monoceratis[14] has a period of 27 days which is increasing at the approximate rate of 10^{-4} per year.

The values of $(dt/d \lg\delta)_N$ are sufficiently large to be consistent with the constancy of period observed for most variables; e.g., a value of $dt/d \lg\delta = 10^{15}$ seconds leads to a period change $\sim10^{-6}$ percent per year. The lifetime of red giants according to Table II is of the order 10^{15} to 10^{16} seconds or 10^{8} to 10^{9} years.

Combining Eqs. (7) and (20) and integrating, one obtains δ or the radius as a function of the

[14] P. ten Bruggencate, Ergeb. d. exakt. Naturwiss. **10** (1931).

time while the star is evolving under the influence of some particular nuclear reaction.

$$t_f - t_i = \frac{x_0 M_0 Q_0 P_0}{L_0 m_0 P_n e^{\tau_n}} \varphi^{-1/3} \exp[(\delta/\varphi)^{1/3}\tau_n] \times (\delta^{7/3} - 3.75W)_f^i, \quad (24)$$

where

$$W = 6! \sum_1^7 \frac{\delta^{(7-n/3)}}{(7-n)!(\tau_n/\varphi^{1/3})^n}(-1)^{n+1}. \quad (25)$$

It may be noted that with increasing time the radius decreases at an increasing rate. The corresponding relation for gravitational contraction is:

$$t_f - t_i = \frac{4\gamma G M_0^2}{L_0 r_0 \varphi^{3.25}}(\delta^{0.25})_f^i.$$

In Fig. 4 each group of stars has been associated with some element responsible for the energy production. It is interesting to note the lower limit of the element concentration x. This value corresponds to the concentration of the element at the point where the star has evolved to the conflict line. If the concentration were less, gravitational contraction would be predominant in the entire region where the reaction in question is occurring. Equally important is the upper limit to the concentration. The latter quantity should not exceed the value obtained when the star living on B^{11} say, was just to the left of the Be^9 conflict line. If the concentration were larger, then the B^{11} reaction should start before the Be^9 reaction is completed and there would then be no stratification as is observed. This may be considered from another point of view. Consider a star living on B^{11}. If one considers the state of this star going backwards in time, then the B^{11} concentration grows larger. If one accepts the hydrogen concentration to be 35 percent, then, even neglecting the presence of any other elements, the maximum B^{11} concentration could not exceed 65 percent. If the position of the star when it contained this amount of B^{11} was to the right of the Be^9 conflict line, then gravitational contraction would not occur between the end of the Be^9 reaction and the start of the B^{11} reaction. This would not produce the observed stratification. The concentration of any light element, after the star has passed the conflict line corresponding to it, will be affected by later history of the star and will continue to decrease faster and faster due to the progressively higher interior temperatures. Another complicating factor is the presence of convection currents of unknown period.

TABLE III.

PERIOD (DAYS)	ELEMENT	x MIN.	LOG δ
0.5	B^{10} (gas)	4×10^{-6}	0.79
2	B^{10} (rad.)	2×10^{-5}	0.87
4.75	B^{11}	1×10^{-4}	1.45
33	Be^9	9×10^{-5}	1.96
300	Li^7	1×10^{-4}	2.37
300	Li^6	5×10^{-7}	2.37

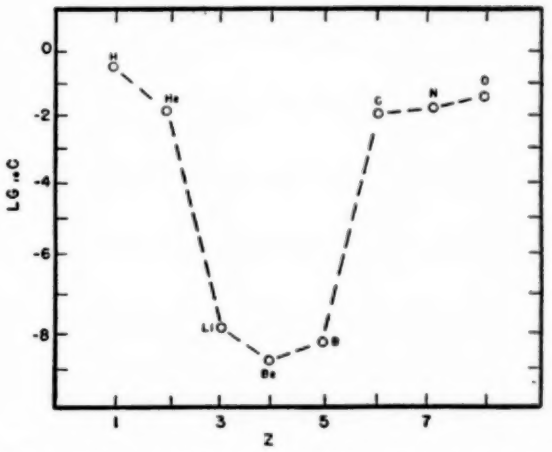

FIG. 5. Observed abundance of light elements in stellar atmospheres *versus* atomic number.

The third column of Table III gives the calculated minimum concentrations $x_{\min}$, the fourth column, the values of log δ which would correspond to an element concentration of 65 percent. (Compare with actual positions of star groups in Fig. 4.) Figure 5 gives the observed abundance of light elements as found in the stellar atmospheres. Examination of the distribution indicates that Li, Be and B were probably present in greater concentrations in the past. According to the above theory these are the only elements that could have been consumed in stellar interiors to any appreciable extent.

The above conflict lines have been obtained (Fig. 4) such that gravitational contraction was predominant to the left of the line while nuclear reaction was predominant to the right.

In conclusion, the author wishes to express his gratitude for the invaluable advice and guidance of Dr. G. Gamow, George Washington University, who suggested this problem, and to Dr. E. Teller and Dr. E. Feenberg for stimulating discussions.

Rare-Earth and Transuranic Elements*

M. GOEPPERT MAYER
Department of Chemistry, Columbia University, New York, New York

(Received May 31, 1941)

The possible existence of a second rare-earth-like group of elements beginning with uranium and extending to the transuranic elements, is discussed by a calculation of the atomic eigenfunctions of the 4*f* and 5*f* electrons. Energy and spatial extension of the 4*f* eigenfunctions drop suddenly at the beginning of the rare-earth group; the binding energy is calculated to be 0.95 ev in lanthanum, $Z=57$, and 5 ev in neodymium, $Z=60$. The 5*f* eigenfunctions undergo the same type of change around $Z=92$. The binding energies were calculated to be 1.35 ev for $Z=86$, 8.5 ev for $Z=91$ and 14 ev for $Z=93$.

INTRODUCTION

THE chemical behavior of element 93, recently discovered by McMillan and Abelson[1] is strikingly similar to that of uranium and has led these authors to the assumption that a second rare-earth group might start at uranium. In this paper this possibility is discussed from the theoretical point of view.

The first rare-earth group is due to a sudden decrease in energy and size of the 4*f* electronic orbits. A second rare-earth group could occur due to a similar change in the 5*f* eigenfunctions. For this reason, a calculation was made of the shape and energy of the 5*f* eigenfunctions in the neighborhood of $Z=92$. To get a clearer insight into the question, the 4*f* eigenfunctions at the beginning of the first rare-earth group, around $Z=58$, were also studied.

This same problem has been discussed by Sugiura and Urey[2] on the basis of the old quantum theory.

THE POTENTIAL ENERGY

The potential energy used for the computation of the eigenfunctions is the statistical, or Thomas-Fermi[3] potential, of the form

$$-\frac{e^2}{r}[1+(Z-1)\varphi(r/\mu)], \qquad \mu=\frac{3^{2/3}h^2}{2^{13/3}\pi^{4/3}me^2}\frac{1}{Z^{1/3}}, \tag{1}$$

where $\varphi(x)$ is a universal function, the same for all atoms, decreasing from 1 at $x=0$ to 0 at $x=\infty$. $\varphi(x)$ has been computed numerically by Fermi.[3] The scale of x, that is the value μ, depends on the atomic number Z.

The differential equation for the determination of the radial part v of $r\cdot\psi$ for an *f* function, with $l=3$, is

$$v''=\frac{8\pi^2m}{h^2}[E-V(r)]v, \tag{2}$$

with

$$V=-\frac{e^2}{r}[1+(Z-1)\varphi(r/\mu)]+\frac{h^2}{8\pi^2m}\cdot\frac{12}{r^2}. \tag{3}$$

The effective potential V, potential energy plus potential of the centrifugal force, is plotted in Figs. 1a, 1b, for the two extreme cases that were treated, $Z=57$ and $Z=93$. Figure 1b, which pictures V for small r, is drawn in a scale of energies one hundred times that of Fig. 1a.

It is seen that V is negative in two different regions. The valley for large r is very broad and shallow. In this region, $(Z-1)\varphi(r/\mu)$ is already small compared to 1 in all cases, so that position and depth of the minimum scarcely change with Z, and are, indeed, practically the same as for hydrogen. For hydrogen, $Z=1$, there exists only this one minimum of V.

As Z increases, a second minimum of the effective potential V develops at small values of r. Its position shifts to the inside with increasing Z—from $r=0.22$A for $Z=57$ to $r=0.09$ for $Z=93$. The depth increases very rapidly, from 101 electron volts at $Z=57$ to 1335 electron volts at $Z=93$. At the same time, the valley

* Publication assisted by the Ernest Kempton Adams Fund for Physical Research of Columbia University.

[1] E. McMillan and P. H. Abelson, Phys. Rev. **57**, 1185 (1940).

[2] Y. Sugiura and H. C. Urey, Kgl. Danske Vid. Sels. Math.-fys. Medd. **7**, 3 (1926).

[3] E. Fermi, Leipziger Vorträge, 95–111, 1928.

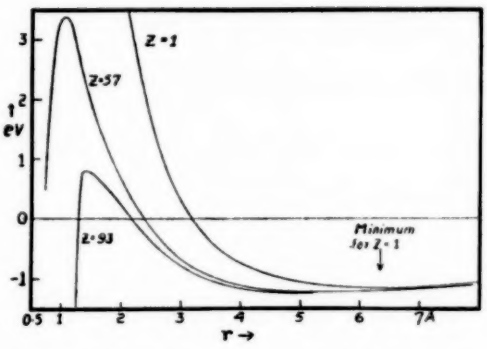

FIG. 1a. Effective potential energy $V(r)$, Eq. (3), for large values of r.

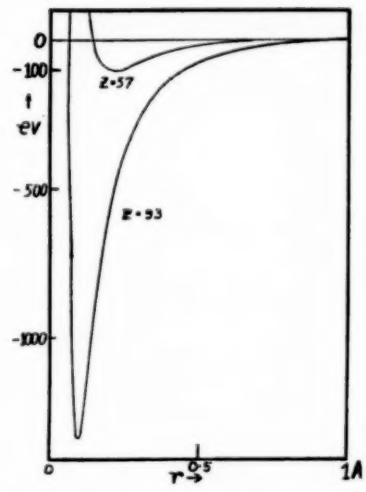

FIG. 1b. Effective potential energy $V(r)$, Eq. (3), for small values of r.

becomes narrower and the curvature at the minimum increases.

The positions of the two minima and their values for different atomic numbers are given in Table I.

QUALITATIVE DISCUSSION

The qualitative behavior of the $4f$ and $5f$ eigenfunctions can now be readily deduced. Perhaps this can be done most clearly by speaking of the potential barrier between the two valleys as if it were infinitely high. In that case, the two valleys would have independent sets of levels. Since the first valley is very much narrower, its levels are much more widely spaced than those of the second one. For small Z, the first level of the inner valley will be positive (above ionization). In that case, the lowest level of the total system is that of the outer valley. Since here the potential is practically that of hydrogen, and hardly varies with Z, the binding energy of the $4f$ electrons will be approximately constant and about the same as for hydrogen, 0.85 ev. Actually, the lowest eigenfunction will have two maxima, at the place of the two valleys, but the value of v at the outer maximum will be much larger than at the inner one.

There comes a value of Z when the inner valley is so deep that its first electron level sinks below the first level of the outer valley. At that point the shape of the $4f$ eigenfunction changes abruptly to one corresponding to an internal orbit. As Z increases, the bottom of the inner valley sinks rapidly, carrying down the $4f$ level. Since, however, the valley becomes not only deeper but also narrower, the decrease of the level is not as rapid as that of the bottom.

Experimentally, we know that just this occurs at the rare-earth group, around $Z=58$. The sudden spatial shrinkage of the $4f$ orbit agrees with the experimental fact that these functions, although containing the most loosely bound electrons, do not influence the valence properties of the atoms.

At the place in the periodic system where the $4f$ function changes its character, the $5f$ function also undergoes some changes. For lower values of Z, the $5f$ level is simply the second level of the outer valley; the $5f$ function is hydrogen-like in shape and energy (about 0.52 ev), with one node somewhere in the outer valley. After the lowest level of the inner valley has sunk below that of the outer one, that is after the rare-earth group, the second level of the total system is the lowest level of the outer valley. The $5f$ function will consequently behave in that region like a $4f$ hydrogen function; its node occurs somewhere

TABLE I. *Positions and depth of minimum values of V.*

Z	Position of 1st Minimum A	Depth of 1st Minimum ev	Position of 2nd Minimum A	Depth of 2nd Minimum ev
1	—	—	6.35	1.13
57	0.22	101	5.7	1.18
60	0.17	147	5.6	1.21
86	0.11	984	5.5	1.23
91	0.094	1218	5.5	1.23
93	0.092	1335	5.5	1.23

in the region of the inner valley. As Z increases, the energy of the level will remain practically constant around 0.85 ev.

But then a Z value is reached at which the inner potential trough becomes so deep that even the second level of the inner valley drops below the lowest level of the outer valley. One will predict that at that point a second rare-earth group sets in, with all the characteristics of the first one; the energy of the $5f$ level starts to drop, and from then on keeps decreasing with increasing atomic number; the orbits shrink suddenly and become inner eigenfunctions, therefore do not influence the valence character of the atoms.

In order to determine where the shrinkage of the $4f$ and $5f$ eigenfunctions occurs, some numerical integrations of Eq. (2) were undertaken.

The $4f$ Eigenfunctions

Lanthanum, $Z=57$, is the first of the rare earths, the one which does not yet have a filled $4f$ orbit. Calculation shows that the binding energy is 0.92 ev, not much changed from that of hydrogen (0.85 ev). The eigenfunction is still located essentially outside the atom. It has two maxima, at $r=0.54$A and $r=7.3$A (the maximum of the $4f$ function of hydrogen occurs at 8.47A), but the value of v, the radial part of $r\psi$, at the second maximum is about six times the value of the first maximum.

At $Z=60$, neodymium, the eigenfunction has undergone the expected radical change. The binding energy has dropped to 5 electron volts, considerably below the value of the potential energy in the outer valley. The first maximum of the eigenfunction occurs at 0.36A, but the second one has entirely disappeared; at $r=2$A the function has already dropped to one-tenth of its value at the maximum. The $4f$ function is now entirely an inner function.

Table II. *Binding energies.*

	$4f$			$5f$	
Z	Substance	Binding Energy in ev	Z	Substance	Binding Energy in ev
1	Hydrogen	0.85	1	Hydrogen	0.54
57	Lanthanum	0.95	86	Radon	1.35
60	Neodymium	5	91	Protactinium	8.5
86	Radon	250	93	Neptunium	14

For $Z=86$, radon, the binding energy of the $4f$ function lies between 200 and 300 electron volts.

The $5f$ Eigenfunctions

The $5f$ eigenfunction of hydrogen crosses the x axis at about 10.5A. In lanthanum, $Z=57$, this node occurs somewhere around 8A. At $Z=60$, the node has come down suddenly to about one-tenth of that value, namely to $r=0.75$A. For subsequent values of Z, up to about $Z=85$, the node moves still further inside. Beyond this node, the eigenfunction has two maxima of absolute value, the first one still located in the inner potential valley, the second one, higher and wider, in the outer potential valley, at about 6A. It is the neighborhood of this outermost maximum of absolute value of v which gives the essential contribution to $|\psi|^2$; the effective potential energy in this range determines the energy. The eigenfunction is here essentially an outer eigenfunction and, according to the qualitative discussion above, we shall expect the energy to be about constant and of the order of that of the $4f$ function of hydrogen, 0.85 electron volt.

The first actual determination of energy was made for radon, $Z=86$. Here, however, the second shrinkage of the $5f$ eigenfunction has already just set in. The energy has fallen to 1.35 electron volts, just below the minimum of the outer potential valley. The function $v=r\psi$ has a maximum at 0.14A, a node at 0.27A, and a minimum (maximum of absolute value) at 0.7A. The outer minimum has just disappeared, but the function does not fall off very rapidly with distance. In short, the ψ function is just on the verge of becoming an inner eigenfunction.

At $Z=91$, protactinium, the shrinkage is more complete. The energy has dropped to 8.5 electron volts. For $Z=93$, neptunium, it is 14 electron volts.

The energies obtained are tabulated in Table II.

Comparison with d Orbits

The sudden change in character and energy of the eigenfunction with a change in the atomic number is typical for the f orbits only, and does not occur in the same manner for any other angular quantum number. Only for $l=3$ does the

effective potential energy V possess two ranges of negative values, separated by a region of positive V.

This is seen most easily by considering, instead of V, a function proportional to r^2V, namely

$$[\mu e^2(Z-1)]^{-1}r^2V(r) = -(r/\mu)\varphi(r/\mu) + l(l+1)(4/3\pi)^{\frac{2}{3}}Z^{\frac{1}{3}}/(Z-1) - r/\mu(Z-1). \quad (4)$$

$x\varphi(x)$ is plotted against $x=r/\mu$ in Fig. 2. The straight lines

$$l(l+1)(4/3\pi)^{\frac{2}{3}}Z^{\frac{1}{3}}/(Z-1) - x/(Z-1) \quad (5)$$

are also plotted for some values of Z, and for $l=2$ and $l=3$. Wherever $x\varphi(x)$ is larger than this straight line for a given Z, the effective potential energy is negative. Figure 2 shows that for Z less than about 47 the solid straight lines (5) with $l=3$ intersect the curve only once. For these values of Z there exists only one range of negative potential. For $Z=50$, and also for all larger values of Z, the straight lines with $l=3$ intersect the curve three times, which shows that there exist two separate ranges of negative potential energy.

For the d electrons, $l=2$, the function (4) differs from that for the f electrons only in that 12 in the second term has to be replaced by 6. The corresponding straight lines are parallel to the lines with $l=3$ for the same value of Z, and their intersection with the y axis is half as high. These lines are dotted in Fig. 2 for various values of Z. It is seen that for all values of Z the lines for $l=2$ intersect the curve once only. The effective potential energy for the d electrons has, therefore, only one range of negative values.

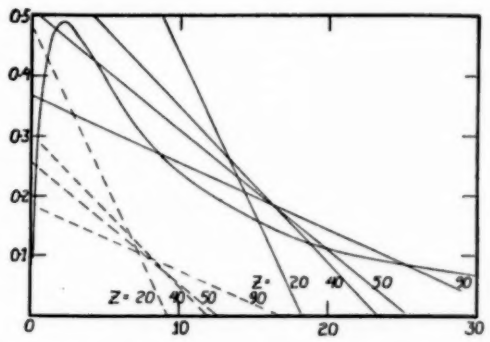

FIG. 2. Curved line represents $x\varphi(x)$ (see Eq. (4)). Solid straight lines represent Eq. (5) for $l=3$, dotted lines for $l=2$.

CONCLUSION

The calculations for the rare-earth group agree moderately well with the experimental facts. The theory would predict that the $4f$ orbits start to be filled at $Z=61$ or $Z=60$, at the earliest. Actually, the first $4f$ electron occurs at $Z=58$.

In the neighborhood of $Z=92$, the theory predicts occurrence of a second rare-earth group; the first filled $5f$ level should occur at $Z=91$ or 92. Experimentally it appears that uranium does not yet possess a $5f$ electron. Inaccuracies of a few units in Z are to be expected in a calculation based on the statistical model.

Sincere thanks are due to E. Fermi, who suggested the problem and took a great deal of interest in it.

The Gamma-Radiation from Long-Lived Yttrium

J. REGINALD RICHARDSON
Department of Physics, University of Illinois, Urbana, Illinois
(Received June 16, 1941)

The gamma-radiation emitted by the 100-day yttrium isotope has been investigated. The momentum distribution of the recoil electrons from a thin paper radiator situated near the center of a cloud chamber falls into two groups. These groups correspond to gamma-ray energies of 0.95 ± 0.05 Mev and 1.92 ± 0.03 Mev. The relative number of quanta in the gamma-ray lines is one to 0.9, or approximately equal. Because the energy of one of the lines is half that of the other, a coincidence experiment must be done before a level diagram can be drawn with certainty.

INTRODUCTION

A RADIOACTIVE isotope of yttrium has been reported[1,2] with a half-life of about 100 days. This substance has been produced both by proton bombardment of strontium and by high energy deuteron bombardment of the same element. The reactions are presumably $Sr^{86}(p, n)Y^{86}$ and $Sr^{86}(d, 2n)Y^{86}$, although the evidence is not quite conclusive on the assignment of the atomic weight of the product. The activity of this isotope consists principally of K and gamma-radiation. Using the gamma-rays, Pecher[2] has shown that this isotope should be suitable for industrial radiography. He has also produced some photo-neutrons from Be and has indicated the suitability of the Y-γ-Be reaction as a source of monokinetic neutrons. With this in mind, it was thought that it would be desirable to have a better knowledge of the energy distribution of the gamma-radiation emitted by this substance.

APPARATUS

The method used to measure the gamma-radiation was to investigate the momentum distribution of the secondary electrons ejected from a thin radiator in a cloud chamber. The cloud chamber was twelve inches in diameter and was filled with hydrogen to a pressure slightly above atmospheric. The chamber was situated in a magnetic field of 415 gauss constant to within 0.5 percent throughout the usable volume of the chamber. This field is produced by coils wound with square copper tubing which is double cotton covered and which has a round hole through the center for water cooling. These coils can dissipate 50 kw in continuous operation, when they will produce a field of 2000 gauss. The current through the coils is kept constant to within 0.5 percent by an automatic electronic regulator.[3]

Two radiators were used as a source of secondary electrons. One was of paper coated with lamp black in oil and having a surface density of 20 mg/cm². The other was a platinum foil of surface density 17 mg/cm².

The yttrium source was produced in the sixty-inch cyclotron at Berkeley by bombarding strontium oxide with 16-Mev deuterons. It was sent by Dr. Pecher to Professor Goldhaber, who intended using it as a source of photo-neutrons. It had a gamma-ray strength of approximately 5 mg Ra equivalent. The gamma-radiation passed through the hole in a lead collimator and also through about 1 cm of glass before reaching the radiator.

In order to test and calibrate the apparatus, two thousand pictures were taken of the recoil electrons ejected from the carbon radiator by the gamma-radiation of Th C″. The measurements indicated a gamma-ray energy of 2.65 Mev, instead of the accepted 2.62 Mev. The measured field constant of the coils was then adjusted to take care of this slight difference.

RESULTS

Photographs were taken of some six thousand cloud-chamber expansions. In the case of the

[1] L. A. DuBridge and J. Marshall, Phys. Rev. **58**, 7 (1940).
[2] C. Pecher, Phys. Rev. **58**, 843 (1940).
[3] J. W. Coltman, not yet published.

carbon radiator, only those tracks were chosen which were within ten degrees of the forward direction, were at least ten cm long and otherwise fulfilled the conditions demanded in previous papers.[4]

The results in the case of the carbon radiator are shown in Fig. 1, giving the momentum distribution of the Compton recoil electrons. The electrons seem to fall clearly into two groups indicating the presence of gamma-radiation of at least two energies. The method used to find the gamma-ray energy from the momentum distribution of the recoil electrons has been explained previously in detail.[4] It consists essentially of drawing the best straight line through the experimental points on the high energy side of the distribution. The intercept of this line with the axis corresponds to the maximum momentum that an electron can receive in the Compton process. Thus in the high energy group in Fig. 1 this momentum is 7160 $H\rho$, corresponding to an energy of 1.70 Mev. To this must be added the minimum energy given to the scattered gamma-quantum, which in this case is 0.22 Mev. Thus we have obtained 1.92 Mev as the initial energy of the quantum. A probable error of ± 0.03 Mev should be assigned. Dr. Scharff-Goldhaber[5] has investigated the energy of the recoil protons knocked on by the photo-neutrons produced by this gamma-radiation from beryllium. Her data indicate an energy for the gamma-radiation of 1.87 ± 0.05 Mev. These values are obviously consistent.

The probable error assigned to the lower energy group in this work must be somewhat larger because of the presence of background from the higher energy group in the region where the straight line would otherwise intersect the axis. The maximum electron energy here is 0.75 Mev and 0.20 Mev goes to the scattered quantum. This gives a value for the low energy radiation of 0.95 ± 0.05 Mev.

The distribution of Compton and photoelectrons from the platinum radiator was investigated to find out if there were any prominent

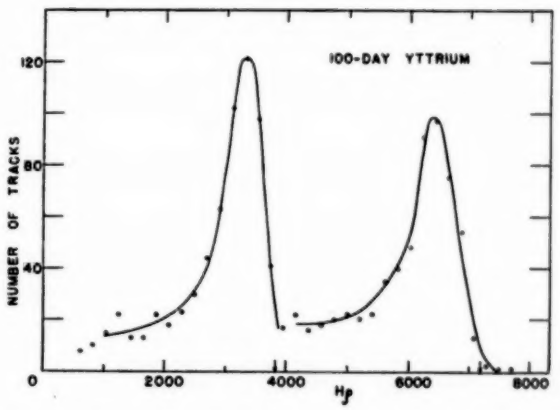

FIG. 1. The momentum distribution of the recoil electrons produced by the gamma-radiation of the 100-day yttrium isotope. The electrons were ejected from a paper radiator of 20 mg/cm² surface density. The gamma-ray energies corresponding to the two groups are: 0.95 ± 0.05 Mev and 1.92 ± 0.03 Mev.

lines between 100 kv and 500 kv. None were found. There was a slight indication of some radiation around 200 kv, but in any case the number of quanta of this energy is less than 10 percent of the total number emitted.

The relative numbers of quanta of different energy emitted by the source are of considerable interest and may be obtained by taking account of the Compton cross section and straggling, as explained in previous papers.[4] Doing this one obtains the following result. If one denotes the number of quanta of 0.95 Mev by unity, the number of energy 1.92 Mev will be 0.85. This result is uncertain by about 20 percent.

These radiations presumably correspond to transitions in the Sr^{86} nucleus, which results from K electron capture. It is interesting to note that the energy of the lower group of quanta is almost exactly half the energy of the upper group. Thus it is quite possible that there are actually two transitions involved, each of energy 0.95 Mev, as an alternative to the single transition 1.92 Mev. The fact that the lower energy group of electrons is somewhat broader than one would expect is slight evidence that this may be so. On the other hand, the fact that there are almost equal numbers of quanta of the two energies means that one cannot rule out the possibility that the transitions are in series. Although a small number of very high energy electrons were observed, they were not in excess of

[4] J. R. Richardson and F. N. D. Kurie, Phys. Rev. **50**, 999 (1936); J. R. Richardson, Phys. Rev. **53**, 124 (1938); J. R. Richardson, Phys. Rev. **55**, 609 (1939).
[5] G. Scharff-Goldhaber, Phys. Rev. **59**, 937A (1941).

what could be accounted for by cosmic radiation.

It seems fairly obvious that the only way in which one can decide between these possibilities is by performing an experiment with coincidence counters and investigating the variation of coincidences with absorption.

It is a pleasure to acknowledge my debt to Louise Richardson, who photographed the expansions and developed the pictures necessary for this work. This research was supported by the Graduate School Research Board of the University of Illinois.

AUGUST 1, 1941 PHYSICAL REVIEW VOLUME 60

The Scattering of Electrons from RaE by Thin Metal Foils

J. L. SAUNDERSON* AND O. S. DUFFENDACK
Randall Laboratory of Physics, University of Michigan, Ann Arbor, Michigan
(Received June 13, 1941)

Beta-rays from radium E of energy greater than 0.2 Mev were scattered by thin foils of metal and the distribution of the scattered electrons was measured with a Geiger-Müller counter between the angles 0° and 45°. Two thicknesses each of aluminum, copper, silver, and gold foils were used as the scattering material. The thinner set of foils was made of thickness such that each had the same cross section for single scattering, that is, Z^2nt was kept constant, while the second set of foils was made twice as thick. The Wentzel angle was 22° for the first set and 33° for the second. A comparison of the experimental results with the Mott theory in the range above the Wentzel angle was made by integrating over the energy spectrum of the radium E source used. For the energy and angular ranges investigated, it is concluded that such deviations from the Mott formula which exceed experimental error are due to the effects of multiple scattering and the inadequacy of the Wentzel criterion for elements of small Z. The check in absolute magnitude of the scattering is considered satisfactory.

I. INTRODUCTION

ALTHOUGH considerable work has been done on the problem of the scattering of electrons, a survey of the literature indicates that there still remains a great deal of contradictory evidence concerning the validity of the theory.[1] Doubtless part of the disagreement is due to the different geometrical arrangements used, as well as to the inherent difficulties of the problem. It appears that the matter will be settled only by the accumulation of more data obtained under carefully controlled and defined geometrical conditions. The work reported here was done to obtain additional information on the scattering of electrons of intermediate energy both in the single scattering and in the multiple scattering regions.

In this work, a collimated beam of electrons from a deposit of RaE was scattered by thin foils of Al, Cu, Ag, and Au. The scattered electrons were measured at various angles with a Geiger-Müller counter. The number of electrons scattered between 20° and 45° was compared with that predicted by the single scattering formula of Mott, after this formula had been modified to take account of the variation in energy of the scattered electrons and also the small angular spread of the incident beam of electrons. The experimental results at angles smaller than 20° were not compared quantitatively with any theory, but a variation of the scattering with the atomic number of the scattering element was found to be in quantitative agreement with the multiple scattering formula of Goudsmit and Saunderson.[2]

The observed scattering at the larger angles was compared with the single scattering formula of Mott,[3] which may be written

$$I_{(\theta)}d\omega=(Ze^2/2mc^2)^2(1-\beta^2/\beta^4)\csc^4\tfrac{1}{2}\theta \times[1-\beta^2\sin^2\tfrac{1}{2}\theta +\pi z\alpha\beta\sin\tfrac{1}{2}\theta\cos^2\tfrac{1}{2}\theta+\cdots]d\omega. \quad (1)$$

* Now with Dow Chemical Company, Midland Michigan.
[1] See, for example, M. E. Rose, Phys. Rev. **57**, 280 (1940).
[2] S. Goudsmit and J. L. Saunderson, Phys. Rev. **58**, 36 (1940), Eq. (14).
[3] N. F. Mott, Proc. Roy. Soc. **A124**, 425 (1929).

In this expression, $I(\theta)$ represents the probability that an electron will be scattered into the solid angle $d\omega$ which is situated at an angle θ with the original direction of motion, and $\alpha=e^2/\hbar c$. For a beam of electrons, the formula represents the distribution in angle of electrons scattered from a single scattering center. A test of the theory must, therefore, be made under conditions of single scattering.

In order to select from the measurements the data which are in the region of single scattering, it is necessary to apply some criterion for their selection. The best known criterion for single scattering is that of Wentzel,[4] according to which the scattering is single for angles θ greater than 12ω, where

$$\omega=2\cot^{-1}\frac{mv^2}{Ze^2}\left(\frac{2}{\pi nt}\right)^{\frac{1}{2}}. \quad (2)$$

In this equation, n is the number of atoms per cc in the scattering material, t is the thickness of the foil, and v is the velocity of the electrons.

An estimate of the fractional error caused by plural scattering in a measurement of the single scattering at the angle θ has been given by Chase and Cox,[5] who obtained the expression

$$\epsilon^2[\csc^2\tfrac{1}{2}\theta-\tfrac{1}{2}]. \quad (3)$$

Here, ϵ^2 is the mean square deflection of the scattered electrons, and may be calculated or determined experimentally. The average angle can be calculated with sufficient accuracy for the purpose at hand by the expression[2]

$$\langle\sin\theta\rangle_{Av}=\{3.08\mu[\log\xi+\tfrac{1}{2}\log\mu+0.60]\}^{\frac{1}{2}}, \quad (4)$$

where

$$\mu=24.8\times10^{-26}Z^2nt\frac{w^2}{(w^2-1)^2}$$

and $\xi=150(\mu^2-1)^2/Z^{\frac{1}{3}}$.

TABLE I. *Foil thicknesses.*

Element	Set I Thickness cm $\times10^{-4}$	$Z^2nt\times10^{-20}$	Element	Set II Thickness cm $\times10^{-4}$	$Z^2nt\times10^{-20}$
Al	2.5	25	Al	5.5	55
Cu	0.35	25	Cu	0.70	50
Ag	0.19	25	Ag	0.38	50
Au	0.076	25	Au	0.15	50

[4] G. Wentzel, Ann d. Physik **69**, 333 (1912).
[5] C. T. Chase and R. T. Cox, Phys. Rev. **58**, 243 (1940).

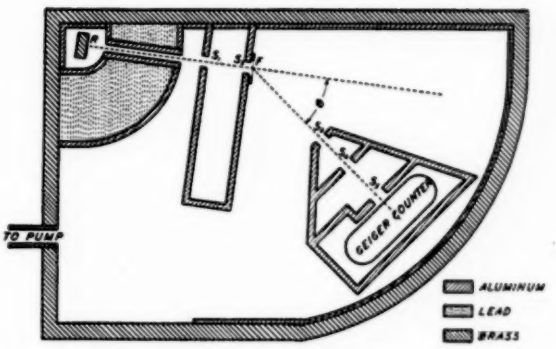

FIG. 1. Plan of the scattering chamber. The parts are labeled as follows: R is a block containing the RaE; S_1, S_2, S_3, S_4, S_5 are slits; F is the scattering foil; θ is the angle of scattering which was varied by moving the counter. The electrical leads to the counter are omitted from the drawing.

The scattering foils for this work were made in two sets of thicknesses, the first set being of such thickness that Wentzel's criterion is satisfied for $\theta=22°$ and $\beta=0.75$, while the second set was made twice as thick as the first set. The data on the foils are given in Table I. For the first set of foils with $Z^2Nt=25\times10^{20}$, an intermediate Z (~40) and an average energy $w=1.7$ in units of mc^2, Eq. (4) gives for the average angle,

$$\epsilon=\langle\sin\theta\rangle_{Av}=3°.$$

At the Wentzel angle of 22°, formula 3 predicts an error of 7.5 percent in the measurement of single scattering due to multiple scattering. The Wentzel criterion was, therefore, considered sufficiently accurate in this case and was used to designate the region of single scattering.

II. Description of Apparatus Used

A. The vacuum chamber

The chamber in which the scattering took place is shown in Fig. 1. The source of electrons, a deposit of radium E, was placed at R. A lead block shielded the rest of the chamber from the source, except for an aluminum tube which allowed electrons to pass through in the form of a beam. All exposed surfaces of the lead block were covered with sheet aluminum in order to reduce the production of x-rays which might affect the counter background. The beam of electrons passing through the aluminum tube was further defined by two apertures, S_1 and S_2. The scattering foil was placed directly behind S_2 at F.

The Geiger-Müller counter tube was placed in an aluminum box and was thus shielded from electrons except for those which came through the three apertures, S_3, S_4, S_5. The last aperature, 7 mm in diameter, determined the effective solid angle of the counter subtended at F. The function of S_3 and S_4 was to limit the electrons which could get to the counter to those coming from the foil. Suitable aluminum lining on the inside of the chamber was used to reduce the number of electrons scattered from the walls.

The aluminum box containing the counter was placed on a carriage which could be rotated through various angles with the center of rotation at the position of the foil. This was done by means of a tapered brass plug, made vacuum tight with stopcock grease, which extended through the bottom of the chamber and which could be rotated from outside by means of a pointer extending beyond the circular end of the chamber. The position of the counter inside was indicated by a scale calibrated in degrees. The electrical connections to the counter were brought into the chamber near the position of the foil, so that the capacity of the leads was practically constant at all positions of the counter. The top of the chamber was put on with a rubber gasket, and the pressure was maintained at 10^{-4} mm of mercury, or less, during all measurements.

B. The counting system

The Geiger-Müller tube was constructed of a hollow nickel cylinder, 2 cm long and 1.2 cm in diameter, with a 3-mil tungsten anode wire at the center. An oval hole was cut in one side of the cylinder and the enclosing glass envelope was thinned out at the corresponding place to allow electrons of energy greater than 0.2 Mev to pass through. The tube was made by the usual method employed in this laboratory.[6] The tube was filled with hydrogen to a pressure of 106 mm of mercury, and was regularly operated at 1050 volts, about 300 volts above the counter threshold.

The recording system was designed by Dr. Lifschutz[7] and consisted of a stabilized high voltage supply, Neher-Harper coupling circuit and a vacuum-tube scale-of-eight circuit which drove a Cenco mechanical counter. The resolution time of the circuit was 6.5×10^{-6} second, and the maximum counting rate of the Geiger-Müller counter and the circuit under the operating conditions of this work was 96,500 counts per minute. This maximum counting rate is much lower than that of which the circuit is normally capable, being lowered in this case because of the unavoidable capacity of the leads running through the scattering chamber to the movable counter inside. Nevertheless, the counting losses in the Cenco counter were negligible for a random input up to about 25,000 counts per minute. This counting rate was never exceeded in this work.

C. Preparation of the scattering foils

Foils of aluminum, copper, silver, and gold were used in this investigation. Aluminum foil 0.00055 cm thick was rolled down to 0.00025 cm, these two thicknesses being used for the scattering. The thinner foil satisfied the Wentzel criterion at 22° for $\beta=0.75$. Foils of the three other metals were made of such thickness that they would have the same scattering power, that is, Z^2nt was kept constant. These foils were made by evaporation of the metal in a vacuum from a tungsten filament onto a thin pyroxylin film. The film was formed by placing a drop of a pyroxylin solution on a water surface. The film was then removed from the water and fixed upon an aluminum holder containing a 1-cm hole, so that when dry the pyroxylin film was stretched tightly over the hole. The scattering power of such a film was determined by weighing a large area and calculating the average value of Z^2nt, in which the average Z^2 and average atomic weight obtained from the chemical formula for pyroxylin are used. In this way it was calculated that the scattering by the pyroxylin film should amount to about 4 percent of that by the thinner set of metal foils and was neglected.

A small amount of the metal to be evaporated was placed upon a 1-mil tungsten ribbon which was bent in the form of a V-shaped trough. The pyroxylin film to receive the evaporated metal was held 8 cm directly above the filament. The thickness of the evaporated foil was controlled by weighing the sample placed on the filament and evaporating it completely each time. By weighing a larger area of the foil, a relation between the

[6] Duffendack, Lifschutz, and Slawsky, Phys. Rev. **52**, 1231 (1939).
[7] H. Lifschutz, Rev. Sci. Inst. **10**, 21 (1939).

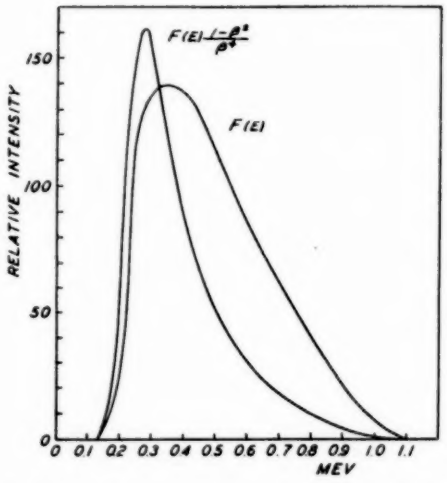

FIG. 2. $F(E)$ is the energy distribution of the RaE source as determined in a magnetic spectrometer with the same counter as used in the scattering experiments. The second curve is Eq. (6) of text, and is used for graphical integration.

mass evaporated and the mass per unit area of the foil was obtained. For the area of foil used, simple calculation showed that the foil thickness should vary a negligible amount. This relation was constant for any given geometry and kind of surface on which metal was evaporated. It was found advantageous to carry out the evaporation rather slowly, as this reduced the chance of breaking the pyroxylin film.

D. Experimental procedure

For purposes of comparison, all data were corrected for the decay of the source by multiplying by a decay factor, thus referring all measurements to a common time. This procedure was complicated by the fact that only the RaE decayed, while the natural background of the counter remained constant. This fact was important in determining the probable statistical fluctuation of the data. In order to correct for electrons scattered from the sides of the chamber and from the apertures defining the beam, the chamber background (so-called to distinguish this from the natural counter background) was measured, without any scattering foil in place, for all angles where the scattering was to be subsequently determined. The chamber background was then subtracted from the observed scattering to obtain the true scattering intensity. It is evident that this is justifiable only when the beam is not much altered by the presence of the scattering foil, as is the case for a study of single scattering at small angles. In order to reduce the statistical error as much as possible, the chamber background was determined with the same accuracy as the scattering measurements themselves.

III. Comparison of Results with Theory

Equation (1) expresses the probability that an electron of total energy $mc^2/(1-\beta^2)^{\frac{1}{2}}$ will be scattered by a nucleus of charge Z through the angle θ into the small solid angle $d\omega$. This formula is, of course, an ideal case, not physically realizable, so that certain modifications must be applied to it. Beginning with this equation, we shall obtain an expression for the theoretical scattering of a beam consisting of A electrons per minute, which have a known distribution of velocities, a certain angular spread because of imperfect collimation, being scattered by a foil consisting of n nuclei per cc and nZ electrons per cc, and which are scattered into a finite $d\omega$ solid angle such that θ cannot be considered constant from one extreme of $d\omega$ to the other. The above modification, characteristic of this experiment, will be applied to the fundamental Mott formula to obtain an expression for the predicted scattering. The expression thus obtained will be compared directly with the true observed scattering as described in II D.

A. Measurement of the intensity of the beam

Measurement of the number of electrons incident upon the foil was made after the RaE had decayed to about one-tenth its original strength in order to avoid high counting rates. The measurement was made by removing the scattering foil and placing the Geiger-Müller tube at the foil position. The fraction of the count thus measured which might be due to gamma-rays was shown to be negligible by blocking off the electrons with a suitable thickness of aluminum. The theoretical decay factor was verified experimentally for the RaE source used.

B. Measurement of the beta-ray spectrum of RaE

Although the spectrum of radium E has been determined many times, it is well known that the observed distribution depends very much on the thickness of the radioactive substance as well as

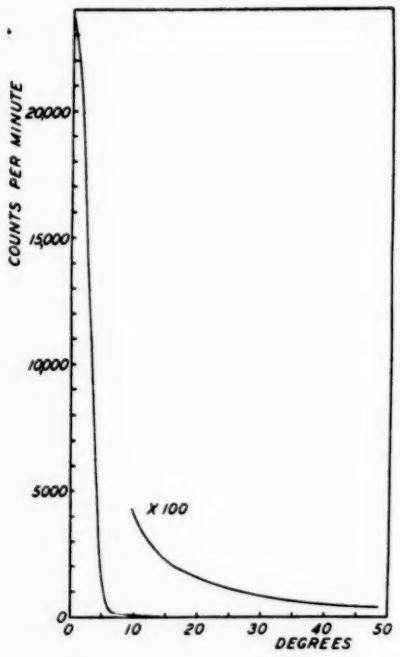

FIG. 3. The chamber background distribution curve, showing the angular distribution of electrons in the absence of any scattering foil (see II D).

upon the material upon which it is deposited. For this reason, the spectrum of the same source as used in the scattering experiments was determined by using the magnetic spectrometer built in this laboratory by Drs. Lawson and Tyler.[8] For this determination, the same counter tube was used in the spectrometer as was used in the scattering experiment.

Figure 2 shows the energy spectrum of the source as determined by the counter. The counter window absorbs strongly below 0.3 Mev and becomes practically opaque to electrons of energy below 0.2 Mev. The most probable energy is 0.35 Mev and the maximum energy is about 1.1 Mev. The energy distribution as experimentally determined will be referred to as $F(E)$; it is the apparent energy spectrum for the combination of source and counter used. For the calculation of the intensity of nuclear scattering, the apparent energy spectrum is the one desired, since its use eliminates the necessity for knowing the true energy spectrum of the source and also the variation of counter efficiency with energy.

[8] J. L. Lawson and A. W. Tyler, Rev. Sci. Inst. **11**, 6 (1940).

C. Integration over the energy distribution

The fact that the source of electrons used had a distribution of electron velocities will now be considered in regard to the way in which the different velocities influence the scattering. During the measurement of the beam intensity, the energy distribution of the electrons which are counted is given by $F(E)$. Thus,

$$\int F(E)dE = A, \tag{5}$$

where A is the number of electrons per unit time in the incident beam. Electrons which are scattered at the angle θ do not, however, have an energy distribution given by $F(E)$, since the slower electrons are scattered more often than the faster ones. From the Mott formula, it is evident that the scattered electrons have an energy distribution given by

$$F(E)(1-\beta^2)/\beta^4 \tag{6}$$

and that this distribution is the same for all angles of scattering. This conclusion follows from the single scattering hypothesis and, therefore, does not apply to regions of plural and multiple scattering. Such regions must, therefore, have a greater number of the faster electrons than represented by $F(E)$, since the single scattering region has a larger number of the slower ones.

An integration must be performed over

$$F(E)(1-\beta^2)/\beta^4$$

to find the number of electrons scattered to the angle θ, with the condition that $F(E)dE$ be normalized to A, the intensity of the entire beam. The number of electrons scattered per unit time into $d\omega$ at θ is given by

$$N = nt\left(\frac{Ze^2}{2mc^2}\right)^2 \cdot \int F(E)\frac{1-\beta^2}{\beta^4}dE \cdot \csc^4 \tfrac{1}{2}\theta \cdot d\omega \cdot K(\theta). \tag{7}$$

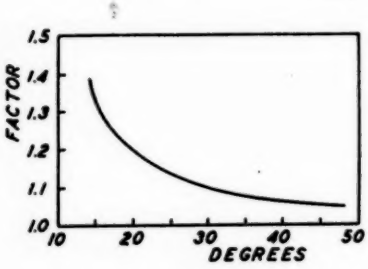

FIG. 4. The angular correction factor $K(\theta)$ used for correcting for the finite size of the apertures.

With A equal to 111,000 electrons per minute, graphical integration (see Fig. 2) yields the result that

$$\int F(E)\frac{1-\beta^2}{\beta^4}dE = 72{,}100 \text{ electrons per minute.}$$

$K(\theta)$ is explained in the following paragraph.

D. Angular spread of the beam

Because of the very small intensity of scattering at angles for which the scattering is mainly single, it was necessary to use fairly large apertures to define the incident beam as well as the scattered beam. It was possible from the geometry of the apparatus to find the uncertainty in angle and to make an approximate correction to the intensity of scattering. The angular uncertainty of the scattered beam $\pm\gamma$ was found to be

$$\gamma = 0.0175\cos\theta + 0.0307. \tag{8}$$

At $\theta=0$, γ is 5.1°, and becomes smaller as the angle θ becomes larger. The shape of the chamber background distribution curve (Fig. 3) agrees well with this value for γ.

The main angular dependence of the Mott formula is the term $\csc^4\frac{1}{2}\theta$. The angular correction factor $K(\theta)$ was taken as the average of $\csc^4\frac{1}{2}\theta$ over the angular interval $\theta\pm\gamma$, assuming all directions equi-probable, that is,

$$K_{(\theta)} = \frac{1}{\csc^4\frac{1}{2}\theta}\cdot\frac{1}{2\gamma}\int_{\theta-\gamma}^{\theta+\gamma}\csc^4\tfrac{1}{2}\theta d\theta. \tag{9}$$

The value of this function is plotted in Fig. 4.

E. The electronic scattering

The Mott formula, Eq. (1), expresses only the scattering of electrons by the nucleus. We shall now consider the effect which the atomic electrons may have upon the total observed scattering. Scattering by the atomic electrons should be of the order of $1/Z$ times as great as the nuclear scattering for smaller angles. For aluminum this amounts to a correction of several percent to be added to the nuclear scattering; for the remaining elements used, electronic scattering may be neglected. The formula of Mott[9] expressing the

[9] N. F. Mott, Proc. Roy. Soc. **A126**, 259 (1930).

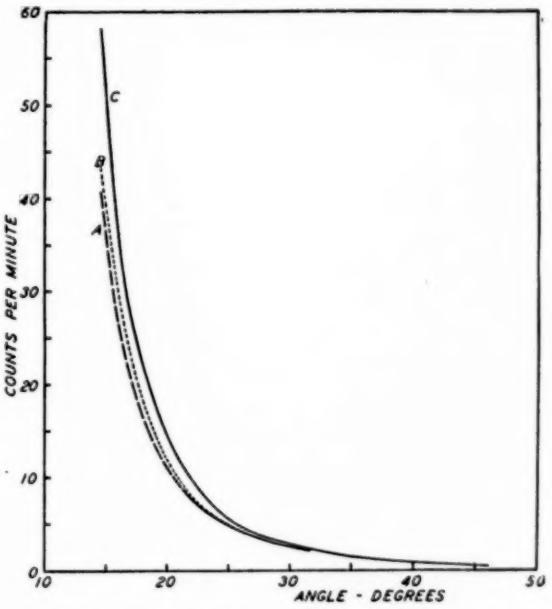

FIG. 5. Curve A is the theoretical scattering distribution, Eq. (7), for the thin set of Cu, Ag, and Au foils. Curve B shows the additional scattering by atomic electrons for a foil of Al. Curve C is 10 percent higher than curve B to indicate the increased scattering from Al for the thick set of foils (see Table I and Fig. 7).

scattering distribution for electrons scattered by electrons,

$$I_e(\theta) = \left(\frac{2e^2}{mc^2}\right)^2\frac{1-\beta^2}{\beta^4}\cos\theta\left[1+\tan^4\theta - \tan^2\theta\left(\cos\frac{\alpha}{\beta}\log\tan^2\theta\right)\right]\csc^4\theta \tag{10}$$

was used and an integration over energy performed as in the nuclear case. The situation here is somewhat more complicated than the nuclear case, since the fraction of the original energy retained by a scattered electron depends upon both the energy and the angle of scattering. Hence, the integration over energy must be carried out separately for each angle. As stated above, the electronic scattering was negligible for all metals except aluminum. The magnitude of the electronic scattering in the case of aluminum may be seen from Fig. 5. Except for aluminum Eq. (7) represents the theoretical scattering. For aluminum, the theoretical scattering is given by Eq. (7) plus the contribution of electronic scattering, as indicated in Fig. 5.

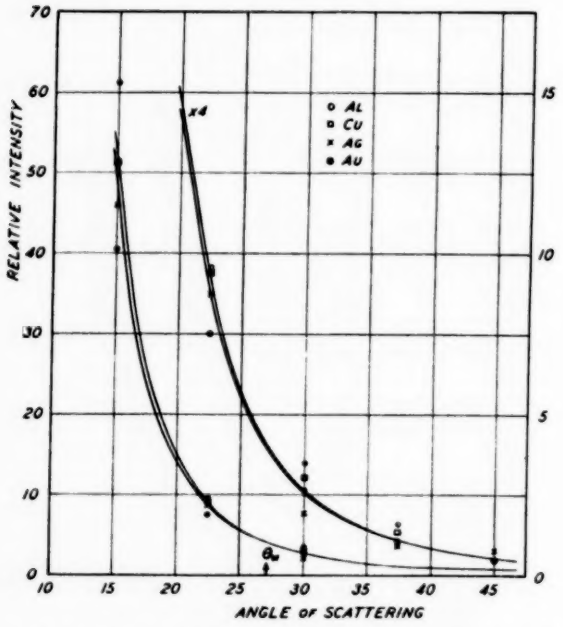

FIG. 6. Foils of set I for region of "single" scattering. The upper curve is the theoretical distribution of scattering for the Al foil, the lower that for the other foils. The Wentzel angle is shown by θ_w. The ordinates are in counts per minute. Right ordinate scale is for the $\times 4$ curves.

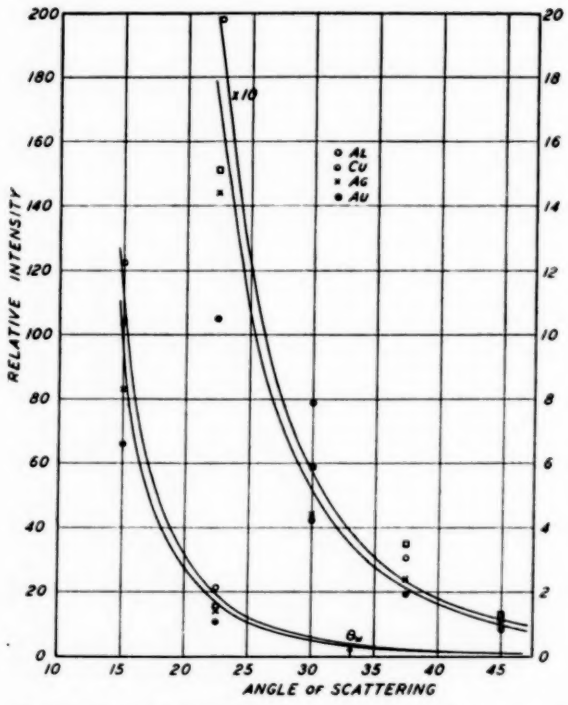

FIG. 7. Foils of set II for region of "single" scattering. Meaning of curves same as in Fig. 6. Right ordinate scale is for the $\times$ 10 curves.

IV. DISCUSSION OF RESULTS

The range for "single scattering" is at angles greater than the Wentzel angle (Figs. 6 and 7). It is evident that the agreement of the experimental points with the single scattering formula becomes progressively better as the angle of observation increases. The order of the points for the different values of Z is quite regular throughout the "single scattering" region, the points for aluminum falling consistently above the theoretical curve and those for gold falling somewhat below. The explanation for this behavior is to be found by a consideration of the effects of multiple scattering.

The region of multiple scattering near 0° is shown in Figs. 8 and 9. The results shown in these figures can be summarized by the statement that, for a constant scattering cross section (Z^2nt), the scattering becomes less multiple as the atomic number of the scattering substance increases. This accounts for the fact that the curve at 0° is highest for large Z, and in the multiple scattering range (but less than the Wentzel angle) is highest for small Z. This behavior was pointed out in the paper previously referred to,[2] in which a formula which approximated the actual calculations was given for the value of the scattering distribution curve at 0°, $f(0)$. According to this formula,

$$4\pi f(0) \sim 0.43/\mu[\log\xi + \tfrac{1}{2}\log\mu + 0.60], \quad (11)$$

in which the symbols have the same meaning as for Eq. (4), the ratio of the intensity at 0° for the first gold foil as compared to the first aluminum foil is 1.37 : 1, where $w = 1.7$ for the average energy as before. The experimental data for these two foils give for the same ratio 1.32/1. For the second set of foils, the gold to aluminum ratios are 1.46 and 2.05 for the theoretical and experimental, respectively.

Much more than a qualitative check with the multiple scattering theory mentioned above is not to be expected for several reasons. In the first place, the theory does not yield a dependable multiple scattering distribution curve when the scattering is too nearly single; the series do not converge rapidly enough. For this reason, and because of the fact that in this work a heterogeneous velocity beam was used, the multiple scattering distribution curve was not calculated.

The approximate formulas given above were fitted to actual calculations for multiple scattering cases for which the energy was considerably greater and the foils much thicker. To extrapolate the approximate formulas as was done above is thus doubly uncertain. We can obtain from the theory, nevertheless, a qualitative explanation of the behavior of the experimental curves in the region of multiple scattering; the scattering is more multiple for elements of small Z.

With this qualitative understanding of multiple scattering, we may now return to the discussion of single scattering. At the Wentzel angle the order of the points for the different values of Z is just reversed from that at 0°. The fact that the points for aluminum lie above the theoretical curve until 45° is reached indicates that multiple scattering carries over into the so-called single scattering range. This effect is less noticeable for copper and silver, and entirely absent for gold, which is in agreement with the conclusion pointed out earlier that the scattering is more multiple for small Z. The extent of the validity of the Wentzel criterion for single scattering is now more clear. For the conditions of this experiment, at least, the Wentzel criterion is seen to be inadequate for elements of small Z.

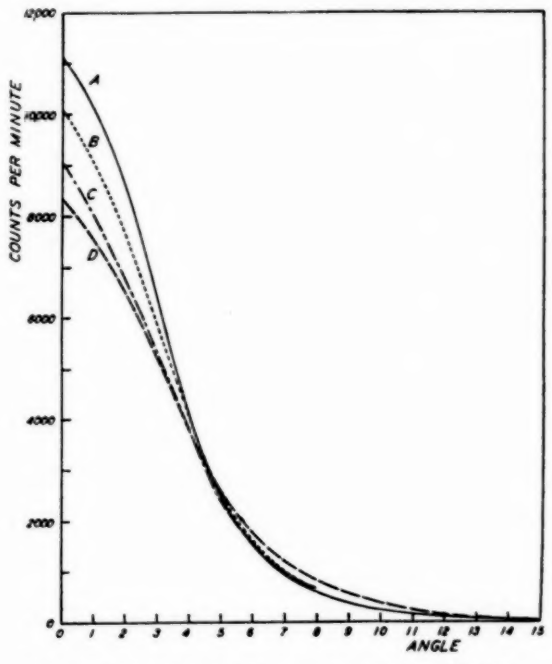

FIG. 8. Foils of set I for region of "multiple" scattering. Curve A is for Au, B for Ag, C for Cu, and D for Al.

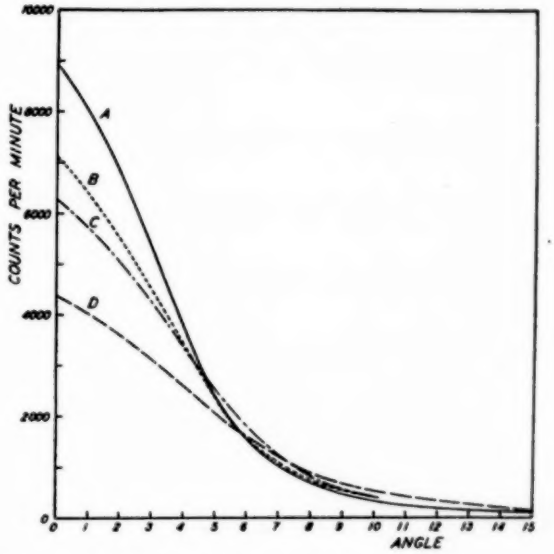

FIG. 9. Foils of set II for region of "multiple" scattering. Curves designated as in Fig. 8.

The fact that the points for large Z lie rather consistently below the theoretical curves may point to a small discrepancy in the absolute magnitude of the scattering for these elements, since multiple scattering present near the Wentzel angle should always increase the observed scattering. However, the rather large statistical fluctuations plus the various experimental errors (the foil thicknesses may be in error by as much as 10 percent) make any conclusion on this point dubious, and, in general, the check in absolute magnitude is considered satisfactory. The Wentzel criterion seems to be an adequate condition for the presence of predominantly single scattering for elements of large Z, but is too lenient for elements of small Z.

The authors are grateful to Professor Goudsmit for his interest in this work and for a great deal of help in interpreting the data. The radioactive material for this project was kindly furnished by Professor J. A. Bearden of the Johns Hopkins University, for which we acknowledge our thanks. This investigation was undertaken in connection with work supported by the Horace H. Rackham Fund.

Disintegration of Slow Mesotrons

FRANCO RASETTI
Department of Physics, Laval University, Quebec, Canada
(Received June 13, 1941)

The disintegration of mesotrons at the end of their range was investigated by means of an improved arrangement of the type already described by the author. The absorption of a mesotron by a block of aluminum or iron is recorded by a system of coincidence and anticoincidence counters. Another system of counters and circuits registers the delayed emission of a particle, which is interpreted as the disintegration electron associated with the absorbed mesotron. The present apparatus enables one to determine the time distribution of the emitted particles and hence the mean life of the decay process, independently of the effects produced by the scattering of mesotrons. The mean life is found to be 1.5 ± 0.3 microseconds, in substantial agreement with the value deduced from the atmospheric absorption effect. The absolute number of disintegration electrons per absorbed mesotron has also been determined (for an Al absorber) and found to be about one-half. This result suggests that, in agreement with theoretical predictions, positive mesotrons undergo spontaneous decay, while the negative ones react with nuclear particles.

1. INTRODUCTION

THE anomalous absorption of the hard component of cosmic rays in the atmosphere has received a satisfactory explanation through the assumption of the mesotron decay. Recent and more accurate experiments[1,2] have confirmed the hypothesis, which was at first based on rather doubtful experimental material, and given a fairly accurate evaluation of the proper lifetime of the free mesotron.

Nevertheless, there remains much to be learned about the process of mesotron disintegration. Since the mesotron is usually identified with the particle which, in the theory of Yukawa,[3] is responsible for the nuclear forces, it is assumed to transform, by a process of β-decay, into an electron and a neutrino. The electrons should, on the average, take up half of the energy of the disintegrating mesotrons. Whether the intensity of the electron component in the atmosphere is sufficiently high to agree with the measured lifetime of the mesotron, is a much discussed and still unsettled point.[4,5]

Even assuming that the process of disintegration of free mesotrons were completely known, there would remain the important point of determining what happens to the mesotrons that have been brought to the end of their range by ionization energy losses. According to the Yukawa theory, the mesotron possesses strong interactions with the heavy particles. The most important process for a slow (negative) mesotron would be an analog of the photoelectric effect,[6] by which the mesotron would disappear transferring its total energy to a bound proton which would be transformed into a neutron. A similar process could take place between a positive mesotron and a neutron.

Recent calculations by Tomonaga and Araki[7] seem to indicate that, owing to the Coulomb field of the nucleus, which attracts the negative mesotrons and repels the positive ones, the above-mentioned process should be much less probable than spontaneous decay for positive mesotrons. For negative mesotrons, on the contrary, nuclear interactions should be so probable that spontaneous decay of mesotrons at rest in dense materials should not take place.

Prior to the author's work, the only observation of mesotrons decaying at the end of their range were two cloud-chamber tracks photographed by Williams and Roberts.[8]

Preliminary reports[9] announced the observation of disintegration electrons by means of a counter arrangement and a rough measurement of the mean life. The present paper contains an

[1] B. Rossi and D. B. Hall, Phys. Rev. **59**, 223 (1941).
[2] W. M. Nielsen, C. M. Ryerson, L. W. Nordheim, and K. Z. Morgan, Phys. Rev. **59**, 547 (1941).
[3] H. Yukawa, Proc. Phys. Math. Soc. Japan **20**, 319 (1938).
[4] G. Bernardini, B. N. Cacciapuoti, B. Ferretti, O. Piccioni, and G. C. Wick, Phys. Rev. **58**, 1017 (1940).
[5] L. W. Nordheim, Phys. Rev. **59**, 554 (1941).
[6] H. Euler and H. Heisenberg, Ergeb. d. exakt. Naturwiss. **17**, 1 (1938).
[7] S. Tomonaga and G. Araki, Phys. Rev. **58**, 90 (1940).
[8] E. J. Williams and G. E. Roberts, Nature **145**, 102 (1940).
[9] F. Rasetti, Phys. Rev. **59**, 706, 613 (1941).

account of more complete and precise measurements, whose aim was not only to determine directly the mean life of the decay process, but also to attempt to settle the important point whether all slow mesotrons, or only half of them, undergo spontaneous disintegration.

2. Experimental Procedure

Counter arrangement

The principle adopted consists of selecting, by means of a coincidence-anticoincidence system of counters, the events in which a mesotron is stopped in an absorbing block (of iron or aluminum) and observing the delayed emission of an ionizing particle from the absorber. The delayed particle, detected by means of a suitable system of counters and circuits, is assumed to be the disintegration electron of the absorbed mesotron.

The general scheme of the counter set-up and of the recording circuits is illustrated in Fig. 1. Counters designated by the same letter are connected in parallel. Cross-marked counters are employed as anticoincidence counters or anticounters. The circles represent the effective cross sections of the counters.

The fourfold coincidence system ($ABCD$) defines a beam of mesotrons, the soft component of cosmic rays being filtered out by 15 cm of lead placed above and between the counters. Counters A, B, C, and D have an effective length of 22 cm. The anticounters F (effective length 52 cm) cover the whole solid angle subtended by the system ($ABCD$), so that anticoincidences ($ABCD-F$), when no absorber is present between D and F, are mostly due to lack of efficiency of the counters F. This number is found to be 1.5 percent of the number of coincidences ($ABCD$).

The absorber has a cross section of 2.5×10 cm^2 and a length of 40 cm. About 75 percent of the mesotrons defined by the coincidences ($ABCD$) traverse the absorber. The two anticounters in position G were added, in parallel with the others, to discriminate against mesotrons associated with showers.

The six counters E are placed in such a way that a particle emitted from the absorber has a fairly large probability of being detected by one of them. They have an effective length of 37 cm, and lie wholly outside of the solid angle defined by the system ($ABCD$), as is clearly indicated in Fig. 1.

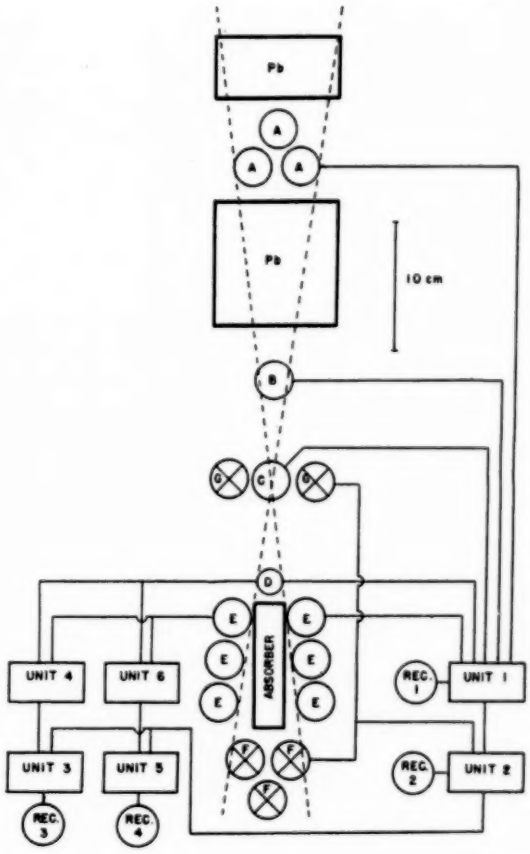

FIG. 1. Arrangement of counters, illustrating connections to amplifier units.

The inside diameter of all counters is 29 mm, except for counter D which has a diameter of 20 mm. The counters have a brass cathode and a 4-mil tungsten wire as anode. The electrodes are sealed in a glass tube filled with a mixture of commercial argon (5 cm Hg) and ethyl alcohol vapor (1 cm Hg). Extreme care was employed in selecting the counters, especially the critical ones of groups D and E, which are connected to the high resolving power amplifiers. The pulses were carefully studied on a cathode-ray oscilloscope, and no counter was accepted unless the pulses were all of equal size and of satisfactory shape. Most counters were found to answer the requirements, provided that the leak resistance was not lower than 10^8 ohms, and the coupling capacity not larger than 10 or 20 $\mu\mu$f. Such values of these

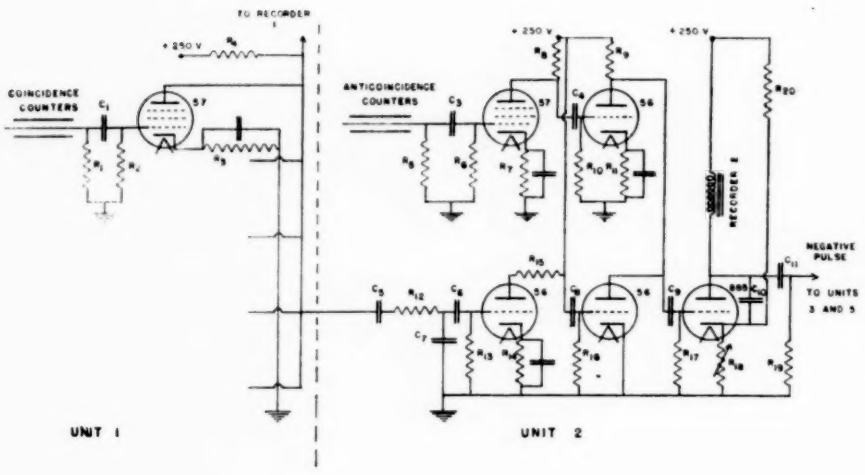

FIG. 2. Fivefold coincidence circuit (unit 1) and anticoincidence circuit (unit 2). Only one of the five Rossi tubes is shown. $R_1=R_5=10^8$; $R_2=R_6=R_8=500{,}000$; $R_3=5000$; $R_4=1$ Meg; $R_7=3000$; $R_9=7500$; $R_{10}=R_{13}=R_{16}=2$ Meg; $R_{11}=R_{19}=50{,}000$; $R_{12}=200{,}000$; $R_{14}=30{,}000$; $R_{15}=15{,}000$; $R_{17}=300{,}000$; $R_{18}=10{,}000$ adjustable; $R_{20}=25{,}000$; $C_1=0.00001$; $C_3=0.00005$; $C_4=0.03$; $C_5=0.0001$; $C_6=0.001$; $C_7=0.00003$; $C_8=C_9=0.001$; $C_{10}=0.1$; $C_{11}=0.0001$. Resistance in ohms, capacity in μf.

constants were actually employed (see Figs. 2 and 3).

The essential check of the counters, however, consisted in showing that they were practically 100 percent efficient in recording double coincidences when the resolving time of the circuit was as low as 5×10^{-7} sec. This check will be discussed in a later section.

The counters had a threshold voltage of about 900 volts and were operated at 1050 volts through a pentode-stabilized circuit. No replacement of any of the counters and no readjustment of the voltage were required during a series of measurements which extended over a period of five months. The size and shape of the pulses of each counter were checked on the cathode-ray oscilloscope at least once a week.

Circuits

The general scheme of the recording circuits has already been described,[9] except for the addition of the units 5 and 6 (Fig. 1) and may be briefly explained as follows. Counters A, B, C, D, and E are connected to a fivefold coincidence set (unit 1). The pulse from unit 1 is passed onto the anticoincidence unit 2, so that recorder 2 is operated only when a coincident discharge ($ABCDE$) is not associated with a discharge of F (this process will be designated by $(ABCDE-F)$). For instance, a mesotron which discharges counters A, B, C and D, is stopped by the absorber, and emits a disintegration electron which trips one of the counters E, will be registered by recorder 2. A scattered mesotron may produce the same effects.

The negative pulse from the plate of the thyratron which operates recorder 2 is passed onto both the double coincidence units 3 and 5. Each one of these operates a recorder (recorders 3 and 4) only when a coincident pulse (within about 10^{-4} sec.) is transmitted to it by, respectively, unit 4 or 6. These are two double coincidence sets of short resolving time, both connected to counters D and E.

Thus, recorder 2 registers a process $(ABCDE-F)$, recorders 3 and 4 each a process which we may designate by $\{(ABCDE-F)(DE)\}$. Were all coincidences between counters produced by the same particle, or by particles associated in a practically instantaneous process (such as a shower), the numbers of events n_2, n_3, and n_4 registered, respectively, by recorders 2, 3, and 4 would be exactly equal. However, delayed processes such as the disintegration of a mesotron may give a fivefold coincidence ($ABCDE$) on unit 1 which is not recorded as a double coincidence (DE) on unit 6, or on both units 4 and 6, on account of their shorter resolving time.

The essentials of units 1, 2, 4, and 6 are illustrated in Figs. 2 and 3. Unit 1 is a conventional Rossi fivefold coincidence set. Its output pulse may be fed to a thyratron operating recorder 1, besides being passed onto the anticoincidence unit 2. The anticoincidence circuit does not embody any novel features, but since it proved to be simple and 100 percent efficient, its diagram

is given in Fig. 2. The capacity-resistance circuit $R_{12}-C_7$ delays the positive pulse from unit 1. The pulse from the anticounters is longer and after two stages of amplification has a square form, amply covering the time interval occupied by the coincidence pulse.

The short resolving time units 4 and 6 are three-stage double coincidence amplifiers, the Rossi tubes constituting the third stage, and comprise a type 885 thyratron which transmits a negative pulse to, respectively, unit 3 or 5 (Fig. 3). All coupling resistances, of course, are low, and capacities small, to insure selective amplification of the high frequency components of the pulse and make the resolving time short. The two units differ only in the value of the coupling capacity C_2 and in the bias of the thyratron cathode, which is determined by the adjustable resistance R_{13}.

All leads from the counters to the amplifiers are provided with low capacity shielding.

The two double coincidence units 3 and 5 are conventional Rossi circuits and do not need description.

Measurement of resolving time

The procedure employed was the usual one of counting the number n of random coincidences when the counters were operated at high counting rates, N_1 and N_2, measured by means of a vacuum tube scaling circuit. At counting rates of several thousands per minute (as are necessary if random coincidences are to be recorded in sufficient number by a circuit having a resolving time of the order of one microsecond), a fraction of the pulses has a size smaller than normal, due to the slow recovery of the voltage across the counter after a discharge. This led to an investigation of the dependence of resolving time upon counting rate and pulse size.

All other counters being left in their normal position, counter D was displaced at a considerable distance from group E, without in the least changing the length of the leads, stray capacities, or other factors which may affect the resolving time. Counter D was also shielded by 20 cm lead. Under such conditions, the rate of systematic coincidences (DE) was only 2.0 ± 0.3 per hour. Counters D and E were then irradiated with weak radioactive sources, and the number of random coincidences (DE) was simultaneously registered on the three units 1, 4 and 6. For this measurement, the circuits were employed in exactly the same way as in the actual experiments, except for unit 1, which is here used only as a double coincidence circuit. However, the exact knowledge of its resolving time is not required for the evaluation of the final experiments.

Table I contains the results on the dependence of resolving time upon counter voltage (which affects the pulse size) and upon counting rate. The resolving time (respectively t_2, t_3 and, t_4 for units 1, 4, and 6) was calculated from the usual formula $t=n/2N_1N_2$.

The result is that the resolving time does not appreciably change within the range of voltage and counting rate investigated. Since the pulses at high counting rates ($2N_1N_2=4900$ sec.$^{-2}$) have the same average size at 1065 volts as they have at background rate and 1035 volts, it seems reasonable to assume that the resolving times measured are valid for the conditions under which the counters were actually employed in the experiments.

The measurements reported in Table I were performed before the beginning of the runs. At the end of the run with an iron absorber, another determination (at 1050 volts) gave: $t_2=14.7\pm0.3$; $t_3=2.08\pm0.1$; $t_4=0.85\pm0.07$. At the end of the run with an aluminum absorber the values found were: $t_2=14.0\pm0.2$; $t_3=1.92\pm0.1$; $t_4=0.66\pm0.04$. The figures indicate that the resolving times t_2 and t_3 remained practically constant,

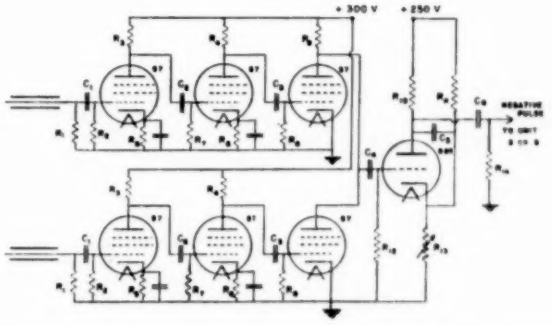

FIG 3. High resolving power double coincidence circuits (unit 4 or 6). $R_1=10^6$; $R_2=R_3=R_4=R_7=R_8=50{,}000$; $R_5=R_6=10{,}000$; $R_9=150{,}000$; $R_{10}=5{,}000$; $R_{11}=25{,}000$; $R_{12}=300{,}000$; $R_{13}=10{,}000$ adjustable; $R_{14}=50{,}000$; $C_1=0.00001$; $C_2=0.00001$ in unit 4, $=0.00005$ in unit 6; $C_3=0.00005$; $C_4=C_6=0.0001$; $C_5=0.1$. Resistance in ohms, capacity in μf.

TABLE I. *Resolving time of three double coincidence circuits.*

NUMBER OF HOURS	VOLTAGE ON COUNTERS	$2N_4N_2$ SEC.$^{-2}$	RANDOM COINCIDENCES IN SEC.$^{-1}\times10^3$	t MICRO-SECONDS
		Unit 1		
14.4	1065	4900	77 ±2	15.7 ±0.3
23.1	1065	4730	72 ±1	15.2 ±0.2
23.2	1035	4625	68 ±1	14.7 ±0.2
23.3	1035	1350	20.3±0.5	15.0 ±0.3
		Unit 4		
23.1	1065	4730	8.6±0.3	1.81±0.07
23.2	1035	4625	8.9±0.3	1.93±0.07
23.3	1035	1350	2.5±0.15	1.88±0.12
		Unit 6		
14.4	1065	4900	4.9±0.3	1.00±0.06
23.1	1065	4730	4.2±0.2	0.90±0.05
23.2	1035	4625	4.6±0.2	0.99±0.05
23.3	1035	1350	1.3±0.15	0.97±0.12

whereas the value of t_4 evidently decreased throughout the series of experiments. This variation is not surprising, as the characteristics of the tubes may have changed to some extent through more than 3000 hours of uninterrupted service. We shall use the following values of the resolving times (in microseconds):

$t_2=15$
$t_3=1.95$
$t_4=0.95$ for the Fe measurements
$t_4=0.76$ for the Al measurements.

Efficiency of the high resolving power circuits

The results of the present experiment are significant only if it has been ascertained that all truly coincident discharges (e.g., those produced by a single cosmic-ray particle) are registered by all three recorders 2, 3, and 4.

A simple procedure to check this point is the following. In unit 1, the Rossi tubes connected to counters A, B and C are disconnected, so that recorder 2 now counts processes of the type $(DE-F)$ at the rate of 900 per hour. All the rest of the circuit is left as in the actual experiment. Thus, recorders 3 and 4 each register the process $\{(DE-F)(DE)\}$.

If random coincidences (DE) are neglected, all recorders should register the same number of counts. Actually, recorders 3 and 4 were observed to lag behind recorder 2 at the rate of about 5 per hour (0.5 percent of the counts, against 15 to 25 percent in the actual experiments), which is the theoretical rate of random coincidences (DE) recorded by circuit 1. Hence, we may safely assume that the circuits 4 and 6 do not miss any systematic coincident discharges. An experiment performed with a resolving time of 0.5 microsecond still showed full efficiency in coincidence recording.

The check described above was repeated every day, at least for a few minutes. During the whole series of the final experiments reported in the next section (over a period of three months) the apparatus functioned uninterruptedly, without requiring the slightest readjustment or replacement. All circuits were fed through a Raytheon voltage stabilizer.

3. RESULTS AND DISCUSSION

Measurement of the mean life

In order to measure the distribution in time of the particles emitted from the absorber, the number n_2 of $(ABCDE-F)$ processes was counted on recorder 2, and simultaneously the numbers n_3, n_4 of processes $\{(ABCDE-F)(DE)\}$, respectively, on recorder 3 and 4. Iron and aluminum were used as absorbers. Blank runs without absorber were interpolated.

The results are summarized in Table II.

The mean life τ of the disintegration process is calculated from the differences of the numbers of counts, according to the formula:

$$\exp\left(-\frac{t_3-t_4}{\tau}\right)=\frac{n_2-n_3}{n_2-n_4}$$

and hence the result is not affected by instantaneous processes (such as the scattering of mesotrons) which contribute the same number of counts on the three recorders.

The small effect observed without absorber was not subtracted, since it is considerably larger than the expected random coincidence rate, and hence probably results from mesotrons disintegrating in the counter walls or in the support of the absorber, which, together, represent a thickness of about 4 g/cm^2 between counters D and F.

It is interesting to note that the presence of the Fe or Al absorber increased the counting rate n_2 by, respectively, 0.45±0.05 and 0.30 ±0.05 per hour. Now, from the difference

n_2-n_4 and from $\tau=1.5$ microseconds, we find for the total number of mesotron disintegrations which should be recorded between $t=0$ and $t=\infty$ the respective rate:

Fe	0.35 ± 0.07
Al	0.20 ± 0.06.

Since these rates are not considerably lower than the ones observed, we may conclude that, even with Fe, most of the additional processes $(ABCDE-F)$ produced by the absorber are due to disintegrations and not to scattered mesotrons. Experiments with a Pb absorber seem to indicate that this is not the case for such a heavy element.

In conclusion, the mean life of the disintegration process is about 1.5 microseconds, no significant difference being observed between the experiments with Al and Fe.

Number of disintegration electrons

To measure the absolute number of disintegration electrons, one must know: (a), the number of absorbed mesotrons; (b), the number of recorded disintegration electrons; (c), the probability that a disintegration electron will be recorded by the counters.

The absorption of disintegration electrons in iron would be exceedingly difficult to evaluate theoretically under the geometrical conditions prevailing in the experiments, and hence the measurements with an iron absorber are practically useless for the present purpose.

In aluminum, however, the range of the electrons should[10] be about 6 cm if their energy is 40 Mev. Therefore, absorption should have little effect on the number of electrons that reach the counters, and the probability of detection can be roughly evaluated from purely geometrical factors. In the present case it also seems reasonable to assume that most of the anticoincidences produced by the absorber are due to stopped rather than to scattered mesotrons.

The number of mesotrons absorbed by the aluminum was directly determined by counting the anticoincidences $(ABCD-F)$ with and without absorber. The results are summarized in Table III.

The geometrical probability for an electron to hit one of the counters E was evaluated graphically as 0.56. The effect of absorption should not be large, considering that the thickness of the absorber (2.5 cm) is much less than the average range of the electrons. We may, therefore, estimate the probability of detection of a disintegration electron as, roughly, 0.5.

By using this factor, we conclude that the counters E should record 0.48 ± 0.08 electron per hour, on the assumption that there is an electron for each absorbed mesotron. The actual rate recorded (extrapolated at the time zero) is only 0.20 ± 0.06 per hour. This gives as the number of disintegration electrons per mesotron 0.42 ± 0.15.

TABLE II. *Distribution in time of mesotron disintegrations.*

ABSORBER	HR.	n_2	n_3	n_4	n_2-n_4	n_2-n_3	τ MICROSEC.
None	311	106	102	102	4 ± 2	4 ± 2	—
10 cm Fe	602	473	417	360	113 ± 11	56 ± 8	1.4 ± 0.3
10 cm Al	514	331	301	268	63 ± 8	30 ± 6	1.6 ± 0.4

TABLE III. *Absorption of mesotrons in aluminum.*

ABSORBER	HOURS	ANTI-COINCIDENCES	ANTI-COINCIDENCES PER HOUR	DIFFERENCE
None	175	258 ± 16	1.48 ± 0.09	0.97 ± 0.15
10 cm Al	175	428 ± 21	2.45 ± 0.12	

Interpretation of results

The value obtained for the mean life of slow mesotrons in dense materials agrees, as satisfactorily as can be expected from the accuracy of the measurements, with the proper lifetime of fast mesotrons in the atmosphere. Actually, our value is lower than the one found by Rossi and Hall,[1] but higher than that reported by the Duke University group.[2]

The proper lifetime for fast mesotrons is deduced from the measurement of the disintegration probability per unit length of path

$$w=\mu/p\tau,$$

p being the momentum and μ the mass of the mesotron. It is gratifying to find that two so widely different methods have yielded consistent

[10] H. Bethe and W. Heitler, Proc. Roy. Soc. **A146**, 83 (1934).

results. This agreement, and the substantially equal values for the mean life measured in Al and Fe, render it plausible to assume that these values represent the mean life for spontaneous decay.

The present experiments seem to indicate a number of disintegration electrons per mesotron definitely smaller than unity. The statistical error is certainly large, and systematic errors are not to be excluded, although it seems rather unlikely that they might be large enough to account for a discrepancy by more than a factor two.

The results, however, are in agreement with the assumption that only half of the mesotrons undergo free decay. Since the analysis of mesotron tracks in a magnetic field has shown that there are about as many positive as negative mesotrons, or a small excess of positive,[11] the result found is what should be expected if only mesotrons of one sign (positive) undergo free decay. Actually, if, according to the calculations of Tomonaga and Araki, reactions with nuclear particles are much more probable than spontaneous disintegration for negative mesotrons, then we should only record an electron for each positive mesotron absorbed. The nuclear reactions produced by negative mesotrons will probably lead to excited states of nuclei and eventually give rise to electrons through processes of β-decay. It is exceedingly unlikely, however, that such particles could be emitted with sufficient energy and within a sufficiently short time to be registered in the present experiments.

[11] See H. Jones, Rev. Mod. Phys. **11**, 235 (1939), also for earlier literature.

AUGUST 1, 1941 PHYSICAL REVIEW VOLUME 60

Theory of Nuclear Surface Energy

EUGENE FEENBERG
Department of Physics, New York University, Washington Square College, New York, New York
(Received May 26, 1941)

The eigenvalues of a free particle in a spherical potential well of finite depth are computed and used to calculate the surface energy of nuclear systems. No assumptions are made concerning the specifically nuclear forces. For depth and radius $56mc^2$ and $\frac{1}{2}A^{\frac{1}{3}}e^2/mc^2$, respectively, the computed surface energy is about two-thirds the empirical value. A well of infinite depth yields a surface energy more than double the empirical value. One-dimensional and cubical wells are discussed for the purpose of orientation.

INTRODUCTION

THE empirical packing fraction curve[1] and the phenomenon of fission[2] require the existence of a nuclear surface energy having the magnitude $26A^{\frac{2}{3}}mc^2$ within limits of perhaps ± 10 percent. There exists no adequate theoretical calculation of this quantity, although estimates have been obtained by Weizsäcker[3] and Bethe.[4] A complete theoretical discussion is not possible without the use of special assumptions about the nuclear forces, but it is clear without calculation that the specifically nuclear forces must make a positive contribution to the surface energy. If γ is written for the coefficient of $A^{\frac{2}{3}}$ in the semi-empirical formula for nuclear energies, and γ_K, γ_P for the contributions from the kinetic and potential energy operators, respectively, these remarks may be summarized in the relations

$$\gamma=\gamma_K+\gamma_P\sim 26mc^2, \quad \gamma_K<26mc^2. \qquad (1)$$

The difficulties and uncertainties barring a theoretical determination of γ_P are not present to the same degree for γ_K. It is, therefore, desirable to obtain a first approximation for γ_K

[1] A. J. Dempster, Phys. Rev. **53**, 869 (1938).
[2] N. Bohr and J. A. Wheeler, Phys. Rev. **56**, 426 (1939).
[3] C. F. v. Weizsäcker, Zeits. f. Physik **96**, 431 (1935).
[4] H. A. Bethe and R. F. Bacher, Rev. Mod. Phys. **8**, 82 (1936).

before attempting to estimate γ_P. This is done in the last section with the model of free particles in a spherical potential well of depth D and radius R. For the purpose of orientation, one-dimensional and cubical wells are also studied.

The free-particle model is useful chiefly for the calculation of the kinetic and Coulomb energies, quantities which do not depend sensitively on the exact form of the short range correlations between the positions of the heavy particles. These calculations as customarily made involve two approximations: (a) the correct single particle eigenfunctions are replaced by plane waves which vanish abruptly at the boundary of the well and (b) sums over the occupied energy levels are replaced by integrals in momentum space. For the kinetic energy one obtains

$$E_K=\frac{3}{40}\left(\frac{3}{\pi}\right)^{2/3}\frac{h^2}{M}V^{-\frac{1}{3}}\{(N/V)^{5/3}+(Z/V)^{5/3}\}$$

$$\cong 28.64A\left\{1+\frac{5}{9}\left(\frac{N-Z}{A}\right)^2\right\}(R_0/R)^2mc^2, \quad (2)$$

where V is the volume of the sphere and $R_0=\frac{1}{2}A^{\frac{1}{3}}e^2/mc^2$. The absence of a surface term in Eq. (2) is characteristic, not of the free-particle model, but of the simplifying assumptions (a) and (b).

One-Dimensional Well of Infinite Depth

The vanishing of the single particle wave functions at $x=0$ and $x=L$ determines the eigenvalues

$$\epsilon_n=h^2n^2/8ML^2, \quad n=1, 2, 3, \cdots. \quad (3)$$

With one particle per orbit, and a total of μ particles, the kinetic energy of the degenerate gas is

$$E=(h^2/8ML^2)\textstyle\sum_1^\mu n^2=(h^2/24M)$$
$$\times\{L(\mu/L)^3+\frac{3}{2}(\mu/L)^2+(1/2L)(\mu/L)\}. \quad (4)$$

If the breadth of the well is assumed proportional to the number of particles, the first term in brackets may be interpreted as the "line" energy and the second and constant term as the "end" energy. The third term has no simple geometrical interpretation and vanishes for infinite L.

One-Dimensional Well of Depth D

The results are stated only for a well of sufficient depth to satisfy the inequality

$$(h^2/8ML^2)\mu^2<\tfrac{1}{3}D \quad \text{with} \quad \mu\gg 1.$$

Under this restriction the effect of raising the bottom of the well is to subject the occupied levels to a uniform compression. The eigenvalues are

$$\epsilon_n=-D+(h^2n^2/8ML^2)\{1-(2h^2/\pi^2MDL^2)^{\frac{1}{2}}\} \quad (5)$$

yielding the total energy

$$E=-\mu D+(h^2/24M)\{L(\mu/L)^3$$
$$+\tfrac{3}{2}(\mu/L)^2[1-(8\mu^2h^2/9\pi^2MDL^2)^{\frac{1}{2}}]+O(1/L)\}. \quad (6)$$

Thus the "line" energy is unaffected by putting a bottom on the well, while the "end" energy is reduced by the factor

$$1-(8\mu^2h^2/9\pi^2MDL^2)^{\frac{1}{2}}.$$

The artificial boundary condition that the phase of the wave function have the value $\frac{1}{4}\pi$ at $x=0$ and $\pm\frac{1}{4}\pi$ at $x=L$ determines eigenvalues

$$\epsilon_n=(h^2/8ML^2)(n-\tfrac{1}{2})^2, \quad n=1, 2, 3, \cdots. \quad (7)$$

In this case there is no "end" term in the expression for the energy of a completely degenerate gas. We note that for a well of finite depth the phases $\pm\frac{1}{4}\pi$ at the boundaries correspond to $\epsilon_n\sim\frac{1}{2}D$.

Cubical Well of Infinite Depth

The eigenvalues are

$$\epsilon_{lmn}=(h^2/8ML^2)(l^2+m^2+n^2), \quad l, m, n=1, 2, 3, \cdots. \quad (8)$$

To calculate the kinetic energy of a degenerate gas we should sum ϵ_{lmn} over all the points of lmn space included in an octant of a sphere. The calculations are greatly simplified without materially altering the results if instead of summing over an octant of a sphere we sum over a cube. With two

TABLE I. *Average energy per particle (mc^2 units).*

A	4	16	40	68	80	116	136	180	212	264	276
Table II	80.6	56.9	48.4	44.9	44.0	41.6	41.4	39.7	39.5	38.2	38.0
Eq. (12)	79.8	57.0	48.3	44.6	43.6	41.7	40.9	39.7	39.0	38.2	38.1

particles in each orbit, and N particles altogether, this procedure yields

$$\begin{aligned} E_N &= (3h^2/4ML^2)\{\tfrac{1}{3}(N/2)+\tfrac{1}{2}(N/2)^{\frac{2}{3}}+\tfrac{1}{6}(N/2)^{\frac{1}{3}}\}(N/2)^{\frac{2}{3}} \\ &= (h^2/2^{11/3}M)\{V(N/V)^{5/3}+2^{-5/3}S(N/V)^{4/3}+2^{-1/3}L(N/V)\}, \end{aligned} \tag{9}$$

where V and S are written for the volume and surface area, respectively, of the cube. If the volume is proportional to the number of particles, Eq. (9) represents a sum of volume, surface and edge energies. The absence of a constant term which might be interpreted as a "corner" energy indicates that the geometrical identifications must not be taken too literally.

Comparison of Eq. (9) with Eq. (2) shows that the coefficient of the volume energy is 8 percent too large because of the approximation involved in summing over a cubical region in the quantum number space. Correcting this discrepancy and interpreting V and S as the volume and surface area, respectively, of a sphere of radius R we find

$$E_K = E_N + E_Z = 28.64A\left[1+\frac{5}{9}\left(\frac{N-Z}{A}\right)^2+\frac{1.92}{A^{\frac{1}{3}}}\left\{1+\frac{2}{9}\left(\frac{N-Z}{A}\right)^2\right\}+\frac{1.26}{A^{\frac{2}{3}}}\right](R_0/R)^2mc^2. \tag{10}$$

The surface energy given by this crude calculation is about double the empirical value. The significance of the last term in brackets is very uncertain, but it is retained because a similar term is found necessary to fit the exact energies of a spherical well of infinite depth.

SPHERICAL WELL OF INFINITE DEPTH

The eigenvalues are determined by the equation

$$J_{l+\frac{1}{2}}(kR)=0, \quad k=2\pi(2M\epsilon/h^2)^{\frac{1}{2}}, \tag{11}$$

where $J_{l+\frac{1}{2}}$ is a Bessel function of half-integral order. Values of kR/π are listed in the last section of Table II. A table of values of $(kR)^2$ is given by Margenau.[5] The numerical results for the average energy per particle follow closely the law

$$E_K/A = 28.64\left[1+\frac{5}{9}\left(\frac{N-Z}{A}\right)^2+\frac{1.92}{A^{\frac{1}{3}}}\left\{1+\frac{2}{9}\left(\frac{N-Z}{A}\right)^2\right\}+\frac{1.45}{A^{\frac{2}{3}}}\right](R_0/R)^2mc^2. \tag{12}$$

Table I shows how the computed values compare with Eq. (12) for the radius $R=R_0=\frac{1}{2}A^{\frac{1}{3}}e^2/mc^2$ and $N=Z$.

SPHERICAL WELL OF FINITE DEPTH

Calculations have been made for depths and radii defined by the equations

$$D=56mc^2/\eta^2, \quad R=\eta R_0/\lambda, \tag{13}$$

with $\lambda=1.05$, 1.00, 0.95 and 0.90. No restriction is required on η. Tables of Bessel functions computed by the W.P.A. Mathematical Tables Project greatly facilitated the numerical work. Margenau's[5] form of the equation expressing the continuity of the logarithmic derivative of the wave function was found convenient for use in connection with the W.P.A. tables. Some results for $\lambda=\eta=1$ are exhibited in Table II. All values are uncertain in the third decimal place.

[5] H. Margenau, Phys. Rev. **46**, 613 (1934).

TABLE II. *Values of* $kR/\pi=[8M(D+\epsilon)/\hbar^2]^{\frac{1}{2}}R$, $\lambda=\eta=1$.

A	$(8MD/\hbar^2)^{\frac{1}{2}}R$	$l=0$	$l=1$	$l=2$	$l=3$	$l=4$	$l=5$	$l=6$
4	0.832	0.689						
16	1.320	0.794	1.118					
40	1.792	0.844 1.635	1.200	1.526				
68	2.138	0.867 1.706	1.237 2.057	1.579	1.901			
80	2.257	0.873 1.724	1.245 2.089	1.591	1.919	2.232		
116	2.555	0.887 1.758	1.267 2.145	1.620 2.489	1.958	2.283		
136	2.694	0.893 1.771	1.274 2.164	1.631 2.523	1.972	2.301	2.623	
180	2.958	0.901 1.793 2.649	1.288 2.195	1.649 2.568	1.995 2.913	2.331	2.657	
212	3.124	0.907 1.804 2.673	1.296 2.210	1.659 2.589	2.007 2.945	2.346	2.676	3.004
264	3.361	0.912 1.817 2.702	1.304 2.229 3.100	1.671 2.615	2.023 2.980	2.365	2.700	3.030
276	3.411	0.914 1.821 2.708	1.307 2.233 3.108	1.673 2.620	2.026 2.988	2.369	2.704	3.033
	∞*	1.000 2.000 3.000 4.000	1.430 2.459 3.471 4.475	1.835 2.895 3.922	2.224 3.314	2.605	2.978	3.342

* Here $kR=(8\pi^2M\epsilon/\hbar^2)^{\frac{1}{2}}R$ with ϵ the kinetic energy measured from the bottom of the well.

Table III shows the average energy per particle, measured from the bottom of the well, as a function of λ and A when $N=Z$ and $\eta=\lambda$. The generalization from $\eta=\lambda$ to arbitrary values of η follows in an obvious manner from the invariance of the quantity $RD^{\frac{1}{2}}$ under changes in η. The numerical results in Table III follow

TABLE III. *Values of* $(E+ADmc^2)/Amc^2$ *for* $N=Z$, $\eta=\lambda$.

A	$\lambda=0.90$	$\lambda=0.95$	$\lambda=1.00$	$\lambda=1.05$
4	41.1	39.5	38.3	37.1
16	36.8	35.7	34.6	33.4
40	35.1	34.4	33.6	32.8
68	34.2	33.7	33.1	32.4[b]
80	33.9[b]	33.3	32.7	32.1
116	33.1	32.7	32.2	31.6
136	33.3	32.7[b]	32.2[b]	31.7
180	32.6	32.2	31.8	31.3
212	32.6[b]	32.3	31.8	31.4
264	—	—	31.4	—
276	—	—	31.3	—

closely the formula

$$E=[28.64A+\{17.8+50(1-\lambda)\}A^{\frac{2}{3}}]\times(\lambda/\eta)^2mc^2-AD. \quad (14)$$

From Eq. (14) we obtain

$$\gamma_K=(R_0/R)^2\times[17.8+50\{1-(56mc^2/D)^{\frac{1}{2}}R_0/R\}]mc^2, \quad (15)$$

in agreement with the inequality (1) for reasonable values of λ and η. Depths greater than $86mc^2$ are excluded by the inequality. The use of Eqs. (14) and (15) for values of A which do not correspond to completely filled shells implies the reasonable assumption that discontinuities in the energy due to shell effects are, to a large extent, smoothed out in actual nuclear systems. Because of the restriction of the numerical work to completely filled shells, it was not found possible to determine the dependence of energy on $N-Z$. The calculation of such second-order terms must await the development of a satisfactory method of smoothing out shell effects.

Studies of the Afterglow in Mercury Vapor

I. Intensity Pressure Relations‡

ROBERT C. GARTH* AND GEORGE E. MOORE†
Columbia University, New York, New York

(Received June 12, 1941)

The intensities of the stronger lines in the subordinate series of the afterglow spectrum of mercury were measured by photographic methods as a function of vapor pressure from 0.1 mm to 2.0 mm Hg in a stream of vapor distilled from a mercury arc into a side tube. Measurements made with the ion concentration held constant at the point of observation showed that increasing the pressure not only greatly increased the intensity of a given line but also caused a marked change in the intensity distribution in a given series. At constant pressure the intensities varied approximately linearly with ion concentration. The introduction of fast electrons into the stream quenched the line spectrum of the afterglow. Quenching also resulted from the removal of positive ions. The results indicate that the line spectrum of the afterglow is produced by a complex recombination process in which collisions with neutral atoms are important, probably resulting in the formation of molecular particles which later break up to produce the excited atoms responsible for the spectrum. Diffuse bands, attributable to molecules each composed of a neutral atom and an atom in one of the $6^3P_{0,1,2}$ states, were observed under certain conditions.

INTRODUCTION

THE afterglow in mercury vapor has been extensively studied[1] and it has been assumed that it is associated with the disappearance from the vapor of ions and electrons in some type of "recombination" process. The afterglow consists of a line spectrum and continua associated with the series limits, and under certain conditions includes also diffuse bands. The fact that the line spectrum of the afterglow is characterized by much greater values of the ratios of the intensities of the higher members of the spectral series to the intensities of the lower members than are observed in the normal arc spectrum, and the fact that in vapor emitting only the afterglow the electron temperatures are usually comparatively low[2] (about 1500°K or less), so that there is little probability of new excitation by electron impact, give support to the assumption that the afterglow line spectrum is a "recombination spectrum." There is, however, strong evidence that the recombination process is much more complex than the direct union of a positive ion and an electron with no third body involved, which latter process we shall refer to as "ion-electron recombination."[3]

The coefficient of ion-electron recombination, α, has been defined for a plasma ($n_+ \approx n_- = n$) by the equation, $dn/dt = -\alpha n^2$. In the theory of such recombination[4] α varies inversely as the square root of the electron temperature and is practically independent of the vapor or gas pressure, except so far as this may affect the electron temperature. Mohler and Boeckner[5] made a quantitative study of the continua emitted by a cesium discharge, and found that the intensity distribution depended upon the electron temperature in a manner agreeing well with this theory. Using purely electrical methods Mohler[6] later studied the rate of disappearance of electrons in the afterglow of cesium at 0.03 mm pressure. From these measurements the value of α for cesium was

* Now at Brooklyn College.
† Now at Bell Telephone Laboratories.
‡ Publication assisted by the Ernest Kempton Adams Fund for Physical Research of Columbia University.

[1] J. Stark, Ann. d. Physik **14**, 520 (1904); R. J. Strutt, Proc. Roy. Soc. **A91**, 92 (1914); Rayleigh, Proc. Roy. Soc. **A108**, 262 (1925); **114**, 620 (1927); L. J. Hayner, Zeits. f. Physik **35**, 365 (1926); H. W. Webb and D. Sinclair, Phys. Rev. **37**, 182 (1931).

[2] R. H. Randall and H. W. Webb, Phys. Rev. **48**, 544 (1935).

[3] L. B. Loeb, *Fundamental Processes of Electrical Discharge in Gases* (John Wiley and Sons, New York, 1939), p. 87; F. L. Mohler, Bur. Stand. J. Research **10**, 771 (1933); (Mohler refers to this process as "spontaneous recombination").

[4] R. Seeliger, Physik. Zeits. **30**, 329 (1929).

[5] F. L. Mohler and C. Boeckner, Bur. Stand. J. Research **2**, 489 (1929).

[6] F. L. Mohler, J. Research Nat. Bur. Stand. **19**, 447 (1937).

computed to be 3.4×10^{-10}. Similar measurements in the afterglow of mercury[7] at 0.27 mm pressure gave 2.3×10^{-10} as the value of α for mercury. Mohler pointed out that the coefficients which he measured are not necessarily to be regarded as coefficients of ion-electron recombination, and that in cesium pressures as low as 0.01 mm could enhance the probability of capture of an electron by an ion.

Rayleigh[1] has shown that the line spectrum of the afterglow of mercury can be extinguished, or "quenched," by applying potentials to electrodes which remove positively charged particles from the vapor. These auxiliary electrodes were located in a stream of mercury vapor which had passed through a region in which there was a strong arc discharge. The diffuse band spectra were only indirectly affected by this treatment. Webb and Sinclair[1] investigated in considerable detail the quenching process in which positive potentials were applied to a gauze electrode placed across the stream in a tube similar to that used by Rayleigh. They concluded that this type of quenching resulted from increasing the concentration of fast electrons, and since the quenching was much greater than was to be expected from the change in the coefficient of ion-electron recombination with an increase of electron temperature they further concluded that the afterglow is not due to ion-electron recombination. They also found that the intensity of the afterglow increased linearly with ion concentration and rapidly with the pressure.

In the investigations to be described in the present paper (I) and in a second paper by the same authors (to be referred to as II) some of the conditions affecting the afterglow have been further studied. In this paper the effect on the intensity of varying the vapor pressure and the ion concentration was investigated. Since the primary object of the study was to determine how the intensity of the lines in the afterglow depended upon pressure, and whether such dependence was consistent with the assumption that the afterglow is the result of ion-electron recombination, the results will be first stated from that point of view. Further observations on the quenching phenomena, on the rate of disappearance of ions and on the diffuse band spectra, which appeared in the afterglow at high pressure and with low ion concentrations, will also be presented. In II studies of the spectral intensity distribution of the afterglow and of its absolute intensity will be described, and the source of the afterglow discussed.

[7] F. L. Mohler, J. Research Nat. Bur. Stand. **19**, 559 (1937).

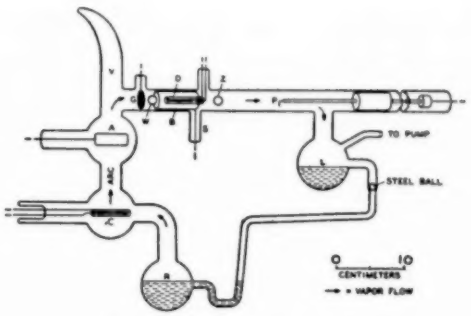

FIG. 1. Experimental tube.

EXPERIMENTAL PROCEDURE

The experimental tube used is shown in Fig. 1 and was similar to that used by Randall and Webb.[2] Mercury was distilled from a reservoir, R, at the lower end of a vertical tube, V, 3.5 cm in diameter and 30 cm long, the upper end of which terminated in a light trap. C was an oxide-coated cathode, and A an anode. After passing the cathode and anode the stream of vapor flowed into a horizontal, superheated branch tube, 3.5 cm in diameter and 30 cm long, terminating in a condenser, L, from which the condensed mercury returned to R. About 400 grams of mercury were retained in L, as it was found that this reduced fluctuations of temperature at the condenser and improved the constancy of experimental conditions. The tube was connected to a diffusion pump which was continuously operated during all observations. Spectroscopic observations of the afterglow were made through a plane quartz window, W, 1 cm in diameter.

Two centimeters upstream from the window in the branch tube was an auxiliary electrode, G, consisting of a plane sheet of gauze, of nickel wire 0.03 cm in diameter and 0.6 cm spacing, placed perpendicular to the axis of the tube. This electrode was connected to A during all observations except as specified below. For experiments on "quenching" an auxiliary, indirectly heated, cylindrical, oxide-coated cathode, D, was mounted

coaxially in the branch tube, with its secondary anode, *B*, a sheet nickel cylinder 5 cm in length, resting against the wall of the tube. About 2 cm below its downstream end there was a second quartz window, *Z*. The electrodes, *B* and *D*, and the window, *Z*, were removed from the tube after the quenching experiments were completed and were not present during any of the other measurements described in this paper or in II.

Velocity and pressure measurements

The velocity of the vapor was controlled by the difference in temperature between the well, *R*, and the condenser, *L*, and could be held very constant. It was measured using the method developed by Ricker,[8] as described by Randall and Webb.[2] The pressure was controlled by the temperature of *R*.

The concentration of atoms in the branch tube was determined from the saturation temperature measured in the small vertical tube, *S*, located 6 cm downstream from *W*. This was immersed in a stirred bath of transparent oil which could be heated electrically or cooled by a current of air through a copper spiral. The bath temperature was measured with a thermocouple and potentiometer. By observing the appearance or disappearance of the mercury droplets on the wall of the tube, as the bath was successively cooled and heated, the saturation temperature could be determined with an average precision of 0.5°C. From this, after correcting for the difference in temperature between the branch tube and *S*, the concentration in the branch tube was found. This is stated throughout this paper as vapor pressure reduced to 140°C. The values of the concentration obtained by this method were found to be in excellent agreement with the values determined by means of the vapor velocity and the time required for a known mass of mercury to overflow from the condenser. This latter was measured in a trap of known volume, which could be closed by a steel ball controlled by a magnet. It was found that the vapor pressure and vapor velocity were practically constant from the anode to the condenser, *L*.

Probe measurements

The probe, *P*, used for measuring ion and electron concentrations and electron temperatures, was of tungsten wire, 0.0025 cm in diameter and 0.4 cm long, mounted at right angles to the axis of the branch tube in such a way that it could be moved along the axis of the branch tube by means of an external electromagnet. Measurements were made in the usual manner, as described by Langmuir and Mott-Smith.[9] During intensity measurements the probe was moved downstream.

Intensity measurements

The intensities of the spectral lines studied were measured photographically with a precision of about 5 percent. The details of the measurement will be described in II.[10] In addition, as a check, a visual photometer with filters was used to measure the combined intensities of λ5461 and the pair of lines λλ5770–5790.

Results

Effect of vapor pressure and ion concentration upon the intensities of various lines

By means of homochromatic methods the changes of the intensities of twenty-one lines in the afterglow, between 5790A and 2482A, were measured at *W* as the pressure was varied from 0.1 mm to 2.0 mm. For pressures above 0.3 mm ten additional lines were included in the measurements. Four of the above "lines" consisted of groups of lines having common lower levels, which were not sufficiently resolved by the spectrograph for separate measurement. Only the sharp and diffuse series were studied.

In order to test the hypothesis that the afterglow was the direct result of simple ion-electron recombination, throughout the measurements first described the concentration of positive ions at the point of observation, opposite the window *W*, was maintained approximately constant at 2.5×10^{11} ions per cc by adjusting the arc current. Throughout these tests the vapor velocity varied between 2500 and 3200 cm/sec., which was not sufficient variation to affect the results appreciably. (The results shown in curve (b) of Fig. 4 have however been reduced to constant vapor velocity, by assuming as a first

[8] N. H. Ricker, Phys. Rev. **17**, 195 (1921).

[9] Langmuir and Mott-Smith, Gen. Elec. Rev. No. 27, 449, 538, 616, 762, 810 (1924).

[10] G. E. Moore and H. W. Webb, J. Opt. Soc. Am. **30**, 413 (1940).

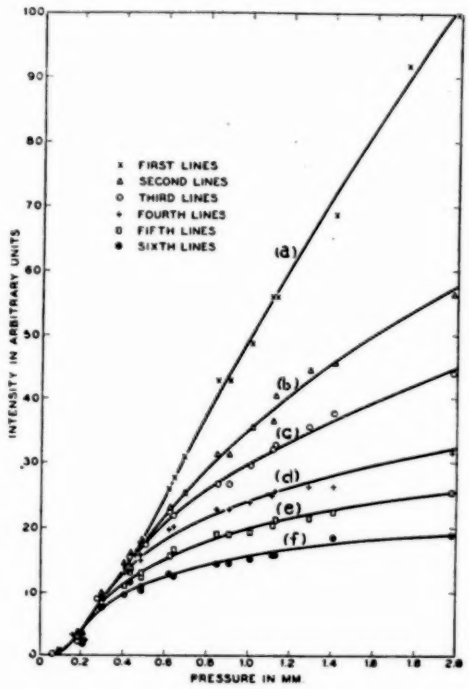

FIG. 2. Intensity of first six members of subordinate series as a function of vapor pressure, with ion concentration constant at point of observation.

(a) First members

5770–90	$6^1P_1-6^1D_2$, $6^1P_1-6^3D_2$, $6^1P_1-6^3D_1$
5461	$6^3P_2-7^3S_1$
4358	$6^3P_1-7^3S_1$
4077	$6^3P_1-7^1S_0$
4047	$6^3P_0-7^3S_1$
3650–63	$6^3P_2-6^3D_1$, -6^3D_2, -6^3D_3
3125–31	$6^3P_1-6^3D_1$, -6^3D_2
2967	$6^3P_0-6^3D_1$

(b) Second members

4916	$6^1P_1-8^1S_0$
3341	$6^3P_2-8^3S_1$
3021, etc.	$6^3P_2-7^1D_2$, $6^3P_2-7^3D_1$, -7^3D_2, -7^3D_3
2893	$6^3P_1-8^3S_1$
2753	$6^3P_0-8^3S_1$
2655, etc.	$6^3P_1-7^3D_1$, -7^3D_2

(c) Third members

3906	$6^1P_1-8^1D_2$
2925	$6^3P_1-9^3S_1$
2804	$6^3P_1-8^3D_2$

(d) Fourth members

3704	$6^1P_1-9^1D_2$
2699	$6^3P_1-9^3D_2$

(e) Fifth member

2639	$6^3P_1-10^3D_2$

(f) Sixth member

2603	$6^3P_1-11^3D_2$

approximation that the concentration at W varied as the vapor velocity.)

The results of the tests are shown in Fig. 2, the abscissae being pressure in millimeters of Hg and the ordinates intensities on an arbitrary scale. It was found that the curves for the first members of all the series studied could be made to coincide within the limits of precision of measurement by suitably adjusting the intensity scale for each, so that only one curve (a) is shown for the first members. It was also found that the behavior of the second members of these series could be shown by a single curve (b), and similarly curves (c), (d), (e) and (f) show the behavior of the third, fourth, fifth and sixth members, respectively. The wave-lengths and series designations of the lines in each of these six groups are listed beneath the figure.

The results show that for constant ion and electron concentration at the point of observation there is a marked dependence of the strength of the afterglow upon the pressure. For pressures above 0.4 mm curve (a) may be approximated by a straight line intercepting the pressure axis at about 0.2 mm. There was a marked difference in behavior between the "higher" and "lower" lines in the series. Although the absolute intensities were much less for the higher lines the intensity scales for (b), (c) and (d) were chosen so that they follow curve (a) below 0.4 mm. Above this pressure, however, they depart from (a) with slopes decreasing with increase in pressure, the departure increasing progressively as we go from the lower to the higher lines. In curves (e) and (f) the decrease in slope with increase in pressure is even more marked, the latter curve becoming nearly parallel to the pressure axis at high pressures. The intensity of nearly all lines fell to values too small to measure at pressures of about 0.1 mm, even with an arc current of 14 amperes.

The dependence of the intensity of the lines in the afterglow on the ion concentration at W with constant pressure was also studied. These measurements were made at three pressures, 0.20, 0.53 and 1.0 mm, but since no marked change in the shape of the intensity-concentration curves was noted for different pressures the results for 0.53 mm only are shown in Fig. 3. The concentrations, ions per cc, are plotted as abscissae, the intensities in arbitrary units as ordinates. Again the intensity scale for each line has been so chosen that a single curve would represent the results for a single group, curve (a) for the first members, (b), (c), (d), (e), and (f) for the second, third, fourth, fifth and sixth members, respectively, as it was found that the behavior of all the lines of each group was sufficiently alike to justify this. It will be noted that all the curves are intermediate in form between straight lines and parabolas, the latter being the form predicted by the theory of ion-electron recombination. It will be further noted that, excepting the curve for the first members, there is a progressive change in the form of the curves as we pass from the second to the higher members.

Measurements were made of the variation with

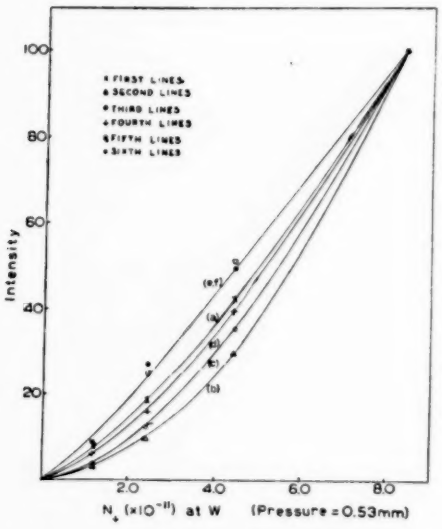

FIG. 3. Intensity of first six members of subordinate series as a function of ion concentration at point of observation, with pressure constant.

the pressure of the ion concentration in or near the region of the arc discharge. Since it was not possible with the experimental tube to place the probe adjacent to the anode A, this was disconnected and the gauze, G, used as the anode. The probe was placed close to G and the ion concentration was there found to be closely proportional to the arc current, the constant of proportionality increasing with the pressure. In Fig. 4, curve (a), the abscissae are pressures in mm and the ordinates ion concentrations near the anode per unit arc current. From this curve and the values of the arc current used in determining the relation between intensity and pressure, the ion concentration near the anode required to produce a given value of the concentration at W (2.5×10^{11} ions per cc) was computed for different pressures and plotted in curve (b), the ordinates giving of course only relative values. This curve has a minimum at 0.45 mm, the required concentration near the anode being four times greater at 0.1 mm than at the minimum and five times greater at 1.8 mm.

Measurements of the percentage change of the ion concentration with time was measured at five pressures in the branch tube by moving the probe along the vapor stream. This was found to be nearly independent of the arc current and to be largest for pressures below 0.3 mm. It had a minimum between 0.3 mm and 0.9 mm, the position of which could not be precisely determined from the measurements made. The percentage change with time of the visible intensity was also measured as a function of pressure, and the results were similar to those found for the percentage change of ion concentration. For example, at a pressure of 0.2 mm and again at 1.6 mm the intensity fell to one-half in about 2×10^{-3} sec. while at 0.4 mm the same change occurred in about 4×10^{-3} sec. At 0.4 mm pressure with a vapor velocity of about 3×10^{3} cm/sec. the intensity decreased 10 percent in a distance of approximately 3 cm.

Quenching experiments

When the gauze, G, was made positive with respect to the anode, A, a marked intensity decrease or "quenching" of the afterglow was produced in the stream immediately beyond the gauze. Beyond the region of greatest quenching the intensity of the afterglow increased again, but at points downstream never completely regained the values observed before the application of the quenching voltage. With pressures below 0.2 mm the quenched region extended the full length of the branch tube but became shorter as the pressure was raised, extending approximately one centimeter beyond G at a pressure of 1.0 mm. This quenching process produced a diminution in the ion and electron concentrations and increased the electron temperature. It further resulted in a large increase in the intensity of λ2537. All these effects became much less pronounced as the pressure was increased, being especially weak for pressures greater than 0.5 mm. Further, it was found that higher potentials on G were required to produce appreciable quenching as the pressure was raised. For example, at a pressure of 0.26 mm a potential difference of 1.8 volts applied to the gauze caused the electron temperature at a point a few centimeters downstream to change from 1200°K to 2000°K, while the intensity of λ5461 decreased to 10 percent of its normal value, and the ion concentration was reduced to 50 percent of its normal value. In contrast with this, at 1.3 mm a potential difference of 3 volts caused a small increase in the electron temperature near the gauze (from 2500°K to 2700°K), while the intensity of λ5461 fell to 70 percent of its normal value and there was very little change in concen-

tration. Another method of quenching was employed, which was also found to have its greatest effect below 0.4 mm pressure. A potential difference of a few volts was applied between the auxiliary anode, *B*, and the oxide-coated cathode, *D*, with no connections between these and the other electrodes. No observable effect on the afterglow was produced when the cathode was cold, but when it was hot and emitting electrons a marked quenching resulted which extended some distance downstream from the space between *B* and *D*. For example, at a pressure of 0.2 mm, with an arc current of 10 amperes the electron temperature at the window, *Z*, was raised from 500°K to 4000°K by applying 1.6 volts between *B* and *D*. The current between these electrodes was then 0.4 ampere. The intensity of λ5461 was reduced to about one-tenth of the normal and the ion concentration fell to one-half. Spectrograms taken through the quartz window, *Z*, showed that the intensity of λ2537 was simultaneously increased 100-fold. Smaller voltages produced less change in the electron temperature, while higher voltages increased the temperature but little. With 3.5 volts between *B* and *D* there was evidence of new excitation produced in this region.

Except in the quenching experiments, no systematic relation was found between the electron temperature at *W* and the intensity of the glow. In the intensity *vs.* pressure measurements the temperatures observed were between 1200°K and 3000°K, depending upon the arc current used, but were not related to the pressure in any simple manner.[1]

Diffuse band spectra

The well-known diffuse band spectra were found in considerable intensity in the afterglow under certain conditions. Our observations are substantially in agreement with the earlier work of Rayleigh.[11] When the pressures were high (above 0.6 mm) and the ionic concentrations were low (i.e., arc currents small) the total energy radiated in the diffuse bands was greater than that emitted in the line spectrum in the region 7000A to 2100A. (Rayleigh has shown that it is possible to pass from a nearly pure line spectrum to a nearly pure band spectrum by increasing the pressure, an effect which we have also observed). In addition a marked enhancement of the intensity of the bands relative to that of the line spectrum was obtained by applying a positive voltage to *G*. It was further noted that for pressures above 0.6 mm the first two of these factors which enhance the band spectra, high pressure and low current, tend to decrease the intensities of the higher series lines relatively to those of the lower members.

The following features of the band spectrum which were observed by Rayleigh were also found: (1) Broad intensity maxima at 4850A, 3300A and 2650A, (2) a narrow band without apparent structure, extending a short distance on both sides of λ2537, (3) a band, apparently with the regular structure described by Rayleigh, on the short wave-length side of 2482A, (4) a region of very definite band structure between 2700A and 3005A. The wave-lengths for all of these bands agree well with those found by Rayleigh, although precise measurements are difficult. In addition to these, other bands not previously reported were observed. These were almost as well defined as atomic lines and were found at the following wave-lengths in A.U.: (a) 4316 and 4145; (b) 4038, 4020, 3994, 3982, 3920, 3900, 3878, 3850, 3827, 3811, 3792, 3778, 3768, 3758, 3736, 3720, 3700, 3675; (c) 3563, 3550, 3488, 3474, 3466, 3443, 3433; (d) 3098, 3065, 3060, 3045, (these were relatively very strong); (e) 2822 and 2816.

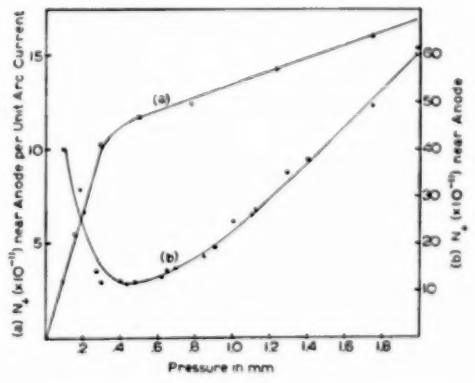

FIG. 4. Curve (a), variation with vapor pressure of ion concentration near anode per unit arc current. Curve (b), variation with vapor pressure of the ion concentration near anode required to obtain 2.5×10^{11} ions per cc at window.

[11] Rayleigh, Proc. Roy. Soc. **A114**, 620 (1927); **116**, 702 (1927).

Discussion

The measurements described above were for the most part made under conditions for which over ninety-nine percent of the radiation in the afterglow was in the lower six lines of eight subordinate series (see II). The diffuse bands were relatively very weak except under the special conditions of high pressure and low currents. The higher lines of the series and the continua were of such low intensity that quantitative measurements of their behavior with changes of pressure were not made, and consequently the conclusions drawn from these results do not necessarily apply to this part of the afterglow radiation.

The curves in Fig. 2, which were plotted for constant ion concentration at the point of observation, show a large change of intensity with pressure for all the lines of the afterglow which were studied. (For the first members the intensity at 2.0 mm is approximately one hundred times greater than at 0.1 mm). The curves also show that changes of pressure had a very marked effect upon the energy distribution in the spectrum, for in each series the ratios of the intensities of the higher members to those of the lower members became much smaller as the pressure was raised. Again, the curves show an abrupt change in nature near 0.1 mm, below which the intensity was very nearly zero. Now, according to the accepted theory of ion-electron recombination the intensity of the radiation for a given ion concentration is proportional to the recombination coefficient, which is practically independent of the vapor pressure, as discussed in the introduction to this paper. Furthermore, from the theory of this type of recombination we should not expect the marked change with pressure observed in the intensity distribution among the lines of a spectral series. Again, the behavior of the intensity *vs.* pressure curves in the neighborhood of 0.1 mm is not in accord with the assumption that we are dealing with ion-electron recombination. These results indicate, therefore, that if the afterglow derives its energy from the ions it does so by a much more complex process, involving collisions with neutral atoms. Other evidence, to be presented in II, leads us to conclude that these collisions result in the formation of particles of molecular nature, which later break up to furnish the excited atoms which emit the line spectrum of the afterglow.

That the rate of disappearance of positive ions in the vapor stream depends upon the pressure is shown directly by curve (b) of Fig. 4, which is a plot of the ion concentration near the anode necessary to give a constant number of ions at the window as a function of pressure. Since the data have been corrected, so that the time required for the vapor to travel from the anode to W was constant, the curve shows the effect of pressure upon the rate of disappearance of ions in this region. The two causes of ion disappearance in the stream are loss to the walls and some kind of volume recombination. The former is more important at low pressures, and the form of the intensity *vs.* pressure curves in Fig. 2 below 0.4 mm is presumably due to the fact that for these pressures relatively few ions make impacts which result in volume recombination. If we assume, as a first approximation, that the loss to the walls varies inversely as the pressure[6] we may compute from curve (b) the approximate values of the ratio of the loss by volume recombination to the loss by diffusion to the walls. We find in our tests that this ratio was very small for pressures less than 0.2 mm, about three-tenths at 0.4 mm, unity at 0.6 mm, seven at 1.0 mm, and nearly thirty at 2.0 mm. From these results and from curve (b) we then find an approximate relation between pressure and rate of loss by volume recombination. This loss increases rapidly with pressure, its value being twenty times greater at 2.0 mm than at 0.4 mm. In view of this large effect of pressure upon the rate of loss by volume recombination, it is probable that the value of α, 2.3×10^{-10}, which Mohler[7] found for mercury at 0.27 mm pressure, depended to some extent upon a more complex type of recombination involving atoms as well as ions, and so was not simply the ion-electron recombination coefficient.

The afterglow spectrum is not observed in the region between the cathode and anode of the arc discharge but first appears in the stream several centimeters above the anode. The energy necessary to excite the glow is presumably brought up in the vapor streaming from the arc either by atomic ions or by atoms in the $6^3P_{0,1,2}$ states, since these are the only particles known to be in the arc discharge which have sufficient concen-

tration and energy and have a long enough life to be carried by the stream for several centimeters. (The mean lives of the atomic states associated with the strong lines of the afterglow are probably all less than 10^{-5} second.)[12] The results point to the positive ions as the source of the excitation, for the marked increase of intensity with the pressure parallels the large increase with pressure of the volume recombination of ions. Again, Rayleigh[13] has shown that the removal of positive ions from the streaming vapor completely quenches all the lines of the afterglow, except λ2537, which comes in part from other sources of excitation. (The measurement of the velocity of the vapor in the present experiments depended upon this quenching phenomenon.) As further evidence of the dependence of the afterglow upon the positive ions we note the similarity in behavior with pressure change of the rate of disappearance of positive ions and the rate of decrease of intensity along the stream, both rates having a minimum in the pressure range of 0.3 to 0.9 mm.

The evidence is fairly conclusive that atoms in the $6^3P_{0,1,2}$ states are the source of excitation for the diffuse band spectra. It is generally accepted[14] that these band spectra are radiated by molecules which are each composed of a normal atom and an atom in one of the $6^3P_{0,1,2}$ states, the broad maximum at 4850A involving a 6^3P_0, that at 3300A a 6^3P_2, and that near 2537A a 6^3P_1 excited atom. Foote, Ruark and Chenault[15] suggest that the maximum at 4850A is due to a molecule composed of two metastable atoms, at least one of which is in the 6^3P_0 state. The results of the present experiments are in agreement with these assumptions, since it was found that the diffuse band spectra were enhanced by conditions favoring the production of $6^3P_{0,1,2}$ excited atoms, such as increased pressure and application of positive potentials to the gauze G.[16] However, the latter condition which greatly increased the concentration of $6^3P_{0,1,2}$ atoms did not result in an increased intensity of the line spectrum, but produced instead a marked quenching of the lines. Hence, it seems very improbable that the line spectrum derives its energy from the $6^3P_{0,1,2}$ atoms.

The fact that the afterglow line spectrum first appeared several centimeters above the anode is consistent with the assumption that molecular particles were there formed if, as suggested by Webb and Sinclair,[1] the quenching of the line spectrum is due to the breaking up of such particles by fast electrons. They showed further that to do this electrons having energy of approximately one electron volt or more were required. Hence, only after the number of high energy electrons in the arc had decreased sufficiently, usually indicated by a marked fall in electron temperature, should we have expected these molecular particles to appear in quantity in the stream. This explanation is consistent with the results of Hayner,[1] who found that if an arc discharge was cut off the afterglow did not appear until after an interval of 0.0001 sec., when it grew to a maximum 0.0002 sec. after the cut-off, and then gradually fell off as the excited particles became exhausted. The quenching experiments reported in the present paper also support this explanation. For example, greatest quenching was obtained with the auxiliary cathode D and anode B when about 1.6 volts were applied between these electrodes and the cathode was hot, while when D was cold such low potential differences produced no observable effect on the afterglow. This indicates that the quenching was primarily due to electrons supplied by the hot cathode which were accelerated in its immediate neighborhood until they had the energy required to dissociate the particles responsible for the afterglow radiation. The probable nature of the assumed molecular carriers of the energy radiated in the line spectrum will be further discussed in II.

In conclusion, the authors wish to express their indebtedness to Professor Harold W. Webb, at whose suggestion and under whose guidance this work was done. The authors also wish to thank Mr. Frederick Spector for assistance in the experimental work.

[12] R. H. Randall, Phys. Rev. **35**, 1161 (1930).
[13] Rayleigh, Proc. Roy. Soc. **A108**, 262 (1925).
[14] G. Herzberg, *Molecular Spectra and Molecular Structure, I. Diatomic Molecules* (Prentice-Hall, Inc., New York, 1939), pp. 417–427.
[15] Foote, Ruark and Chenault, Phys. Rev. **37**, 1685 (1931).
[16] H. W. Webb and S. C. Wang, Phys. Rev. **33**, 329 (1929).

Studies of the Afterglow in Mercury Vapor

II. Spectral Intensity Distribution‡

GEORGE E. MOORE* AND ROBERT C. GARTH†
Columbia University, New York, New York

(Received June 12, 1941)

The relative intensities of two hundred of the most intense lines of the spectrum of the afterglow in mercury vapor were measured photographically. The glow was observed in a stream of vapor which had previously passed through a region in which an arc discharge was maintained. By measuring the absolute intensity of the group of lines 3650–3663A radiated by one cubic centimeter of the vapor, the absolute intensities of these lines were determined and the total number of quanta radiated per second from unit volume calculated. From these results and from the measured rate of change of the positive ion concentration near the point of observation, it was shown that the total number of quanta radiated per second was much too great to be accounted for by assuming the afterglow to be produced by simple recombination of ions and electrons. Furthermore, a comparison of the number of quanta entering each atomic state by radiative transitions with the number similarly leaving this atomic state showed that the average energy possessed by the excited atoms emitting the line spectrum was about 9 electron volts. These results can best be explained by assuming that molecular particles with a mean life of about 10^{-3} second are formed by multiple impacts between the atomic ions produced in the arc, and neutral mercury atoms and that these particles dissociate to produce the excited atoms which radiate the afterglow. Some of the observed properties of the afterglow, especially the dependence of the intensity upon the pressure, are well accounted for by the assumption that this molecular particle is the excited molecule proposed by Arnot and Milligan.

INTRODUCTION

IN a preceding paper,[1] which in this paper will be referred to as "I" the present authors described an experimental study of the dependence upon vapor pressure of the intensity of the line spectrum of the afterglow in mercury vapor. They also made further observations on the "quenching" of the afterglow by auxiliary fields, and measured by electrical means the rate of disappearance of the ions. From these results they concluded that the bulk of the line spectrum in the afterglow does not result from "ion-electron recombination," by which is meant the direct union of a positive ion and an electron without any intermediate steps involving other bodies. They further interpreted the marked dependence upon pressure of the total intensity and of the distribution of intensity among the series lines of the spectrum as evidence that the process resulting in the line spectrum of the afterglow involves neutral atoms and is probably one in which molecular particles are formed from ions and neutral atoms, which particles later break up to furnish the excited atoms radiating the line spectrum. It was further concluded that metastable atoms are not directly involved in the production of these molecular particles, although they are intimately related to the diffuse bands which under special conditions were found in the afterglow with considerable intensity. The present paper describes further experiments with the afterglow which strongly confirm the conclusions of I.

EXPERIMENTAL

(1) Tube

The tube was in general similar to that described in I, but was considerably larger and did not have the electrodes *G*, *B* and *D*. The anode and a large oxide-coated cathode,[2] capable

* Now at Bell Telephone Laboratories.
† Now at Brooklyn College.
‡ Publication assisted by the Ernest Kempton Adams Fund for Physical Research of Columbia University.
[1] R. C. Garth and G. E. Moore, Phys. Rev. **60**, 208 (1941).

[2] Acknowledgment is made to the Bell Telephone Laboratories, Inc., for their courtesy in furnishing this cathode.

of supporting an arc current of 25 amperes, were mounted in the vertical tube, 5 cm in diameter. The horizontal branch tube was 5 cm in diameter and 40 cm long, joining the vertical tube 3 cm above the anode. For observing the afterglow spectrum in the mercury stream, a fused quartz window, 2 cm in diameter, was attached to the branch tube about 9 cm from the center of the vertical tube. Immediately adjacent to this window was a probe of tungsten wire, 0.005 cm in diameter and 6 mm long, for the measurement of ion concentration and electron temperature at the point of observation. The concentration of mercury atoms was determined as in I.

(2) Intensity measurements

The intensities of the lines in the afterglow were too weak to measure with a thermocouple, even with arc currents of 25 amperes. Consequently the measurements were made in three steps: First, the relative intensities of seventeen reference lines emitted by a quartz mercury arc, operated under very constant conditions were measured to a precision of about one percent with a non-selective vacuum thermocouple.[3] This couple was so mounted on a screw driven carriage that the collector was maintained with its face perpendicular to the incident beam, in the focal plane of the quartz lens of a spectrograph (focal length = 30 cm; aperture = 2.5 cm), constructed to permit interchangeable use of couple and plate-holder. The voltage of the quartz arc was held constant to within ±0.2 volt by a control device described in another paper.[4] The relative intensities of the lines emitted were constant to better than one percent over periods of several hours, while the absolute intensities of all but the resonance lines remained constant to within three percent, the changes being so slow that they could readily be corrected for. These measurements were corrected for the transmission of the spectrograph, which was determined for ten lines in the region 10,140 to 2537A, by a procedure essentially that described by Forsythe and Barnes.[5] The measurements were, however, much simplified by the use of the controlled arc, which remained so constant throughout any one set of measurements that a single thermocouple could be used.

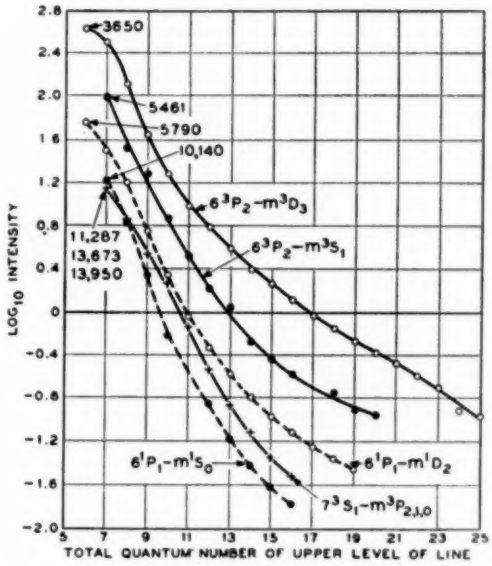

FIG. 5. Intensity relationships for five series in the mercury afterglow.

In the second step, the measurements of the relative intensities of the lines in the arc were used to determine the relative intensities of these same lines in the afterglow spectrum by determining for each line the ratio of its intensity in the arc to its intensity in the afterglow. The method of making this comparison has been described elsewhere[4] and will be only outlined here. On a single photographic plate one or more exposures of the afterglow and several of the controlled arc were taken, all with the same exposure times. The light from each source was diffusely reflected from a magnesium carbonate block into the slit of the spectrograph on which was mounted a calibrated sputtered step weakener of five steps. By varying the distance of one or both of the sources from the carbonate block, which was fixed with respect to the spectrograph, the intensity of the light entering the spectrograph could be controlled, since it was very closely proportional to the inverse square of the distance. Exposure distances were so selected that extrapolation was never necessary. Because of the step weakener, each exposure gave for each line five spectra of known intensity ratios. From the calibration of the weakener and the inverse

[3] G. E. Moore and H. W. Webb, Rev. Sci. Inst. **11**, 101 (1940).
[4] G. E. Moore and H. W. Webb, J. Opt. Soc. Am. **30**, 413 (1940).
[5] W. E. Forsythe and B. T. Barnes, Rev. Sci. Inst. **1**, 569 (1930).

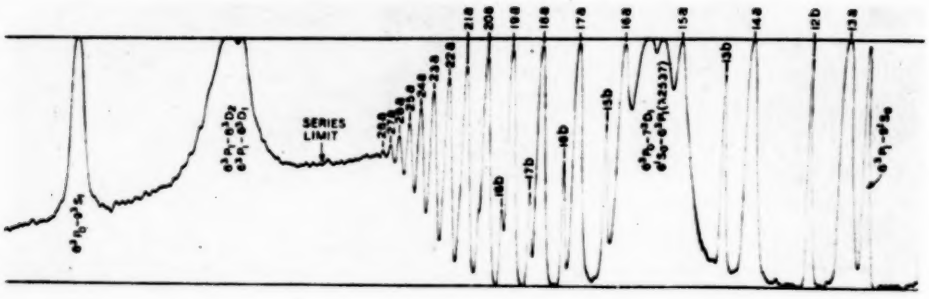

FIG. 6. Microphotometergraph showing convergence of triplet diffuse and sharp series. Series $a = 6^3P_2 - m^3D_{123}$; values of m from 13 to 28 inclusive are shown. Series $b = 6^3P_2 - m^3S_1$; values of m from 12 to 19 inclusive are shown. $6^3P_1 - 9'S_0 = 2563.88$; $6^3P_1 - 8^3D_1 = 2482.721$; $6^3P_0 - 7^3D_1 = 2534.771$; $6^3P_0 - 9^3S_1 = 2464.059$; $6^3P_1 - 8^3D_2 = 2482.008$.

square law, the relative intensities of the reference lines in the afterglow could be calculated from their relative intensities in the arc.

In the third step the ratio of the intensity of each of the weaker lines to that of the nearest of the seventeen reference lines was determined with a quartz spectrograph of higher dispersion, again with the step weakener over the slit. Since the ratio of the intensities of the strongest and weakest lines in the afterglow was of the order of 10^4, and the maximum ratio of intensities which could be measured with the step weakener alone was about five, this part of the measurements had to be performed in steps. For large ratios two auxiliary homogeneous weakeners were employed, whose spectral transmission had been measured with the spectrograph and thermocouple. These weakeners were made by sputtering platinum on quartz plates and each transmitted about 10 percent. By combining the homogeneous and step weakeners intensity ratios as large as 300 could be measured from three exposures, all taken on one photographic plate with constant exposure times. With the weaker lines thus measured as secondary reference lines, the above process was repeated and the measurements extended to lines whose intensities were 10^{-4} times that of the strongest lines in the spectrum. The measurements were repeated so that there were three to five separate measurements of the intensity of each line.

RESULTS

Energy distribution

The energy distribution in the spectrum of the afterglow was studied under conditions selected to give relatively high intensity. For the results described below, the arc was operated at 9.5 amperes and 6.5 volts. At a point in the stream opposite the window, the vapor pressure was 0.37 mm (10^{16} atoms per cc), the concentration of positive ions 6.7×10^{11} per cc, and the electron temperature 1890°K. There were approximately 200 lines of substantial intensity in the spectrum. Of these, 126 in twenty-two spectral series were measured directly, while the intensities of the remaining lines were evaluated by indirect methods.

The relative intensities of the lines in five of the more intense series are plotted in Fig. 5. Other data are given in Table I. Throughout this paper, the intensity of 5461A is arbitrarily taken as 100, whenever relative intensities are discussed. The most intense line was 3650A, $6^3P_2 - 6^3D_3$, the intensity of which was 350. The precision of the intensity determination of every directly measured line stronger than 5461A was on this scale between 1 and 3. For weaker lines it was in general better than 1; for example for 4916A the intensity was 6.4 ± 0.6, for 4970A, 0.065 ± 0.015.

The three series $6^3P_2 - m^3D_{123}$ are treated as one in Fig. 5 since the higher members could not be resolved by the spectrographs used. Similarly the two series $6^3P_1 - m^3D_{12}$ were measured as one beyond the second members. Twenty-two lines of the former series were separately measurable (under favorable conditions 24 lines[6] can be resolved) before the lines merged into the continuum about 10A on the long wave-length

[6] I. Walerstein, Phys. Rev. **46**, 874 (1934).

side of the series limit. A microphotometer trace showing the higher series lines and the continuum is shown in Fig. 6. Lines of the $6^3P_2-m^3S_1$ series are also clearly shown on the trace. The position of the series limit is indicated by an arrow.

Only the first six lines of the $6^3P_1-m^3D_{12}$ series were measured directly, since the higher members fell outside of the range in which the quartz arc was calibrated. As expected, the relative intensity distribution among these lines was very closely the same as for the corresponding lines in the $6^3P_2-m^3D_{123}$ series, and the intensities of the remaining lines in the series were therefore computed by assuming the same distribution throughout each series. The intensities for the other ultraviolet lines beyond λ2400 listed in the table were similarly estimated.

The intensity of 2537A ($6^1S_0-6^3P_1$) was measured but that of 1849A ($6^1S_0-6^1P_1$) could only be roughly estimated. Reversal is large with both lines so that their intensities could not be determined with precision. The higher members of the two series of which these lines are the first members lie too far in the ultraviolet to be photographed with the instruments available.

Of the numerous infra-red lines in the mercury spectrum, only eleven are listed in Table I as of sufficient intensity in the afterglow to be significant in this problem. No infra-red lines except 10,140A and 11,287A were observed on infra-red plates sensitive to 13,000A, and the direct photographic intensity determinations of these two lines were not very reliable. Since these lines were weak in comparison with the stronger lines in the visible and ultraviolet, their intensities could be estimated with sufficient accuracy. For example, the line 10,140A is the first member of the series $6^1P_1-m^1S_0$ of which the second and higher members were measured directly and found to have closely the same relative intensities as was observed for the corresponding lines in other series. Hence, from the intensity distributions in the other series, the intensity of 10,140A was computed as 17 ± 4. Approximately the same value was computed from the measured intensity of 4077A ($6^3P_1-7^1S_0$), which originates on the same upper level, by assuming that the ratio of the intensities of 10,140A and 4077A in the afterglow was the same as in the controlled arc, in which it was accurately measured with

TABLE I. *Intensities of lines not plotted in Fig. 5. Intensity of 5461 = 100.*

Term Designation	Relative Intensity
$6^1P_1-m^3D_2$	
$m=6$	48
7	10.2
8	3.8
	*
$6^3P_2-m^3D_2$	
$m=6$	52.0
7	30.0†
$6^3P_1-m^3D_2$	
$m=6$	151.0
7	99.0
8	48.0
9	25.0§
10	‡
$7^1S_0-m^1P_1$	
$m=7$	4.0
8	1.9
9	0.6†
10	0.29
11	0.17†
12	0.08
13	0.03
14	0.02
$6^3P_2-m^3D_1$	
$m=6$	39.2
7	14.0†
	*
$6^3P_1-m^3D_1$	
$m=6$	111.0
7	40.0
8	22.0
9	10.0§
10	‡
$6^3P_0-m^3D_1$	
$m=6$	91.0
7	48.0
8	20.0
9–16	‡
$6^3P_2-m^1D_2$	
$m=6$	26.4
7	12.5
8	6.6
9	1.8
	*
$6^3P_1-m^1D_2$	
$m=6$	96.0
7	25.0
8	9.8
	*
$6^3P_1-m^1S_0$	
$m=7$	3.7
8	1.8
9	0.75
10	0.24
11–16	‡

Term Designation	Relative Intensity
$7^3S_0-m^1P_1$	
$m=7$	0.63
8	1.15‖
9	0.44
10	0.17
11	0.065
$6^1P_1-m^3S_1$	
$m=8$	0.072
9	0.027
$7^3S_1-m^3P_{1,0}$	
$m=8$	1.7
9	0.86
10	0.29
11	0.096
12	0.043
$6^3P_0-m^3S_1$	
$m=7$	30.5
8	13.2
9	6.0
10	2.5
11–15	‡
$6^3P_1-m^3S_1$	
$m=7$	102.0
8	34.0
9	14.0
10	5.8
11	2.5
12–24	‡
Infra-red lines	
$6^1P_1-7^1S_0$	17.0
$7^3S_1-7^3P_2$	7.9
$7^1S_0-7^1P_1$	3.9
$7^3S_1-7^3P_1$	3.8
$7^3S_1-7^3P_0$	1.4
$6^1D_2-6^1F_3$	2.5
$6^3D_1-6^3F_2$	1.8
$7^3P_2-7^1D_1$	2.6
$6^3D_2-6^3F_3$	2.3
$6^3D_3-6^3F_4$	0.4
$6^1P_1-7^3S_1$	0.8
Other lines not listed above	
λ2537	62.2
λ1849	‡
λ1942	‡
λ6124	0.77

* Other lines of series not resolved.
† Estimated because of partial masking.
‡ Observed but not measured.
§ Estimated, only, because of short wave-length.
‖ Note: This line is apparently an exception to the general rule since it is more intense than the preceding line.

the thermocouple. Similarly, the intensities of 11,287A, 13,673A and 13,950A were computed by extrapolation from the intensities of the measured lines in their respective series as 10, 3.1 and 1.2, respectively. A satisfactory check on these computations giving values of 8.0, 3.8 and 1.4 was made with the above value for the intensity of 10,140A and the results of McAlister,[7] who measured the relative intensities of all the more prominent infra-red lines in a mercury arc. The intensities of the other seven infra-red lines, which were considerably weaker than these four, were similarly estimated as given in Table I.

Figure 5 gives the intensities of the lines of five of the more intense spectral series in the afterglow. The ordinates are the common logarithms of the intensities (intensity of 5461A = 100) and the abscissae the total quantum numbers of the levels from which the lines originate. The wavelength of the first member observed in each series is given on the curve to assist in identification. The intensities of the lines not plotted in the figure are given in Table I.

About 99 percent of the total radiation in the line spectra was in the first six members of the various series. Somewhat less than one percent of the total radiation was due to the series limit continua which were observed for eight different series.

The rate of direct excitation into each atomic level was computed by subtracting from the number of quanta leaving the level per second by radiative processes the number of quanta entering the level by radiation. These rates are given in Table II for most of the levels for which the values were sufficiently large to be of interest. The first and second columns give the series designations of the levels and the energies in wave numbers, respectively, the third and fourth give the quanta leaving and entering by radiative transitions, respectively, and the fifth column gives the difference, or the rate of direct excitation into the level. The scale in the last three columns was so chosen that the figures in the last column give the percent of the total number of direct excitation processes taking place into each level.

In computing these results, the values of the rates for the principal series levels m^1P_1 and m^3P_{012} have been taken as zero. Although no accurate measurement of the intensity or weakening by reversal of 1849 was made, the fact that it was comparable in intensity with the normally weak line 1942 suggests that most of the observed radiation was due to the transitions into the 6^1P_1 level from higher levels rather than to direct excitation. Similarly no accurate estimate was possible for the effect of reversal on the intensity of 2537A which was only one-sixth of that to be expected from the observed transitions into the 6^3P_1 level from higher levels. Since 2537A was very weak relatively to the other lines in the afterglow as compared with its value in the radiation from other mercury sources of comparable pressure, the net direct excitation of this level has been assumed to be zero. The direct excitation of the 6^3P_0 and 6^3P_2 levels and higher levels of the same series have also been neglected. As will be evident later these assumptions have no effect on the conclusions to be drawn from the results. For other lines reversal was neglected, since the work of Barnes and Adams[8] has shown that, for the conditions under which the present investigation was made, only minor reversal effects for all but the resonance lines are to be expected.

Absolute intensity

The absolute intensity of each of the lines in the afterglow spectrum emitted per second by a cubic centimeter of the vapor opposite the window was calculated from the above measurements of the relative intensities of the lines and from a measurement of the absolute intensity of the group of lines 3650A–3663A, which were not individually resolved by the thermocouple. This measurement was made by first determining the sensitivity of the thermocouple-galvanometer system, with a standardized incandescent lamp. The thermocouple and galvanometer were then used with the quartz spectrograph to measure the absolute intensity of the 3650A–3663A group emitted per unit solid angle from a measured area of the controlled quartz arc. The computations involved the geometry of the arc and spectrograph combination and corrections for the transmission

[7] E. D. McAlister, Phys. Rev. **34**, 1142 (1929).

[8] B. T. Barnes and E. Q. Adams, Phys. Rev. **53**, 545–563 (1938).

of the spectrograph at these wave-lengths. The relative intensity of this group of lines in the afterglow and in the arc was then determined photographically with the magnesium carbonate block and step weakener before the slit and varying the distances to the sources until equal photographic densities were obtained. From the known absolute intensity of the arc radiation, the absolute intensity of the group of lines in the afterglow was computed.

The total energy radiated per second as 3650A–3663A from one cubic centimeter of the afterglow, computed from this value and the volume of glowing vapor from which radiation reached the carbonate block, was 5.4×10^{-4} watt. From Table II we find that the direct excitation into the 6^3D_{123} levels, measured in quanta, was 38 percent of the total of such excitation processes. This gives the result that, in the experimental tube, from each cc of vapor at the window there were emitted as the result of direct excitation at least 2.6×10^{15} quanta per second.

A repetition of this measurement of absolute intensity with a photo-cell and a quartz mercury arc, calibrated in another laboratory, gave results in good agreement with the above.

Discussion

In this investigation of the mercury afterglow, as well as that described in I, measurements were made primarily on the line spectra. The series limit continua, which involved considerably less than 1 percent of the quanta radiated under the conditions used in the present work, were of such low intensity that relatively few quantitative data were obtained in regard to their behavior. The intensity of the band spectrum was so low that it was not observed with the large tube used in the work described in this paper, although under special conditions with the tube used in I more energy was radiated in the band than in the line spectrum. The conclusions drawn below apply primarily to the atomic line radiation.

The measurements of total intensity indicate that the radiation of this line spectrum is not due to ion-electron recombination. From the work of Randall and Webb[9] and from the data reported in I, the velocity of the vapor stream in the present experiments was estimated to be somewhat less than 10^4 cm per second. Randall[10] has shown that the lifetimes of the 7^3S_1 and 6^3D_{123} levels are less than 10^{-7} second, and if we assume that the lifetimes of the states in a given series are approximately proportional to the cube of the effective total quantum numbers as in hydrogen, we find that the lifetimes of those states which contribute substantially to the afterglow are all less than 10^{-5} second. Hence in the present experiments an excited atom travelled less than 1 mm in an excited state between excitation and radiation.

The product of the vapor velocity (10^4 cm/sec.) and the concentration of ions near W, (6.7×10^{11} ions per cc) gives the maximum number of ions passing through each cc per second, 6.7×10^{15}. But the total intensity was found to involve 2.6×10^{15} radiating atoms per cc per second in this region. Therefore if the line radiation were due only to ion-electron recombination, the ionization in the vapor would have been exhausted in moving about 3 cm. This is however, contrary to the experimental observations made earlier under similar conditions that the ion concentration decreases by only about 10 percent in 3 cm. Furthermore, the total amount of energy radiated by the vapor beyond the window was estimated and the corresponding number of quanta involved was found to be at least 20 times greater than the ion concentration at the window.[11]

The conclusion that the afterglow line spectrum is not due to ion-electron recombination is apparently supported by the observations of Mohler[12] who measured by electrical means the rate of decay of the ion concentration in a mercury arc after extinction. Using approximately the same vapor pressure and electron

[9] R. H. Randall and H. W. Webb, Phys. Rev. **48**, 544 (1935).

[10] R. H. Randall, Phys. Rev. **35**, 1161 (1930).

[11] The pressure 0.37 mm, at which these intensity measurements were made was judged to be sufficiently low to avoid the possibility of any substantial error in the measurement of the ion concentration such as has been suggested. [F. L. Mohler, Nat. Bur. of Stand. Research Paper R.P.948]. As a further check on this, the measurements of absolute intensity were repeated at a pressure of 0.1 mm for which the probe measurements could not have been significantly in error, and again it was found that the number of excited atoms which were radiating was much too large to be due to ions recombining near the point of observation.

[12] F. L. Mohler, Nat. Bur. Stand. Res. Paper R.P.1045.

temperature as in the present experiments, he found that an initial ion concentration of 6.7×10^{11} per cc decayed at the rate of 1.3×10^{14} per cc per second or approximately 5 percent of the rate, 2.6×10^{15}, which was found above to be the required rate of ion disappearance, if the afterglow were the result of ion-electron recombination.

This conclusion is further supported by the results given in Table II in which it is shown that the radiating atoms have an average initial energy of about 9 electron volts (somewhat less if the assumption of negligible excitation into the principal levels is incorrect.) If ion-electron recombination produced the afterglow line spectrum directly, the difference between the ionization potential and 9 volts, or 1.4 electron volts, must on the average have been carried off in the process of exciting each atom radiating the afterglow line spectrum. But in such recombination, this could have occurred only by the radiative process since no third body was involved to carry off the 1.4 electron volts as kinetic energy. However, from the data in the third and fourth columns of the table, it is evident that this could not have occurred since the number of quanta entering the upper energy state of nearly every line of substantial intensity in the afterglow is considerably less than the number leaving by radiative transitions. For example, in the case of the 7^3S_1 state, more than four quanta leave for each quantum entering from higher states. Similarly in the case of the three 6^3D states, the ratio is greater than five and is still larger for higher states. Continua, such as are observed especially with the alkalis and interpreted as resulting from ion-electron recombination, were very weak in the mercury afterglow, being detected only for the $6P$ states where they accounted for less than one percent of the total quanta radiated. Consequently, they need not be considered in discussing the excitation of the strong lines. For example, ion-electron recombination into the 7^3S_1 state would have produced a continuum starting at 4550A and extending to shorter wave-lengths, but no series limit continua were observed except for the $6P$ series. Since then there is no evidence that radiative transitions from higher levels, discreet or continuous, account for more than a small fraction of the excitation of the more important states, we conclude that, if some type of recombination of ions and electrons is responsible for the line spectrum of the afterglow, this cannot be ion-electron recombination, but must be a much more complex process and must involve collisions with neutral atoms, in order that the excess energy can be accounted for as kinetic energy. It is concluded that neutral atoms rather than electrons carry away this energy, since the average energy of the electrons in the afterglow, as measured by the electron temperature, is usually low.

From the results described in I, it was concluded that in these experiments the ions from the arc discharge were the primary source of the energy of excitation of the afterglow. If this is correct, the measurements of the absolute intensity show that whatever process was involved was initiated at some point near the anode, since

TABLE II. *Excitation data.*

SERIES DESIGNATION	ENERGY IN ν	QUANTA LEAVING	QUANTA ENTERING	RELATIVE EXCITATION RATE
7^1S_0	20,253	2.37	2.16	0.21
8^1S_0	10,219	0.56	0.21	0.35
9^1S_0	5,964	0.14	0.01	0.13
6^1P_1	30,112	?	18.3	0?
7^1P_1	12,886	?	0.36	0?
6^1D_2	12,848	10.7	2.01	8.69
7^1D_2	7,117	3.85	0.14	3.71
8^1D_2	4,521	1.29	0.014	1.28
7^3S_1	21,830	16.1	3.74	12.4
8^3S_1	10,219	3.46	0.057	3.40
9^3S_1	5,965	1.57	0.01	1.56
10^3S_1	3,912	0.57		0.57
11^3S_1	2,765			0
6^3P_2	40,138		2.35	0?
7^3P_2	12,973	1.29	0.52	0.77
8^3P_2	7,357	0.22	0	0.22
6^3P_1	44,787	4.0	22.8	0?
7^3P_1	14,519		4.0	0?
6^3P_0	46,536	0?	5.6	0?
7^3P_0	14,664	0.20	0.23	0
8^3P_0	7,734	0.054	0.014	0.04
6^3D_3	12,750	18.4	0.575	17.8
7^3D_3	7,052	10.4	0.011	10.4
8^3D_3	4,479	5.04	0	5.04
6^3D_2	12,785	13.5	2.52	11.0
7^3D_2	7,073	5.75	0.04	5.71
8^3D_2	4,491	2.34	0	2.34
6^3D_1	12,845	11.1	1.77	9.3
7^3D_1	7,096	3.74	0.043	3.70
8^3D_1	4,503	1.58	0	1.58

only near the arc discharge was the ion concentration sufficiently large to account for the total energy radiated as afterglow throughout the tube. An approximate calculation, based on the theory of the arc developed by Tonks and Langmuir[13] showed that the ion concentration near the anode was of the same order of magnitude as the total number of quanta emitted in the afterglow throughout the tube. Hence, if the ions were the source of the excitation, in order to explain the intensity distribution observed in the tube, it must be assumed that long-lived molecular particles (mean life $\sim 10^{-3}$ second) were formed near the anode, carried several centimeters down stream and then became dissociated, thus furnishing the excited atoms which radiated the afterglow line spectrum. The results discussed in the preceding paragraph indicate that the multiple collisions necessary for the formation of such a molecule did occur. Moreover, the dependence of the rate of volume recombination of the ions on the pressure, described in I, can best be explained by assuming such recombination to have resulted from multiple impacts involving neutral atoms.

In I it was concluded that atoms in the 6^3P_{012} states were not directly involved in the excitation of the line spectra, although they are the source of the molecules which radiate the diffuse band spectra. It does not seem probable, therefore, that the molecule just postulated to explain the behavior of the afterglow can be identified with any formed from atoms in the $6P$ states. For similar reasons, it is concluded that it cannot be formed from the negative molecule ions which Nielsen[14] showed to be formed by the union of neutral atoms, electrons and metastable atoms. Other mercury molecules have been suggested, but the properties of the afterglow seem best to be explained by assuming that the molecule is that proposed by Arnot and Milligan.[15] These authors observed that mercury molecule ions can be produced by bombardment of neutral atoms with electrons of 9.5 volts energy, 0.9 volt less than the ionizing potential of the atom, and presented strong evidence that these molecule ions were formed by the process

$$Hg' + Hg \rightarrow Hg'Hg \rightarrow Hg_2^+ + \epsilon,$$

where Hg′ represents an excited mercury atom in the $7D$, or a higher atomic state and Hg′Hg an excited molecule formed by its combination with a neutral mercury atom.[16]

We assume that the first of the above reactions is easily reversible; that is, the Hg′Hg molecule can dissociate readily into an excited atom and a neutral atom. This assumption is plausible, at least for the $7D$ and higher states, because the energy differences between the excited atomic states and corresponding molecular states are small. Since there is a large energy difference between any of the molecular states and the $6D$ and $7S$ atomic states, any transitions into these states must be nearly irreversible.

The marked dependence of the intensity of the afterglow on the pressure, reported in I (see Fig. 2) implies that the concentration of Hg′Hg at W, for a fixed concentration of positive ions at this point, was approximately proportional to the pressure, p. This proportionality is also suggested by Fig. 4, which shows that, for a given concentration at W, that part of the positive ion concentration near the anode which was not lost to the walls by diffusion, and which we may take as the measure of the useful excitation at that point, was very nearly proportional to p. The form of the intensity-pressure curves (Fig. 2) suggests that a better approximation to actual conditions is obtained if we take the concentration of HgHg′ to be proportional to $p-0.1$ (mm), the latter term roughly compensating for the loss to the walls.

Since the probability, Q, that the excited molecule will reform before the excited atom radiates is given by[17]

$$Q = \frac{A\sigma^2 \tau p}{A\sigma^2 \tau p + 1},$$

where σ^2 is the collision cross section for the above

[13] L. Tonks and I. Langmuir, Phys. Rev. **34**, 876 (1929).
[14] W. M. Nielsen, Phys. Rev. **27**, 716 (1926); Proc. Nat Acad. Sci. **16**, 721 (1930).
[15] F. L. Arnot and J. C. Milligan, Proc. Roy. Soc. **A153**, 359 (1935).

[16] A similar molecule was suggested by Franck to explain the photo-ionization of cesium by absorption of radiation of the frequency of its lower principal series lines as observed by Mohler, Foote and Chenault (Phys. Rev. **27**, 37 (1926)). F. L. Mohler and C. Boeckner subsequently gave evidence strongly supporting Franck's suggestion (Nat. Bur. Stand. Research Paper, R.P.186).
[17] L. A. Turner, Phys. Rev. **23**, 464 (1924).

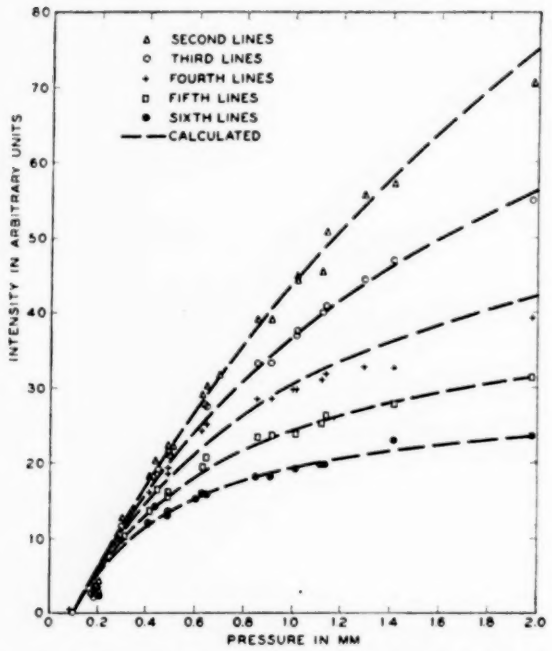

FIG. 7. Comparison of experimental and calculated forms of the intensity-pressure relationships in the mercury afterglow.

process, τ the lifetime of the atomic state in question and $p\sigma^2A$ the number of collisions per second between excited and neutral atoms. For a given ion concentration, the intensity J in the afterglow will then be proportional to the product of $1-Q$ and the concentration of the Hg'Hg molecules, or

$$J \propto \frac{p-0.1}{A\sigma^2\tau p+1}. \qquad (1)$$

Now if in this equation we use for all the excited states an average value of σ, 5×10^{-8}, which value lies in the range given by Turner[17] for similar collisions, and values of τ computed for the different states from the data of Randall[9] as in the first paragraph of this discussion, J is found to vary with p as shown by the dotted curves in Fig. 7. The experimental points shown are taken from the data plotted in Fig. 2 of I. Only the form of the curves is of interest since the intensity scale was arbitrarily chosen for each line. In view of the probability that the actual process involved is somewhat more complex than that assumed, the agreement between the calculated curve and experiment is satisfactory. To simplify the figure, curves are given only for the second to the sixth lines. The very much smaller value of σ which must be assumed because of the nearly irreversible processes producing the $6D$ and $7S$ atoms gives a linear relation between J and p for the 6^3D-6^3P and 7^3S-6^3P lines, which also agrees well with experiment. (See Fig. 2.)

The observation made by Rayleigh[18] that the afterglow is quenched by the removal of positive ions can be explained on the assumption that the second reaction postulated by Arnot and Milligan is highly probable, since the complete withdrawal of ions from the vapor stream would necessarily result in the disappearance of the excited molecules.

The quenching phenomena observed with a positively charged grid in the vapor stream are, however, not satisfactorily explained, although they are consistent with the hypothesis that fast electrons break up the molecules which carry the energy necessary to produce the afterglow. The large increase in the intensity of λ2537 accompanying the quenching suggests that the molecules are broken up into atoms in the 6^3P_{012} states, but the recovery of the glow beyond the quenched region is difficult to explain on this assumption. Adequate data are not yet available on this type of quenching.

With the methods of calculation developed by Mohler[19] the intensity distribution in the various spectral line series and the continua were examined for a possible correspondence with a Boltzmann distribution. No evidence of such a distribution was found in the line spectra. The intensity distribution in the continuum in the neighborhood of 2537A was found to correspond to a "temperature" of 1150°K as compared with the measured electron temperature of 1890°K.

The writers wish to express their thanks to Professor Harold W. Webb, who proposed this investigation, for his many suggestions and continued help throughout the work.

[18] Rayleigh, Proc. Roy. Soc. **A108**, 262 (1925).
[19] F. L. Mohler, Nat. Bur. Stand. Research Papers, R.P.901 and R.P.1036.

Zeeman Effect of the Forbidden Lines of Pb I

II. An Interference Effect in the Mixed Line, λ7330

F. A. JENKINS AND S. MROZOWSKI*
Department of Physics, University of California, Berkeley, California
(Received June 13, 1941)

The transverse Zeeman effect of this line, which contains mixed magnetic dipole and electric quadrupole radiation, is investigated with a Fabry-Perot interferometer, and with magnetic fields up to 4000 gauss. The pattern obtained, −2.68, −2.42, (−1.49), (−1.215), (−0.945), −0.255, 0, 0.255, (0.945), (1.215), (1.47), 2.42, 2.68, is in substantial agreement with expectations. Quantitative intensity measurements of all components are reported. In the σ pattern, the sum of the intensities of the four outer electric quadrupole components is found to be 0.02 of the three central magnetic dipole components. The relative intensities of the latter, 28, 45 and 27, and of the π components, agree with the theory developed in the following article by E. Gerjuoy, provided that the intensities contributed by the Zeeman components of the hyperfine structure are taken into account. These components are investigated at various magnetic fields, and the development of the Back-Goudsmit effect is verified. For the six π components, in the above order, the measured intensities at 3880 gauss are 22, 23, 7, 7, 18 and 23. Comparison with theory indicates 2.2 ± 0.5 percent of quadrupole radiation, and proves that interference exists between the two types of radiation.

THE preceding part of this paper[1] dealt with the Zeeman effect of three forbidden lines of lead, one of which was pure magnetic dipole radiation, and the others pure electric quadrupole radiation. In this part we wish to report on the effect in the stronger of the two remaining forbidden lines, λ7330 and λ9250. These are due to transitions from the $6p^2\ {}^1D_2$ state to $6p^2\ {}^3P_1$ and $6p^2\ {}^3P_2$, respectively. They are permitted by the selection rules for both magnetic dipole and electric quadrupole radiations, and hence may be called "mixed" lines. There are no existing data on the Zeeman effect of such lines, and, since it should have some interesting features, we have made a detailed investigation of the splittings and intensities in λ7330. A study of λ9250 was not undertaken, because its predicted splitting is only about $0.03\Delta\nu_n$, and extremely high fields would be required to separate the components by a distance greater than their Doppler width. It is probable that the pattern of this line cannot be resolved by using the techniques now known.

The interest in these forbidden lines of Pb I arises partly from the fact that they are the analogs of the forbidden lines coming from transitions within the p^2 configuration of light atoms which give rise to well-known lines in cosmic sources. Thus, λ7330 of Pb is like the strong green nebular line of O III called N_2, and also like the red nebular line λ6548. Condon[2] calculated that the N_2 line contains only 0.1 percent of quadrupole radiation, the rest being magnetic dipole. These forbidden lines of light ions would be difficult to observe in the laboratory, but in Pb I they are more intense, thanks to the breakdown of Russell-Saunders coupling. Furthermore, the quadrupole moment is relatively greater in this case, and the proportion of quadrupole radiation to magnetic dipole should be large enough to be measurable. An attempt to detect the pure quadrupole component in the hyperfine structure of λ7330 was made by Mrozowski[3] but was not successful. He estimated an upper limit of 9 percent for the proportion of quadrupole radiation in the line. He also made measurements of the relative intensities of all the observed lines. As is shown in the article by E. Gerjuoy,[4] these intensities lead to a value of slightly less than 5 percent quadrupole radiation. Since this result was unexpectedly low, as ex-

* Now at Ryerson Physical Laboratory, University of Chicago.

[1] F. A. Jenkins and S. Mrozowski, Phys. Rev. **59**, 808 (1941).

[2] E. U. Condon, Astrophys. J. **79**, 217 (1934).

[3] S. Mrozowski, Phys. Rev. **58**, 1086 (1940).

[4] E. Gerjuoy, Phys. Rev. **60**, 233 (1941), this issue.

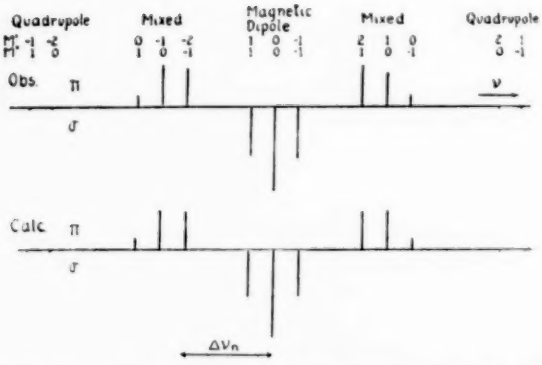

FIG. 1. Theoretical and observed Zeeman patterns for λ7330. Relative intensities are shown by the heights of the lines, and the calculated values are based on 2.0 percent of quadrupole radiation. The intensities of the two components of the outer pairs of quadrupole components were not measured separately, but only that of the pairs as a whole.

plained by Gerjuoy, we undertook a study of the Zeeman effect, which should provide a more accurate determination. Our final result, 2.2 ±0.5, is still lower, and this apparent discrepancy with theory is discussed in Gerjuoy's paper.

A feature of special interest in the Zeeman effect of this mixed line was the predicted interference between electric quadrupole and magnetic dipole radiation, which was first pointed out to us by Dr. L. I. Schiff. Using the theoretical equations derived by Gerjuoy in the accompanying paper, we have been able to prove definitely, for the first time, the existence of this effect. It is, perhaps, of interest to point out that of all forbidden lines now known, only this line λ7330 affords an opportunity of observing the interference effect.

EXPERIMENTAL

The spectrograms

A description of the discharge tube and of the spectrographic apparatus has been given in Part I. The special difficulties involved in the study of λ7330, chief among which is the presence of the strong allowed line λ7229, were pointed out in Mrozowski's paper[5] on the hyperfine structure. The temperature of the oven surrounding the tube had to be higher for maximum intensity of this line—slightly above 800°C—than for the other forbidden lines. It could be regulated quite accurately to the optimum value by raising it slowly until the helium lines had practically disappeared. In photographing the Zeeman effect of the hyperfine structure, no gain in intensity was obtained by using the ring electrodes around the ends of the tube because the Zeeman splittings of the hyperfine components are rather small, and higher fields had to be used than for the other lines. Eastman I-U plates, hypersensitized for only 30 seconds in a solution of 4 percent ammonia in 40 percent alcohol, were sufficiently sensitive and were quite free of fog. No trouble with non-uniformity of sensitization was experienced in the intensity measurements to be described below. Exposure times of from 25 to 90 minutes were required. The parallel (π) and perpendicular (σ) components were photographed separately, by the use of a Nicol prism immediately in front of the spectrograph slit.

The choice of Fabry-Perot etalon spacers and of magnetic fields was governed by several considerations, which will be explained with the aid of the complete Zeeman pattern shown in Fig. 1. The mixed components, which have parallel polarization, are the most interesting, since it is in these that we expect the interference effect. If this effect is present, their relative intensities should be strongly dependent on the proportion of quadrupole radiation present. Calculation showed that with the magnetic field available, 4000 gauss, these π components would not be resolved even by increasing the etalon spacer up to the maximum value possible with-

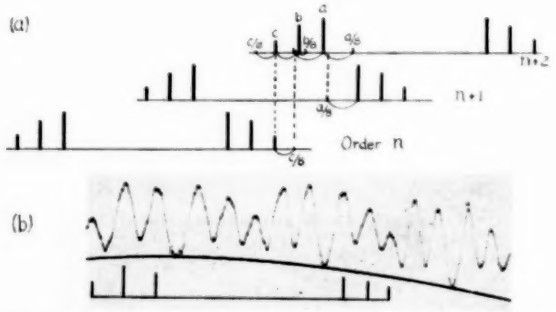

FIG. 2. (a) Diagram of the relative positions of the π components in three successive orders with magnetic field 3880 gauss and etalon spacer 19 mm. The weak components labeled $a/8$, etc., are from the hyperfine structure, and are explained later. (b) Microphotometer trace of a plate taken under these conditions. The π components in one order are indicated beneath the trace.

[5] Reference 3, p. 1091.

out overlapping of successive orders. This limitation is imposed not by the reflecting power of the etalon surfaces but by the Doppler width of the lines at the high temperature of the source. By further increasing the spacer until the triplets in each order cross over those in the next order, they were found to be well resolved. A diagram of the relative position of the lines under these conditions is given in Fig. 2. To facilitate the intensity measurements, it was found convenient to adjust the magnetic field to a value such that the outermost and weakest component in the pattern of one order was exactly superimposed on that in the next order but one, as indicated by the vertical broken line connecting the components c in Fig. 2. This yields a pattern consisting of groups of five lines of comparable intensity, a condition favorable for accurate intensity measurements. An enlargement of such a pattern is shown in the right-hand strip of Fig. 3. When the magnetic field was decreased somewhat, it was found that the pattern was still fairly well resolved, and here all six components in each order can be seen, as in the pattern for $H=3560$ of Fig. 3.

In photographing the σ components, two combinations of magnetic field and etalon spacer were found convenient. That used in obtaining the pattern in Fig. 3 gave ample resolution of the strong magnetic dipole triplet in the center of the pattern. However, it did not reveal the weak quadrupole components, the total intensity of which is only about 1 percent of the whole pattern. To observe these, we decreased the spacer to 7 mm and the magnetic field to 3025 gauss, so that the quadrupole components of one order were superimposed on those of the next order. This showed the components with sufficient intensity to be measurable, although they were not resolved into two separate lines under these conditions and only their total intensity could be found. Of course, any number of combinations of magnetic field and spacer could have been used to bring about this superposition. The combination given above was chosen because of the presence of a weak line at λ7346, which was too close to λ7330 to be separated by the auxiliary dispersion of the prism.[6] With the 7-mm spacer, the two σ components of this line were well separated from both the quadrupole and magnetic dipole components of λ7330, and did not interfere with the measurements.

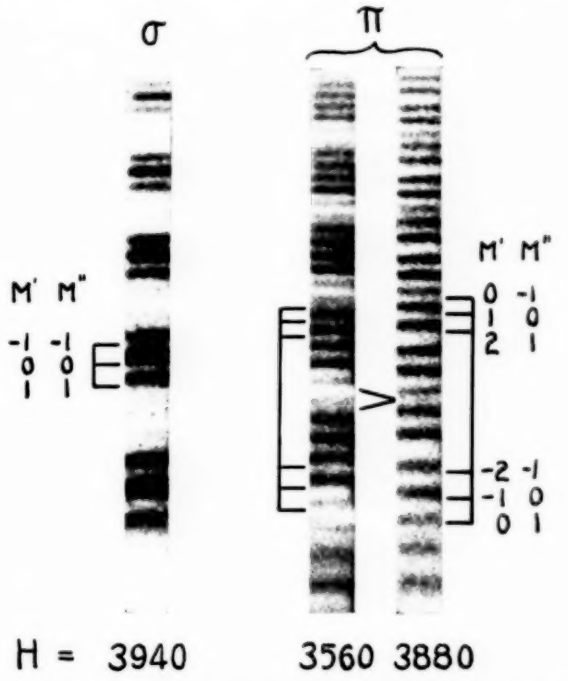

FIG. 3. Fabry-Perot patterns taken with an etalon spacer of 19 mm, and with the magnetic fields indicated. Exposures, 45 minutes each. In the σ components, two weak lines flanking the main triplet may be discernible. These are due to the hyperfine structure, as explained later. The main components belonging to one order are marked in each case.

Intensity measurements

All plates were calibrated with two sets of density marks, one above and one below the Fabry-Perot pattern. These were impressed by the use of a step-slit in the spectrograph, in the manner previously used by Mrozowski in his measurements of intensities in the hyperfine structure.[3] Photographic densities were determined by means of a Zeiss recording microphotometer, and were converted to intensities by means of a calibration curve for each plate.

Since the relative intensities of the mixed, or π components were of the greatest interest, considerable care was taken to get the best values

[6] This line was also observed by Mrozowski, reference 3, and may be seen in his Fig. 2 just below the long wavelength hyperfine component. We first assumed it to be the cadmium line $6^3S-7^3P_2$, arising from an impurity. Its Zeeman effect, however, does not confirm this assignment, since it yields an approximately normal triplet. The continued presence of the line after long running of the tube, which should eliminate the cadmium, indicates that it is a faint unclassified line of lead itself.

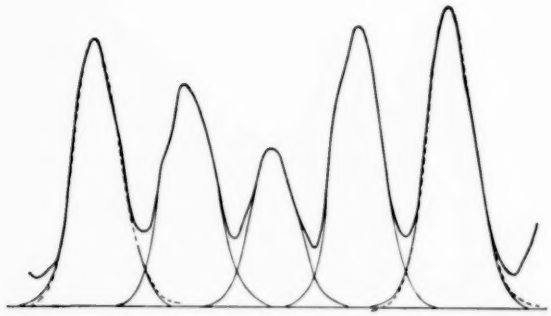

FIG. 4. Analysis of the intensity curves of the π components. The heavy curve is the experimental one, while the light ones give the analysis used. Broken curves on the extreme components are of the theoretical Doppler shape.

of these from the plates showing the "groups of five" referred to above. Two original plates were available, and for each of these two microphotometer curves were made, one for the three higher orders and one for the three lower ones, using a narrower slit in the latter case because the lines in the lower orders are narrower. The peak intensities and the corresponding values of the background, the latter being taken according to the black line on Fig. 2(b), were then evaluated. A curve of the variation of peak intensity with order was then used to find the factor by which the intensities in different orders should be multiplied to render them comparable. The values from the six orders were then averaged. Finally, the whole process was repeated with a new pair of microphotometer plates, and the result averaged with that from the first pair.

The above procedure of measuring the peaks and subtracting the apparent background is open to two objections, one of which requires a correction to the values obtained by its use. This concerns the true background, which might be appreciably lower than that indicated by a curve drawn through the lowest points on the microphotometer trace. A change in the assumed background is rather important for the relative intensities, because it is fairly large, amounting to between 30 and 50 percent of the total intensity at the stronger peaks.[7] The other question is whether the weakest components were exactly superimposed; for, if not, the peak intensity is obviously not a true measure of the sum of the two lines. Both of these matters were investigated by an analysis of the intensity curves in two different orders. The results for one of these are shown in Fig. 4. The heavy solid line is the experimental curve transformed to a linear scale of frequencies by the use of a parabolic formula. It also contains the correction for the variation of intensity with order. The two extreme components were fitted to empirical curves of the Doppler shape, and the bases of these taken as the true background. By subtraction, the curves for the other three components were then drawn (light solid lines). The areas of the five curves were then measured with a planimeter. The relative values of these areas were the same to within 2 percent as the peak intensities corrected by the new background. This was to be expected, because the half-widths of all the lines were very nearly the same, with an average value of 0.031 cm^{-1}. The theoretical Doppler half-width at 850°C is 0.023 cm^{-1} at this wave-length. The results of these analyses thus show that the superposition is sufficiently exact for peak intensities to be used, but that the apparent background must be reduced by 7 percent of the measured intensity of the strongest peaks. This correction was subsequently applied to all the peak measurements. Measurements of the peak intensities were also made on a plate taken with a smaller field ($H=3560$, Fig. 3), on which all six components were resolved. The resolution was still sufficient to obviate any correction for overlapping of adjacent lines, and here it could be assumed that the true background was measured by the lowest points of the microphotometer curves, between the weakest components.

The main triplet of the σ components was investigated in a similar manner. The analysis in one order is shown in Fig. 5. Here the fitting

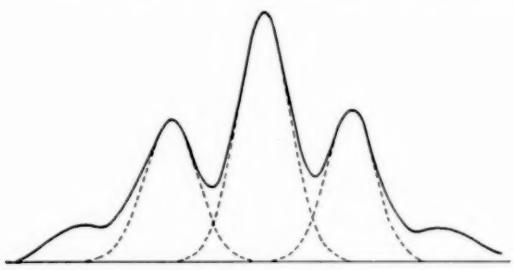

FIG. 5. Analysis of the intensity curves of the σ polarized magnetic dipole components in one order.

[7] For a discussion of the origin of this background, see reference 3, p. 1041. It is relatively more important in the present case, because of the fact that the main line is divided into several components.

TABLE I. *Observed and calculated separations in terms of* $\Delta\nu_n = 4.67 \times 10^{-5} H$.

POLARIZATION	σ	σ	π	π	π	σ	σ	σ	π	π	π	σ	σ
M'	1	2	0	1	2	−1	0	1	−2	−1	0	−2	−1
M''	−1	0	−1	0	1	−1	0	1	−1	0	1	0	1
Obs.	2.68	2.42	1.47	1.215	0.945	0.255	0	−0.255	−0.945	−1.215	−1.49	−2.42	−2.68
Calc.	2.73	2.46	1.50	1.23	0.96	0.27	0	−0.27	−0.96	−1.23	−1.50	−2.46	−2.73

by Doppler curves was made difficult by the presence of the weak lines on either side of the triplet. These belong to the hyperfine structure, as explained below. However, the curves show that peak intensities are equivalent to areas, and that no correction need be applied to the apparent background in this case. The results quoted in Table II below were obtained from two original plates, each of which was photometered only once.

The outer σ components were measured on three plates where they were superimposed in adjacent orders, as explained above. Their intensity relative to the central triplet was determined by integration, which here was essential because the triplet was not quite resolved. Since these quadrupole components are very weak, the measured intensity depends rather critically on the choice of the proper background. Nevertheless, the values obtained from the three plates were surprisingly consistent. A point of interest in connection with these plates was the half-width of the lines, which could be found from the unresolved main triplet where the intensities and separations of the lines were already known. The measured half-width, 0.030 cm^{-1}, turned out to be the same as on the plates taken with larger spacers. This shows clearly that the observed width is intrinsic in the lines themselves, and is not instrumental. If the latter were the case, the width would be a constant fraction of the order separation, and the present measurement would yield a wave number width almost three times as great as the previous ones.

RESULTS

Splitting of the main component

We measured the wave number separations and the magnetic fields by the methods described in Part I. The results are given in Table I, where the separations are expressed in terms of the normal splitting $\Delta\nu_n = 4.67 \times 10^{-5} H$. The table also includes values calculated from the known g factors of the levels,[8] namely $g(^1D_2) = 1.230$ and $g(^3P_1) = 1.269$. These factors were determined from the Zeeman effect of allowed lines involving the two levels.

As regards our observed values, it should be stated that those for the four inner π components (± 0.945, ± 1.215) were obtained under the assumption that their splitting is symmetrical about the no-field position. The outer π components, whose total splitting can be accurately found from the field required to overlap them, then appear to be slightly unsymmetrical. This can be seen in the enlargements, Fig. 3. Its probable explanation will be given below under the discussion of the intensities of the π components. A certain amount of arbitrariness is contained in our results for the outer σ components. As stated earlier, these were not observed as resolved pairs, and, in fact, could only be detected by overlapping them in adjacent orders. The results quoted were obtained by taking the observed splitting between the centers of gravity of the unresolved doublets, and by assuming the theoretical value 0.26 cm^{-1} for the doublet separation. All of our splittings are systematically a little smaller than those calculated from Back's g values, a fact which was noted and discussed in connection with the other lines in Part I.[9]

[8] E. Back, Zeits. f. Physik **37**, 193 (1926).

[9] At the time of writing Part I, we were unaware of the more recent work on the mercury lines by Green and Loring, Phys. Rev. **46**, 888 (1934). The g value 1.013 given by them for our calibrating line λ4916 agrees, within experimental error, with the one we adopted and requires no change in our field calibration. However, if one adopts their mean g value for $^1P_1$ from the two lines λ4916 and 5770, namely 1.019, perfect agreement would be obtained with the splittings predicted from Back's values. It is to be noted that the value 1.019 is in close agreement with Houston's equations and with some measurements on λ4916 made by Gehrcke. The anomaly in λ5790, mentioned in our footnote 8, Part I, is completely explained by Green and Loring.

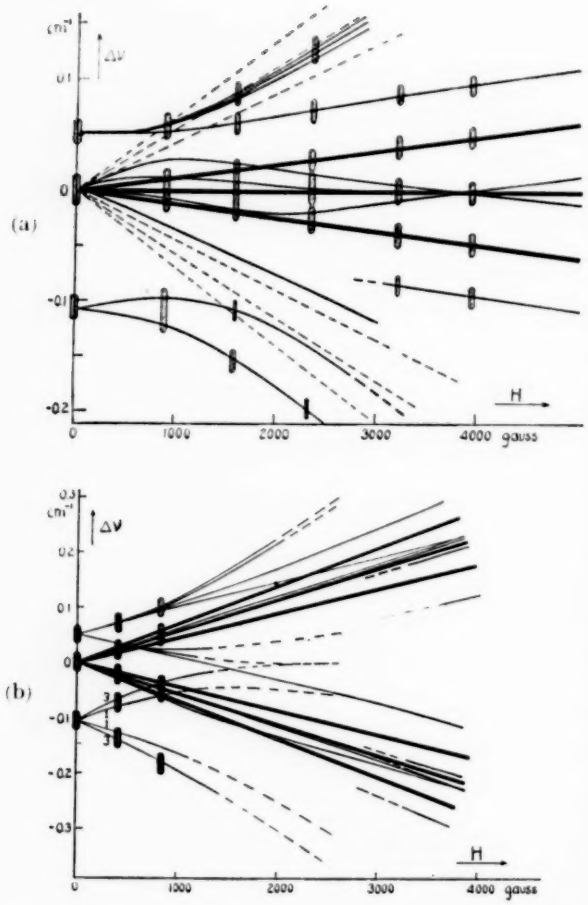

FIG. 6. Predicted and observed patterns for the Zeeman effect of the hyperfine structure. The heights and widths of the shaded marks indicate the approximate widths and intensities of the observed lines. (a) σ components. The three heavy lines show the positions of the magnetic dipole components of the main line. Broken lines show the positions of the main π components. (b) π components. The figure is extended to cover fields up to 4000 gauss although no direct observations of h.f.s. components were made above 1000 gauss, in order to show the origin of the lines which necessitate corrections to the intensities of the main components at high fields.

Zeeman effect of the hyperfine structure

Before we take up the important question of the intensities in the main Zeeman pattern, we must describe our results on the splitting of the three hyperfine-structure components, because these have an appreciable influence on the intensities in the main pattern. Figures 6(a) and (b) show, in the same manner as was used in Part I, the results on the σ and π components respectively of the hyperfine structure. In computing the predicted patterns, we used for the lower state the splittings of the line λ4618, described in Part I. For the upper state, $^1D_2$, a graphical interpolation between weak and strong fields was made. This is sufficiently accurate here because the hyperfine structure of the $^1D_2$ level is very narrow, and the Back-Goudsmit effect is almost complete at fields as low as 1000 gauss. The splittings of the lines were deduced from these two sets of levels. In the σ components of Fig. 6(a), only the magnetic dipole part has been included. The electric quadrupole part, $\Delta M = \pm 2$, would be exceedingly weak for these hyperfine components. In Fig. 6(b) the intensities for the weak field pattern of the low frequency h.f.s. component are given to indicate why we were not able to observe one of the components at $H \sim 900$ gauss. In the σ pattern, the weak field intensities do not play any role because, for the fields at which the lines are separated, the intensities are already distorted by the beginning of the Back-Goudsmit effect. In general, both splittings and intensities agree satisfactorily with theory. From the plots, one can see that at the fields for which we measured the intensities of the main components ($\sim$3900 gauss) the Back-Goudsmit effect of the hyperfine structure is practically complete. The h.f.s. components on either side of the magnetic dipole triplet may be seen in the curve of Fig. 5.

Intensities of the σ components

In the absence of hyperfine structure, the strong magnetic dipole triplet should have the intensities 3 : 4 : 3, as calculated from the usual electric dipole formulas (see Eqs. (7) of the article by Gerjuoy[4]). The observed values, given in Table II, show that the central component is relatively stronger than this. The reason is

TABLE II. *Intensities of magnetic dipole and electric quadrupole components.*

M.D. Components	Obs. Pl. 6	Obs. Pl. 7	Calc. No h.f.s.	Corrections h.f.s.	Corrections E.Q.	Calc. Corrected	Calc. Reduced
$-1 \rightarrow -1$	28	28	30	0	1	31	26
$0 \rightarrow 0$	46	45	40	17	0	57	48
$1 \rightarrow 1$	26	27	30	0	1	31	26
E.Q. Components	**Pl. 8**	**Pl. 9**	**Pl. 10**				
$1 \rightarrow -1$ $2 \rightarrow 0$ $-2 \rightarrow 0$ $-1 \rightarrow -1$	1.8	1.9	1.5	2.0		2.0	1.7

TABLE III. *Intensities of the π components.*

1.	2.	3.	4.	5.	6.	7.	8.	9.	10.	11.	12.	13.	14.	15.	16.
	OBS. ($H=3880$)		CALC. 2% E.Q.			CALC. (WITH CORR.)		CALC. (REDUCED)		OBS. ($H=3560$)		CALC. (WITH CORR.)		CALC. (REDUCED)	
MIXED COMPONENTS	Pl. 3	Pl. 4	INTERF.	NO INTERF.	h.f.s. CORR.	INTERF.	NO INTERF.	INTERF.	NO INTERF.	Pl. 5	h.f.s. CORR.	INTERF.	NO INTERF.	INTERF.	NO INTERF.
−2→−1	22	21	24	30	3	27	34	22	27	22	0	24	30	20	26
−1→ 0	23	23	18	15	9	27	24	22	19	24	8	26	23	22	19
0→ 1	14	14	16	10	0	16	10	13	8	7	1	9	6	8	5
0→−1										7	1	9	6	8	5
1→ 0	18	19	18	15	9	27	24	22	19	18	8	26	23	22	19
2→ 1	23	23	24	30	3	27	34	22	27	22	0	24	30	20	26

apparent from Fig. 6(a). At the magnetic field used, 3940 gauss, two lines of the hyperfine structure cross the central component, while the h.f.s. contributes nothing to the side components. The calculated values may be easily corrected for this, since we know the abundance of the 207 isotope (~ 20 percent). Using the dipole formulas for the intensities in the complete Back-Goudsmit effect, one obtains a 17 percent increase in the central component, as shown in Table II. There is also a slight correction to be made because of the overlapping of the outer components of the triplet by the weak electric quadrupole components belonging to the patterns of the main line two orders away on either side. The intensities of these are discussed in the following paragraph. When the two corrections are applied, and the resulting intensities reduced to a total of 100, the final calculated values compare favorably with the observations, as shown in the table. If anything, the correction for h.f.s. appears to be a little too large. The observed central component is not quite as strong as it should be, although much stronger than predicted without h.f.s. Possibly this is due to the Back-Goudsmit effect not being quite as complete as we have assumed it, although it must be nearly so because the symmetry of the five h.f.s. components is complete, as far as can be seen.

Table II also contains the results of three measurements of the electric quadrupole components from the plates where the two pairs from adjacent orders are superimposed. Since these four components together represent one-half of the total quadrupole radiation (the other half being in the mixed π components), the ratio of their total intensity to that of the magnetic dipole triplet, which contains half the magnetic dipole radiation, gives directly the proportion of quadrupole radiation in the line. If we assume 2.0 percent for this quantity, the observed ratio should be somewhat less, owing to the blending of the h.f.s. components with the magnetic dipole triplet. Thus we find 1.7 percent as a predicted value, and since this agrees exactly with the average observed value, these measurements indicate 2 percent of quadrupole radiation. This result is only approximate, for reasons discussed above under intensity measurements.

Intensities of the π components

These should give a more exact determination of the proportion of quadrupole radiation. Also of interest is the probable existence of the interference effect in such mixed components. The observed intensities are given in Table III, columns 2, 3, and 11, and shown graphically in Fig. 7, for the two cases $H=3880$ (groups of five) and $H=3560$ (groups of six). The calculated intensities, without correction for hyperfine structure, were obtained from Eqs. (7) of Gerjuoy's article. They are given both for the case where interference is assumed to occur, and for that where it is assumed absent. For the latter, Eqs. (7) are also used, merely omitting the terms linear in s_2. In Table III the value 2 percent of quadrupole radiation obtained above has been assumed, while Fig. 7 also includes the intensities for 5 percent quadrupole, the value

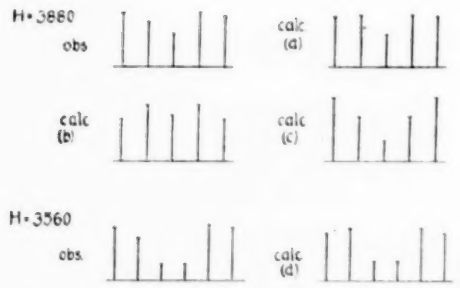

FIG. 7. Observed and computed intensities of the π components. For convenience, the lines are shown as they actually occur in the Fabry-Perot pattern, i.e., three components from each of two different orders. The observed intensities are shown with the weaker components superposed ($H=3880$) and separate ($H=3560$). The calculated values contain the correction for h.f.s. in all cases, and are obtained from the following assumptions: (a) 2 percent electric quadrupole radiation, with interference. $H=3880$. (b) 5 percent E.Q., with interference. (c) 2 percent E.Q., without interference. (d) 2 percent E.Q., with interference. $H=3560$.

obtained by Gerjuoy from Mrozowski's intensity measurements.

Before the calculated intensities in Table III, columns 4 and 5, can be compared with the observations, they must be corrected for the underlying components of the hyperfine structure. If we assume a complete Back-Goudsmit effect of the latter, each π component of the main pattern is accompanied by two hyperfine components at equal distances on either side. The sum of their intensities should be $\frac{1}{4}$ that of the main line, since the odd isotope 207 has an abundance of 20 percent. Let us call the three main components on either side of the center of the pattern, which should be symmetrical, a, b, and c in the order of decreasing intensity (Fig. 2). Using the known h.f.s. splittings in zero field,[3] we find that the satellites of a should be at a distance 0.061 cm^{-1}, of b at 0.0105 cm^{-1}, and of c at 0.040 cm^{-1}. For the case $H=3880$ this places them in the relative positions shown in the diagram of Fig. 2. From this diagram, one sees that the observed intensities for this case should be in the ratio

$$(a+a/8) : (b+a/8+2b/8+2c/8) : (2c).$$

The factor $\frac{1}{8}$ arises upon dividing the abundance ratio by two, for the two h.f.s. components. These corrections are listed in column 6 of Table III. Columns 7 and 8 give the corrected theoretical ratios, and in columns 9 and 10 they are reduced to a scale of 100 for comparison with the observed values in columns 2 and 3.

It will be seen that the agreement with column 9 is good, except for the component $1\rightarrow0$ which appears to be too weak. This observed asymmetry in the intensities, $1\rightarrow0$ being consistently weaker than $-1\rightarrow0$, cannot be explained by the h.f.s. if the Back-Goudsmit effect is taken to be complete, because then one must obtain a symmetrical pattern. If it is not quite complete, the component of intensity $a/8$ to the left of a in Fig. 2 would not be fused with b but would lie between b and c. In fact, there are definite indications of an extra line between these two components, as may be seen in the upper or high frequency triplet of Fig. 3 and in the microphotometer curves. It is probably responsible for the slight asymmetry of the measured splittings of components c that was mentioned above. By omitting the correction $a/8$ for the $1\rightarrow0$ component, its calculated intensity is changed from 22 to 19, and brought into agreement with experiment.

On the other hand, the values in column 10, calculated by assuming no interference, are in definite disagreement with the observations. Nor can they be made to agree by changing the assumed proportion of quadrupole radiation. For any proportion whatever, this theory would give intensities of the two stronger components in the ratio 2 : 1 if h.f.s. is neglected, and about 3 : 2 if h.f.s. is included. Our evidence for the existence of the interference effect is brought out most clearly in Fig. 7 by comparison of the observed intensities for $H=3880$ with those calculated in (a) with interference, and in (c) without it.

The results from the plate taken at the smaller magnetic field, Table III, columns 11 to 16, are of less accuracy because the resolution was not as complete. Here the corrections for h.f.s. come in somewhat differently, but were worked out by the method outlined above. The results bear out those from the other plates. It is especially gratifying that the components c, which are here measured separately, (column 11), are equal in intensity and are each equal to half the combined intensity previously measured (columns 2 and 3). This proves that there can be no serious error in the assumed value of the background.

Some discussion is necessary concerning the accuracy of our assumed value 2.0 for the percentage of quadrupole radiation. Gerjuoy's calculations using the earlier measurements of the relative intensities of the various forbidden lines had indicated a proportion of about 5 percent. This would give for $H=3880$ a group of five lines of comparable intensity, as in Fig. 7(b). The observed intensities require a figure definitely lower than this. A consideration of the way in which the intensities of these π components change with the percentage of quadrupole radiation assumed, and of the accuracy of the measured intensities, led us to conclude that the figure could not be altered by more than 0.3 percent without definite disagreement with experiment.[10] There is another possible source of error, however, in the presence of the weak line λ7346. In the parallel effect this gives a single component which should lie almost symmetrically in the gap between the "groups of five." The gap is not wide enough to see the line as separate, so probably it merely increases the observed background in this region. It is difficult to estimate the uncertainty due to this cause, since the relative intensity of the line changes rapidly with the temperature of the source, decreasing at higher temperatures. Measurements on one plate of the σ components at $H=3025$ gave an intensity relative to λ7330 as high as 7 percent, but it was probably less than this on the plates of the π components. If we decrease the assumed background by this amount, the lines become more nearly equal in intensity, but the estimated percentage of quadrupole is raised by only 0.4 percent. It appears necessary to take this uncertainty into account, and to raise our final estimate and its limit of error to 2.2 ± 0.5 percent. As will be shown in the article by E. Gerjuoy, this result is unexpectedly low. Nevertheless, the internal consistency of our results convinces us that there is no large error involved. Further discussion of our results in connection with the theoretical predictions will be found in Gerjuoy's article.

[10] This was the limit of error given in our preliminary report of the present work, Phys. Rev. **59**, 915A (1941).

AUGUST 1, 1941 PHYSICAL REVIEW VOLUME 60

Interference in the Zeeman Effect of Forbidden Lines

E. GERJUOY
Department of Physics, University of California, Berkeley, California

(Received June 13, 1941)

The Zeeman effect of forbidden lines involving simultaneous electric quadrupole and magnetic dipole radiation will exhibit interference between these two different modes of radiation. The predicted intensity of any Zeeman component includes, in general, a term dependent on the fact that both modes of radiation are possible, as well as the usual transition probabilities for independent electric quadrupole and magnetic dipole radiation. Such additional interference terms appear only in the Zeeman effect and not in total line intensities. Proofs of these assertions and formulas for the Zeeman intensities are developed. The latter are compared with observations of the Zeeman effect of the forbidden lines of the $6p^2$ configuration of Pb I, by Jenkins and Mrozowski. Good agreement with experiment is obtained only if interference is taken into account. Their observations on the Zeeman effect correspond to a somewhat smaller value of the quadrupole moment of the transition electron in Pb I than is computed from comparison of total line intensities. Both these values of the quadrupole moment of the transition electron are 100 percent or more smaller than that given by a rough estimate from screening constant data using hydrogenic wave functions and the known positions of the levels to evaluate the effective nuclear charge. In the absence of Hartree wave functions for Pb I, no better estimate seems possible. A brief discussion of the hyperfine structure of forbidden lines is included, in which it is shown that the rules for determining the relative intensities of electric dipole hyperfine multiplets also give the intensity ratios in the hyperfine structure of magnetic dipole lines.

THE forbidden lines resulting from transitions between levels of the $6p^2$ configuration of Pb I have recently been investigated by Mrozowski and Jenkins. Mrozowski[1] studied the hyperfine structure and relative intensities of the

[1] S. Mrozowski, Phys. Rev. **58**, 1086 (1940).

lines, while Jenkins and Mrozowski[2] have just completed an investigation of the Zeeman effect, including quantitative intensity measurements and the Zeeman effect of the hyperfine structure. Several of the lines of the p^2 configuration, and in particular the lines λ7330 and λ9250 of Pb I, involve simultaneous electric quadrupole and magnetic dipole radiation, and the Zeeman effect of such lines exhibits a new feature of interest, namely interference between the two different modes of radiation. That is, the predicted intensity of any Zeeman component is not, in general, to be found by simply summing the transition probabilities for independent electric quadrupole and magnetic dipole radiation, but must include a term dependent on the fact that both modes of radiation are possible. It is the primary purpose of this paper to derive the expressions for the intensities of the Zeeman components, and compare them with the actual observations of Jenkins and Mrozowski in Pb I. In addition, we shall briefly discuss several problems raised by Mrozowski in his earlier paper on the hyperfine structure and line intensities.[1]

The transition probability for interference radiation may be found by the usual correspondence theory formalism. If the radiation field is due to the presence of simultaneous magnetic dipole and electric quadrupole moments in an oscillating charge distribution of circular frequency ν, then, using the more convenient complex fields, we have at large distances[3]

$$\mathbf{E}=\mathbf{E}_m+\mathbf{E}_q, \qquad \mathbf{H}=\mathbf{H}_m+\mathbf{H}_q,$$

$$\mathbf{E}_m=-\frac{\nu^2}{c^2}(\boldsymbol{\beta}\times\mathbf{M}), \qquad \mathbf{E}_q=\frac{i\nu^3}{2c^3}\{\mathfrak{N}\cdot\boldsymbol{\beta}-(\boldsymbol{\beta}\cdot\mathfrak{N}\cdot\boldsymbol{\beta})\boldsymbol{\beta}\},$$

$$\mathbf{H}_m=\frac{\nu^2}{c^2}(\boldsymbol{\beta}\times\mathbf{M}\times\boldsymbol{\beta}), \qquad \mathbf{H}_q=\frac{i\nu^3}{2c^3}\boldsymbol{\beta}\times(\mathfrak{N}\cdot\boldsymbol{\beta})$$

with the Poynting vector

$$\mathbf{S}=\frac{c}{16\pi}(\mathbf{E}\times\mathbf{H}^*+\mathbf{E}^*\times\mathbf{H}).$$

$\mathfrak{N}$ and $\mathbf{M}$ are the electric quadrupole and magnetic dipole moments, respectively, $\boldsymbol{\beta}$ is the unit vector in the direction of propagation. We have omitted the usual $1/r$ dependence of the field intensities so that $\mathbf{S}$ gives the average radiation into a solid angle $d\Omega$ in the direction $\boldsymbol{\beta}$. The terms in which we are interested are the cross terms due to the presence of both moments, the other terms give the usual magnetic dipole and electric quadrupole radiation fields. That is, we evaluate that part of the Poynting vector which is

$$\mathbf{R}=\frac{c}{16\pi}(\mathbf{E}_q\times\mathbf{H}^*_m+\mathbf{E}_m\times\mathbf{H}^*_q+\mathbf{E}^*_q\times\mathbf{H}_m+\mathbf{E}^*_m\times\mathbf{H}_q).$$

On dividing the magnitude of $\mathbf{R}$ by $h\nu$ ($\mathbf{R}$ is, of course, a vector in the direction of $\boldsymbol{\beta}$) and substituting twice the proper matrix element for the classical moment we then find the transition probability $A_i(A, B)$ for the interference radiation into the solid angle $d\Omega$ in the direction $\boldsymbol{\beta}$ as the result of a transition between the levels A, B. By introducing the notation

$$(\gamma JM|\mathfrak{N}|\gamma'J'M')=e\mathbf{Q},$$

$$(\gamma JM|\mathbf{M}|\gamma'J'M')=\frac{eh}{2mc}(\gamma JM|\mathbf{L}+2\mathbf{S}|\gamma'J'M')=\frac{eh}{2mc}\mathbf{D},$$

$$\mathbf{Q}=\mathbf{Q}_1+i\mathbf{Q}_2, \quad \mathbf{D}=\mathbf{D}_1+i\mathbf{D}_2,$$

where $\mathbf{D}$ is measured in units of h, $\mathbf{Q}$ in units of a^2, a the Bohr radius, we find the transition probability $A_i(A, B)$ between two levels defined by the quantum numbers γJM and $\gamma'J'M'$ will be:

$$A_i(\gamma JM, \gamma'J'M')=\frac{\alpha^5\tau^{-1}\sigma^4}{64\pi}\{(\boldsymbol{\beta}\cdot\mathbf{Q}_1)\cdot(\mathbf{D}_2\times\boldsymbol{\beta})-(\boldsymbol{\beta}\cdot\mathbf{Q}_2)\cdot(\mathbf{D}_1\times\boldsymbol{\beta})\}d\Omega. \quad (1)$$

Here σ the wave number is measured in terms of the Rydberg constant, α is the fine-structure constant, and τ is the so-called Hartree unit of time, $\tau=\hbar^3m^{-1}e^{-4}$.

The expression (1) can actually be obtained with less computation from the quantum-mechanical formula for spontaneous emission (which furnishes a check of the correspondence principle method) but the development given here will probably be more familiar to most readers. The quantum-mechanical formulas also

[2] F. A. Jenkins and S. Mrozowski, Phys. Rev. **60**, 225 (1941), this issue.

[3] E. U. Condon and G. H. Shortley, *Theory of Atomic Spectra* (Cambridge University Press, 1935), p. 90 *et seq.* We shall refer to this book as *TAS*.

give most readily the probabilities of emission of quanta polarized along an arbitrary direction. It is convenient to have these probabilities and we shall write them down; they may be derived with a little more trouble by the correspondence methods. The transition probabilities for the emission of a quantum in the direction $\boldsymbol{\beta}$ with the electric vector polarized along $\boldsymbol{\omega}$ for the quadrupole, dipole, and interference radiations, turn out to be

$$\begin{aligned}
A_q^{\omega}(A,B)&=\frac{1}{4}\frac{\alpha^5\tau^{-1}\sigma^5}{64\pi}\{(\boldsymbol{\beta}\cdot\mathbf{Q}_1\cdot\boldsymbol{\omega})^2\\
&\qquad+(\boldsymbol{\beta}\cdot\mathbf{Q}_2\cdot\boldsymbol{\omega})^2\}d\Omega,\\
A_m^{\omega}(A,B)&=\frac{\alpha^5\tau^{-1}\sigma^3}{64\pi}\{(\mathbf{D}_1\times\boldsymbol{\beta}\cdot\boldsymbol{\omega})^2\\
&\qquad+(\mathbf{D}_2\times\boldsymbol{\beta}\cdot\boldsymbol{\omega})^2\}d\Omega,\\
A_i^{\omega}(A,B)&=\frac{\alpha^5\tau^{-1}\sigma^4}{64\pi}\{(\boldsymbol{\beta}\cdot\mathbf{Q}_1\cdot\boldsymbol{\omega})(\mathbf{D}_2\times\boldsymbol{\beta}\cdot\boldsymbol{\omega})\\
&\qquad-(\boldsymbol{\beta}\cdot\mathbf{Q}_2\cdot\boldsymbol{\omega})(\mathbf{D}_1\times\boldsymbol{\beta}\cdot\boldsymbol{\omega})\}d\Omega.
\end{aligned}\tag{2}$$

That is, $A_q(A,B)$ and $A_m(A,B)$ are simply the usual transition probabilities for the emission of electric quadrupole and magnetic dipole radiation, respectively, and the actual intensity of any Zeeman component will be the sum $A_q+A_m+A_i$. To evaluate explicitly for any transition we must insert in (2) the actual values of $\mathbf{D}_1$, $\mathbf{D}_2$, $\mathbf{Q}_1$, $\mathbf{Q}_2$, which are matrix elements and depend on the quantum numbers of the levels between which the transition is taking place. For convenience in writing formulas, we are not indicating the explicit dependence of $\mathbf{D}$ and $\mathbf{Q}$, which must, however, be kept in mind. The vectorial character of $\mathbf{D}$ and the dyadic character of $\mathbf{Q}$ depends only on the change in magnetic quantum number for the particular transition in question.

$$\begin{aligned}
\Delta M=0\quad&\mathbf{D}=\mathbf{D}_1+i\mathbf{D}_2=d(0)\mathbf{k}\\
&\mathbf{Q}=\mathbf{Q}_1+i\mathbf{Q}_2=q(0)(\tfrac{2}{3})^{\frac{1}{2}}(\mathbf{kk}-\tfrac{1}{2}\mathbf{ii}-\tfrac{1}{2}\mathbf{jj}),\\
\Delta M=\pm1\quad&\mathbf{D}=\frac{1}{\sqrt{2}}d(\pm1)(\mathbf{i}\pm i\mathbf{j})\\
&\mathbf{Q}=q(\pm1)\tfrac{1}{2}[\mathbf{ki}+\mathbf{ik}\pm i(\mathbf{kj}+\mathbf{jk})],\\
\Delta M=\pm2\quad&\mathbf{D}=0\\
&\mathbf{Q}=q(\pm2)\tfrac{1}{2}[\mathbf{ii}-\mathbf{jj}\pm i(\mathbf{ij}+\mathbf{ji})].
\end{aligned}$$

The q's and d's are readily expressible in terms of the notation of *TAS*.[4] For any pair of levels the q's or d's are products $\chi(J)\theta(M,J)$, the second factor giving the usual M dependence and the $\chi(J)$ the appropriate D, E, F for quadrupole, or $(\gamma J\vdots M\vdots\gamma' J')$ for magnetic dipole, in the notation of *TAS*, with, of course, the necessary factors to take care of the change in units. Thus, for example, for a transition (γJM) to $(\gamma' J-1M\pm1)$

$$eq(\pm1)=\tfrac{1}{2}E(J\pm2M+1)[(J\mp M)(J\mp M-1)]^{\frac{1}{2}}.$$

We now immediately obtain the transition probabilities for the three modes of radiation for the separate Zeeman components. β_3 is the component of $\boldsymbol{\beta}$ along the magnetic field, which is parallel to the z axis.

Magnetic dipole:

$$\begin{aligned}
\Delta M=0\quad&A_m(A,B)=\frac{3}{8\pi}\sigma^3T_0d(0)^2(1-\beta_3^2)d\Omega,\\
\Delta M=\pm1\quad&A_m(A,B)=\frac{3}{16\pi}\sigma^3T_0d(\pm1)^2(1+\beta_3^2)d\Omega.
\end{aligned}$$

Electric quadrupole

$$\begin{aligned}
\Delta M=0\quad&A_q(A,B)=\frac{9}{64\pi}\sigma^5T_0q(0)^2(1-\beta_3^2)\beta_3^2d\Omega,\\
\Delta M=\pm1\quad&A_q(A,B)=\frac{3}{128\pi}\sigma^5T_0q(\pm1)^2\\
&\qquad\times(1-3\beta_3^2+4\beta_3^4)d\Omega,\\
\Delta M=\pm2\quad&A_q(A,B)=\frac{3}{128\pi}\sigma^5T_0q(\pm2)^2\\
&\qquad\times(1-\beta_3^2)(1+\beta_3^2)d\Omega.
\end{aligned}\tag{3}$$

Interference:

$$\begin{aligned}
\Delta M=0,\pm2\quad&A_i(A,B)=0,\\
\Delta M=\pm1\quad&A_i(A,B)=\pm\frac{3}{16\pi}\frac{\sigma^4}{\sqrt{2}}T_0d(\pm1)\\
&\qquad\times q(\pm1)(3\beta_3^2-1)d\Omega,\\
&T_0=\alpha^5\tau^{-1}/24.
\end{aligned}$$

The d's and q's are not necessarily real quantities, but will actually be real for all spectro-

[4] pp. 63 and 95.

scopic applications. This is because the form of the atomic Hamiltonian is such that the radial eigenfunctions and off-diagonal elements of the central field approximation are real (with the proper choice of phases, of course, but the formulas are always independent of relative phases of the eigenfunctions), and, therefore, the only possible imaginary parts come from the angle integrations, which have been taken into account. For this reason we have not bothered to put absolute value signs into the formulas (3). The vanishing of the interference term for $\Delta M=0$ is not however contingent on $\mathbf{D}_2$ and $\mathbf{Q}_2$ being zero in (1), but is simply due to the fact that $\boldsymbol{\beta}\cdot\mathbf{Q}$ is a vector in the plane of $\boldsymbol{\beta}$ and $\mathbf{k}$ and therefore perpendicular to $\mathbf{D}\times\boldsymbol{\beta}$. From (2) we readily discover that for $\Delta M=0$ the quadrupole radiation is always plane polarized with its electric vector in the plane of $\boldsymbol{\beta}$ and the magnetic field, whereas the magnetic dipole radiation is polarized perpendicular to that plane. The vanishing of the interference terms for these transitions is thus simply an expression of the fact that radiations polarized in perpendicular planes will not interfere.

Similarly, in the direction of observation perpendicular to the magnetic field, where the interfering components $\Delta M=\pm 1$ are plane polarized, they are polarized in the same plane, namely with the electric vector parallel to the magnetic field.

By inserting the M dependence of $d(\pm 1)$ and $q(\pm 1)$ in (3) and summing over all M, M', for the separate cases $J-J'=0,\ \pm 1,\ \pm 2$, it is possible to prove directly, though rather tediously, that the sum of the interference terms over all Zeeman components will be zero in any direction, thereby justifying the addition of A_m and A_q for ordinary line intensities. In other words the interference can only be observed in the Zeeman effect, the intensity of any line as a whole will simply be the sum of the separately computed magnetic dipole and electric quadrupole intensities. This conclusion is again valid for complex d's and q's which merely insert absolute value signs and the cosine of a phase difference in (3). We may, however, note more simply that the integral of $(3\beta_3^2-1)$ over all angles is zero. The interference term does not change the total transition probability between any two levels, it merely changes the angular distribution of the radiation. The total radiation, summed over M and M', must, of course, be spherically symmetric, and the independent electric quadrupole and magnetic dipole terms are also spherically symmetric when summed over M and M'. Therefore, it follows that the sum of the interference terms over all Zeeman components must be zero in any direction, since the sum must be the same over all directions by the requirement of spherical symmetry, and the integrated intensity of any interference term over all angles is zero. The way in which the vanishing of the integral of the interference term over all angles comes about can be readily seen from (2). $\mathbf{Q}$ is a symmetric dyad and $\mathbf{D}$ a vector. The interchange of $\boldsymbol{\beta}$ and $\boldsymbol{\omega}$ in (2) changes the sign of $A_i^{\omega}(A, B)$. The contributions from directions with interchanged polarization and propagation vectors cancel out.

Without any desire to belabor the point we may mention that, from the general expansion of the radiation into multipole orders, it can be shown quite generally that the line strengths from different multipoles will not interfere, but for low multipole orders such as quadrupole and dipole, the elementary methods of this paper are much simpler. In conclusion, the intensities at any angle are most conveniently found from (3) by re-expressing the d's and q's in terms of the line strengths. We shall do this for Pb I. The sign of the interference term in the $\Delta M=\pm 1$ transitions is, of course, crucial. The correct sign will, however, follow naturally from our formulas; and rules for determining the sign have been stated concisely by Shortley and his collaborators.[5]

Comparison with Experiment in Pb I

The $6p^2$ configuration and some of the data for Pb I as given by Mrozowski[1] are summarized

[5] These conclusions on the Zeeman effect of mixed lines have been arrived at independently by G. H. Shortley, L. H. Aller, J. G. Baker, and D. H. Menzel, Astrophys. J. **93**, 178 (1941), in connection with their tabulations of the strengths of forbidden lines as a function of coupling. They start from the Dirac radiation theory and give the relative intensities at arbitrary angle with the magnetic field of the π and σ components of those Zeeman lines showing interference. These expressions can be readily obtained from our formulas (2). As the only experiments, in Pb I, have been carried out perpendicular to the magnetic field, where the polarizations are plane, it has been sufficient for our purposes to give only the formulas (3) which are nothing more than (2) summed over the two independent directions of polarization.

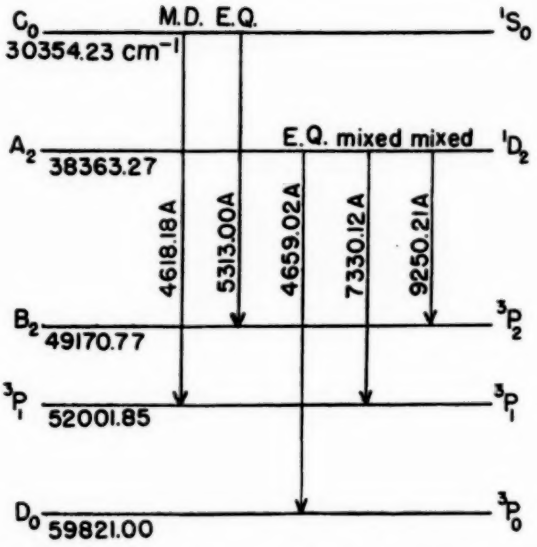

FIG. 1. The lowest levels of Pb I all belonging to the $6s^26p^2$ configuration. Arrows show the transitions giving the forbidden lines investigated. M.D. = magnetic dipole, E. Q. = electric quadrupole.

in Fig. 1. In the past year several papers have appeared giving general formulas and methods for the calculation of the intensities of forbidden lines in intermediate coupling.[6] It will therefore be sufficient merely to write down the formulas for the line intensities. The line strengths, quadrupole:

$$\begin{aligned}
S_q(A_2\,{}^3P_1) &= {}^9\!/_{15}b^2s_2^2,\\
S_q(A_2B_2) &= {}^{63}\!/_{15}a^2b^2s_2^2,\\
S_q(A_2D_0) &= {}^{16}\!/_{15}(ad+{}^1\!/_2bc)^2s_2^2,\\
S_q(B_2D_0) &= {}^{16}\!/_{15}(bd-{}^1\!/_2ac)^2s_2^2,\\
S_q(C_0B_2) &= {}^{16}\!/_{15}(bc+{}^1\!/_2ad)^2s_2^2,
\end{aligned} \tag{4}$$

magnetic dipole:

$$\begin{aligned}
S_m(A_2\,{}^3P_1) &= {}^5\!/_2b^2,\\
S_m(A_2B_2) &= {}^{15}\!/_2a^2b^2,\\
S_m(C_0\,{}^3P_1) &= 2d^2.
\end{aligned}$$

The lines are labeled as on the left of Fig. 1, with the approximate Russell-Saunders labeling on the right. The constant a, b, c, d measure the departure from Russell-Saunders coupling and define the actual wave functions ψ for the various levels in terms of the Russell-Saunders eigenfunctions φ. s_2 is the radial integral

$$s_2=\int_0^\infty r^2R^2(6p)dr.$$

The wave functions ψ are:

$$\begin{aligned}
\psi(A_2) &= a\varphi(^1D_2)+b\varphi(^3P_2),\\
\psi(B_2) &= -b\varphi(^1D_2)+a\varphi(^3P_2),\\
\psi(C_0) &= c\varphi(^1S_0)+d\varphi(^3P_0),\\
\psi(D_0) &= -d\varphi(^1S_0)+c\varphi(^3P_0).
\end{aligned} \tag{5}$$

With s_2 measured in units of the Bohr radius squared, the transition probabilities in terms of the line strengths are:
quadrupole:

$$A_q(A,B)=\frac{3}{40}T_0\frac{\sigma^5}{2J_A+1}S_q(A,B),$$

magnetic dipole:

$$A_m(A,B)=T_0\frac{\sigma^3}{2J_A+1}S_m(A,B). \tag{6}$$

Jenkins and Mrozowski[2] studied the Zeeman effect of the line $(A_2\,{}^3P_1)$, λ7330. From the formulas (3) and the line strengths we can write the transition probabilities for the various components in terms of s_2:

M	M'	Transverse to magnetic field
2	1	$G_0(3.85s_2^2\times10^{-5}+0.25-6.2\times10^{-3}s_2)$
1	0	$G_0(1.93s_2^2\times10^{-5}+0.125+3.1\times10^{-3}s_2)$
0	1	$G_0(5.8s_2^2\times10^{-5}+0.0416+3.1\times10^{-3}s_2)$
2	0	$G_0(7.7s_2^2\times10^{-5})$
1	−1	$G_0(3.85s_2^2\times10^{-5})$
1	1	$G_0(0.25)$
0	0	$G_0(0.33)$
		Parallel to magnetic field
2	1	$G_0(7.7s_2^2\times10^{-5}+0.5+12.4\times10^{-3}s_2)$
1	0	$G_0(3.85s_2^2\times10^{-5}+0.25-6.2\times10^{-3}s_2)$
0	1	$G_0(11.6s_2^2\times10^{-5}+0.083-6.2\times10^{-3}s_2)$

$$G_0=3b^2\sigma^3T_0/8\pi. \tag{7}$$

The transitions are symmetric, $M\to M'=-M\to-M'$.

It is seen that the intensities of the $\Delta M=\pm1$ transitions are quite sensitive to the value of s_2.

[6] G. H. Shortley, L. H. Aller, J. G. Baker, and D. H. Menzel, Astrophys. J. **93**, 178 (1941); G. H. Shortley, Phys. Rev. **57**, 225 (1940); S. Pasternack, Astrophys. J. **92**, 129 (1940).

The experiments were only performed transverse to the magnetic field. In Tables II and III of reference 2 are summarized the observed data, the expected intensities from (7), the intensities without interference, and the theoretical intensities corrected for the influence of hyperfine structure. s_2 is determined by the percentage quadrupole, defined as the ratio of electric quadrupole to magnetic dipole intensity in λ7330. Jenkins and Mrozowski obtain good agreement with (7) with the assumption of 2 percent quadrupole, with an upper limit of 2.6 percent.

It is interesting to compare the value of s_2 obtained from these Zeeman measurements with that deduced from Mrozowski's direct comparison of total line intensities. The coefficients a, b, c, d in (5) are calculated by diagonalizing the spin-orbit matrix and then fitting to the energy levels. The necessary values of the parameters may be obtained from Robinson and Shortley.[7] They are $F_2=921$ cm^{-1}, $\zeta=7290$ cm^{-1} and the coefficients, line strengths, and transition probabilities then have the values,[8] obtained from formulas (4) and (6).

$$a=0.756, \quad b=0.654, \quad c=0.927, \quad d=-0.375.$$

Quadrupole:

$$\begin{aligned}
S_q(A_2\,{}^3P_1)&=0.257s_2^2\\
S_q(A_2B_2)&=1.025s_2^2\\
S_q(A_2D_0)&=0.000897s_2^2\\
S_q(B_2D_0)&=0.369s_2^2\\
S_q(C_0B_2)&=0.229s_2^2\\
A_q(A_2\,{}^3P_1)&=1.133\times10^{-7}\,T_0s_2^2\\
A_q(A_2B_2)&=1.418\times10^{-7}T_0s_2^2\\
A_q(A_2D_0)&=3.902\times10^{-9}\,T_0s_2^2\\
A_q(B_2D_0)&=0.4754\times10^{-7}\,T_0s_2^2\\
A_q(C_0B_2)&=25.08\times10^{-7}\,T_0s_2^2
\end{aligned} \tag{8}$$

Magnetic Dipole:

$$\begin{aligned}
S_m(A_2\,{}^3P_1)&=1.83\\
S_m(A_2B_2)&=1.07\\
S_m(C_0\,{}^3P_1)&=0.281\\
A_m(A_2\,{}^3P_1)&=4.087\times10^{-4}\,T_0\\
A_m(A_2B_2)&=3.484\times10^{-4}\,T_0\\
A_m(C_0\,{}^3P_1)&=21.47\times10^{-4}\,T_0.
\end{aligned}$$

The observed intensity ratios are: $I_{4618}:I_{5313}=5.0\pm0.3$, $I_{4659}:I_{7330}:I_{9250}=0.023\pm0.006:1:0.84\pm0.07$.[9] Comparing the observed intensities of λ4618 and λ5313 with the formulas (8) gives $s_2^2=171$, corresponding to 4.76 percent quadrupole, which will not fit the Zeeman data at all. It is not possible to make any further comparisons. The ratio of the intensities of λ7330 and λ9250 is practically independent of s_2^2. Thus with 4.75 percent quadrupole, I_{7330}/I_{9250} is 0.87, which is no more gratifying a fit of the observed data than 0.85, the ratio to be expected if there were no quadrupole present at all. On the other hand, the theoretical prediction of very low intensity for λ4659, less than 0.002 compared to I_{7330} with $s_2^2=171$, is essentially accidental. It simply arises from the fact that with the parameters of Robinson and Shortley, the value of $ad+\frac{1}{2}bc$ is 0.019. This, when squared, cuts down sharply the value of the transition probability. These parameter values differ slightly from those obtained from a least square fit to the observed energy levels, which, in turn, do not fit to better than two percent. a, b, c, d cannot, therefore, be considered known to better than two percent. A two percent change in the coefficients can multiply $ad+\frac{1}{2}bc$ by a factor of three and the transition probability by a factor of nine, which is enough to bring the theoretical intensity within the experimental error, when 5 percent quadrupole is used. The change in the coefficients is, of course, to be accompanied by the inclusion of terms from other configurations, to whose action is to be ascribed the lack of fit of the energy levels. These configuration interaction terms will contribute to the intensity through cross terms with the ground configuration, and it does not seem at all unlikely that the transition probability could be increased by another factor of three, which would bring it well within the observed value for 2 percent quadrupole.

Actually, the disparities between the Zeeman measurements and Mrozowski's values for the line intensities need not be taken too seriously. As may be seen from (7), the relative intensities

[7] H. A. Robinson and G. H. Shortley, Phys. Rev. **52**, 713 (1937).

[8] The coefficients and line strengths may also be calculated from the tables of reference 5, and lead to values for the transition probabilities differing very slightly from our own.

[9] We may add that Mrozowski also measured the ratio I_{5313}/I_{4659}, this ratio varying between 15 and 12, corresponding to having level A_2 occupied a little more than 3 times as frequently as level C_0.

of the Zeeman components of λ7330 are independent of the coupling, so that the Zeeman measurements furnish a more unambiguous determination of the integral s_2 than is possible from the comparison of line intensities. It is also probable that, despite the reduced intensities, the measurements of the Zeeman effect are capable of less experimental error than the observations on the multiplet structure. In the spectrum of a heavy element like Pb I, where the coupling is almost *jj*, the fine-structure lines occur in widely separated portions of the spectrum, and the computation of actual intensities from observed plate intensities requires difficult corrections for the variation of plate sensitivity. The sensitive dependence of the Zeeman intensities on s_2 and the good agreement for 2 percent quadrupole would seem to indicate that, despite the complicating hyperfine structure, the Zeeman effect does give a good value for

$$s_2=\int_0^\infty r^2R^2(6p)dr \text{ in Pb I.}$$

This value may now be compared with estimates of the integral using hydrogenic wave functions with approximate screening constants as determined from Robinson and Shortley.[7] As Hartree fields have not yet been calculated for the $6s^26p^2$ configuration, this is the only procedure possible. 2 percent and 4.75 percent quadrupole correspond, always using hydrogenic wave functions, to effective charges of about 20 and 15, and values of s_2 of about 13 and 8. If we use the short isoelectronic sequence Pb I, Bi II to determine the slopes for the variation of F_2 and ζ, as in reference 7, we obtain, for both F_2 and ζ, effective charges of about 4, with $s_2\sim180$. The slope of the hydrogen-like formula for F_2 is a slowly varying function of $1/n^2$ as may be seen from Pasternack's equations,[10] and if we extrapolate to $n=6$, we obtain the effective charge $Z\sim12$, $s_2\sim22$. The acceptance of either experimental value for s_2 forces us to conclude that using screening constants and hydrogenic wave functions gives much too large an estimate of the quadrupole moment of the transition electron in Pb I. This confirms a trend, noted by Pasternack,[10] that estimates of s_2 from screening constant data are always larger than more accurate evaluations with, for example, Hartree wave functions. Two percent quadrupole, $Z\sim20$, corresponds, however, to a rather more tightly bound and penetrating electron than we expect, and a more accurate way of estimating s_2 at this time would certainly be welcome. In addition, it might be worth while measuring the Zeeman effect parallel to the magnetic field, where the change in intensity as a result of interference is exactly opposite to that observed in transverse measurements.

[10] S. Pasternack, Astrophys. J. **92**, 129 (1940). See pp. 144 and 145.

Hyperfine Structure of Magnetic Dipole Lines

It is well known that the relative intensities of the components of an electric dipole line in hyperfine structure can be found from the usual theory of Russell-Saunders multiplet intensities by merely replacing the quantum numbers *L*, *S*, and *J*, by *J*, *I*, and *F*, and it is clear that the same correlations in the Rubinowicz formulas will give the correct intensities for the hyperfine structure of electric quadrupole lines. It does not seem to have been pointed out, however, that the intensity ratios in the hyperfine structure of a magnetic dipole line will be the same as in an electric dipole line with the same correlations. Mrozowski noted the applicability of the intensity rules for electric dipole hyperfine multiplets to magnetic dipole multiplets in Pb I, and using these rules for the study of the mixed line λ7330, was able to conclude that the percentage quadrupole was less than about 10 percent. He also remarked that the applicability of the rules needed some theoretical clarification.

The reason may be stated quite simply. The intensity ratios in electric dipole radiation are determined completely by the commutation rules between the operators **J**, **I**, and **F**, and the electric dipole moment **P**. In particular, since **P** commutes with **I** and satisfies the usual commutation rule $[\mathbf{J},\mathbf{P}]=-ih\mathbf{P}\times\mathbf{E}$, $\mathbf{E}=\mathbf{ii}+\mathbf{jj}+\mathbf{kk}$, with respect to **J**, which are exactly the commutation laws for **P** with **S** and **L**, the electric dipole hyperfine intensities are evaluated from the usual Russell-Saunders fine-structure formulas with the correlations given. Now for magnetic dipole radiation we must evaluate the matrix

elements of

$$\frac{eh}{2mc}(\mathbf{L}+2\mathbf{S})+\frac{eg_N h}{2Mc}\mathbf{I}=\mathbf{M}+\frac{eg_N h}{2Mc}\mathbf{I}$$

for the various components of the multiplet, and with the assumption that the levels are not mixed by the nuclear interaction, that is, with the assumption that J remains a good quantum number and the Russell-Saunders formulas are applicable, all the matrix elements $(\gamma JFM|\mathbf{I}|\gamma' J'F'M')$ vanish. This is because $\mathbf{I}$ commutes with $\mathbf{J}$ and the wave functions ψ in (5) have been chosen orthogonal for the different levels of the configuration. Therefore, all the contribution to the intensities comes from the matrix elements of $\mathbf{M}$, and since $\mathbf{M}$ commutes with $\mathbf{I}$ and satisfies the same commutation rule with respect to $\mathbf{J}$ as does $\mathbf{P}$, the intensity ratios for magnetic dipole radiation in hyperfine structure will be the same as for electric dipole radiation. It is readily seen that the inclusion of terms in the wave functions due to the mixing by the nuclear interaction will, by first-order perturbation theory, give an error of order of magnitude of the ratio of hyperfine- to fine-structure splitting in the intensities as predicted from the Russell-Saunders formulas. This conclusion is valid for both electric quadrupole and magnetic dipole radiation, as well as for light elements or for small values of b and d defined by (5). That is, the conclusion is not affected by the fact that the forbidden lines themselves only arise as a result of small departures from Russell-Saunders coupling. The effects of perturbations by terms from other configurations may also be neglected. The interaction with the nucleus cannot connect states of opposite parity and it is, therefore, not possible to introduce a term which, though present in small amount, could, by permitting electric dipole transitions, considerably affect the intensities. This explains the failure of Mrozowski to observe the line (C_0D_0), which could become permitted for magnetic dipole transitions through coupling of the ground state with the $^3P_1$ level, in some analogy with the Hg I line λ2665.8. The ratio of hyperfine to fine structure splitting is almost 10^{-5} which would make the intensity of (C_0D_0) at most 10^{-8} the intensity of λ4618.

I wish to thank Professor J. R. Oppenheimer, Dr. L. I. Schiff, and especially Dr. J. Schwinger, for their cooperation and advice during the course of this investigation. I am indebted to Professors F. A. Jenkins and S. Mrozowski for many stimulating discussions and for their kindness in letting me have their data in advance of publication.

Paramagnetic Dispersion Measurements at 77.3°K*

C. STARR
Massachusetts Institute of Technology, Cambridge, Massachusetts
(Received June 7, 1941)

The dispersion of the magnetic susceptibility of some paramagnetic compounds of Fe, Mn, and Cr, was studied at 77.3°K over a frequency range of 2 to 10 megacycles/sec. with magnetic fields up to 60,000 gauss. The results substantiate the theory of Casimir and du Pre, which is based upon the thermal coupling between the magnetic spin system and the lattice vibrations. The magnitude of the crystalline field splitting of the energy levels of the ground state was determined from the experimental results, for an assumed type of crystalline field and ionic arrangement. The splitting of chromic ammonium alum was found to differ from that of chromic potassium alum. The relaxation time for ferric ammonium alum was studied as a function of the magnetic field, and was found to fit an empirical formula which is based upon the theoretical conclusions of Van Vleck.

INTRODUCTION

THE dispersion of the magnetic susceptibility of some paramagnetic compounds in an alternating magnetic field was discovered by Gorter in 1936. Subsequent experimental work by Gorter, Brons, Teunissen, and others,[1,2] on the frequency dependence of the susceptibility, and the associated energy absorption has clarified the nature of the phenomenon. They have shown that the dynamic susceptibility of paramagnetic compounds in an alternating magnetic field can be approximately described as a function of frequency by a simple dispersion formula, characterized by a relaxation time which is increased by a decrease of temperature or by the application of a constant parallel magnetic field. When a constant magnetic field is not present, the dispersion apparently disappears, and the dynamic susceptibility is the same as the static susceptibility determined by the customary static force methods. At the temperature of boiling N_2 (77.3°K) and above, the dispersion has been found in the radiofrequency range. Because the volume susceptibility of paramagnetics at these temperatures is small ($<10^{-3}$) a beat frequency method was used to study the dispersion. The energy absorption was determined by calorimetric methods. At the temperature of liquid helium (1°–4°K), the phenomenon has been studied by de Haas and du Pre[3,4] and the dispersion range was found to be less than 60 cycles/sec. Since the volume susceptibility at liquid-helium temperatures is quite large, a.c. bridge technique was used. The frequency dependence of the susceptibility and the energy absorption was determined directly from the bridge balance.

A thermodynamic explanation of paramagnetic dispersion has been presented by Casimir and du Pre[5] and has been generalized by others.[6] A thermal coupling between the magnetic spin system and the crystal lattice is assumed to exist. An applied magnetic field directly influences the energy (and thus the temperature) of the spin system only. In an alternating magnetic field the energy flows into and out of the spin system in a manner determined by the specific heats of the spin system and the crystal lattice, and the thermal conductance between the two. At temperatures where the lattice specific heat is large, the dynamic susceptibility at very high frequencies is effectively that of an adiabatic spin system, and at very low frequencies is that of an isothermal spin system. The nature of the thermal conductance mechanism between the spins and lattice has been the subject of detailed

* Contribution No. 472 from the Research Laboratory of Physical Chemistry. This research was aided by a grant from the Rumford Fund of the American Academy of Arts and Sciences.

[1] C. J. Gorter, Physik. Zeits. **39**, 815 (1938), a review of the early work.

[2] P. Teunissen and C. J. Gorter, Physica **7**, 33 (1940).

[3] W. J. de Haas and F. K. du Pre, Physica **5**, 501, 969 (1938); **6**, 705 (1939).

[4] F. K. du Pre, Physica **7**, 79 (1940).

[5] H. B. G. Casimir and F. K. du Pre, Physica **5**, 507 (1938).

[6] H. B. G. Casimir, Physica **6**, 156 (1939); R. de L. Kronig, Physik. Zeits. **39**, 823 (1938); P. Debye, Physik. Zeits. **39**, 616 (1938).

theoretical investigation, chiefly by Kronig[7] and by Van Vleck.[8]

The susceptibility of most paramagnetic compounds is primarily due to the electron spin magnetic moment of the paramagnetic ions involved.[9] The lowest energy states of these ions are degenerate, but in solids the degeneracy is completely or partially removed by the electrostatic field of the crystal lattice and by weak magnetic interaction. The resulting distribution of energy levels gives rise to a specific heat of atomic excitation (Schottky anomaly) for the magnetic spin system. In the case of the paramagnetic alums used for the adiabatic demagnetization cooling process, this anomaly reaches its maximum below 1°K. The determination of the absolute temperature from susceptibility measurements, below 1°K, requires a knowledge of the anomaly in the specific heat. Direct calorimetric measurements below liquid-helium temperatures involve major experimental difficulties, and at higher temperatures the anomalies are masked by the lattice specific heat. The paramagnetic dispersion in these compounds permits the separation of the spin specific heat from the lattice specific heat at temperatures very much higher than 1°K, since the high frequency susceptibility involves the adiabatic properties of the spin system. It is, therefore, possible to determine from dispersion measurements the constants involved in the spin specific heat anomalies (to a first approximation), and thus to aid in the establishment of the absolute temperature scale below 1°K. The present work was intended to verify the validity of the thermodynamic theory and to determine the constants of the spin specific heat for several compounds.

Theory

The theory of Casimir and du Pre is based upon the thermodynamics of two coupled systems, the magnetic spin system and the lattice vibration system. The time required to establish temperature equilibrium within each system is assumed to be very small compared to the time required for equilibrium between the two systems. Since the theory is concerned with the latter time interval, each system is considered as internally in equilibrium, the spin system at a temperature T_S and the lattice system at a temperature T_L. Designate $\Theta = T_L - T_S$; α the thermal conductance between the spin system and the lattice; L the specific heat of the lattice; C_σ and C_H the spin specific heat at constant magnetization and constant field, respectively. The magnetic field H is the internal applied field (equal to the external applied field plus the demagnetizing field), and σ is the magnetization per unit quantity of the spin system. The case of interest is that of a constant field H_0 plus a parallel alternating field of amplitude h and frequency ν, so that $H = H_0 + he^{i\omega t}$ where $\omega = 2\pi\nu$ and t is the time.

The heat content of the spin system changes according to the equation

$$dq = dU - Hd\sigma = -\alpha\Theta dt,$$

where U is the internal energy of the spin system. With the assumption of adiabatic conditions for the paramagnetic compound as a whole, the resulting change of the spin system temperature $dT = d\Theta + \alpha\Theta L^{-1}dt$. Application of the fundamental thermodynamic relations of magnetization[10] (T and H independent variables) gives the solution for the above field suddenly applied:

$$\Theta = \Theta_0 e^{-t/\tau} - T_S\left(\frac{\partial\sigma}{\partial T}\right)_H \frac{he^{i\omega t}}{C_H}\frac{i\omega\tau}{1+i\omega\tau},$$

where the relaxation time $\tau = C_H/\alpha(1+C_HL^{-1})$. The first term of this equation represents a transient temperature change due to the sudden application of H_0, causing the spin temperature to increase isentropically[11] by an amount Θ_0. The second term is the steady-state condition, and shows the frequency dispersion.

The dynamic susceptibility (measured by the change in inductance of the coil producing the alternating field in the specimen) at any frequency of the alternating field is found from the

[7] R. de L. Kronig, Physica **6**, 33 (1939).
[8] J. H. Van Vleck, Phys. Rev. **57**, 426 (1940).
[9] E. C. Stoner, *Magnetism and Matter* (Methuen, 1934), p. 310.
[10] P. S. Epstein, *Thermodynamics* (John Wiley and Sons, 1937), p. 346.
[11] The isentropic temperature rise may be computed from the equation $T_2 = T_1(1+cH^2/a)^{\frac{1}{2}}$, where T_1 and T_2 are spin temperatures before and after application of a field H, and a, c are constants defined later in the paper.

relation

$$\frac{d\sigma}{dH}=\left(\frac{\partial\sigma}{\partial H}\right)_T+\left(\frac{\partial\sigma}{\partial T}\right)_H\frac{dT_s}{dH}.$$

The steady-state condition is then

$$\frac{\chi_\omega}{\chi_0}=1-\frac{C_H-C_\sigma}{C_H}\left(\frac{i\omega\tau}{1+i\omega\tau}\right)-\frac{C_H-C_\sigma}{C_H+L}\left(\frac{1}{1+i\omega\tau}\right), \quad (1)$$

where $\chi_\omega=d\sigma/dH$ is the dynamic susceptibility and $\chi_0=(\partial\sigma/\partial H)_T$ is the isothermal susceptibility. The dynamic susceptibility is the adiabatic susceptibility of the specimen as a whole, but only at very high frequencies is it the adiabatic susceptibility of the spin system.

The lattice specific heat L follows the Debye T^3 law at low temperatures. At liquid-hydrogen temperatures ($\sim 20°$K) or above, the value of L for most paramagnetics is so much greater than the magnetic specific heats that Eq. (1) reduces to

$$\frac{\chi_\omega}{\chi_0}=1-\frac{C_H-C_\sigma}{C_H}\left(\frac{\omega^2\tau^2+i\omega\tau}{1+\omega^2\tau^2}\right). \quad (2)$$

Below liquid-helium temperatures L becomes negligible, and Eq. (1) gives as the ratio of the adiabatic to isothermal susceptibilities $\chi_\omega/\chi_0=C_\sigma/C_H$ at all frequencies. At liquid-helium temperatures it is possible to increase the effective L by placing the crystals of the specimen in direct contact with the liquid helium. The effectiveness of this procedure depends upon the thermal conductance from all parts of the crystal lattice to the liquid helium, and this is as yet an uncertain quantity. For the remainder of this paper, only high temperatures will be considered and Eq. (2) will be used.

Thermodynamics contributes the additional relation

$$C_H-C_\sigma=T\left(\frac{\partial\sigma}{\partial T}\right)_H^2\Big/\left(\frac{\partial\sigma}{\partial H}\right)_T. \quad (3)$$

The value of C_σ is the same as that of C_0 (specific heat at zero field) for the spin system, since, when σ is constant, no magnetic work is involved and C_σ is thus independent of the field strength. (This is true only of perfect magnetics where σ is a function of H/T, and U is therefore independent of H.) The value of C_0 may be computed from the partition function for the lowest energy state of the paramagnetic ion, when split by the crystalline field and magnetic interaction. This has been done by Van Vleck,[12] and by Hebb and Purcell.[13] At temperatures where kT is large compared to the energy difference between the split levels, the specific heat anomaly has the customary form $C_0=a/T^2$ where the constant a involves the magnitude of the splitting. The alums and most of the other compounds investigated behave as ideal paramagnetics at liquid-helium temperatures and above, i.e., the magnetization $\sigma=cH/T$ where c is the Curie constant for the paramagnetic ions involved. Substitution of these relations into Eq. (3) gives

$$C_H T^2=a+cH^2. \quad (4)$$

For the purpose of dispersion studies, the only part of the applied field that need be considered in Eq. (4) is the constant field H_0 (henceforth used without the subscript). The effect of the alternating field may be neglected because of its relatively small magnitude. The alternating field also modulates χ_ω at a frequency double that of the applied frequency, but this is not detectable by the usual measurements.

The magnetic work $Hd\sigma$ used in the above thermodynamic treatment is more precisely the scalar product $(\mathbf{H}\cdot d\boldsymbol{\sigma})$. Since the change of magnetization is produced by the alternating field, only that component of the alternating field parallel to the constant field is involved in the dispersion. This conclusion has been experimentally investigated by Teunissen and Gorter,[14] and they found it to be correct.

Method of Measurement

A schematic diagram of the apparatus used in the present research is shown in Fig. 1. The constant magnetic field was created by a solenoid electromagnet (No. 4 of the M.I.T. magnet

[12] J. H. Van Vleck, J. Chem. Phys. **5**, 320 (1937).
[13] M. H. Hebb and E. M. Purcell, J. Chem. Phys. **5**, 338 (1937).
[14] P. Teunissen and C. J. Gorter, Physica **5**, 486 (1938).

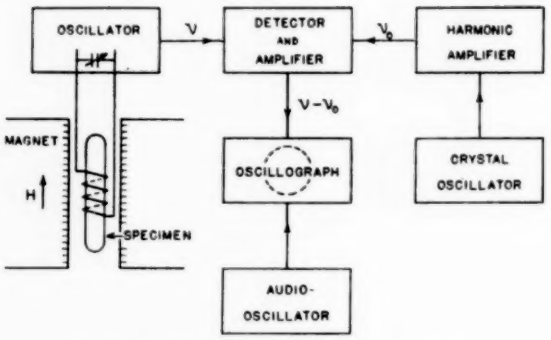

FIG. 1. Schematic diagram of the apparatus.

laboratory)[15] which permitted investigations up to 60,000 gauss. The coil in which the specimen was placed was connected in parallel with a capacitance, and the resulting resonant circuit determined the frequency of a stable oscillator.[16] The output of this specimen oscillator was beat with the output of a crystal controlled oscillator. The crystal had a fundamental frequency of 100 kc/sec. and by means of a harmonic amplifier any multiple of this frequency could be selected. The two signals were fed into an ordinary radio receiver and the audiofrequency beat note was amplified and appeared across one set of plates of a cathode-ray oscillograph. The output of a calibrated audiofrequency oscillator was connected to the other set of plates, and the frequency of this oscillator was adjusted to maintain a standing pattern on the oscillograph. In this manner any change of frequency of the specimen oscillator could be followed by the audio-oscillator. Since the inductance of the coil surrounding the specimen was a function of the dynamic susceptibility of the specimen, the effect of the applied constant magnetic field could be determined from the resulting frequency change of the specimen oscillator.

The electromagnet had a cylindrical core 4 inches in diameter into which was placed a Dewar flask containing the specimen and coil. The paramagnetic compounds were sealed off with helium gas in Pyrex specimen tubes 6 cm long and 1.3 cm in diameter. By means of a string the specimens could be lowered into another Pyrex tube of slightly greater diameter, upon which was wound the coil. The tube with the coil fitted into another Pyrex tube sealed off at the bottom, and the whole assembly was then placed in the Dewar. The purpose of this last tube was to separate the coil from the liquids in the Dewar. It was found that, without this protection, the gas bubbles of the boiling liquid caused transient disturbances of the distributed capacitance of the coil. The coil used for investigations over the frequency range of 2–10 megacycles/sec. was about 4 mm wide and consisted of 10 turns of No. 28 copper wire. The apparatus was arranged so that the coil was in the center of the magnet and was also at the center of the specimens inserted in it. When liquid nitrogen was used in the Dewar, the tubes contained hydrogen gas to provide thermal contact between the specimen and the liquid nitrogen. A specimen originally at room temperature required about 2 minutes to reach thermal equilibrium with the bath.

The dynamic susceptibility, as given by Eq. (2), consists of a real and imaginary component,

$$\chi_\omega = \chi' - i\chi'',$$

$$\frac{\chi'}{\chi_0} = 1 - F\frac{\omega^2\tau^2}{1+\omega^2\tau^2},$$

$$\frac{\chi''}{\chi_0} = F\frac{\omega\tau}{1+\omega^2\tau^2},$$

where

$$F=(C_H-C_s)/C_H=[1+(a/cH^2)]^{-1}. \qquad (5)$$

The inductance of the coil surrounding the specimen is $L=L_0+A\chi'$, where L_0 is the inductance when no specimen is present, and A is a constant (maximum value $=4\pi L_0$) depending upon the volume of the coil field filled by the specimen. The frequency of the specimen oscillator is given by the equation $\omega^2LC=1-(CR^2/L)$, where R is the effective radiofrequency resistance of the coil. The resistance term of this equation is generally negligible, although it may produce a second-order effect at very low temperatures.

[15] F. Bitter, Rev. Sci. Inst. **10**, 373 (1939).

[16] The oscillator was designed for maximum frequency stability, and used a push-pull circuit which required only two coil leads. Since varying load on the oscillator causes frequency variation by changing the grid current, and thus the input capacitance of the vacuum tubes, the circuit was designed to compensate automatically for this effect. At 10 megacycles/sec. the frequency did not wander more than 1 cycle/sec. during the time required for a set of measurements (about 15 minutes).

If this term is neglected, the fractional change of frequency due to the specimen is given by $2d\nu/\nu = -dL/L$, where $dL = A\chi'$ and $L \approx L_0$, since the specimen susceptibility is very small. At liquid-nitrogen temperatures the value of $d\nu/\nu$ for most of the paramagnetics was approximately 10^{-4} to 10^{-5}.

The energy absorption accompanying the frequency dispersion is represented by the out-of-phase component of the susceptibility, χ''. This results in an increase of the effective radio-frequency resistance of the coil equal to $A\omega\chi''$. A simple calculation shows that the energy absorbed per second is $W = \frac{1}{2}h^2\omega\chi''$, (per unit volume if χ is the volume susceptibility). It is apparent that, as a function of increasing frequency, R and W increase rapidly in the dispersion region and reach a constant value at high frequencies. The energy absorbed per cycle (W/ν) is a maximum when $\omega = \tau$. The increase of the coil resistance has two effects on the frequency of the oscillator. The first is that due to the resistance term in the frequency formula, and this is usually negligible. The second is that due to the increased load on the oscillator, and this may be appreciable. As mentioned in footnote 16 the present oscillator compensated for this effect.

The procedure used for a set of measurements was as follows. The variable capacitance of the specimen oscillator was adjusted to give a suitable beat note with the desired crystal harmonic. The frequency of the beat note as a function of the applied constant field was then measured. Inasmuch as the maximum field (60,000 gauss) was more than sufficient to make χ_ω negligible at the high frequencies, the total change of the beat frequency from zero field to the maximum field was assumed to represent the total effect of χ_0. The value of χ_ω/χ_0 for any intermediate field was then the ratio of the frequency change from the maximum field to the intermediate field, to the total frequency change to zero field. This method was used because when the specimen is inserted into the coil a very large frequency change results from the effect of the dielectric constant of the specimen upon the distributed capacity of the coil. This capacitance change is, of course, independent of the applied field, and may be approximately evaluated by the use of a non-magnetic dummy specimen with similar dielectric properties (such as aluminum alum). The dummy method has been used in all previous researches,[1,2] but has the serious objection that the dielectric behavior of the specimen depends not only on chemical similarity but also on geometric similarity. Since the compounds are either powders or small crystals, the packing density would be a variable of major importance and uncertainty. A Faraday screen would help to reduce the capacitance effect, but this was not used since the method described at the beginning of the paragraph appeared to be adequate, and there is no evidence to raise any doubts concerning it.

Results

The present investigation was confined to the frequency range of 2–10 megacycles/sec. and to room temperature and liquid-nitrogen temperature (77.3°K). The compounds studied were all of analytical reagent purity, some commercial and some prepared in the laboratory. In addition to those listed in Table I, the following substances were investigated and showed no dispersion; $FeCl_3$ (anhydrous sublimed), $MnCO_3$, and MnF_2. These three compounds and the $CrNH_4(SO_4)_2 \cdot 12H_2O$ have not been studied before. The isothermal susceptibilities of all the substances that have shown dispersion follow the Curie law at the temperatures used.

A detailed comparison between the present results and those of Teunissen and Gorter[2] will not be made, although there is general qualitative agreement. Their frequency range did not go higher than 4 megacycles/sec. (except for one instance where the frequency was 7 Mc),[17] and

TABLE I. *Spin system data determined from dispersion measurements.*

	$10^{-6}a/c$					
	STARR 77°	TEUNISSEN AND GORTER 77°	DU PRE 1°–4°	$10^{-6}a$	η	δ
$FeNH_4(SO_4)_2 \cdot 12H_2O$	0.263	0.248	0.256	1.14	0.0472°	0.193°
$CrK(SO_4)_2 \cdot 12H_2O$	0.64	0.7	0.80	1.19	0.0204	0.231
$CrNH_4(SO_4)_2 \cdot 12H_2O$	2.68			4.99	0.0200	0.486
$MnSO_4 \cdot 4H_2O$	4.2	6.2		18.2	0.126	0.903
$MnCl_2 \cdot 4H_2O$	19.8	19.5		85.9	0.135	2.11

[17] P. Teunissen and C. J. Gorter, Physica **6**, 1113 (1939).

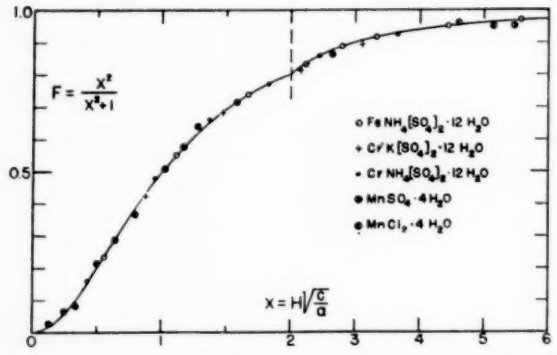

FIG. 2. The factor $F=(C_H-C_\sigma)/C_H$ as a function of the parameter $H(c/a)^{\frac{1}{2}}$. The solid line represents the formula $F=[1+(a/cH^2)]^{-1}$. The second half of the graph has a condensed scale.

their maximum field was 3200 gauss. Most of their data involve extrapolation and approximation. Their early results are based upon a combination of absorption and dispersion measurements, and apparently contain some undetermined experimental error;[17] only their very latest data[2] are free from this error. A detailed comparison is also made difficult by the fact that Teunissen and Gorter found that specimens from different sources gave different quantitative results. This was probably due to variations in the water of hydration, since many of the compounds are unstable in this respect. The results of the present work are more precise and reliable than those of Teunissen and Gorter, for the following reasons. First, the use of higher frequencies enabled the determination of the F values without extrapolation. Second, as explained in the section on measurement, the strong magnetic fields available permitted the author to dispense with the correction for the dielectric constant effect, and therefore the large errors involved in the use of the non-magnetic dummy do not enter into the present results.

The general formula for dispersion effects, resulting from systems with a relaxation time, has the frequency dependence given by Eq. (2).[18] However, the model assumed by Casimir and du Pre is uniquely responsible for the factor $F=(C_H-C_\sigma)/C_H$. The validity of their theory would be proven if the paramagnetic dispersion followed Eqs. (2) and (5). The dependence of F upon the applied field is given by Eq. (5), and, since a and c are constants independent of field and temperature (except for very low temperatures), F should be independent of temperature.

In order to study the F values, the present measurements were made at 10 megacycles/sec. At 77°, for the compounds investigated, this frequency results in a value of $\omega \gg \tau$. In those cases where there was a dependence of χ' upon frequency in the range studied, this could be corrected by calculation of the relaxation time. In no case did this correction amount to more than a few percent. The author's experimental results are shown in Fig. 2. The experimental curve of F *vs.* H has been replotted for each compound in terms of the parameter $X=H(c/a)^{\frac{1}{2}}$. The value of a/c is chosen so that when $F=0.5$, $X=1$. The a/c values found this way are given in Table I. The solid curve of Fig. 2 represents the plot of Eq. (5). It is apparent that, within the experimental error (about 2 percent), the field dependence of F is the same for all the compounds and is that theoretically predicted. The effect of temperature on F is not very certain. The comparison of the results of different investigators in Table I is not very conclusive because of the reasons discussed above. In the case of the most investigated compound, $FeNH_4(SO_4)_2 \cdot 12H_2O$, the a/c value appears to be reasonably independent of temperature. Teunissen and Gorter[17] made a detailed study of this point and also came to the same conclusion. An investigation of paramagnetic absorption and dispersion in $CrK(SO_4)_2 \cdot 12H_2O$ at 64°, 77°, and 90°K has recently been made by Gorter, Dijkstra, and Groendijk.[19] Their dispersion results gave the same value of $a/c=0.76\times10^6$ at all the temperatures, but their absorption measurements are not easily interpreted. Both $MnSO_4 \cdot 4H_2O$ and $MnCl_2 \cdot 4H_2O$ show dispersion at room temperature, and the present work showed that the a/c value at this temperature is the same as that at 77°. In general, the evidence seems to indicate that the F function is independent of temperature and that the model of paramagnetic dispersion assumed by Casimir and du Pre is correct.

[18] The electrical system consisting of an inductance connected in parallel with a resistance has a resulting impedance which exhibits the frequency dependence given by the frequency term of Eq. (2).

[19] C. J. Gorter, L. J. Dijkstra, and H. Groendijk, Physica **7** (July, 1940).

The specific heat constant a consists of two terms, one due to the crystalline field splitting and the other due to the splitting caused by the magnetic spin-spin interaction. Waller,[20] Van Vleck,[12] and Hebb and Purcell[13] have theoretically evaluated these terms. At the comparatively high temperatures involved in these dispersion measurements, the value of a for the Cr^{+++} compounds is

$$a=0.250R\delta^2+2.40R\eta^2 \text{ ergs deg. mole}^{-1},$$

where R is the gas constant per mole, δ is the crystalline field splitting in degrees, and η is the characteristic temperature of the magnetic spin-spin interaction (approximately the ferromagnetic Curie temperature). For the Cr^{+++} compounds, the Curie constant is $c=1.86$ erg deg. gauss^{-2} mole^{-1}. The value of a for the Fe^{+++} and Mn^{++} compounds, for the case of a cubic crystalline field and a face-centered arrangement of the paramagnetic ions, is

$$a=0.222R\delta^2+2.40R\eta^2,$$

and the Curie constant is $c=4.34$. The structure of the ferric ammonium alum is such that this formula has been assumed to be applicable. The crystal structures of the Mn^{++} compounds investigated have not been determined. However, the above formula was arbitrarily assumed to hold in this case also, in order to arrive at some estimate of the quantities involved. Table I contains the values of a and δ based upon the a/c values of the present research. The characteristic temperature η was computed from the following definitory formula given by Van Vleck[12] (the τ of his paper), $\eta=Ng^2\beta^2J(J+1)/k$, where N is the number of magnetic ions per cc, and the remaining symbols have their customary meaning.

Kronig and Bouwkamp[21] have shown on theoretical grounds that in the case of $FeNH_4(SO_4)_2\cdot 12H_2O$ magnetic fields greater than about 900 gauss should suppress the magnetic interaction between spins, so that only the splitting due to the crystalline field should remain. From the values in Table I, the crystalline splitting specific heat is about 60 percent of the total. According to Kronig and Bouwkamp the low field value of $F=[1+(a/cH^2)]^{-1}$ should change at high fields to $F=[1+(0.53a/cH^2)]^{-1}$. A field of 900 gauss corresponds to an $F=0.75$, and any marked deviation from the low field F formula should, therefore, be observable. No such deviation was found, as can be seen from Fig. 2. If this effect should occur at a very much higher field, so that $F\approx 1$, it would not be detectable. The conclusion that the effect predicted by Kronig and Bouwkamp does not exist in the experimentally detectable range was also reached by du Pre,[4] from his measurements at liquid-helium temperatures.

The properties of $CrNH_4(SO_4)_2\cdot 12H_2O$ differ from those of $CrK(SO_4)_2\cdot 12H_2O$, as shown in Table I. According to Lipson and Beevers[22] the crystal structures of these two alums are the same. The Cr^{+++} ion in the alums is surrounded by an octahedron of six water molecules. The distortion of this octahedron, giving rise to a trigonal crystalline field, is responsible for the crystalline splitting. The difference in distortion required to produce the differing fields in the two alums is probably not very large. In this connection, the work of Kraus and Nutting[23] on the absorption spectra of the chrome alums is of interest. They found that the ammonium alum goes through a crystal structure transition at 81°K with a change in the absorption spectrum. The transition is sluggish and the alum is easily

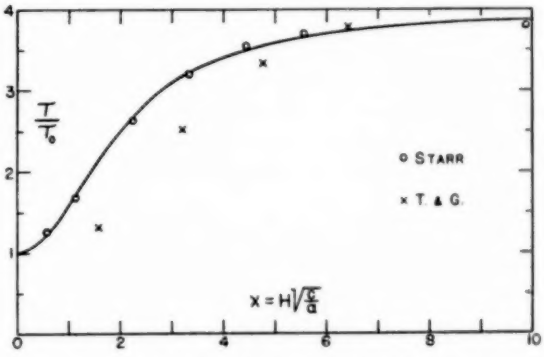

FIG. 3. The relaxation time of $FeNH_4(SO_4)_2\cdot 12H_2O$ as a function of the parameter $H(c/a)^{\frac{1}{2}}$. The solid line represents the formula $\tau=\tau_0 4(1+X^2)/(4+X^2)$.

[20] I. Waller, Zeits. f. Physik **104**, 132 (1936).
[21] R. de L. Kronig and C. J. Bouwkamp, Physica **5**, 521 (1938); **6**, 290 (1939).
[22] H. Lipson and C. A. Beevers, Proc. Roy. Soc. **A151**, 347 (1935).
[23] D. L. Kraus and G. C. Nutting, J. Chem. Phys. **9**, 133 (1941).

supercooled. The potassium alum does not have this transition. It is possible that this difference in the two alums is related to the difference in the observed crystalline field splittings.

In the frequency range studied, sufficient dispersion was found in $FeNH_4(SO_4)_2 \cdot 12H_2O$ at 77° to permit the determination of the relaxation time τ as a function of the applied field. The definition and Eq. (4) give

$$\tau = C_H/\alpha = (a+cH^2)/T^2\alpha.$$

The previous experimental work[2] (with which the present is in qualitative agreement) has shown that α, the thermal conductance, is a function of the applied field and temperature. The theoretical study of α by Van Vleck[7] has shown that α should be proportional to $(1+bH^2)$ where b is a constant. This suggestion has been included in the following empirical equation, which has been found to fit the present results for the ferric alum at 77°.

$$\tau = \tau_0 4(1+X^2)/(4+X^2),$$

where $X = H(c/a)^{\frac{1}{2}}$ and $\tau_0 = 4.05 \times 10^{-8}$ seconds. The solid curve shown in Fig. 3 represents this equation, with the a/c value from Table I. The experimentally determined values of τ, also shown, fit this curve within the experimental error (2 percent). The factor 4 in the equation is the ratio of the relaxation times in infinite field and zero field. The value 4 is within the theoretical limits (1.7–4.5) found by Van Vleck[8] for ferric alum. The relaxation times found by Teunissen and Gorter[17] are also shown in Fig. 3, with an assumed $\tau_0 = 7.0 \times 10^{-8}$ second. There is no possible adjustment of the constants of the above type of formula which will make it fit their data. With the τ_0 found in the present research ($\tau_0 = 4.05 \times 10^{-8}$) the formula

$$\tau = \tau_0 7(1+X^2)/(7+X^2)$$

is in very rough agreement with the results of Teunissen and Gorter, but the ratio 7 is much greater than that theoretically permitted by Van Vleck.

The paramagnetic compounds which do not exhibit dispersion ($FeCl_3$, $MnCO_3$, MnF_2, and the long list of Teunissen and Gorter[2]) appear to fall into two classifications. The first includes ions of the first transition series which are not known to exhibit dispersion in any of their compounds, i.e., all ions except Fe^{+++}, Mn^{++}, Cr^{+++}, and V^{++}. According to Kronig[7] and Van Vleck[8] the energy separation of the ground state from the excited states is very small in the ions of this group. This results in a large spin-lattice coupling through the orbital moment of the excited states. As a consequence of the resulting large α, the relaxation time is very small and the dispersion region involves frequencies very much higher than is experimentally practical. The second group which does not exhibit dispersion includes compounds of Fe^{+++}, Mn^{++}, Cr^{+++}, and V^{++} which have little or no water of hydration. It is unlikely that any effect of dehydration in these compounds would cause a sufficient decrease in relaxation time to move the dispersion region outside the experimental range. The absence of dispersion in the second group is probably due to the increased specific heat of the spin system, as a result of the increased crystalline field asymmetry and the increased magnetic spin-spin interaction caused by the dehydration. In the present research, $FeCl_3$, MnF_2, and $MnCO_3$ were investigated up to 60,000 gauss without any detectable effect upon the dynamic susceptibility. Since a value of $H(c/a)^{\frac{1}{2}} = 0.2$ may be easily detected, the a/c value for these compounds must be greater than 10^{11} for the dispersion effect to be undetectable. This is about 4×10^5 times as large as the value for ferric ammonium alum. Inasmuch as the value of c is approximately independent of the state of hydration, the specific heat of the spin system would have to be responsible for this large ratio ($a = C_0T^2$). This is not an unreasonable situation. It is known that the unusual magnetic properties of the anhydrous compounds of the iron group[24] are probably due to strong magnetic exchange interaction, as in ferromagnetism. In the case of $FeCl_3$ this produces a Curie point[24] of $-12°$, and in MnF_2 an antiferromagnetic Curie point of 70° has been found.[25] Since the specific heat is roughly proportional to the square of the Curie point temperature, the spin

[24] C. Starr, F. Bitter, and A. R. Kaufmann, Phys. Rev. **58**, 977 (1940); C. Starr, Phys. Rev. **58**, 984 (1940).
[25] W. J. de Haas, B. H. Schultz, and J. Koolhaas, Physica **7**, 57 (1940).

system specific heat of $FeCl_3$ due to magnetic causes alone is about 0.65×10^5 times as great as that of ferric alum ($\eta=0.047°$), and that of MnF_2 is 22×10^5 times that of ferric alum. As most of the dehydrated compounds have Curie point temperatures of similar magnitudes, the explanation given above for the apparent absence of dispersion in these compounds is probably correct.

The author is indebted to the Rumford Fund of the American Academy of Arts and Sciences for a grant enabling this research to be undertaken. The author thanks Professor F. G. Keyes for his encouragement during the research.

AUGUST 1, 1941 PHYSICAL REVIEW VOLUME 60

Remarks on the Volume Magnetostriction of Nickel

R. SMOLUCHOWSKI
Palmer Physical Laboratory, Princeton University, Princeton, New Jersey

(Received June 14, 1941)

Results of a theory of volume magnetostriction developed in a recent paper and applied there to iron are applied here to the case of nickel, and a correction is made of the data on iron. The molecular field factor N, its dependence on volume, the magnetization at absolute zero I_0 and its dependence on volume are calculated and discussed. Contrary to the results of magnetocaloric effect, and in accord with the expectations based on the dependence of the exchange integral on interatomic distance, N appears to decrease in nickel with increasing volume (for $j=1$). To account for the dependence of the magnetization, at absolute zero, on volume it is necessary to assume a dependence of the number of holes in the 3*d* band on the interatomic distance. This dependence can be understood on the basis of the band structure, which can be obtained by extrapolating Krutter's calculations on copper. Corrected numerical values for iron are given.

IN a recent paper,[1] referred to as I, certain relations were developed between the observed change of volume $(1/V)(\partial V/\partial H)=(\partial\omega/\partial H)$ of magnetized ferromagnetic metals at saturation, the molecular field factor N, and the magnetization at absolute zero I_0. The formulas were applied to the case of iron and some conclusions relative to specific heat were drawn. The aim of the present paper is twofold. Similar considerations will be made for nickel, and at the same time an error, kindly pointed out to the author by Drs. Primakoff and Holstein, will be corrected. This correction, though not affecting the main conclusions of I, introduces some small changes of the numerical values.

We indicate first the corrections: from the formula[2]

$$(\partial V/\partial H)_{Tp}=-(\partial VI/\partial p)_{TH}$$

we have

$$(\partial I/\partial p)_{TH}=-(\partial\omega/\partial H)_{Tp}+I\kappa$$

and similarly

$$\left(\frac{\partial I}{\partial T}\right)_v=\left(\frac{\partial I}{\partial T}\right)_p-\frac{3\alpha}{\kappa}\left(\frac{\partial\omega}{\partial H}\right)_{Tp}+3\alpha I. \quad (1)$$

Therefore in formulas (7, I) and (8, I) one has to substitute $(\partial\omega/\partial H)_{Tp}-I\kappa$ for $(\partial\omega/\partial H)_{Tp}$. Similar corrections in (9, I) are necessary but they cancel out finally so that formula (10, I) remains valid.[3] The corrected numerical values for iron are given in the last part of this paper. Let us now go over to the case of nickel.

The main difficulty in applying the theory to the case of nickel is the fact that very few data on volume magnetostriction in the saturated state are known. Systematic studies of this effect at various temperatures, such as were made for iron by Kornetzki, are not available. The effect itself is much smaller than in the case of iron and corrections due to magnetocaloric effect are

[1] R. Smoluchowski, Phys. Rev. **59**, 309 (1941).
[2] R. Becker, Zeits. f. Physik **87**, 547 (1934).

[3] There is a misprint in the formula following formula (9, I): it should be $N(\partial I/\partial T)_v$ instead of $(\partial I/\partial T)_v$; also, on p. 313, in the fifteenth line from the bottom, ρ should read τ.

TABLE I. *Data on nickel.*

	$-(\partial I/\partial T)_p$	I_p	$3\alpha\cdot10^5$	$\kappa\cdot10^{13}$	$-(\partial I/\partial T)_v$	I/T	$D(a)$
0°C	0.211	489.2	3.95	5.25	0.198	1.792	0.099
20°C	0.244	484.7	4.02	5.275	0.232	1.654	0.123
		N		I_0		N	I_0
0°C	$j=\frac{1}{2}$	18,680		500.2	$j=1$	15,305	502.1
20°C	$j=\frac{1}{2}$	19,130		498.8	$j=1$	15,290	501.9

essential. The most accurate measurements seem to be those of Snoek[4] made at 0°C and at room temperature. They agree with the result of Döring[5] at 4°C. The result is that the relative change of volume with increasing field strength $\partial\omega/\partial II$ is practically constant in this range of temperature and equal to 0.95×10^{-10}. Additional tests made at −55°C seem to confirm the conclusion that the temperature dependence of this effect, if any, is small. We therefore assume the same value at the temperatures, 0°C and 20°C, at which we shall apply the formulas. Data on magnetization and its dependence on temperature were taken from Weiss and Forrer,[6] other data from standard tables.

With the help of formula (1) we can calculate $(\partial I/\partial T)_v$ and then from (10, I) obtain N for the two cases $j=\frac{1}{2}$ and $j=1$. This was done for the two temperatures and the results are given in Table I. From this we obtain easily that $(1/N)(\partial N/\partial\omega)$ is equal to $+29.8$ for $j=\frac{1}{2}$ and -1.2 for $j=1$. We see that the difference between the two cases is pronounced. The value of N is, similarly to the case of iron, greater for $j=\frac{1}{2}$ than for $j=1$. It is also larger than that obtained from measurements not involving any particular form of the function L. This has been discussed fully by Stoner.[7]

The interesting fact is that for $j=1$ we get N decreasing with increasing volume. In iron this dependence has the opposite sign.[1] Although the absolute value of this change of N is small as compared with the case $j=\frac{1}{2}$, or with the results for iron, nevertheless, its sign seems to be certain. It would be very interesting to have accurate data to check this point over a larger range of temperatures. The factor N is, on the basis of Heisenberg theory of ferromagnetism, directly related to J, the exchange integral between the d electrons in a ferromagnetic crystal. One can get a general idea about the dependence of this integral upon the interatomic distance from various data,[8] as, for instance, comparing the Curie points, the expansion anomaly at this point and the relative size of the d shell as compared with the interatomic distance. All these data lead to the same known conclusion, that for iron J increases with interatomic distance, and for nickel it decreases. Since N is proportional to J, we see that this is in accord with the results obtained here for $j=1$ and definitely disagrees with them for $j=\frac{1}{2}$.

The magnetocaloric effect, observed below the Curie point, can be described by a formula which contains N. Conversely, from the measurements, one can compute N. This has been done by Potter[9] at various temperatures and one obtains a rather small value which shows a steady increase with rising temperature. Stoner[7] has pointed out that N obtained in this way is very much affected by the difference between the apparent and the intrinsic magnetization, and does not correspond to the conditions within the domains. The "true" N is larger and comparable with that deduced from susceptibility measurements above the Curie point. The large value of N as obtained in this paper apparently corresponds to the intrinsic magnetization. In particular, its dependence on volume, which agrees with other considerations mentioned above, seems to support this conclusion.

We can now calculate I_0 for both cases from the equation $I_0=I/L_j(a)$ and obtain the values given in Table I. Since, as we see, the change of I_0 with volume is very small it seems more advisable to compute $(1/I_0)(\partial I_0/\partial\omega)$ from the formula

$$\frac{1}{I_0}\frac{\partial I_0}{\partial\omega}=-\frac{1}{N}\frac{\partial N}{\partial\omega}D(a)-\frac{I-(1/\kappa)(\partial\omega/\partial II)}{I-T(\partial I/\partial T)_v}, \quad (2)$$

which was derived before. One obtains $(1/I_0)\times(\partial I_0/\partial\omega)=-3.8$ for $j=\frac{1}{2}$ and $(1/I_0)(\partial I_0/\partial\omega)=-0.5$ for $j=1$. The quantity I_0 can be ex-

[4] J. L. Snoek, Physica **4**, 853 (1937).
[5] W. Döring, Zeits. f. Physik **103**, 560 (1936).
[6] P. Weiss and R. Forrer, Ann. de physique **12**, 279 (1929); P. Weiss, Comptes rendus **198**, 1893 (1934).
[7] E. C. Stoner, Trans. Roy. Soc. **235**, 165 (1935).
[8] See, e.g., F. Seitz, *Modern Theory of Solids* (McGraw Hill, New York, 1940), p. 614; W. Shockley, Tech. Pub. Bell Sys. **18**, 645 (1939); R. M. Bozorth, Tech. Pub. Bell. Sys. **19**, 1 (1940).
[9] H. H. Potter, Proc. Roy. Soc. **146**, 362 (1934).

pressed in the form $\rho L\tau\mu_B/A$ where ρ is the density, A is the atomic weight, L is the Loschmidt number and τ is the average number of electrons responsible for ferromagnetism per atom, which, for nickel, has the value 0.6. From the point of view of the electron band structure of metals, τ is the number of holes in the partially unfilled $3d$ band. Since this number depends upon the position of the bands and their overlapping, one might expect it to be volume dependent. We have, therefore, with $\partial\rho/\partial\omega=-\rho$, the relation

$$\frac{1}{\tau}\frac{\partial\tau}{\partial\omega}=\frac{1}{I_0}\frac{\partial I_0}{\partial\omega}+1, \tag{3}$$

giving here the values -2.8 and $+0.5$ for $j=\frac{1}{2}$ and $j=1$, respectively. Although the bands for nickel are not known exactly, we can assume that they do not differ much from the results of calculations made for copper by Krutter[10] and Slater.[11] The number of electrons filling up these bands is now 10 instead of 11 for copper. Because of a change of the interatomic distance, the spread and the position of the $4s$ and $3d$ bands changes. This results in a shift of the distribution of electrons between the two bands. A simple consideration shows that, for small changes of interatomic distance, the change of the number of holes in the $3d$ band is approximately given by

$$\frac{\partial\tau}{\partial r}=\frac{n_s n_d}{n_s+n_d}\left(\frac{\partial d'}{\partial r}-\frac{\partial s'}{\partial r}+q\frac{\partial d}{\partial r}-p\frac{\partial s}{\partial r}\right), \tag{4}$$

where n_s and n_d is the density of electronic states at the top of the Fermi surface in the s and d bands, respectively, s' and d' the energy of the bottom of the bands and s and d their width. The quantities p and q indicate what fraction, on an energy scale, of the s and d bands is full. Using Krutter's data we get $r(\partial\tau/\partial r)\sim+0.39$ or $(1/\tau)(\partial\tau/\partial\omega)\sim+0.2$. Although these values are very rough and depend on many assumptions, they seem to agree with the case $j=1$ rather than with the case $j=\frac{1}{2}$. Thus, in all comparisons with information obtainable from other sources, the case $j=1$ is more satisfactory. It should be stressed that in the case of nickel the volume effect is small and therefore the absolute value of N is not much influenced by $(\partial\omega/\partial H)$. On the other hand, the dependence on volume of N, I_0, and τ is much more sensitive to this magnitude, and a comparison with some more systematic measurements might be interesting.

TABLE II. *Data (corrected) on iron.*

	$\left(\frac{\partial I}{\partial T}\right)_v$	$D(a)$	a	$j=\frac{1}{2}$ N	I_0	a	$j=1$ N	I_0
20°C	0.177	0.0294	3.000	7660	1720.3	5.152	6560	1722.0
40°C	0.204	0.0360	2.884	7870	1718.5	4.950	6750	1720.2
60°C	0.230	0.0430	2.777	8080	1716.6	4.725	6875	1718.8
80°C	0.257	0.0507	2.675	8270	1714.6	4.528	7000	1717.1
100°C	0.284	0.0589	2.584	8480	1712.6	4.335	7105	1716.0

TABLE III. *Data (corrected) on iron.*

		$\frac{1}{N}\frac{\partial N}{\partial\omega}$	$\frac{1}{N}\frac{\partial N}{\partial T}\cdot10^4$	$\frac{1}{I_0}\frac{\partial I_0}{\partial\omega}$	$\frac{1}{I_0}\frac{\partial I_0}{\partial T}\cdot10^4$
20°C	$j=\frac{1}{2}$	44.1	14.15	−1.60	−0.52
	$j=1$	41.2	13.2	−1.44	−0.46
100°C	$j=\frac{1}{2}$	32.2	11.62	−1.62	−0.58
	$j=1$	22.2	8.0	−1.01	−0.36

Certain results of Döring[5] on linear magnetostriction of nickel seem to indicate that there is a reversal of sign of that effect at higher temperatures. Since, in that region, the corrections due to magnetocaloric effect are large, direct measurements of volume magnetostriction are difficult. Thus there might be a negative volume magnetostriction at higher temperatures. This does not mean, of course, that there is a reversal of sign of $\partial N/\partial\omega$, since the connection between these two magnitudes is not very close and a negative magnetostriction is easily compatible with a decrease of N with increasing volume.

We now give in Tables II and III the corrected results for iron, which should be substituted in I.

As compared with I, the differences amount to a small increase of absolute value of the quantities involved. The quantity $(1/\tau)(\partial\tau/\partial\omega)$ as computed from (3) is here definitely negative. There is, however, no possibility of checking this result in view of lack of knowledge of the structure and position of bands in iron.

The additional specific heats obtained from these data are at 20°C: 0.45 and 0.70; at 100°C: 0.38 and 0.58 for $j=\frac{1}{2}$ and $j=1$, respectively. The agreement with experiment is better for the case $j=1$.

The author wishes to express his sincerest thanks to Professor E. Wigner for his advice and interest during the course of this work.

[10] H. M. Krutter, Phys. Rev. **48**, 664 (1935).
[11] J. C. Slater, Phys. Rev. **49**, 537 (1936).

Statistics of the Two-Dimensional Ferromagnet. Part I

H. A. KRAMERS, *University of Leiden, Leiden, Holland*

AND

G. H. WANNIER, *University of Texas, Austin, Texas*[1]

(Received April 7, 1941)

In an effort to make statistical methods available for the treatment of cooperational phenomena, the Ising model of ferromagnetism is treated by rigorous Boltzmann statistics. A method is developed which yields the partition function as the largest eigenvalue of some finite matrix, as long as the manifold is only one dimensionally infinite. The method is carried out fully for the linear chain of spins which has no ferromagnetic properties. Then a sequence of finite matrices is found whose largest eigenvalue approaches the partition function of the two-dimensional square net as the matrix order gets large. It is shown that these matrices possess a symmetry property which permits location of the Curie temperature if it exists and is unique. It lies at

$$J/kT_c = 0.8814$$

if we denote by J the coupling energy between neighboring spins. The symmetry relation also excludes certain forms of singularities at T_c, as, e.g., a jump in the specific heat. However, the information thus gathered by rigorous analytic methods remains incomplete.

TRANSITION temperatures of various types are a well-known phenomenon in the study of matter, and the statistical distribution laws form a generally accepted piece of theory. It is also generally believed that the former are a consequence of the latter. This is, however, by no means immediately obvious and an examination of the literature shows that there is not more than one case in which a proof of this fact has been attempted. The case which has received successful treatment is the condensation of vapors.[2] This paper wishes to carry out a similar treatment for the Curie transition of ferromagnets.

The problem has a mechanical and a statistical aspect. On the mechanical side we wish to improve our understanding of the responsible coupling forces. On the statistical side we wish to derive with certainty the thermal properties from a reasonably accurate mechanical model. Both aspects have received extensive attention. Quantum theory has explained satisfactorily the origin and nature of the coupling forces. There are also several theories available which explain in terms of them the thermal behavior of ferromagnets. Not one, however, applies just straight statistics to the mechanical data.[3] Generally some simplifying assumption is introduced to facilitate the evaluation of the partition function. It follows that the results obtained are not necessarily a consequence of the mechanical model, but may well be due to the statistical approximation.

The present paper is an attempt to gain sound statistical information about some model of a ferromagnet. The Ising model has been chosen because its extreme simplicity makes it particularly suitable for such a purpose.

In Part I, we shall show that the task of finding the state sum can be reduced to finding the largest eigenvalue of some matrix. The matrix will be very simple in the case of the linear chain and we shall re-derive by this method the results of Ising. No such simple solution will be possible for the two-dimensional square net where the matrix is infinite. However, some precise information can still be gained which will be collected in the latter sections of this paper.

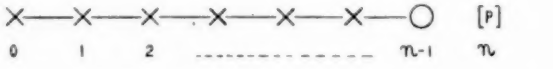

FIG. 1. Building up the linear chain. The elementary step consists in placing a spin in position $[P]$, whose sign depends only on the spin ○.

[1] Owing to communication difficulties, one of the authors (G. H. W.) is entirely responsible for the printed text.

[2] J. E. Mayer, J. Chem. Phys. **5**, 67 (1937); J. E. Mayer and Ph. G. Ackermann, J. Chem. Phys. **5**, 74 (1937); M. Born, Physica **4**, 1034 (1937); B. Kahn, Dissertation Utrecht, 1938. The last paper has the most rigorous treatment of the matter.

[3] For a detailed discussion of various approximations see Part II.

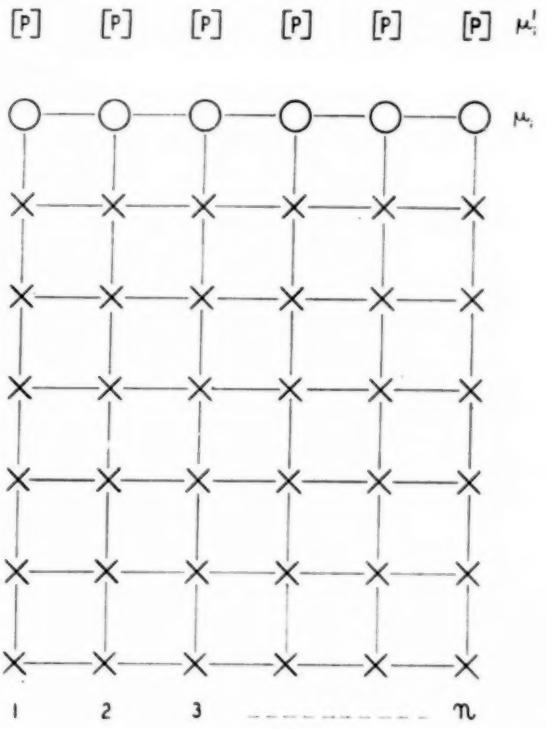

FIG. 2. Building up the infinite strip. Elementary step consists in filling all positions [*P*] whose situation depends on each other and the spins ○.

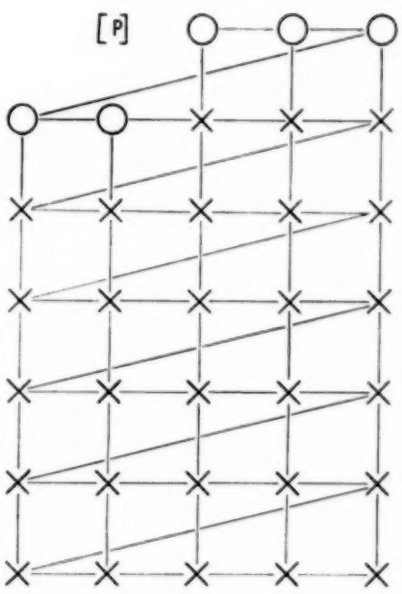

FIG. 3. Building up the infinite screw. Elementary step [*P*] demands knowledge of spins ○, partly for the step itself, but mostly for later similar steps to follow.

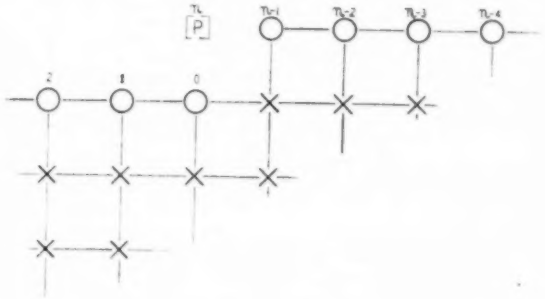

FIG. 4. Numbering of spins in the infinite screw problem.

In Part II, we shall complement this knowledge by approximate treatments. Some of them are already well known, as for instance the power series approximations, the Heisenberg method, the order-disorder method of Bethe. In addition, we wish to add two treatments of our own. Both are based on the matrix method. One will be a semi-numerical treatment to answer a specific question left open in Part I, the other a new approximation method giving results in closed form. It will be shown that this latter is very much superior to the older procedures.

1. The Mechanical Model

The Ising model can be explained as follows. Assume a set of spins $\mu_1, \mu_2, \mu_3 \cdots \mu_N$ arranged in some regular order. Let each of the spins be capable of two orientations which we characterize by $\mu_i = +1$ and $\mu_i = -1$. Then the Ising model assumes that the forces on each spin depend only on the orientation of its immediate neighbors in addition to an eventually applied magnetic field. In particular, if all direct neighbors of a given spin are equivalent the model contains only two parameters, namely the magnetic moment m of each spin and a quantity J which is the energy gained if two neighbors change from an antiparallel to a parallel position. With these two definitions the total energy E takes the form

$$E = -\tfrac{1}{2} J \sum_{\langle i,k \rangle} \mu_i \mu_k - mH \sum_i \mu_i, \qquad (1)$$

where here as in the future $\sum_{\langle i,k \rangle}$ shall mean that the sum is carried out over all pairs (i, k) which are direct neighbors.

Most statistical questions concerning (1) can be considered solved if we can evaluate the

so-called partition function f

$$f=\sum_{\mu_i=\pm 1}\exp[K\sum_{(i,k)}\mu_i\mu_k+C\sum_i\mu_i] \tag{2}$$

with

$$K=\tfrac{1}{2}J/kT \tag{3}$$

and

$$C=mH/kT. \tag{4}$$

The bold face summation sign $\sum_{\mu_i=\pm 1}$ is to be understood to extend over all possible states of the system, i.e., it would have to be written explicitly as

$$\sum_{\mu_i=\pm 1}\sim\sum_{\mu_1=\pm 1}\sum_{\mu_2=\pm 1}\sum_{\mu_3=\pm 1}\cdots\sum_{\mu_N=\pm 1}.$$

Once f is obtained most important physical consequences can be derived from it. We obtain for instance the total magnetization M and the total energy E:

$$M=m\,\partial\log f/\partial C \tag{5}$$

and

$$E=-MH-\tfrac{1}{2}J\,\partial\log f/\partial K. \tag{6}$$

2. The Linear Chain

Ising himself carried out the calculation (2) for the linear chain.[4] However, we shall reconsider this problem since it forms an easy introduction for the eigenvalue method of evaluating f.

Let us suppose first the chain to be finite with n members $\mu_0, \mu_1, \mu_2, \cdots\mu_{n-1}$, as indicated in Fig. 1. Then, by Boltzmann's theorem, the probability for a particular arrangement of spins $\mu_0=+1$, $\mu_1=+1$, $\mu_2=-1$, $\mu_3=+1$, $\cdots\mu_{n-1}=-1$ is proportional to $\exp(-E/kT)$, because every arrangement has weight 1. Since the energy E is given by (1) this probability is proportional to

$$\exp[K(\mu_0\mu_1+\mu_1\mu_2+\mu_2\mu_3+\cdots+\mu_{n-2}\mu_{n-1})+C(\mu_0+\mu_1+\mu_2+\cdots+\mu_{n-2}+\mu_{n-1})],$$

where K and C are given by (3) and (4). Exactly the same consideration is possible if we add one extra spin in the position $[P]$ of Fig. 1. The resulting expression is the same as above except that both sums extend to μ_n. It follows that the two probabilities differ from each other only through the factor

$$\exp[K\mu_{n-1}\mu_n+C\mu_n].$$

From these all-over probabilities others answering more simple questions can be obtained by summation. Let us determine for example from our first expression the probability $P(\mu_{n-1})$ that μ_{n-1} has either value regardless of the values of $\mu_0, \mu_1, \mu_2, \cdots\mu_{n-2}$. This is easily found to be

$$P(\mu_{n-1})\sim\sum_{\mu_0,\mu_1,\cdots\mu_{n-2}=\pm 1}\exp[K(\mu_0\mu_1+\mu_1\mu_2+\cdots\mu_{n-2}\mu_{n-1})+C(\mu_0+\mu_1+\cdots\mu_{n-1})].$$

By summing the second probability containing μ_n over the same μ's a probability $P(\mu_{n-1}, \mu_n)$ can be obtained giving the chance for any one of the four combinations $++$, $+-$, $-+$, $--$. The quantities $P(\mu_{n-1})$ and $P(\mu_{n-1}, \mu_n)$ still differ by the same factor, *viz.*,

$$\lambda P(\mu_{n-1}, \mu_n)=P(\mu_{n-1})\exp[K\mu_{n-1}\mu_n+C\mu_n],$$

the unknown factor λ entering because the Boltzmann exponentials are only proportional to probabilities.

If we sum both sides in the above expression over $\mu_{n-1}=\pm 1$ we get the probability $P(\mu_n)$ for μ_n having either value in terms of the same probabilities for μ_{n-1} before μ_n was added. However, *if the chain is very long*, the physical situation described by the two P's is identical. Hence $P(\mu_n)$ and $P(\mu_{n-1})$ must be the same mathematical functions of their argument

$$\lambda P(\mu_n)=\sum_{\mu_{n-1}=\pm 1}P(\mu_{n-1})\exp[K\mu_{n-1}\mu_n+C\mu_n].$$

These two linear equations have the form of a matrix eigenvalue problem. If we symmetrize the

[4] E. Ising, Zeits. f. Physik **31**, 253 (1925).

matrix by the substitution

$$a(\mu)=P(\mu)\exp\tfrac{1}{2}C\mu$$

the problem takes the form

$$\sum_{\mu'=\pm1}\mathfrak{K}(\mu,\mu')\,a(\mu')=\lambda\,a(\mu) \tag{7a}$$

with

$$\mathfrak{K}(\mu,\mu')=\exp[K\mu\mu'+\tfrac{1}{2}C\mu+\tfrac{1}{2}C\mu']. \tag{7b}$$

We shall consider the solutions of (7) later on.

Before doing so let us clear up the significance of the two eigenvalues λ_1 and λ_2.[5] This can be done most easily by using the fundamental theorem which develops any matrix in terms of its eigenvectors:

$$\mathfrak{K}(\mu_1,\mu_2)=\lambda_1a_1(\mu_1)a_1(\mu_2)+\lambda_2a_2(\mu_1)a_2(\mu_2),$$

where $a_1(\mu)$ and $a_2(\mu)$ denote the eigenvectors belonging to λ_1 and λ_2, respectively. They are orthogonal and may be assumed normalized

$$\sum_{\mu=\pm1}a_i(\mu)a_k(\mu)=\delta_{ik}.$$

This permits us to unite two $\mathfrak{K}$'s as follows

$$\sum_{\mu_2}\mathfrak{K}(\mu_1,\mu_2)\mathfrak{K}(\mu_2,\mu_3)=\lambda_1^2a_1(\mu_1)a_1(\mu_3)+\lambda_2^2a_2(\mu_1)a_2(\mu_3)$$

and next

$$\sum_{\mu_2}\sum_{\mu_3}\mathfrak{K}(\mu_1,\mu_2)\mathfrak{K}(\mu_2,\mu_3)\mathfrak{K}(\mu_3,\mu_4)=\lambda_1^3a_1(\mu_1)a_1(\mu_4)+\lambda_2^3a_2(\mu_1)a_2(\mu_4)$$

and so on until finally

$$\sum_{\mu_2,\,\mu_3\cdots\mu_N}\mathfrak{K}(\mu_1,\mu_2)\mathfrak{K}(\mu_2,\mu_3)\mathfrak{K}(\mu_3,\mu_4)\cdots\mathfrak{K}(\mu_N,\mu_{N+1})=\lambda_1^Na_1(\mu_1)a_1(\mu_{N+1})+\lambda_2^Na_2(\mu_1)a_2(\mu_{N+1}).$$

If we close the ring of spins by the assumption $\mu_{N+1}=\mu_1$ and sum over this last spin we get

$$\sum_{\mu_1}\mathfrak{K}(\mu_1,\mu_2)\mathfrak{K}(\mu_2,\mu_3)\cdots\mathfrak{K}(\mu_N,\mu_1)=\lambda_1^N+\lambda_2^N.$$

Substituting for the matrices $\mathfrak{K}$ their values as given by (7) we verify that the expression on the left-hand side is exactly the partition function f, as defined by (2), for a closed ring of N spins

$$f_N=\lambda_1^N+\lambda_2^N. \tag{8}$$

Finally, if the length N of the chain tends to infinity the smaller root λ_2 may be neglected.

What is the value of this larger root? The eigenvalue problem (7) reads

$$\begin{pmatrix}e^{K+C} & e^{-K}\\ e^{-K} & e^{K-C}\end{pmatrix}\begin{pmatrix}a(+)\\ a(-)\end{pmatrix}=\lambda\begin{pmatrix}a(+)\\ a(-)\end{pmatrix} \tag{7c}$$

and hence

$$\lambda=e^K\cosh C+(e^{2K}\sinh^2C+e^{-2K})^{\frac{1}{2}}. \tag{9}$$

It has already been pointed out by Ising himself[1] that a linear chain of spins is not ferromagnetic. This can easily be verified by calculating the total magnetization with the help of (5) and (8):

$$M=mN\sinh C/(\sinh^2C+e^{-4K})^{\frac{1}{2}}, \tag{10a}$$

an expression which, because of (4), vanishes with H. The initial molecular paramagnetic susceptibility comes out to be

$$\chi=(m^2/kT)\exp(J/kT). \tag{10b}$$

[5] The elegant form of procedure used here is due to Mr. E. Montroll who applied it first to the theory of molecular chains.

At low temperatures this value is very much larger than without the cooperative coupling J, but it is still finite.

In the absence of a magnetic field we have

$$\lambda = 2\cosh K,$$

which gives for the energy as a function of temperature

$$E = -\tfrac{1}{2}NJ\tanh K = -\tfrac{1}{2}NJ\tanh(J/2kT). \tag{11}$$

This is a smooth increase from $-\frac{1}{2}NJ$ to 0 as the temperature rises.

3. Matrix Form of the Square Net Problem

The successful calculation of Section 2 has unfortunately no bearing upon ferromagnetism since the model proves to be paramagnetic only. The situation is entirely different if we consider the still simplified case of a square net of spins having two infinite dimensions. Peierls[6] has proved that this model is ferromagnetic in the sense that it has a non-zero magnetization at absolute zero. We can conclude from that result that the spontaneous magnetization cannot possibly be represented by a single analytic function of temperature since it vanishes identically in the high temperature range. This in turn would make us suspect the existence of a singular point at which the magnetization ceases to vanish identically. It follows that the two-dimensional Ising model is a fair test case for the general statistical theory of ferromagnets.

The reduction of the linear chain problem can be described in a qualitative way as follows. It is possible to build up a chain by repeating constantly one and the same operation, namely adding another spin beyond the one just placed previously. In fact, if the chain is really very long no physical change takes place through the addition of one more spin. The successful mathematical treatment is based on this identity on the one hand and on the other on the fact that the *state of the last spin μ_n is only dependent upon the state of its predecessor μ_{n-1}*. It follows that the function $P(\mu_n)$ depends operationally on $P(\mu_{n-1})$, yet is the same mathematical function of its argument. Exactly this is expressed in Eq. (7).

A strip of spins having infinite length but finite width can obviously be built up in an analogous manner. Let us recall briefly the steps with the help of Fig. 2. First we write down two probability expressions, one referring to all spins marked by crosses and rings (we assume the positions $[P]$ to be vacant), and the other to all crosses, rings and positions $[P]$. Both expressions follow directly from Boltzmann's theorem, that is they are proportional to $\exp(-E/kT)$, E being given by (1). In interpreting (1) we must remember that the neighborhood in $\sum_{\langle i,k\rangle}$ is now both horizontal and vertical, as expressed by the connecting rods in Fig. 2. As a consequence, the factor by which the probabilities differ is equal to

$$\exp[K(\mu_1'\mu_2'+\mu_2'\mu_3'+\cdots+\mu_{n-1}'\mu_n')+K(\mu_1\mu_1'+\mu_2\mu_2'+\cdots\mu_n\mu_n')+C(\mu_1'+\mu_2'+\cdots+\mu_n')],$$

where the indices of the μ's refer to the column number. Only the μ's of the two top lines are involved in the expression, the very top one being indicated by μ_i', the next one by μ_i (see Fig. 2). Probabilities referring only to the two lines just mentioned can be gained by summing over all crossed spins. We are left with a function $P(\mu_i)$ of n variables and $P(\mu_i, \mu_i')$ of $2n$ variables. The two probabilities still differ from each other by the same factor

$$\rho\, P(\mu_i, \mu_i') = P(\mu_i)\exp[K\sum_{i=1}^{n-1}\mu_i'\mu_{i+1}'+K\sum_{i=1}^{n}\mu_i\mu_i'+C\sum_{i=1}^{n}\mu_i'],$$

[6] R. Peierls, Proc. Camb. Phil. Soc. **32**, 477 (1936). Ising's erroneous conclusions for the two-dimensional case are still quoted in some papers, e.g., Lamek Hulthen, Arkiv för Matematik Astronomi och Fysik **26A**, No. 11 (1940).

the constant ρ appearing for the same reason as above (§2). Finally, if the strip is very long $P(\mu_i') = \sum_{\mu_i} P(\mu_i, \mu_i')$ must be the same function of its variables as $P(\mu_i)$. The substitution

$$a(\mu_i) = P(\mu_i) \exp[\tfrac{1}{2}K \sum_{i=1}^{n-1} \mu_i\mu_{i+1} + \tfrac{1}{2}C \sum_{i=1}^{n} \mu_i]$$

will make the resulting eigenvalue problem symmetrical. It reads then

$$\sum_{\mu_i'} \mathfrak{K}(\mu_i, \mu_i')\, a(\mu_i') = \rho\, a(\mu_i) \tag{12a}$$

with

$$\mathfrak{K}(\mu_i, \mu_i') = \exp\,[K \sum_{i=1}^{n} \mu_i\mu_i' + \tfrac{1}{2}K \sum_{i=1}^{n-1} \mu_i\mu_{i+1} + \tfrac{1}{2}K \sum_{i=1}^{n-1} \mu_i'\mu_{i+1}' + \tfrac{1}{2}C \sum_{i=1}^{n} \mu_i + \tfrac{1}{2}C \sum_{i=1}^{n} \mu_i']. \tag{12b}$$

To find the significance of ρ we turn again to the matrix development theorem. We have this time 2^n roots ρ_i since the matrix is of that order. As a starting point, we use the two basic statements

$$\sum_{\mu_i} a_p(\mu_i) a_q(\mu_i) = \delta_{pq},$$

$$\mathfrak{K}(\mu_i, \mu_i') = \sum_{p=1}^{2^n} \rho_p\, a_p(\mu_i)\, a_p(\mu_i').$$

If we consider now a finite ring which is n spins wide and m spins in circumference we find that its partition function can be written in terms of the "nuclei" $\mathfrak{K}$ thus

$$f = \sum_{\mu_i^k} \mathfrak{K}(\mu_i^1, \mu_i^2)\mathfrak{K}(\mu_i^2, \mu_i^3)\mathfrak{K}(\mu_i^3, \mu_i^4) \cdots \mathfrak{K}(\mu_i^{m-1}, \mu_i^m)\mathfrak{K}(\mu_i^m, \mu_i^1).$$

Putting in the development for each matrix $\mathfrak{K}$, interchanging summations and remembering the orthogonality conditions we find

$$f = \sum_{p=1}^{2^n} \rho_p{}^m. \tag{13}$$

If we make the strip very long while keeping the width the same, m will become very large and all but the largest root ρ can be neglected. It is well known from the theory of matrices that the largest root has an eigenvector $a(\mu)$ with only positive components. This must be so, of course, because of their probability significance.

The doubly infinite square net results from (12) and (13) only in the limit when the width n of the strip tends to infinity as well as m. It has therefore been our endeavor to find a way of connecting n and $n+1$ just as our Eq. (12) carries out the reduction from $m+1$ to m. It has been impossible so far to do this in a rigorous manner. However, a very powerful approximation method can be based upon Eq. (12) which will be discussed in Part II, Section 7.

In spite of this failure some exact results can be obtained for the two-dimensional case; they are based on certain matrix identities. In order to obtain them we have to take up once more our basic steps which led to the eigenvalue problem (12). For it is possible to use instead of the matrix $\mathfrak{K}$ another equivalent one which does not have some of its inconveniences. The matrix $\mathfrak{K}$ is of order 2^n; it is filled solidly with elements which take up various values in a more or less haphazard way. In addition, its largest eigenvalue changes its meaning as n increases because it does not refer to one spin but to a whole line of them, i.e., we do not have $\rho^{nm} = f$, but only $\rho^m = f$. The reason for these features is that we built up the strip in large steps, filling a large number of vacant positions $[P]$ at one time (Fig. 2).

This situation can be amended partly by arranging the spins along the thread of a screw instead of a simple strip. For this purpose we dispose of the free right- and left-hand edges in Fig. 2 by bringing together each left end spin with the right end spin of the next line; the resulting order is

visualized in Fig. 3. Its advantage is that the whole net can now be built up through the simple operation of placing a new spin immediately beside its predecessor as we move along the thread of the screw. Figure 3 indicates this operation by a $[P]$ as in the two previous figures.

The mathematical build-up of the eigenvalue problem follows the two previous procedures. Boltzmann's theorem may be used to give the probabilities for all μ's with or without a spin being placed at $[P]$. As a second step we may eliminate, just as before, all explicit reference to the crossed spins by summation. If we denote by n the number of spins making up one pitch of the screw we can re-label the ring spins as indicated on Fig. 4. Let us call $A(\mu_{n-1}, \mu_{n-2}\cdots\mu_1, \mu_0)$ the probability referring to them alone and $P(\mu_n, \mu_{n-1}\cdots\mu_0)$ the one including μ_n in position $[P]$ as well. The factor by which the two quantities differ is now much simpler than it was in our previous treatment in §3. It contains only the two couplings which link up μ_n with μ_{n-1} and μ_0 in addition to the action of the field H on μ_n

$$\lambda\, P(\mu_n, \cdots\mu_0) = A(\mu_{n-1}, \cdots\mu_0)\exp[K\mu_n(\mu_{n-1}+\mu_0)+C\mu_n].$$

The eigenvalue problem follows from this equation if we sum $P(\mu_n, \cdots\mu_1, \mu_0)$ over μ_0 and notice that the resulting situation is identical with the one described by $A(\mu_{n-1}, \cdots\mu_0)$, provided the screw is very long. The only difference is that μ_1 now occupies the place of μ_0, μ_2 of μ_1, and so forth. It follows that we get the equation

$$\sum_{\mu_0} \exp[K\mu_n(\mu_{n-1}+\mu_0)+C\mu_n]\, A(\mu_{n-1}, \cdots\mu_0) = \lambda\, A(\mu_n, \cdots\mu_1). \tag{14}$$

If we compare (14) with (12) we notice that the matrix has become essentially asymmetric and that we have not achieved any reduction of its order. But we have realized two improvements: Each line contains now only two non-zero elements and the eigenvalue λ is now the partition function per individual spin regardless of the order of the matrix.

The proof of this latter proposition repeats the pattern outlined after Eq. (12), except that we have to take into account the asymmetry of the matrix. Let λ_i be its 2^n eigenvalues and $A_i(\mu_n\cdots\mu_1)$ the corresponding eigenvectors to the right. Then we have to consider in addition the eigenvectors to the left which we call $B_i(\mu_n, \cdots\mu_1)$ and which satisfy the equations

$$\sum_{\mu_n} \exp[K\mu_n(\mu_{n-1}+\mu_0)+C\mu_n]\, B(\mu_n, \cdots\mu_1) = \lambda\, B(\mu_{n-1}, \cdots\mu_0). \tag{15}$$

Before applying the basic equations it is advantageous to eliminate the appearance of identical μ's on either side of our Eqs. (14) and (15). This can be done by repeating n times the matrix operation indicated. If we discard the terms in C, i.e., let the magnetic field be zero for simplicity, we get

$$\sum_{\mu_1, \mu_2\cdots\mu_n} \exp[K\sum_{i=n}^{2n-1}\mu_i\mu_{i+1}+K\sum_{i=1}^{n}\mu_i\mu_{i+n}]A(\mu_n\cdots\mu_1) = \lambda^n A(\mu_{2n}\cdots\mu_{n+1})$$

and

$$\sum_{\mu_{n+1}, \mu_{n+2}, \cdots\mu_{2n}} \exp[K\sum_{i=n}^{2n-1}\mu_i\mu_{i+1}+K\sum_{i=1}^{n}\mu_i\mu_{i+n}]B(\mu_{2n}\cdots\mu_{n+1}) = \lambda^n B(\mu_n\cdots\mu_1).$$

It follows that with proper normalization

$$\sum_{\mu_i} B_p(\mu_n\cdots\mu_1)A_q(\mu_n\cdots\mu_1) = \delta_{pq}$$

and

$$\exp[K\sum_{i=n}^{2n-1}\mu_i\mu_{i+1}+K\sum_{i=1}^{n}\mu_i\mu_{i+n}] = \sum_{p=1}^{2^n}\lambda_p{}^n A_p(\mu_{2n}\cdots\mu_{n+1})B_p(\mu_n\cdots\mu_1).$$

We can write down this same formula for the next pitch of the screw

$$\exp[K\sum_{i=2n}^{3n-1}\mu_i\mu_{i+1}+K\sum_{i=n+1}^{2n}\mu_i\mu_{i+n}] = \sum_{p=1}^{2^n}\lambda_p{}^n A_p(\mu_{3n}\cdots\mu_{2n+1})B_p(\mu_{2n}\cdots\mu_{n+1}).$$

Now we multiply these two formulas with each other and sum over the spins of the middle row $\mu_{n+1}, \mu_{n+2} \cdots \mu_{2n}$. We get

$$\sum_{\mu_{n+1}, \mu_{n+2} \cdots \mu_{2n}} \exp[K \sum_{i=n}^{3n-1} \mu_i \mu_{i+1} + K \sum_{i=1}^{2n} \mu_i \mu_{i+n}] = \sum_{p=1}^{2^n} \lambda_p{}^{2n} A_p(\mu_{3n} \cdots \mu_{2n+1}) B_p(\mu_n \cdots \mu_1).$$

We can continue building up that way on the left the complete partition function of the problem. If we dispose of the ends of our screw by making it endless on a torus-shaped body, i.e., if we put

$$\mu_{mn+1} = \mu_1,$$

then we get finally

$$f = \sum_{p=1}^{2^n} \lambda_p{}^{mn} = \sum_{p=1}^{2^n} \lambda_p{}^N, \tag{16}$$

where $mn = N$ is the total number of spins present. If m is made sufficiently large while keeping n fixed, all but the largest eigenvalue λ may be neglected.

It has proved necessary in the study of the matrix (14) to avoid all unnecessary complications of the problem. One such complication is the dependence of λ on two parameters K and C, corresponding physically to the temperature and the magnetic field (Eqs. (3), (4)). It is an obvious simplification to study the square net at zero field only. Unfortunately the disadvantage of such a step is greater than is immediately obvious, for Eq. (5) shows us that it will be impossible under those circumstances to study even zero-field magnetization as a function of temperature. This reduces us henceforth entirely to the study of the energy and the specific heat. It is fortunate that these quantities show singularities concurrently with the magnetization at the Curie point, and their behavior as functions of T should be sufficient to discern the complete behavior of our model. From (6) and (16) we can thus deduce the following simplified expressions for the energy E and the molar specific heat C

$$E = -\tfrac{1}{2} NJ \, d \log\lambda / dK \tag{17}$$

and

$$C/R = K^2 \, d^2 \log\lambda / dK^2, \tag{18}$$

where R is the gas constant $R = Nk$.

If we make this assumption of zero magnetic field the parameter C in (14) is zero and the matrix operator is invariant with respect to inversion of all spins. It follows that the eigenvectors are either symmetric or antisymmetric with respect to that operation. Since the largest eigenvalue has only positive components it must belong to the symmetric class

$$A(\mu_n, \mu_{n-1} \cdots \mu_1) = A(-\mu_n, -\mu_{n-1}, \cdots -\mu_1). \tag{19}$$

This follows also from the significance of the A's as probabilities. Equation (19) reduces the number of components of **A** from 2^n to 2^{n-1}.

It has proved to be convenient to write the matrix in (14) as a thing with lines and columns. This implies some ordering of the components of **A**. The following scheme has been adopted.

Take a given arrangement of μ's, for instance

$$+ \; + \; - \; - \; + \; + \; - \; +,$$

replace all the plus signs by zeros and all the minus signs by ones, thus:

$$0 \; 0 \; 1 \; 1 \; 0 \; 0 \; 1 \; 0;$$

read the number thus obtained as if 2 were our decimal unit and let it be the order number of the arrangement. The above arrangement for instance has the order number 50. As an example let us write down the components for the case $n = 5$:

+	+	+	+	+	0		+	−	+	+	+	8
+	+	+	+	−	1		+	−	+	+	−	9
+	+	+	−	+	2		+	−	+	−	+	10
+	+	+	−	−	3		+	−	+	−	−	11
+	+	−	+	+	4		+	−	−	+	+	12
+	+	−	+	−	5		+	−	−	+	−	13
+	+	−	−	+	6		+	−	−	−	+	14
+	+	−	−	−	7		+	−	−	−	−	15

Because of the symmetry condition (19) the components 16 to 31 are identical with 15 to 0. We find generally

$$\text{component } (i) = \text{component } (2^n - i - 1).$$

From here on it is a straightforward matter to bring the matrix (14) into its customary square form. In the case $n=5$ we find, for example,

$$\mathfrak{M}(K)=\begin{vmatrix}
\alpha & 1 & 0 & 0 & 0 & 0 & 0 & 0 & 0 & 0 & 0 & 0 & 0 & 0 & 0 & 0 \\
0 & 0 & \alpha & 1 & 0 & 0 & 0 & 0 & 0 & 0 & 0 & 0 & 0 & 0 & 0 & 0 \\
0 & 0 & 0 & 0 & \alpha & 1 & 0 & 0 & 0 & 0 & 0 & 0 & 0 & 0 & 0 & 0 \\
0 & 0 & 0 & 0 & 0 & 0 & \alpha & 1 & 0 & 0 & 0 & 0 & 0 & 0 & 0 & 0 \\
0 & 0 & 0 & 0 & 0 & 0 & 0 & 0 & \alpha & 1 & 0 & 0 & 0 & 0 & 0 & 0 \\
0 & 0 & 0 & 0 & 0 & 0 & 0 & 0 & 0 & 0 & \alpha & 1 & 0 & 0 & 0 & 0 \\
0 & 0 & 0 & 0 & 0 & 0 & 0 & 0 & 0 & 0 & 0 & 0 & \alpha & 1 & 0 & 0 \\
0 & 0 & 0 & 0 & 0 & 0 & 0 & 0 & 0 & 0 & 0 & 0 & 0 & 0 & \alpha & 1 \\
0 & 0 & 0 & 0 & 0 & 0 & 0 & 0 & 0 & 0 & 0 & 0 & 0 & 0 & \beta & 1 \\
0 & 0 & 0 & 0 & 0 & 0 & 0 & 0 & 0 & 0 & 0 & 0 & \beta & 1 & 0 & 0 \\
0 & 0 & 0 & 0 & 0 & 0 & 0 & 0 & 0 & 0 & \beta & 1 & 0 & 0 & 0 & 0 \\
0 & 0 & 0 & 0 & 0 & 0 & 0 & 0 & \beta & 1 & 0 & 0 & 0 & 0 & 0 & 0 \\
0 & 0 & 0 & 0 & 0 & 0 & \beta & 1 & 0 & 0 & 0 & 0 & 0 & 0 & 0 & 0 \\
0 & 0 & 0 & 0 & \beta & 1 & 0 & 0 & 0 & 0 & 0 & 0 & 0 & 0 & 0 & 0 \\
0 & 0 & \beta & 1 & 0 & 0 & 0 & 0 & 0 & 0 & 0 & 0 & 0 & 0 & 0 & 0 \\
\beta & 1 & 0 & 0 & 0 & 0 & 0 & 0 & 0 & 0 & 0 & 0 & 0 & 0 & 0 & 0
\end{vmatrix}. \tag{20}$$

where $\alpha=e^{2K}$ and $\beta=e^{-2K}$. For other values of n the order of the matrix is a different power of two. Apart from that the matrix stays the same. The non-zero elements occupy a characteristic, turned-over V-shape. On the top arm e^{2K} and 1 are alternating, on the bottom e^{-2K} and 1. Altogether each line and each column has two non-zero elements.

Our statistical problem is now reduced to finding the largest eigenvalue $\lambda(K)$ of the matrix $\mathfrak{M}$:

$$\mathfrak{M}(K)\ \mathbf{A}(K)=\lambda(K)\ \mathbf{A}(K) \tag{21}$$[7]

and to studying the behavior of $\lambda(K)$ as the order of $\mathfrak{M}(K)$ increases indefinitely. For only in that limit does the solution correspond to the doubly infinite square net. The parameter K represents the temperature variable as defined in Eq. (3).

4. Properties of the Square Net Solution

It has been mentioned already that we have failed to find an exact solution in closed form for our problem. This does not mean, however, that no information concerning λ can be obtained. For some of the properties of the matrix $\mathfrak{M}$ have a bearing upon the properties of λ.

It is possible, for instance, to replace K by $-K$ in (20) through a simple re-ordering of terms. Using the case $n=5$ again as a test case this re-ordering matrix $\mathfrak{R}$ takes the following form

$$\mathfrak{R}=\begin{vmatrix}
0 & 0 & 0 & 0 & 0 & 0 & 0 & 0 & 0 & 0 & 1 & 0 & 0 & 0 & 0 & 0 \\
0 & 0 & 0 & 0 & 0 & 0 & 0 & 0 & 0 & 0 & 0 & 1 & 0 & 0 & 0 & 0 \\
0 & 0 & 0 & 0 & 0 & 0 & 0 & 0 & 1 & 0 & 0 & 0 & 0 & 0 & 0 & 0 \\
0 & 0 & 0 & 0 & 0 & 0 & 0 & 0 & 0 & 1 & 0 & 0 & 0 & 0 & 0 & 0 \\
0 & 0 & 0 & 0 & 0 & 0 & 0 & 0 & 0 & 0 & 0 & 0 & 0 & 0 & 1 & 0 \\
0 & 0 & 0 & 0 & 0 & 0 & 0 & 0 & 0 & 0 & 0 & 0 & 0 & 0 & 0 & 1 \\
0 & 0 & 0 & 0 & 0 & 0 & 0 & 0 & 0 & 0 & 0 & 0 & 1 & 0 & 0 & 0 \\
0 & 0 & 0 & 0 & 0 & 0 & 0 & 0 & 0 & 0 & 0 & 0 & 0 & 1 & 0 & 0 \\
0 & 0 & 1 & 0 & 0 & 0 & 0 & 0 & 0 & 0 & 0 & 0 & 0 & 0 & 0 & 0 \\
0 & 0 & 0 & 1 & 0 & 0 & 0 & 0 & 0 & 0 & 0 & 0 & 0 & 0 & 0 & 0 \\
1 & 0 & 0 & 0 & 0 & 0 & 0 & 0 & 0 & 0 & 0 & 0 & 0 & 0 & 0 & 0 \\
0 & 1 & 0 & 0 & 0 & 0 & 0 & 0 & 0 & 0 & 0 & 0 & 0 & 0 & 0 & 0 \\
0 & 0 & 0 & 0 & 0 & 0 & 1 & 0 & 0 & 0 & 0 & 0 & 0 & 0 & 0 & 0 \\
0 & 0 & 0 & 0 & 0 & 0 & 0 & 1 & 0 & 0 & 0 & 0 & 0 & 0 & 0 & 0 \\
0 & 0 & 0 & 0 & 1 & 0 & 0 & 0 & 0 & 0 & 0 & 0 & 0 & 0 & 0 & 0 \\
0 & 0 & 0 & 0 & 0 & 1 & 0 & 0 & 0 & 0 & 0 & 0 & 0 & 0 & 0 & 0
\end{vmatrix} \tag{22}$$

and its effect on $\mathfrak{M}(K)$ is given by

$$\mathfrak{R}\ \mathfrak{M}(K)\ \mathfrak{R}=\mathfrak{M}(-K). \tag{23}$$

It is clear that the transformation does not alter the eigenvalue spectrum and hence

$$\lambda(K)=\lambda(-K). \tag{24}$$

The substitution $K\rightarrow -K$ means replacing the ferromagnetic coupling J by an antiferromagnetic coupling of equal strength. It follows that such a coupling would also produce the thermal effects of ferromagnetism. This holds in particular for an eventual Curie point. Many approximate treatments destroy this basic symmetry.

It is easy to extend the definition (22) of $\mathfrak{R}$ to other orders. For if we compare that definition with the list of vector components on p. 259, we see that it simply changes the sign of every other spin. It should be mentioned in this connection that this invariance does not exist for $n=2,\ 4,\ 6\cdots$ because in those cases a completely antiferromagnetic pattern cannot be fitted into our screw arrangement of Fig. 3. For $n=1,\ 3,\ 5\cdots$ the difficulty does not arise and this partial sequence is sufficient to establish the invariance of λ for $n\rightarrow\infty$.

A more interesting result is obtained by operating on $\mathfrak{M}(K)$ with the unitary symmetric matrix $\mathfrak{T}$ which for $n=5$ has the following form:

$$\mathfrak{T}=\frac{1}{4}\begin{vmatrix}
1 & 1 & 1 & 1 & 1 & 1 & 1 & 1 & 1 & 1 & 1 & 1 & 1 & 1 & 1 & 1 \\
1 & 1 & 1 & 1 & 1 & 1 & 1 & 1 & -1 & -1 & -1 & -1 & -1 & -1 & -1 & -1 \\
1 & 1 & 1 & 1 & -1 & -1 & -1 & -1 & -1 & -1 & -1 & -1 & 1 & 1 & 1 & 1 \\
1 & 1 & 1 & 1 & -1 & -1 & -1 & -1 & 1 & 1 & 1 & 1 & -1 & -1 & -1 & -1 \\
1 & 1 & -1 & -1 & -1 & -1 & 1 & 1 & 1 & 1 & -1 & -1 & -1 & -1 & 1 & 1 \\
1 & 1 & -1 & -1 & -1 & -1 & 1 & 1 & -1 & -1 & 1 & 1 & 1 & 1 & -1 & -1 \\
1 & 1 & -1 & -1 & 1 & 1 & -1 & -1 & -1 & -1 & 1 & 1 & -1 & -1 & 1 & 1 \\
1 & 1 & -1 & -1 & 1 & 1 & -1 & -1 & 1 & 1 & -1 & -1 & 1 & 1 & -1 & -1 \\
1 & -1 & -1 & 1 & 1 & -1 & -1 & 1 & -1 & -1 & 1 & 1 & -1 & -1 & 1 & 1 \\
1 & -1 & -1 & 1 & 1 & -1 & -1 & 1 & 1 & 1 & -1 & -1 & 1 & 1 & -1 & -1 \\
1 & -1 & -1 & 1 & -1 & 1 & 1 & -1 & -1 & -1 & 1 & 1 & 1 & 1 & -1 & -1 \\
1 & -1 & -1 & 1 & -1 & 1 & 1 & -1 & 1 & 1 & -1 & -1 & -1 & -1 & 1 & 1 \\
1 & -1 & -1 & 1 & -1 & 1 & 1 & -1 & -1 & -1 & 1 & 1 & -1 & -1 & 1 & 1 \\
1 & -1 & 1 & -1 & 1 & -1 & 1 & -1 & 1 & -1 & 1 & -1 & 1 & -1 & 1 & -1 \\
1 & -1 & 1 & -1 & 1 & -1 & 1 & -1 & -1 & 1 & -1 & 1 & -1 & 1 & -1 & 1 \\
1 & -1 & 1 & -1 & -1 & 1 & -1 & 1 & 1 & -1 & 1 & -1 & -1 & 1 & -1 & 1
\end{vmatrix} \tag{25}$$

[7] When using matrix notation in this and the following paper we shall use uniformly the following convention: matrices will be printed in German type, vectors in bold face Latin type.

For arbitrary values of n the matrix can be formed with the help of the following prescription: Suppose you have the matrix in the case $n-1$. Then you get the matrix for the case n by writing down twice each line of the previous matrix and then continuing on the right-hand side alternately in a symmetric and antisymmetric fashion. In addition, divide by $\sqrt{2}$ to preserve unitary character. The matrix of order 1 you start out with is the number 1.

If we transform $\mathfrak{M}(K)$ with this matrix $\mathfrak{T}$ we find that it goes over from its form (20) into a matrix having upright V-shape. Upon closer inspection we can write it as follows

$$\mathfrak{T}\ \mathfrak{M}(K)\ \mathfrak{T}=\sinh 2K\ \mathfrak{M}^{+}(K^{*}),$$

where the cross on $\mathfrak{M}$ stands for transposition, i.e., exchange of lines and columns and K^{*} is an auxiliary quantity defined through

$$e^{2K^{*}}=\coth K$$

or more symmetrically

$$\sinh 2K\ \sinh 2K^{*}=1 \tag{26a}$$

or also

$$\frac{\sinh 2K}{\cosh^{2}2K}=\frac{\sinh 2K^{*}}{\cosh^{2}2K^{*}}. \tag{26b}$$

The matrix relation can also be brought in a more symmetric form through the substitution

$$\mathfrak{B}(K)=\frac{1}{\cosh 2K}\mathfrak{M}(K), \tag{27}$$

which yields

$$\mathfrak{T}\ \mathfrak{B}(K)\ \mathfrak{T}=\mathfrak{B}^{+}(K^{*}) \tag{28}$$

a relation which, because of

$$\mathfrak{T}=\mathfrak{T}^{+},\quad \text{and}\quad \mathfrak{T}^{2}=1$$

is obviously reversible.

Equation (28) has an important bearing upon λ. Neither transformation with $\mathfrak{T}$ nor transposition of $\mathfrak{M}$ does change its eigenvalues and hence we find for λ

$$\lambda(K)/\cosh 2K=\lambda(K^{*})/\cosh 2K^{*}.$$

We shall have occasion later to study this invariant quotient which we define as $x(K)$:

$$x(K)=\lambda(K)/\cosh 2K \tag{29}$$

and for which

$$x(K)=x(K^{*}). \tag{30}$$

If we interpret (26) with the help of (3) we see that it associates two temperatures with each other. As one of them rises from 0 to ∞ the other one drops from ∞ to 0. The significance of Eq. (30) is then that singular temperatures can only arise in pairs, since every singularity at K will be matched by one at K^{*}. The only exception to this rule is the temperature for which

$$\sinh 2K_{c}=1, \tag{31a}$$

since K_{c} is its own mate. The numerical value of K_{c} is found to be

$$K_{c}=0.44069. \tag{31b}$$

We conclude therefrom that if λ possesses one singularity only it must occur at the temperature given by (31). It is therefore the only possible location of the Curie point.

It is, of course, impossible to determine by such a symmetry argument the nature of the singularity, since we are not even certain of its existence. For the symmetry property in question is common to the whole sequence of matrices of order 1, 2, 4, 8, 16$\cdots$. All these finite matrices have solutions λ which are continuous throughout. But we can use our information in a negative way to exclude with certainty certain types of possible singularities. Using the definition (29) we find from (17) and (18)

$$E=-NJ\{\tanh 2K-\tfrac{1}{2}\,d\log x/dK\} \tag{32}$$

and

$$C/R=K^{2}\{4/\cosh^{2}2K+d^{2}\log x/dK^{2}\}. \tag{33}$$

Now from (26) we can derive the following relations at the Curie point

$$(dK^{*}/dK)_{K=K_{c}}=-1,\quad (d^{2}K^{*}/dK^{2})_{K=K_{c}}=2\sqrt{2}$$

and therefore from (30)

$$(dx/dK)_{K_{c}+0}+(dx/dK)_{K_{c}-0}=0 \tag{34}$$

and

$$\left(\frac{d^{2}x}{dK^{2}}\right)_{K_{c}+0}-\left(\frac{d^{2}x}{dK^{2}}\right)_{K_{c}-0}=-\sqrt{2}\left\{\left(\frac{dx}{dK}\right)_{K_{c}+0}-\left(\frac{dx}{dK}\right)_{K_{c}-0}\right\}. \tag{35}$$

Because of (32) Eq. (34) tells us that if the energy is continuous at the Curie point it must have the value

$$E(K_c) = -\tfrac{1}{2}\sqrt{2}NJ \tag{36}$$

which is a rather slow growth from the low temperature minimum $E=-NJ$ to the high temperature value $E=0$. In case of a phase transition (36) would at least represent the arithmetic mean of the values it has in the two phases.

Equation (35) tells us that *if the energy at K_c is continuous then the specific heat is also continuous unless it is infinite.* This infinity, if existing, would have to be of a rather symmetric nature since $C(K)-C(K^*)$ must tend to zero as we approach the Curie point. This result will be of great importance in Part II since it is in flat contradiction to most approximate solutions, which show a jump of the specific heat at the Curie point.

Both these results can be united into a single statement. If we study the sequence of solutions x_n for $n=1, 2, 3\cdots$ the specific heat as given by (33) must either tend to infinity at $K=K_c$ or else both energy and specific heat are continuous. The question thus formulated is specific enough to permit numerical treatment. It will occupy Section 6 in Part II and will give strong evidence that the specific heat is actually infinite at the Curie temperature.

We hope that the matrix method of solving statistical problems will be of use to other workers in this field. It may be mentioned in this connection that the treatment of the three-dimensional Ising model can also be reduced to the solution of a sequence of V-shaped matrices. It seems altogether as if a better understanding of such V-matrices might be helpful for statistics. One would expect this not to be too difficult in view of the small number of non-zero elements and their periodic structure. Their main drawback as compared to other simple matrices seems to be that the linear system to which they belong does not have the structure of a system of recursion relations.

In conclusion we want to express our thanks to Mr. E. Montroll for a helpful discussion.

Statistics of the Two-Dimensional Ferromagnet. Part II

H. A. KRAMERS, *University of Leiden, Leiden, Holland*

AND

G. H. WANNIER, *University of Texas, Austin, Texas*

(Received June 12, 1941)

The study of the two-dimensional Ising model is continued. Its specific heat at the Curie point is investigated. The quantity in question is computed for six successive finite matrix problems and the conclusion is drawn that the specific heat is infinite at the Curie point. A new closed form approximation of the partition function λ is then developed by using the matrix method in its variational form. The two power series for λ at extreme temperatures are used as a test for this and various other approximations, and it is found that the new result is a considerable improvement over the existing solutions. Finally it is pointed out that these closed form solutions support our conclusion as to the place and nature of the Curie point transition.

AFTER having collected in Part I[8] some exact information concerning the partition function f of the two-dimensional Ising model we wish to present in this paper some approximate methods of our own and compare their results with the exact information available and other well-known approximate schemes.

Before proceeding let us recall the notation. We denoted by λ the partition function per spin, i.e., for N spins we have

$$f=\lambda^N(K). \tag{37}$$

The parameter K is the only variable on which λ depends. It combines the coupling energy J and the temperature T in the form

$$K=J/2kT. \tag{38}$$

The knowledge of $\lambda(K)$ is not sufficient for the computation of the magnetic properties of the model, but it permits calculation of the thermal quantities, particularly the total energy E and the molar specific heat C [Eqs. (17) and (18)].

5. Power Series Developments of λ

The energy of our system can be obtained by elementary reasoning in both the very high and very low temperature region.

At high temperatures (i.e., $K=0$) the spins orient themselves at random regardless of coupling forces. We conclude, therefore, by direct inspection of Eq. (1) that

$$E(0)=0.$$

By a similar reasoning we find for large K

$$E(\infty)=-NJ.$$

Equations (2) and (37) then permit the computation of λ in these two extreme cases. We find

$$\lambda(0)=2, \tag{39}$$

$$\lambda(\infty)\approx e^{2K}. \tag{40}$$

Either one of these two limiting formulas can be continued by a power series. The continuation of (39) is the well-known development of λ in powers[9] of $1/T$ which in our case means powers of K. If we carry out this development in Eq. (2) we get

$$f=\sum_{\mu_i=\pm 1}[1+K\sum_{\langle i,k\rangle}\mu_i\mu_k+\tfrac{1}{2}K^2(\sum_{\langle i,k\rangle}\mu_i\mu_k)^2+\cdots$$

$$=2^N[1+K\langle\sum_{\langle i,k\rangle}\mu_i\mu_k\rangle_{Av}+\tfrac{1}{2}K^2\langle(\sum_{\langle i,k\rangle}\mu_i\mu_k)^2\rangle_{Av}+\cdots.$$

The averages are quite elementary to evaluate because they are to be taken at infinite temperature, that is, regardless of coupling. They are expressions containing various powers of N. But when we raise f to the power $1/N$ in accordance with (37) these powers disappear. Thus we find for λ

$$\lambda=2\left(1+K^2+\frac{4}{3}K^4+\frac{77}{45}K^6+\frac{1009}{315}K^8+\cdots\right). \tag{41}$$

[8] H. A. Kramers and G. H. Wannier, Phys. Rev. **60**, 252 (1941), this issue.

[9] W. Opechowski, Physica **4**, 181 (1937).

TABLE I. *Values of eigenvectors.*

VECTOR A_2	VECTOR A_5	VECTOR A_6	
1.000000	1.000000	1.000000	.094527
.249038	.145548	.137739	.017936
	.100846	.098916	.009995
VECTOR A_3	.129103	.112698	.017578
	.098804	.097652	.010148
1.000000	.019608	.016676	.002709
.186931	.075422	.071758	.008510
.105677	.148388	.114363	.022371
.231108	.096230	.096454	.065628
	.020594	.016343	.017673
VECTOR A_4	.011008	.010661	.008320
	.023617	.016817	.022060
1.000000	.070174	.069010	.056461
.159434	.023648	.016516	.022385
.103346	.066754	.062185	.060217
.160827	.218677	.141720	.216286
.099340			
.026148			
.079123			
.222893			

It is also possible to find a power series valid for low temperatures.[10] In the very lowest state all spins are oriented parallel to each other.[6] The first excited state is given by the reversal of a single spin and requires an excitation energy $4J$. The next higher state corresponds to the reversal of two neighboring spins (excitation energy $6J$), the following to the reversal of two independent spins, and so forth. The development proceeds in inverse powers of

$$k=e^{K}=e^{J/2kT} \tag{42}$$

and yields, after extraction of the Nth root,

$$\lambda=k^2(1+k^{-8}+2k^{-12}+5k^{-16}+14k^{-20}+\cdots). \tag{43}$$

Equations (41) and (43) must be different aspects of one and the same power series, in view of the symmetry property expressed through (26), (29) and (30). This is, in fact, true and can be made explicit through the introduction of the following parameter

$$\kappa=\frac{\sinh 2K}{2\cosh^2 2K}. \tag{44a}$$

Its invariance property

$$\kappa(K)=\kappa(K^*) \tag{44b}$$

has already been pointed out in (26b). It vanishes at either very high or very low temperatures, and behaves as K in the former and as k^{-2} in the latter region. Its maximum value at $K=K_c$ is equal to $\frac{1}{4}$. With the help of this parameter we may unite the two series into

$$x(K)=\lambda(K)/\cosh 2K=2(1-\kappa^2-4\kappa^4-29\kappa^6 -265\kappa^8-2745\kappa^{10}-\cdots). \tag{45}$$

For our problem these series solutions are of no direct interest, for they seem to diverge in the critical region. They are, however, a very agreeable criterion to test the accuracy of approximate solutions by comparing their series development with (41) and (43).

6. THE SPECIFIC HEAT AT THE CURIE POINT

If our model leads to one singular temperature only (which is the standard idea associated with the Curie temperature) then the Eqs. (26), (30), and (31) permit us to limit our attention to the point $K=0.44069$. In addition, the possibilities to be expected at that point are essentially twofold only: Either the specific heat tends to infinity as we approach the infinite problem over a sequence of finite matrix problems, or else it stays finite, in which case both energy and specific heat must be continuous [Eqs. (34) and (35)].

We have applied this test to the sequence of V matrices (20) of order 2, 4, 8, 16, 32. This corresponds physically to the arrangement of spins along the thread of a screw with 2, 3, 4, 5, 6 spins per pitch. In addition, we added the solution λ_1 having one spin per pitch as the first member. This case is equivalent to a linear chain with doubly strong coupling.

There is no difficulty of principle in computing these λ's as functions of K, and in particular their second derivative at $K=K_c$. In practice, however, it is found that the secular equation derived from (20) becomes rapidly unmanageable as the order of the matrix increases. Another, more elegant, method has therefore been followed, which uses a good number of special properties of such V matrices.

In the first place, it is possible to obtain the largest eigenvalue λ for a given value of K by operating repeatedly with the matrix (20) on an arbitrary vector (iteration method).[11] After a

[10] F. Bloch, Zeits. f. Physik **61**, 206 (1930).

[11] Frazer, Duncan and Collar, *Elementary Matrices and some Applications to Dynamics and Differential Equations* (Cambridge University Press and the Macmillan Company, 1938), p. 138.

number of operations which depends on the skill with which the initial vector was chosen the vector becomes the eigenvector of the largest eigenvalue and the matrix multiplies it each time with that eigenvalue. In this fashion eigenvalue and eigenvector of (21) were calculated at $K=K_c$. For the eigenvectors the values in Table I were obtained and for the eigenvalues

$$\lambda_1=2.828427,\quad \lambda_3=2.601145,\quad \lambda_5=2.559762,$$
$$\lambda_2=2.663252,\quad \lambda_4=2.573648,\quad \lambda_6=2.551953.$$

It is well known from matrix calculus that the knowledge of the eigenvector for a given value of some parameter K permits the determination of the first derivative of the eigenvalue with respect to this parameter. For the second derivative, however, the knowledge of all eigenvectors is usually necessary. But in our particular case it can be circumvented. A matrix can be found whose expectation value at K_c equals the second derivative x''; this is due to the special properties of this point.

The method runs as follows. The matrix $\mathfrak{V}$ possesses for each eigenvalue a right-hand and a left-hand eigenvector as pointed out in (14) and (15). With the help of (20), (27), (29) and the cross convention for transposed matrices we get the two equations in the form

$$\mathfrak{V}(K)\mathbf{A}(K)=x(K)\mathbf{A}(K) \tag{46}$$

and

$$\mathbf{B}^+(K)\mathfrak{V}(K)=x(K)\mathbf{B}^+(K). \tag{47}$$

Differentiation of these equations leads to the following formulas for $x'(K)$ and $x''(K)$

$$\mathbf{B}^+(K)\mathbf{A}(K)x'(K)=\mathbf{B}^+(K)\mathfrak{V}'(K)\mathbf{A}(K) \tag{48}$$

and

$$\begin{aligned}\mathbf{B}^+(K)\mathbf{A}(K)x''(K)&=\mathbf{B}^+(K)\mathfrak{V}''(K)\mathbf{A}(K)\\&+\mathbf{B}'^+(K)\mathfrak{V}'(K)\mathbf{A}(K)+\mathbf{B}^+(K)\mathfrak{V}'(K)\mathbf{A}'(K)\\&-x'(K)\{\mathbf{B}^+(K)\mathbf{A}'(K)+\mathbf{B}'^+(K)\mathbf{A}(K)\}.\end{aligned} \tag{49}$$

The special properties of $K=K_c$ come in through (25), (26), and (28)

$$\mathfrak{T}\mathfrak{V}(K)-\mathfrak{V}^+(K^*)\mathfrak{T}=0 \tag{50}$$

with

$$\mathfrak{T}=\mathfrak{T}^+\quad\text{and}\quad\mathfrak{T}^2=1. \tag{51}$$

Because of (46) and (47) the matrix $\mathfrak{T}$ will also relate the eigenvectors $\mathbf{B}$ and $\mathbf{A}$, except for an arbitrary factor. We may let this factor be unity and write

$$\mathbf{B}(K^*)=\mathfrak{T}\mathbf{A}(K)\quad\text{and}\quad\mathbf{A}(K^*)=\mathfrak{T}\mathbf{B}(K). \tag{52}$$

It is important to notice that $\mathfrak{T}$ is a constant matrix. Remembering that

$$K^*_c=K_c\quad\text{and}\quad(dK^*/dK)_{K=K_c}=-1, \tag{53}$$

we thus derive the following relations from (50)

$$\mathfrak{T}\mathfrak{V}'(K_c)+\mathfrak{V}'^+(K_c)\mathfrak{T}=0, \tag{54}$$

$$\mathbf{B}'(K_c)=-\mathfrak{T}\mathbf{A}'(K_c). \tag{55}$$

These equations will simplify (48) and (49). Using (51), (52), (54) and (55) we get

$$\begin{aligned}\mathbf{B}^+(K_c)\mathfrak{V}'(K_c)\mathbf{A}(K_c)&=\mathbf{A}^+(K_c)\mathfrak{T}\mathfrak{V}'(K_c)\mathfrak{T}\mathbf{B}(K_c)\\&=-\mathbf{A}^+(K_c)\mathfrak{V}'^+(K_c)\mathbf{B}(K_c)\\&=-\mathbf{B}^+(K_c)\mathfrak{V}'(K_c)\mathbf{A}(K_c)\\&=0\end{aligned}$$

and

$$\begin{aligned}\mathbf{B}'^+(K_c)\mathfrak{V}'(K_c)\mathbf{A}(K_c)&=-\mathbf{A}'^+(K_c)\mathfrak{T}\mathfrak{V}'(K_c)\mathfrak{T}\mathbf{B}(K_c)\\&=\mathbf{A}'^+(K_c)\mathfrak{V}'^+(K_c)\mathbf{B}(K_c)\\&=\mathbf{B}^+(K_c)\mathfrak{V}'(K_c)\mathbf{A}'(K_c),\end{aligned}$$

which reduces (48) and (49) to

$$x'(K_c)=0, \tag{56}$$

$$\begin{aligned}x''(K_c)=\frac{1}{\mathbf{B}^+(K_c)\mathbf{A}(K_c)}&[\mathbf{B}^+(K_c)\mathfrak{V}''(K_c)\mathbf{A}(K_c)\\&+2\mathbf{B}^+(K_c)\mathfrak{V}'(K_c)\mathbf{A}'(K_c)].\end{aligned} \tag{57}$$

At $K=K_c$ the matrix $\mathfrak{T}$ may serve to transpose the lines and columns of $\mathfrak{V}$. The same thing can be brought about for all K's by reordering the components:

$$\begin{aligned}\mathfrak{S}(K)\mathfrak{V}(K)-\mathfrak{V}^+(K)\mathfrak{S}(K)&=0,\\\mathbf{B}(K)\sim\mathfrak{S}(K)\mathbf{A}(K)&\end{aligned} \tag{58}$$

and hence, because of (52),

$$\mathbf{A}(K^*)\sim\mathfrak{T}\mathfrak{S}(K)\mathbf{A}(K). \tag{59}$$

For $n=5$ the reordering matrix $\mathfrak{S}(K)$, expressed in terms of our parameter k defined by (42), has the following form

$$\mathfrak{S}(K)=\begin{pmatrix}
k^{-4}&0&0&0&0&0&0&0&0&0&0&0&0&0&0\\
0&0&0&0&0&0&0&0&0&0&0&0&0&0&k^{-2}\\
0&0&0&0&0&0&0&0&1&0&0&0&0&0&0\\
0&0&0&0&0&0&0&k^{-2}&0&0&0&0&0&0&0\\
0&0&0&0&1&0&0&0&0&0&0&0&0&0&0\\
0&0&0&0&0&0&0&0&0&0&0&k^2&0&0&0\\
0&0&0&0&0&0&0&0&0&0&0&0&1&0&0\\
0&0&0&k^{-2}&0&0&0&0&0&0&0&0&0&0&0\\
0&0&1&0&0&0&0&0&0&0&0&0&0&0&0\\
0&0&0&0&0&0&0&0&0&0&0&0&k^2&0&0\\
0&0&0&0&0&0&0&0&0&0&k^4&0&0&0&0\\
0&0&0&0&0&k^2&0&0&0&0&0&0&0&0&0\\
0&0&0&0&0&0&1&0&0&0&0&0&0&0&0\\
0&0&0&0&0&0&0&0&0&k^2&0&0&0&0&0\\
0&0&0&0&0&0&0&0&0&0&0&0&0&1&0\\
0&k^{-2}&0&0&0&0&0&0&0&0&0&0&0&0&0
\end{pmatrix} \tag{60}$$

It is immediately generalized to other orders with the help of the list of components in I, p. 259. The matrix inverts the sequence of signs, that is $+++-+$ goes over into $+-+++$. In addition, it multiplies with a factor $\exp(-K\sum_i \mu_i\mu_{i+1})$. $\mathfrak{V}$, $\mathfrak{T}$ and $\mathfrak{S}$ are related by a fundamental identity. Using (50) and (58) we get

$$\mathfrak{T}\mathfrak{S}(K^*)\mathfrak{T}\mathfrak{S}(K)\mathfrak{V}(K)=\mathfrak{V}(K)\mathfrak{T}\mathfrak{S}(K^*)\mathfrak{T}\mathfrak{S}(K),$$

i.e., the expression

$$\mathfrak{T}\mathfrak{S}(K^*)\mathfrak{T}\mathfrak{S}(K)$$

commutes with $\mathfrak{V}$ and hence, assuming no multiple roots, is expressible in terms of it. We find, by direct inspection,

$$\mathfrak{T}\mathfrak{S}(K^*)\mathfrak{T}\mathfrak{S}(K)=\{2[\kappa(K)]^{\frac{1}{2}}\mathfrak{W}^{-1}(K)\}^{n-1}, \quad (61)$$

where n is, as usual, the number of spins per pitch, that is, 2^{n-1} is the matrix order. Because of (59), already $\mathfrak{T}\mathfrak{S}(K)$ commutes with $\mathfrak{V}$ at $K=K_c$ and must equal some square root of (61). The sign varies for different eigenvectors and is found to be positive for our vector $\mathbf{A}(K_c)$. Remembering that $\kappa(K_c)=\frac{1}{4}$ and (46) we get

$$\mathfrak{T}\mathfrak{S}(K_c)\mathbf{A}(K_c)=(1/x(K_c))^{(n-1)/2}\mathbf{A}(K_c). \quad (62)$$

With the help of $\mathfrak{T}\mathfrak{S}(K_c)$ we define a new matrix $\mathfrak{W}$ which shall be a function of $\mathfrak{V}$ not depending directly on K

$$\mathfrak{W}=\alpha+\beta\mathfrak{W}+\gamma\mathfrak{W}^2+\delta\mathfrak{W}^3+\cdots \quad (63)$$

and for which

$$\mathfrak{W}(K_c)=\mathfrak{T}\mathfrak{S}(K_c). \quad (64)$$

Because of (50) and (54), the derivative of $\mathfrak{W}$ obeys the equation

$$\mathfrak{T}\mathfrak{W}'(K_c)+\mathfrak{W}'^{+}(K_c)\mathfrak{T}=0,$$

which, considering (51), means that

$$\mathfrak{A}=\mathfrak{T}\mathfrak{W}'(K_c) \quad (65)$$

is an antisymmetric matrix. Because of (63), $\mathfrak{W}$ admits $\mathbf{A}$ as an eigenvector; if we differentiate this relation as well as (59) and remember (64) we arrive at

$$\mathfrak{W}'(K_c)\mathbf{A}(K_c)+\mathfrak{T}\mathfrak{S}(K_c)\mathbf{A}'(K_c)=(1/x(K_c))^{(n-1)/2}\mathbf{A}'(K_c),$$

$$\mathfrak{T}\mathfrak{S}'(K_c)\mathbf{A}(K_c)+\mathfrak{T}\mathfrak{S}(K_c)\mathbf{A}'(K_c)=-(1/x(K_c))^{(n-1)/2}\mathbf{A}'(K_c).$$

Subtracting and simplifying with (51) and (65) we get

$$\mathbf{A}'(K_c)=\tfrac{1}{2}(x(K_c))^{(n-1)/2}\mathfrak{T}\{\mathfrak{A}-\mathfrak{S}'(K_c)\}\mathbf{A}(K_c). \quad (66)$$

Uniting finally (57) and (66), simplifying with (52) and (54) and leaving off the now superfluous argument K_c we get the final formula

$$x''=\frac{1}{\mathbf{B}^+\mathbf{A}}[\mathbf{B}^+\mathfrak{V}''\mathbf{A}+x^{(n-1)/2}\mathbf{A}^+\mathfrak{V}'^{+}\{\mathfrak{S}'-\mathfrak{A}\}\mathbf{A}]. \quad (67)$$

Expression (67) for x'' has the desired form. The eigenvalue x and the eigenvectors $\mathbf{A}$ and $\mathbf{B}$ are numerically given on page 264 and through (52); the matrices involved are obtainable by differentiation from (20), (27), and (60). The matrix $\mathfrak{A}$ is the only exception, being given through implicit equations. It is easy, however, to obtain for it a number of equations far in excess of the number of its components, particularly since $\mathfrak{A}$ is restricted to be antisymmetric. For we have, for any power p of $\mathfrak{V}$, because of (63)

$$\mathfrak{W}\mathfrak{V}^p-\mathfrak{V}^p\mathfrak{W}=0,$$

which, because of (50), (54), (64), (65), gives

$$\mathfrak{V}^p\mathfrak{A}-\mathfrak{A}\mathfrak{V}^p=\mathfrak{S}(\mathfrak{V}^p)'+(\mathfrak{V}^p)'^{+}\mathfrak{S}. \quad (68)$$

In the case $n=5$, the matrix obtained for $\mathfrak{A}$ looks as follows

$$\mathfrak{A}=\begin{pmatrix}
0 & -2^{\frac{1}{2}}k^{-2} & -2k^{-2} & -2^{\frac{1}{2}}k^{-2} & -2k^{-2} & 0 & -2k^{-2} & -2^{\frac{1}{2}}k^{-2} & -2k^{-2} & 0 & 0 & 0 & -2k^{-2} & 0 & -2k^{-2} & -2^{\frac{1}{2}}k^{-2} \\
2^{\frac{1}{2}}k^{-2} & 0 & 0 & 0 & 0 & 0 & 0 & 0 & -2^{\frac{1}{2}}k^{-2} & -2 & 0 & -2 & -2^{\frac{1}{2}}k^{-2} & -2 & -2^{\frac{1}{2}}k^{-2} & 0 \\
2k^{-2} & 0 & 0 & 0 & 0 & 0 & 0 & 2^{\frac{1}{2}}k^{-2} & 0 & -2^{\frac{1}{2}}k^{2} & -2k^{2} & -2^{\frac{1}{2}}k^{2} & 0 & 0 & 0 & -2^{\frac{1}{2}}k^{-2} \\
2^{\frac{1}{2}}k^{-2} & 0 & 0 & 0 & -2^{\frac{1}{2}}k^{-2} & -2 & -2^{\frac{1}{2}}k^{-2} & 0 & 2^{\frac{1}{2}}k^{-2} & 2 & 0 & 2 & 0 & 0 & 0 & 0 \\
2k^{-2} & 0 & 0 & 2^{\frac{1}{2}}k^{-2} & 0 & -2^{\frac{1}{2}}k^{2} & 0 & -2^{\frac{1}{2}}k^{-2} & 0 & 0 & -2k^{2} & -2^{\frac{1}{2}}k^{2} & 0 & 0 & 0 & 0 \\
0 & 0 & 0 & 2 & 2^{\frac{1}{2}}k^{2} & 0 & 0 & -2 & 2^{\frac{1}{2}}k^{2} & 0 & -2^{\frac{1}{2}}k^{2} & 0 & -2^{\frac{1}{2}}k^{2} & 0 & 0 & 2 \\
2k^{-2} & 0 & 0 & 2^{\frac{1}{2}}k^{-2} & 0 & 0 & 0 & 0 & 0 & 0 & 2k^{2} & 2^{\frac{1}{2}}k^{2} & 0 & -2^{\frac{1}{2}}k^{2} & 0 & -2^{\frac{1}{2}}k^{-2} \\
2^{\frac{1}{2}}k^{-2} & 0 & -2^{\frac{1}{2}}k^{-2} & 0 & 2^{\frac{1}{2}}k^{-2} & 2 & 0 & 0 & 0 & 0 & 0 & -2 & 2^{\frac{1}{2}}k^{-2} & 2 & 0 & 0 \\
2k^{-2} & 2^{\frac{1}{2}}k^{-2} & 0 & -2^{\frac{1}{2}}k^{-2} & 0 & -2^{\frac{1}{2}}k^{2} & 0 & 0 & 0 & 0 & -2k^{2} & 0 & 0 & -2^{\frac{1}{2}}k^{2} & 0 & 0 \\
0 & 2 & 2^{\frac{1}{2}}k^{2} & -2 & 0 & 0 & 0 & 0 & 0 & 0 & -2^{\frac{1}{2}}k^{2} & 0 & 2^{\frac{1}{2}}k^{2} & 0 & -2^{\frac{1}{2}}k^{2} & 2 \\
0 & 0 & 2k^{2} & 0 & 2k^{2} & 2^{\frac{1}{2}}k^{2} & -2k^{2} & 0 & 2k^{2} & 2^{\frac{1}{2}}k^{2} & 0 & -2^{\frac{1}{2}}k^{2} & -2k^{2} & -2^{\frac{1}{2}}k^{2} & 2k^{2} & 0 \\
0 & 2 & 2^{\frac{1}{2}}k^{2} & -2 & 2^{\frac{1}{2}}k^{2} & 0 & -2^{\frac{1}{2}}k^{2} & 2 & 0 & 0 & 2^{\frac{1}{2}}k^{2} & 0 & 0 & 0 & 0 & 0 \\
2k^{-2} & 2^{\frac{1}{2}}k^{-2} & 0 & 0 & 0 & 2^{\frac{1}{2}}k^{2} & 0 & -2^{\frac{1}{2}}k^{-2} & 0 & -2^{\frac{1}{2}}k^{2} & 2k^{2} & 0 & 0 & 0 & 0 & 0 \\
0 & 2 & 0 & 0 & 0 & 0 & 2^{\frac{1}{2}}k^{2} & -2 & 2^{\frac{1}{2}}k^{2} & 0 & 2^{\frac{1}{2}}k^{2} & 0 & 0 & 0 & -2^{\frac{1}{2}}k^{2} & 2 \\
2k^{-2} & 2^{\frac{1}{2}}k^{-2} & 0 & 0 & 0 & 0 & 0 & 0 & 0 & 2^{\frac{1}{2}}k^{2} & -2k^{2} & 0 & 0 & 2^{\frac{1}{2}}k^{2} & 0 & -2^{\frac{1}{2}}k^{-2} \\
2^{\frac{1}{2}}k^{-2} & 0 & 2^{\frac{1}{2}}k^{-2} & 0 & 0 & -2 & 2^{\frac{1}{2}}k^{-2} & 0 & 0 & -2 & 0 & 0 & 0 & -2 & 2^{\frac{1}{2}}k^{-2} & 0
\end{pmatrix} \quad (69)$$

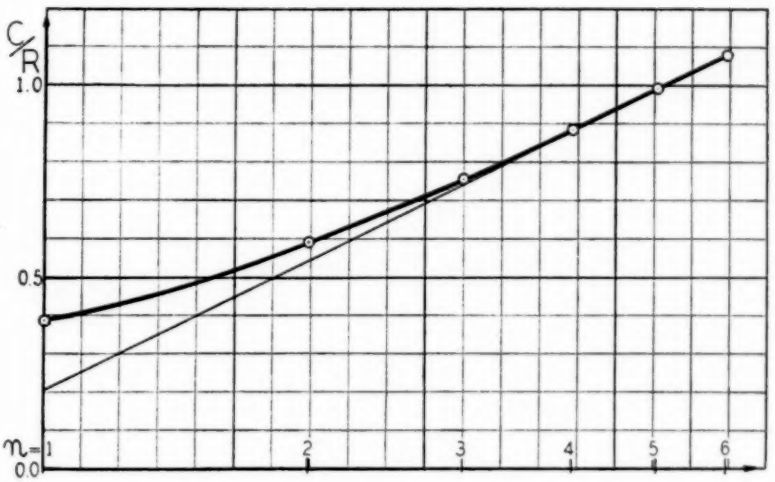

FIG. 5. Behavior of specific heat at T_c in successive "screw" approximations. The logarithm of the number of spins making up one "pitch" of the screw is plotted on abscissa.

It has, unfortunately, not been possible to find a general rule of formation for the matrix for all values of n. But the number of regularities is sufficiently large to permit guessing of the elements with the help of some of the equations (68). Thus our purpose of computing $x''(K_c)$ without the knowledge of the secular equation is achieved. The latter method was used as a cross check for the smaller matrices.

We find, in this fashion, the values for $x(K_c)$ and $x''(K_c)$ as functions of n given in Table II. Because of (56), these numbers are the only variables to enter into the specific heat as given by (33):

$$S=\frac{C}{R}=K_c^2\left(2+\frac{x''}{x}\right). \tag{70}$$

The fundamental question of this section is: does the quantity S tend to infinity or not with increasing n? Since this involves extrapolating to the limit of an infinite sequence from its first six members the answer is somewhat a matter of judgment. This is particularly true in this case because the growth of S is decelerating with n. A careful analysis of the data, however, still indicates strongly that C tends to infinity. The conclusion is reached by comparing S with $\log n$.

TABLE II. *Values of x and x''.*

n	x	x''	n	x	x''
1	2.00000	0.00000	4	1.81984	4.66665
2	1.88320	1.97715	5	1.81002	5.62246
3	1.83929	3.48493	6	1.80450	6.41935

The resulting curve is plotted on Fig. 5. It indicates that the mutual relation approaches linearity. This is borne out even more exactly by the analysis shown in Table III. The first two columns contain the argument n and the function S, then follows the difference quotient dividing the increment of S by the increment of $\log n$. That this quotient tends to a constant is shown in the next two columns. The first shows that the differences between successive quotients decrease rapidly, and the last, by forming the ratios between those differences, shows that the decrease is exponential and therefore sufficient to guarantee convergence of the difference quotients to a constant value.

We conclude therefrom that the specific heat of the two-dimensional square net of spins is infinite at $K_c=0.4407$, insofar as numerical extrapolation methods are able to decide such a question. Whether this means a latent heat or not is beyond the scope of the method.

TABLE III.

n	$S=C/R$	$\frac{\Delta S}{\Delta \log n}$	$\Delta\frac{\Delta S}{\Delta \log n}$	Ratios of Δ's
1	0.38841			
		0.2942		
2	0.59230		0.1105	
		0.4046		0.43
3	0.75637		0.0474	
		0.4520		0.42
4	0.88641		0.0197	
		0.4717		0.45
5	0.99167		0.0088	
		0.4805		
6	1.07928			

7. A New Approximation of λ for All Temperatures

The calculations of the preceding section indicate that we are not able, at present, to dispense with approximate evaluations of λ. But even in this field better results can be obtained with the eigenvalue method. We depart in this case from the eigenvalue problem (12) referring to an infinite strip (Fig. 2). For simplicity we may assume that the free ends of each strip are linked up with each other. This will make it an infinite cylinder in which each level circle consists of n equivalent spins. Our unknown λ is then the nth root of the eigenvalue ρ.

The largest eigenvalue of a matrix can always be expressed in a variational form. In our case we find from (12)

$$\lambda = \operatorname*{Max}_{\text{all } a\text{'s}} \frac{\sum_{\mu_i \mu_i'} \mathfrak{K}(\mu_i, \mu_i') a(\mu_i) a(\mu_i')}{\sum_{\mu_i} [a(\mu_i)]^2}. \tag{71}$$

Expression (71) obviously suggests a variation method in which a restricted set of competing functions are used for the a's. In the first place, the correct a's themselves possess the symmetries of the nucleus $\mathfrak{K}$ as may be verified from Section 3. In the second place, we may restrict ourselves to combinations of the μ's which are linear in each of them, since $\mu_i^2 = 1$. Let us note down a few of them

$$\mu_1+\mu_2+\mu_3+\mu_4+\cdots$$
$$\mu_1\mu_2+\mu_2\mu_3+\mu_3\mu_4+\cdots$$
$$\mu_1\mu_3+\mu_2\mu_4+\mu_3\mu_5+\cdots$$
$$\mu_1\mu_2\mu_3+\mu_2\mu_3\mu_4+\cdots$$
$$\mu_1\mu_4+\cdots.$$

Among them, the first two are outstanding because $\mathfrak{K}$ contains them already explicitly. Let us, therefore, put

$$\sum_{i=1}^{n} \mu_i = nm, \tag{72}$$

$$\sum_{i=1}^{n} \mu_i \mu_{i+1} = nq \tag{73}$$

and evaluate the maximum of (71) under the restriction that the a's be of the form

$$a(\mu_i) = a(q, m). \tag{74}$$

We shall prove now that there is a form of a equivalent to (74), which has, however, great practical advantages. This form is

$$a(\mu_i) = \exp n\{H(K, C)q + A(K, C)m\}, \tag{75}$$

where H and A are constants as far as q and m are concerned, but depend upon temperature and field, i.e., K and C as parameters. This dependence has to be determined by the maximum condition (71).

The first step of the proof is to introduce explicitly the assumption (74) into (71). For this purpose we denote by

$$\exp n g(q, m)\, dq\, dm, \tag{76}$$

the number of arrangements of the μ's lying in a rectangle of sides dq and dm around q and m. Let us also introduce the notation

$$\sum_{\substack{\mu_i, \mu_i' \\ q, m, q', m'}} \exp[nK \sum_i \mu_i \mu_i'] = \exp[n f(q, m, q', m')]\, dq\, dm\, dq'\, dm', \tag{77}$$

where the summation on the left is extended only over those combinations that lie within a volume $dq\,dm\,dq'\,dm'$ around the point q, m, q', m'. Then (71) takes the form

$$\lambda^n = \operatorname*{Max} \frac{\iiiint \exp n\{f(q, m, q', m') + \tfrac{1}{2}K(q+q') + \tfrac{1}{2}C(m+m')\} a(q, m) a(q', m')\, dq\, dm\, dq'\, dm'}{\iint \exp n g(q, m) a^2(q, m)\, dq\, dm}. \tag{78}$$

Now transforming

$$a(q, m) = b(q, m) \exp[-\tfrac{1}{2} n g(q, m)],$$

we write

$$\lambda^n = \operatorname*{Max} \frac{\iiiint \exp n\{f(q, m, q', m') - \tfrac{1}{2}g(q, m) - \tfrac{1}{2}g(q', m') + \tfrac{1}{2}K(q+q') + \tfrac{1}{2}C(m+m')\} b(q, m) b(q', m')\, dq\, dm\, dq'\, dm'}{\iint b^2(q, m)\, dq\, dm}.$$

We can study this maximum problem in two parts; first we may assume the denominator to be normalized to unity and then we may look for the maximum of the numerator. If we do that we see that we shall get λ^n as large as possible if we let b be large wherever the exponent reaches its maximum. If we evaluate then the integral with the saddle point method, $b(q, m)$ will make no contribution to it because of its normalization and we get

$$\log\lambda = \operatorname*{Max}_{q,\,m,\,q',\,m'} [f(q, m, q', m') - \tfrac{1}{2}g(q, m) - \tfrac{1}{2}g(q', m') + \tfrac{1}{2}K(q+q') + \tfrac{1}{2}C(m+m')]. \tag{79}$$

We can eliminate the unknown functions f and g with the help of simpler ones. We introduce the solution χ^n of a two-strip problem

$$\chi^n(I, B, I', B') = \sum_{\mu_i, \mu_i'} \exp[K \sum_{i=1}^{n} \mu_i\mu'_i + I \sum_{i=1}^{n} \mu_i\mu_{i+1} + I' \sum_{i=1}^{n} \mu'_i\mu'_{i+1} + B \sum_{i=1}^{n} \mu_i + B' \sum_{i=1}^{n} \mu'_i] \tag{80}$$

or because of (72), (73), and (77)

$$\chi^n = \int\int\int\int \exp n\{f(q, m, q', m') + Iq + I'q' + Bm + B'm'\}\,dq\,dm\,dq'\,dm'.$$

For large n we can evaluate χ by the saddle point method

$$\log\chi(I, B, I', B') = \operatorname*{Max}_{q,\,m,\,q',\,m'} [f(q, m, q', m') + Iq + I'q' + Bm + B'm']. \tag{81}$$

Similarly we introduce two one-strip solutions

$$\psi^n(II, A) = \sum_{\mu_i} \exp[2H \sum_{i=1}^{n} \mu_i\mu_{i+1} + 2A \sum_{i=1}^{n} \mu_i], \tag{82}$$

which can be written as

$$\log\psi(II, A) = \operatorname*{Max}_{q,\,m} [g(q, m) + 2IIq + 2Am] \tag{83a}$$

and similarly

$$\log\psi(II', A') = \operatorname*{Max}_{q',\,m'} [g(q', m') + 2II'q' + 2A'm']. \tag{83b}$$

It looks incorrect at first sight to substitute (81) and (83) into (79) because the former are already maximized with respect to q, m, q', m'. However, the parameters $I, B, I', B', II, A, II', A'$ are arbitrary, and, as they vary, the quantities q, m, q', m' cover their full range of variability. We may therefore carry out the substitution and write

$$\log\lambda = \operatorname*{Max}_{q,\,m,\,q',\,m'} [\log\chi(I, B, I', B') - \tfrac{1}{2}\log\psi(II, A) - \tfrac{1}{2}\log\psi(II', A') + (\tfrac{1}{2}K - I + H)q + (\tfrac{1}{2}K - I' + II')q' + (\tfrac{1}{2}C - B + A)m + (\tfrac{1}{2}C - B' + A')m']. \tag{84}$$

In studying (84) we have to distinguish three types of relations between the quantities involved:

(a) The extremal conditions on χ and ψ indicated in (81) and (83). We shall use these conditions only in an indirect form. They are sufficient in number to make the expressions $I, B \cdots A'$ functions of q, m, q', m', or vice versa. Another consequence is that first derivatives of χ and ψ may be formed as if q, m, q', m', appearing explicitly in (81) and (83), were constants.

(b) The relations expressing the identity of q, m, q', m' in the various parts. They read

$$\frac{\partial\log\chi}{\partial I} = \frac{1}{2}\frac{\partial\log\psi}{\partial II} = q, \quad \frac{\partial\log\chi}{\partial I'} = \frac{1}{2}\frac{\partial\log\psi'}{\partial II'} = q', \quad \frac{\partial\log\chi}{\partial B} = \frac{1}{2}\frac{\partial\log\psi}{\partial A} = m, \quad \frac{\partial\log\chi}{\partial B'} = \frac{1}{2}\frac{\partial\log\psi'}{\partial A'} = m'.$$

(c) Finally, the extremal conditions on λ

$$\frac{\partial\log\lambda}{\partial q} = \frac{\partial\log\chi}{\partial I}\frac{\partial I}{\partial q} + \frac{\partial\log\chi}{\partial B}\frac{\partial B}{\partial q} + \frac{\partial\log\chi}{\partial I'}\frac{\partial I'}{\partial q} + \frac{\partial\log\chi}{\partial B'}\frac{\partial B'}{\partial q} - \frac{1}{2}\frac{\partial\log\psi}{\partial II}\frac{\partial II}{\partial q} - \frac{1}{2}\frac{\partial\log\psi}{\partial A}\frac{\partial A}{\partial q}$$

$$-q\left(\frac{\partial I}{\partial q} - \frac{\partial II}{\partial q}\right) - q'\frac{\partial I'}{\partial q} - m\left(\frac{\partial B}{\partial q} - \frac{\partial A}{\partial q}\right) - m'\frac{\partial B'}{\partial q} + \tfrac{1}{2}K - I + H = 0$$

and three similar equations. The relations under (b) simplify them to

$$I=\tfrac{1}{2}K+II, \quad I'=\tfrac{1}{2}K+II',$$
$$B=\tfrac{1}{2}C+A, \quad B'=\tfrac{1}{2}K+A'.$$

If we eliminate I, I', B, B' with the help of these four equations, (84) takes the form

$$\lambda=\frac{\chi(\tfrac{1}{2}K+II, \tfrac{1}{2}C+A, \tfrac{1}{2}K+II', \tfrac{1}{2}C+A')}{[\psi(II, A)\psi(II', A')]^{\frac{1}{2}}}$$

and the equations under (b) read

$$\frac{\partial \log\lambda}{\partial II}=\frac{\partial \log\lambda}{\partial II'}=\frac{\partial \log\lambda}{\partial A}=\frac{\partial \log\lambda}{\partial A'}=0,$$

i.e., the four parameters II, II', A, A' must make λ a stationary value. Should there be several sets of solutions leading to several possible sets of q, m, q', m', then the original maximum condition would demand the largest one. This gives, then,

$$\lambda=\operatorname*{Max}_{II, A, II', A'}\frac{\chi(\tfrac{1}{2}K+II, \tfrac{1}{2}C+A, \tfrac{1}{2}K+II', \tfrac{1}{2}C+A')}{[\psi(II, A)\psi(II', A')]^{\frac{1}{2}}}. \tag{85}$$

Our last step is to prove that

$$II=II', \quad A=A'.$$

This is done by substituting (80) and (82) into (85). Remembering the definition (12) of $\mathfrak{K}$ we get it in the form

$$\lambda^n=\operatorname*{Max}_{c, d}\frac{\sum_{\mu_i\mu_i'}\mathfrak{K}(\mu_i, \mu_i')c(\mu_i)d(\mu_i')}{\{[\sum_{\mu_i}c^2(\mu_i)][\sum_{\mu_i'}d^2(\mu_i)]\}^{\frac{1}{2}}}, \tag{86}$$

where the competing c's and d's are a restricted class of functions obeying (75). This maximum problem does not seem to agree in form with our basic equation (71). The greater generality is only apparent, however, for we can prove the following theorem:

If we have a set of c's and d's defining λ *as in (86) a larger* λ *can always be obtained either by replacing the c's by the d's or else the d's by the c's.* We prove, first, the lemma that

$$\sum_{\mu_i, \mu_i'}\mathfrak{K}(\mu_i, \mu_i')a(\mu_i)a(\mu_i')$$

is a positive definite form. We proceed by induction, starting from the fact that the statement is manifestly true if the a's depend only on one spin μ. Now suppose it to be true for $n-1$ spins then we can prove it for n. The nucleus $\mathfrak{K}$ is of the form

$$\mathfrak{K}(\mu_i, \mu_i')=\phi(\mu_i)\phi(\mu_i')\exp K\sum_{i=1}^{n}\mu_i\mu_i'.$$

Absorbing the ϕ's into the a's, which are arbitrary, we must only prove that

$$F=\sum_{\mu_i, \mu_i'}\exp(K\sum_{i=1}^{n}\mu_i\mu_i')a(\mu_i)a(\mu_i')$$

is a positive definite form. Now we single out μ_n and μ_n' and denote by $\Sigma'_{\mu_i, \mu_i'}$ summation over the remaining μ's. Since μ_n is only capable of two values, the dependence of a on μ_n can be made explicit by writing

$$a(\mu_i)=\alpha(\mu_i)+\mu_n\beta(\mu_i),$$

where α and β are independent of μ_n. We can thus carry out the summation over μ_n and μ_n' and get F in the form

$$F=4\cosh 2K \sum'_{\mu_i,\mu_i'} \exp(K\sum_{i=1}^{n-1}\mu_i\mu_i')\alpha(\mu_i)\alpha(\mu_i')+4\sinh 2K \sum'_{\mu_i,\mu_i'} \exp(K\sum_{i=1}^{n-1}\mu_i\mu_i')\beta(\mu_i)\beta(\mu_i').$$

This proves our lemma, for the two right-hand sides are, by assumption, positive. To prove the theorem itself we apply the Schwartz inequality to (86); assuming the c's and d's normalized we get

$$2\sum_{\mu_i,\mu_i'} \mathcal{K}(\mu_i,\mu_i')c(\mu_i)d(\mu_i') \leqq \sum_{\mu_i,\mu_i'} \mathcal{K}(\mu_i,\mu_i')c(\mu_i)c(\mu_i')+\sum_{\mu_i,\mu_i'} \mathcal{K}(\mu_i,\mu_i')d(\mu_i)d(\mu_i'),$$

which proves the theorem. It transforms (85) into the final form

$$\lambda=\operatorname*{Max}_{H,A}\frac{\chi(\frac{1}{2}K+H,\frac{1}{2}C+A)}{\psi(H,A)}. \tag{87}$$

Because of (12), (80), and (82), it is that particular case of (71) in which the a's have the form (75). Hence (75) is a consequence of (74). The approximation could be pushed further, in principle, by making a depend on more than just two parameters among the ones listed on p. 268. One verifies easily that such an expression could still be transformed to the form (75). Other parameters beside H and A would then have to be added to (87).

To evaluate (87) we observe that χ and ψ can be easily obtained by the methods of Sections 2 and 3. The explicit form of ψ is actually given in (9) and χ is obtained from a fourth-order matrix problem of the type (12). Using the definitions

$$e^K=k,\quad e^C=c,\quad e^{2H}=h,\quad e^{2A}=a, \tag{88}$$

we find for ψ

$$\psi=\tfrac{1}{2}h\left(a+\frac{1}{a}\right)+\tfrac{1}{2}\left[h^2\left(a-\frac{1}{a}\right)^2+\frac{4}{h^2}\right]^{\frac{1}{2}} \tag{89a}$$

and χ

$$\chi^3-\chi^2\left\{k^2h\left(ac+\frac{1}{ac}\right)+\frac{1}{k}\left(kh+\frac{1}{kh}\right)\right\}+\chi\left(kh-\frac{1}{kh}\right)\left\{kh\left(ac+\frac{1}{ac}\right)+k^2\left(kh+\frac{1}{kh}\right)\right\}-k\left(kh-\frac{1}{kh}\right)^3=0. \tag{89b}$$

The computation was only carried through for zero field, i.e., $c=0$. In this case $a=1$ is a possible solution since both $\partial\psi/\partial a$ and $\partial\chi/\partial a$ vanish at that point. The equation in χ then factorizes into

$$\left[\chi^2-\chi\left(k+\frac{1}{k}\right)\left(kh+\frac{1}{hk}\right)+\left(kh-\frac{1}{kh}\right)^2\right]\left[\chi-k\left(kh-\frac{1}{kh}\right)\right]=0$$

and the last solution may be discarded. The equation may be considered an equation in λ. The substitution

$$\frac{kh-(1/kh)}{h+(1/h)}=s\lambda$$

brings it in the form

$$\lambda=\operatorname*{Max}_{s}\frac{2}{(s-\sinh K)^2+1-\sinh^2 K},$$

which is immediately maximized to

$$\lambda=\frac{2}{1-\sinh^2 K}. \tag{90}$$

It is obvious that (90) cannot be valid for high values of K. In that region another solution having $a \neq 1$ becomes the correct one (nonvanishing "inner field"). The substitutions

$$\left(kh-\frac{1}{kh}\right)\frac{1}{\psi}=s\lambda, \quad \left(h+\frac{1}{h}\right)\frac{1}{\psi}=y$$

transform (87) into

$$\lambda=\operatorname*{Max}_{s,\,y}\frac{k\left(k+\frac{1}{k}\right)(k-s)+\frac{2}{k}(1-k^3s)y-k\left(k-\frac{1}{k}\right)(k-s)y^2}{k+\frac{1}{k}-\frac{s}{k}\left(k-\frac{1}{k}\right)+s^2k^2\left(k-\frac{1}{k}\right)-s^3k\left(k+\frac{1}{k}\right)-2ks(k-s)y}.$$

Forming $\partial\lambda/\partial y=0$ and eliminating y we find

$$(\lambda-k^2)^2s^2(k-s)^2-(\lambda-k^2)(k-s)\left(\frac{1}{k^2}-s^2\right)\left[k\left(k^2-\frac{1}{k^2}\right)-s\left(k^2+\frac{1}{k^2}\right)\right]+\left(\frac{1}{k^2}-s^2\right)^2=0.$$

After restoring linearity by the substitution

$$(1/k^2)-s^2/s(k-s)=(\lambda-k^2)/z,$$

we may carry out the second differentiation $\partial\lambda/\partial z=0$. We get

$$(1+(2/k^2)z+z^2)^2=[k^2-(1/k^2)]^3z \tag{91a}$$

and

$$\lambda=k^2+\frac{(1+k^2z)(1-z^2)}{k^4[k^2-(1/k^2)]}. \tag{91b}$$

The two pieces (90) and (91) make up the complete solution. They join with a common tangent at the point

$$K_c=\tfrac{1}{2}\log\frac{5+17^{\frac{1}{2}}}{4}=0.4122, \tag{92}$$

which means a transition without latent heat, but with a discontinuity in the specific heat curve. Other features of the solution will be discussed in the next section.

8. Comparison with Other Treatments

Several approximate methods have been developed in the past to arrive at the partition function of a set of regularly arranged spins. The first evaluation of λ is due to Heisenberg in his original paper on ferromagnetism.[12] His method has been systematized recently by Kirkwood[13] who developed a scheme of successive approximations of which Heisenberg's is the first step. It is based on the following consideration. Expression (2) for λ depends on two combinations involving the μ's, namely

$$\sum_{(i,k)}\mu_i\mu_k=2Nq, \quad \sum_i\mu_i=Nm.$$

If we denote the density of arrangements in $q-m$ space by $D^N(q, m)$ we have

$$\lambda^N=\int\int dqdm\,\exp N\{\log D(q, m)+2Kq+Cm\}. \tag{93}$$

Now $D^N(q, m)$ is unknown, but the expression

[12] W. Heisenberg, Zeits. f. Physik **49**, 619 (1928). See also: R. H. Fowler, *Statistical Mechanics* (Cambridge University Press and Macmillan Company, 1936), second edition, p. 485.

[13] John G. Kirkwood, J. Chem. Phys. **6**, 70 (1938); see also F. C. Nix and W. Shockley, Rev. Mod. Phys. **10**, 27, 65 (1938).

that results from it by integration over q is known. It is given by

$$\log D(m)=\log 2-\tfrac{1}{2}(1-m)\log(1-m)$$
$$-\tfrac{1}{2}(1+m)\log(1+m).$$

Hence if the term Kq can be developed in terms of K and m only, the expression can be integrated. This is done by identifying the power series in powers of K resulting from (93) with the one resulting from a hypothetical expression of the form

$$\lambda^N=\int dm\,\exp N\Big\{\log D(m)+Cm+\tau_1 2K$$
$$+\frac{1}{2!}\tau_2(2K)^2+\frac{1}{3!}\tau_3(2K)^3\cdots\Big\}. \quad (94a)$$

The q averages which result can be evaluated along the lines which led to formula (41). The first three τ's have the following values

$$\tau_1=q_{Av}=m^2,$$
$$\tau_2=N(q_{Av}{}^2-q_{Av}{}^2)=\tfrac{1}{2}(1-m^2)^2, \quad (94b)$$
$$\tau_3=N^2(q_{Av}{}^3-3q_{Av}{}^2q_{Av}+2q_{Av}{}^3)=m^2(1-m^2)^2.$$

The evaluation of m as a function of K follows then from the usual extremum condition of the saddle point method.

The result of the Heisenberg approximation which proceeds only to τ_2 is somewhat surprising. It gives a phase transition at

$$K_c=0.3912$$

with a jump of $-E/NJ$ from 0.6370 to 0.3912. The result should not be taken too seriously, however, for the next stage of the Kirkwood method, which is being evaluated numerically for the first time in this paper, brings about a regular Curie transition with specific heat jump, which takes place at

$$K_c=0.3389.$$

A more simple and straightforward treatment is the one developed by Bethe.[14] In its simplest form it treats only one spin with its direct neighbors by statistical methods, but the piece to be studied can be enlarged at will to approach the true solution. At low temperatures this

[14] H. A. Bethe, Proc. Roy. Soc. **A150**, 552 (1935); see also Nix and Shockley, reference 13, pp. 17, 63.

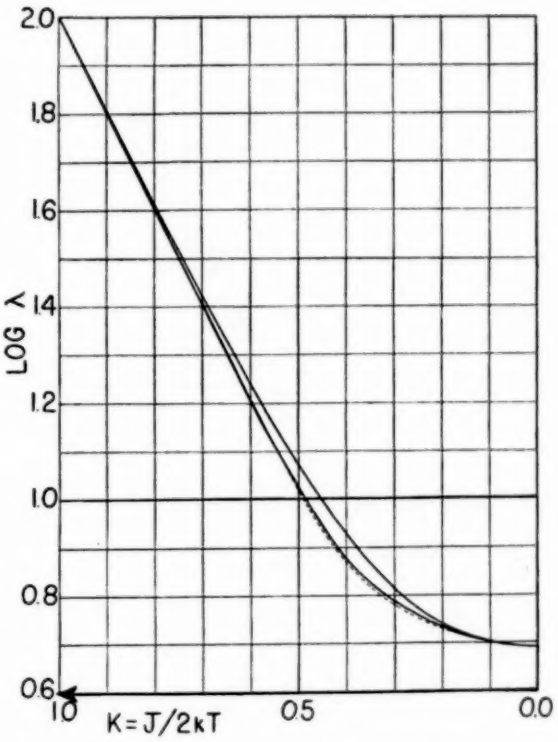

FIG. 6. Logarithm of partition function against reciprocal temperature. ——— 2-screw approximation (upper curve); variational solution (lower curve). - - - - Bethe solution. The slope of the curve is proportional to the energy at that temperature.

simple approximation is improved by assuming an ordering potential acting on the outer spins. It is determined by demanding symmetry in the result between them and the center spin. As a result of this calculation the following expressions are obtained for λ:

$$\lambda=2\cosh^2 K \qquad \text{below } K_c,$$
$$\lambda=e^{2K}+\frac{e^{-2K}}{e^{4K}-2} \qquad \text{above } K_c. \quad (95)$$

The two solutions join with a specific heat jump at

$$K_c=\tfrac{1}{2}\log 2=0.3466.$$

Results on the so-called second approximation of Bethe have been communicated to us by Mr. Groen. Its singular point is located at

$$K_c=0.381.$$

Zernike[15] has indicated a more dynamical approach to the problem by studying the propa-

[15] F. Zernike, Physica **7**, 565 (1940).

gation of order in a lattice. By Boltzmann's theorem we can express the probability that a given spin has either value in terms of the probabilities for its neighbors. If the latter are treated as independent, a system of difference equations is the result. The unknowns are the probabilities $P_{hk}(\mu)$ for each lattice position h, k and the system is such that it permits the computation of any P from one given one. If we now take a certain spin as given, say $P_{00}(+)=1$, we can ask for the probabilities for a spin very far away. At high temperatures, this limiting probability is $\frac{1}{2}$; Zernike is able to show, however, that below a certain temperature limiting probabilities different from $\frac{1}{2}$ will result. In our case this critical temperature is given by

$$\tanh 4K_c + 2\tanh 2K_c - 2 = 0 \qquad (96)$$

or

$$K_c = 0.3236.$$

The method is capable of giving all standard thermodynamic results because $P_{01}(\mu)$ is directly connected with the energy. It is found that the contact between the two branches is rather smooth, giving a discontinuity in the derivative of the specific heat only. It is interesting to notice that these calculations lead to a symmetry between very high and very low temperatures which is similar to (26). The propagation at high temperature of short range order in a generally disordered lattice leads to a difference equation of the same form as the propagation at low temperature of local disorder in a generally ordered lattice [Zernike, Eqs. (5) and (44)].

Among the approximations, the λ's of Section 6 (referred to below as "screw" solutions) should not be forgotten. They are, by their very nature, continuous functions of K, but compare not unfavorably with other approximate solutions.

In comparing various approximations it should be borne in mind that most of them are primarily approximating the partition function λ. It follows that an improved method of approach does not necessarily yield better energy and specific heat data, although it will be the case as a general rule. The differences in λ we have to account for are not large. In Fig. 6 curves having $\log\lambda$ plotted against K are given for the Bethe solution, the variation solution (Section 7) and the 2 screw. Most solutions discussed in this section are too small because they are essentially of the type (71); the screw solutions, on the other hand, are too large.

All λ's agree for very large and very small K and their usefulness may be tested by comparing their series expansions with (41) and (43). Ordering the solutions according to magnitude, we find for small K

$$\begin{aligned}
&\text{3 screw:} && \lambda = 2\left[1+K^2+\tfrac{7}{3}K^4+\cdots\right.\\
&\text{Zernike:} && \lambda = 2\left[1+K^2+\tfrac{4}{3}K^4+\tfrac{227}{45}K^6+\cdots\right.\\
&\text{5 screw:} && \lambda = 2\left[1+K^2+\tfrac{4}{3}K^4+\tfrac{122}{45}K^6+\cdots\right.\\
&\text{correct:} && \lambda = 2\left[1+K^2+\tfrac{4}{3}K^4+\tfrac{77}{45}K^6+\tfrac{1009}{315}K^8+\cdots\right. \qquad (97)\\
&\text{variation:} && \lambda = 2\left[1+K^2+\tfrac{4}{3}K^4+\tfrac{77}{45}K^6+\tfrac{694}{315}K^8+\cdots\right.\\
&\text{Heis-Kirk:} && \lambda = 2\left[1+K^2+\tfrac{1}{2}K^4+\cdots\right.\\
&\text{Bethe I:} && \lambda = 2\left[1+K^2+\tfrac{1}{3}K^4+\cdots.\right.
\end{aligned}$$

For large K we find

$$\begin{aligned}
\text{3 screw:}\quad & \lambda = k^2[1+2k^{-8}+\cdots \\
\text{5 screw:}\quad & \lambda = k^2[1+k^{-8}+3k^{-12}+\cdots \\
\text{correct:}\quad & \lambda = k^2[1+k^{-8}+2k^{-12}+5k^{-16}+14k^{-20}+\cdots \\
\text{variation:}\quad & \lambda = k^2[1+k^{-8}+2k^{-12}+5k^{-16}+14k^{-20}+\cdots \\
\text{Bethe I:}\quad & \lambda = k^2[1+k^{-8}+2k^{-12}+4k^{-16}+\cdots \\
\text{Kirkwood:}\quad & \lambda = k^2[1+k^{-8}+k^{-16}\left(\tfrac{64}{3}K^3+16K^2+8K\right)+\cdots \\
\text{Heisenberg:}\quad & \lambda = k^2[1+k^{-8}+k^{-16}(16K^2+8K)+\cdots \\
\text{Zernike:}\quad & \lambda = k^2[1+\tfrac{1}{2}k^{-8}+\cdots .
\end{aligned} \tag{98}$$

It may be noticed that the Bethe and Kirkwood methods switch places in the two tabulations. The reason is that the Bethe method is more elaborate for low temperatures. The Kirkwood approximation, on the other hand, is poor for very low temperatures because (94) is indirectly based on a $1/T$ expansion.[9] A similar situation exists for the Zernike solution because of his assumption of independent probabilities. Compared to other methods, our variational solution is very satisfactory. Being of the type (71), it lies below the true solution, but extremely close to it. A similar conclusion is reached if we extrapolate the sequence on p. 265 to find the value of λ at $K=0.4407$. We find about $\lambda=2.5335$, which is very close to the variational value $\lambda=67-47\sqrt{2}=2.5320$, but quite above the Bethe value $\lambda=2.5224$.

This simple situation is complicated somewhat when we form the first and second derivatives of λ which give the energy and the specific heat through (17) and (18). A solution whose λ is too large has an energy curve which is too smooth; and if λ is too small the energy passes too rapidly from one extreme to the other. This conclusion is verified by the energy *versus* temperature curves in Fig. 7. Beside various approximations, Fig. 7 has the exact location of K_c marked off together with its energy value (36). The correct curve passes through that point very probably in a vertical direction (Section 6).

If we disregard the Heisenberg solution which carries little weight for reasons mentioned above, we may divide the approximations in two classes. The ones proceeding from finite problems and the one given by Zernike have energy and specific heat continuous throughout. The others, using some kind of an inner field assumption, arrive at one singularity with a jump in the specific heat. As examples, specific heat curves

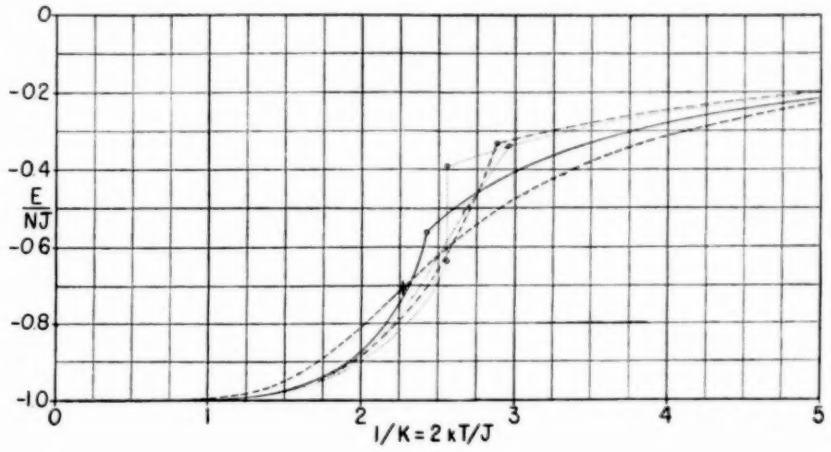

FIG. 7. Energy *versus* temperature in various approximations. – – – – 3-screw approximation. ——— Variation method. –·–·– Bethe method. ····· Heisenberg and Kirkwood. ○ Singular points. Point with vertical bar belongs to exact curve (with vertical slope).

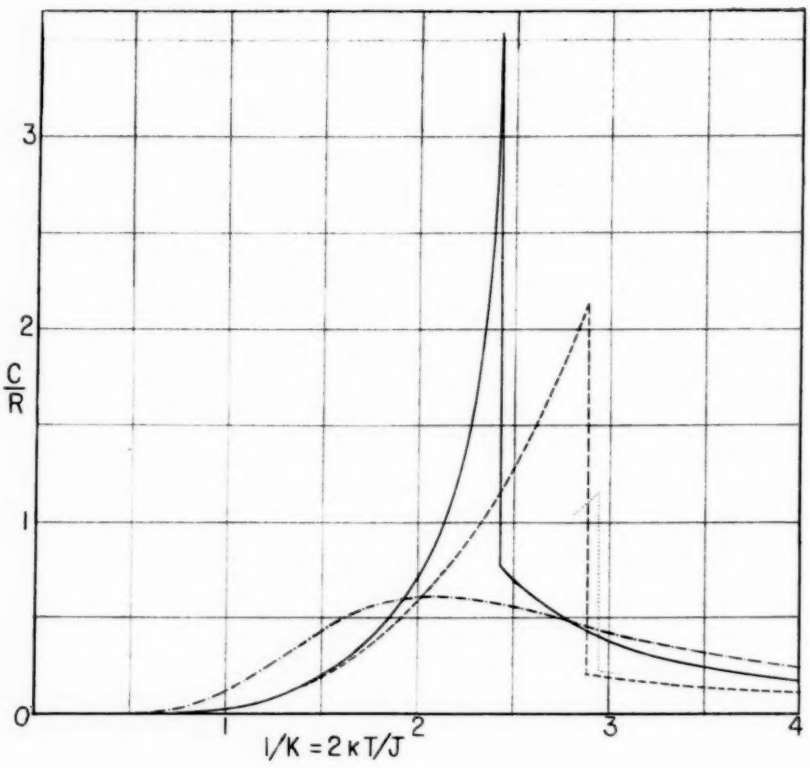

FIG. 8. Specific heat *versus* temperature curves. -·-·-· 2-screw approximation. ——— Variation method. – – – – Bethe method. ····· Kirkwood method.

are plotted in Fig. 8 for the 2-screw and the variational Bethe and Kirkwood solutions. The large discontinuity in the specific heat is the dominant feature of the latter three. However, this result cannot possibly be correct, for it could be disproved by exact methods in Eq. (35). In view of the results of Section 6, it seems, therefore, that the main significance of these approximate results is not to be sought in the jump of C, but rather in its numerical magnitude at the Curie point. This magnitude increases as the approximation improves. Simultaneously, the position of the singularity approaches the value (31), as can be verified from the data of this section and (92). Thus the approximate solutions of the last two sections are not in contradiction to the conclusions of Sections 4 and 6, that the Curie point lies at $K_c = 0.4407$ and that the specific heat at that point is infinite.

In conclusion, we want to express our thanks to Mr. P. Groen who has assisted us in some of the calculations.

The Dipole Character of the Meson, and the Difficulties of Meson Theory

D. IWANENKO AND A. SOKOLOW
Sverdlovsk State University, U. S. S. R.

(Received June 9, 1941)

APPLICATION of Proca gquations to the description of mesons has brought to light many results not verified by experiments and inadmissible from the theoretical point of view. We may remark that the general behavior of mesons can be characterized by a factor $(h\nu/\mu c^2)^2$ appearing in the ultra-relativistic formulae for effects connected with the specific nuclear interaction of mesons with nuclons (g forces), as well as at electromagnetic interactions of charged mesons (e forces).

That the appearance of this factor depends on the effective dipole character of the mesons is made clear by the following consideration, which seems not to have been recognized in its general form. The interaction energy of nuclons with the mesons (described by potentials A_μ and field strengths $H_{\mu\nu}$)

$$U=g_1 d_\mu A_\mu+\frac{g_2}{k_0}\sigma_{\mu\nu}H_{\mu\nu} \tag{1}$$

makes evident the dipole character of the quasi-magnetic effects due to the presence of the internal dipole g_2/k_0 of the nuclons. In quantum theory the ν^2 factor appears then through the commutation rules for the Fourier amplitudes of the meson field[1]

$$[h^k_{\mu\nu}, h^{+k}_{\mu'\nu'}]=k_\mu k_{\mu'}\delta_{\nu\nu'}+k_\nu k_{\nu'}\delta_{\mu\mu'} -k_\mu k_{\nu'}\delta_{\nu\mu'}-k_\nu k_{\mu'}\delta_{\mu\nu'}, \tag{2}$$

where we have chosen the normalization

$$H^k_{\mu\nu}=(2\pi ch/K)^{\frac{1}{2}}h^k_{\mu\nu}, \quad k_y=Ki=i(k^2+k_0^2)^{\frac{1}{2}}.$$

Though the appearance of the ν^2 factor from the quasi-electrical terms with g_1 was not expected from the analogy with classical theory, the commutation rules for the amplitudes of the meson potentials lead to the same ν^2 factor and thus we have an effective dipole character for the mesons

$$[a^k_\nu, a^{+k}_{\nu'}]=\delta_{\nu\nu'}+(k_\nu k_{\nu'}/k_0^2), \qquad A^k_\nu=(2\pi ch/K)^{\frac{1}{2}}a^k_\nu. \tag{3}$$

These latter commutation rules are also responsible for the dipole-type behavior of mesons in the electromagnetic field. It should be recalled that, although the Dirac kinematics also endows the electron with an effective dipole moment, this vanishes in the ultra-relativistic limit.

This reasoning can be illustrated by many examples:

(1) Not only do the nuclear forces given by the meson field involve terms of order r^{-3}, but an r^{-3} potential also arises in the problem of a meson in a Coulomb field.[2]

(2) The scattering of light by mesons gives a cross section[3]

$$\sigma_e\sim(eh/\mu c)^4\mu\nu/c^2h^3, \tag{4}$$

while for the scattering of mesons on nuclons one gets[4]

$$\sigma_\mu\sim(g_2/k_0)^4M\nu/c^2h^3. \tag{5}$$

Both expressions are indeed quite similar; and if one equates the quasi-magnetic moment of the nuclon and magnetic moment of the meson on the one hand, and the masses of scattering particles on the other, one obtains the identical formulae which differ only by a numerical factor of the order of unity. The part played by the effective dipole of the meson in these effects is very striking and the ν^2 rule is made especially evident by the comparison with the ultra-relativistic limit of Klein-Nishina formula for the scattering of light on the electron which goes essentially as $\sim\nu^{-1}$.

(3) The scattering of mesons by a Coulomb field, the production of meson pairs by two photons, and the various effects of the third order such as brems-radiation of light by mesons or the brems-radiation of mesons by nuclons, etc., may serve as further examples both of the validity of ν^2 rule and of a close parallelism

[1] D. Iwanenko and A. Sokolow, J. Phys. (Moscow) **3**, 54 (1940).

[2] Ig. Tamm, Phys. Rev. **58**, 952 (1940).

[3] F. Booth and A. H. Wilson, Proc. Roy. Soc. **A175**, 483 (1940); M. Kobayasi and R. Utiyama, Sci. Pap. Inst. Phys. Chem. Research Tokyo **37**, 221 (1940); Smorodinski, J. Exp.-theor. Phys. (Russ.) **10**, 840 (1940).

[4] A. Sokolow, Comptes rendus (Moscow) **29**, 20 (1940); F. Booth and A. H. Wilson, Proc. Camb. Phil. Soc. **36**, 446 (1940).

between electromagnetic and specific nuclear effects.[5]

(4) The various non-linear effects connected with mesons are also influenced by the dipole character of mesons. One finds here, first, the non-linearities in the equations of the meson field itself, which were shown by Heisenberg to be more pronounced than the analogous terms in the electrodynamics due to the scattering of light on light *via* electron pairs.

On the other hand, the mesons also contribute to the non-linearities in Maxwell's electrodynamics, through the possibility of the virtual production and annihilation of meson pairs. Thus the scattering of light on light can occur also *via* meson pairs. The non-linear additions to usual electrodynamics due to mesons are more pronounced than those due to electrons, in view of the dipole character of mesons. We shall discuss these problems more closely in a paper to appear elsewhere, and content ourselves here with the indication on the non-linear polarization of the vacuum due to mesons. Computing[6] the additional electric density ρ' produced by an external density ρ, we get for ρ' first, the terms independent of the external field which diverge in a stronger manner than analogous terms for the vacuum of Dirac electrons (or spinless particles). The physically important field-dependent term of ρ' also diverges in the meson theory, in contrast to the theory of Dirac vacuum, though only in a logarithmic manner

$$\rho' = -\frac{e^2}{12\pi hc}\left(\frac{h}{\mu c}\right)^2 \lim_{k\to\infty}\left(2\log\frac{2k}{k_0}-\frac{13}{6}\right)\Delta\rho. \quad (6)$$

There is as yet no general method of removing the above difficulties.

In any case we may point that the introduction of damping diminishes the cross sections considerably. In classical mesodynamics, the damping is introduced by the radiation friction forces $\frac{2}{3}(g/c^3)(\partial^3 x/\partial t^3)$ (quasi-electric), or $\frac{2}{3}(1/v^3)(\partial^3 m/\partial t^3)$ (quasi-magnetic, where v is the phase velocity of mesons).[1]

We may remark here that a most general and simple method of formulation of classical mesodynamics is achieved by introduction of Hertz vectors Z_e and Z_m. One gets, then, as equivalent to the inhomogeneous Proca equations

$$\left(\Delta-\frac{1}{c^2}\frac{\partial^2}{\partial t^2}-k_0^2\right)\begin{cases}Z_e\\ Z_m\end{cases}=\begin{cases}-4\pi(g_1P+g_2T/k_0),\\ -4\pi(g_1M+g_2S/k_0),\end{cases} \quad (7)$$

where P, M denote the external quasi-electric and magnetic polarizations, respectively and T, S the vectors of the proper dipole moments of nuclons. This system is readily solved in the general case by means of the Green's function of Proca-Schrödinger equations. The same Green's function essentially determines the four-dimensional commutations rules for all field quantities of Proca, Dirac, Schrödinger, etc., relativistic wave functions.

In quantum theory the damping is taken into account by an exact solution of Dirac's equations for the coefficients $C^k(t)$ that is, without the usual approximation $C^k(0)=1$, or $C^{k'}(0)=0$.

Then, for high energies, the cross sections for the scattering of mesons on nuclons (g forces) become

$$\text{neutral:}\quad \sigma_{cl}=\sigma\frac{1}{1+(\sigma k^2/6\pi)},$$
$$\text{charged:}\quad \sigma_{qu}=\sigma\frac{1}{1+(3\sigma k^2/4\pi)}. \quad (8)$$

(σ denotes the cross sections without damping.) One can expect that the σ's for the effects of third order, which are considered as the sum of scattering acts, will also be diminished.

An hypothesis of Heitler-Ma on the introduction of higher nuclon states is also capable of diminishing the cross sections of the effects of third order for g forces.[7] If one is inclined to generalize this latter method for removing the difficulties of the electromagnetic effects with mesons as well, then the higher spin states of mesons must be introduced also. It is interesting to note that Heitler's hypothesis leading to constant σ is, in this result, equivalent to the proposal of Heisenberg[8] to take into account the reaction on nuclons of the radiated meson field in the form essentially coinciding with the introduction of the term $\partial^3 m/\partial t^3$ in the classical equations of motions of the nuclon dipole.

[5] Oppenheimer, Serber, and Snyder, Phys. Rev. **57**, 75 (1940).

[6] D. Iwanenko and A. Sokolow, Physik. Zeits. Sowjetunion **11**, 590 (1937).

[7] W. Heitler and S. T. Ma, Proc. Roy. Soc. **A176**, 368 (1940).

[8] W. Heisenberg, Zeits. f. Physik **113**, 61 (1939).

Letters to the Editor

PROMPT publication of brief reports of important discoveries in physics may be secured by addressing them to this department. Closing dates for this department are, for the first issue of the month, the eighteenth of the preceding month, for the second issue, the third of the month. Because of the late closing dates for the section no proof can be shown to authors. The Board of Editors does not hold itself responsible for the opinions expressed by the correspondents.

Communications should not in general exceed 600 words in length.

Half-Life of C^{11}

A. K. SOLOMON
Research Laboratory of Physics, Harvard University, Cambridge, Massachusetts
July 15, 1941

MEASUREMENTS of the half-life of C^{11} have been made in connection with biological research in which this element was used as a tracer.[1] The half-life was measured with an alcohol-filled Geiger-Müller counter and a scale-of-16 circuit already described.[1] For these experiments the counting loss at high speeds was determined before and after the measurements and found to be less than 1.7 percent at 10,500 counts per minute, and less than 1.0 percent below 8500 c/min. Half-lives were calculated by the method of Peierls[2] in which the total count of a period of 3 or more half-lives is divided into successive 8-minute intervals. The initial counting rate was below 8500 c/min. except for run 5 in which it was below 10,000 c/min. No corrections were made for this loss. In runs 1 and 2, the experiments terminated when the counting rate was somewhat greater than three times background; in all the other experiments the final rate was greater than eight times background. Background was measured before and after each run, and checks were also made with a uranium standard. Samples were measured as $BaCO_3$. As a check against contamination, in run 3 the C^{11} was synthesized into sodium lactate and measured as such. All the runs gave good straight line plots for logarithm of activity against time. The results are given in Table I.

The half-life of C^{11} calculated from all the runs is 20.42 ± 0.06 minutes. However, in run 1 the background altered by a factor of two during the run; so this result can be discarded. Column 3 in the table gives the ratio of the measured activity of a uranium standard before and after each run. The deviation in runs 2 and 5 seems large, especially since its direction corresponds with the deviation of these runs from the mean. Consequently, the best value is that obtained from the remaining seven runs—20.50 ± 0.6 minutes. This is in good agreement with the value of 20.63 minutes previously obtained graphically[1] as well as the value of 20.35 ± 0.08 minutes given by Smith and Cowie.[3]

Table I. *Data on* C^{11}.

Run	Time Observed (Min.)	Agreement of Standard Activity Before and After Run (%)	Half-Life (Min.)
1	104		20.01
2	120	4.5	19.83
3	88	1.3	20.29
4	88	0.8	20.44
5	72	4.4	20.84
6	96	2.5	20.42
7	96	0.6	20.46
8	96	1.8	20.65
9	88	1.3	20.57
10	72	1.7	20.64

I should like to express thanks to Miss Birgit Vennesland, and Mr. J. Buchanan for their help in preparing the samples; to Dr. B. R. Curtis and the Harvard cyclotron group for the bombardments; and to the Milton Fund for the grant which has made the work possible.

[1] Conant, Cramer, Hastings, Klemperer, Solomon and Vennesland, J. Biol. Chem. **137**, 557 (1941).
[2] R. Peierls, Proc. Roy. Soc. **A149**, 467 (1935).
[3] J. H. C. Smith and D. B. Cowie, J. App. Phys. **12**, 78 (1941).

On the Slowing Down of Neutrons by Elastic Collisions

FELIX ADLER
Institute for Advanced Study, Princeton, New Jersey
April 17, 1941

WE consider a homogeneous medium in which Q neutrons of energy E_0 are produced per sec. Let v be the velocity of the neutrons, m their mass, $\lambda(v)$ the free path for scattering, M the mass of the nuclei of the medium, and p the probability of a neutron of initial energy E' and velocity v' being scattered by an elastic collision into the energy interval dE at E. According to the laws of elastic collisions we get for p

$$p(E, E') = \frac{1}{1-\alpha^2}\frac{dE}{E'} \quad \text{if} \quad E'\alpha^2 \leqslant E, \tag{1}$$

$$p(E, E') = 0 \quad \text{if} \quad E'\alpha^2 > E,$$

$$\alpha = (M-m)/(M+m).$$

In order to describe p by a uniform analytic expression, we introduce a discontinuous factor of the type of the Dirichlet discontinuous factor. We define $\delta(E, E'\alpha^2)$ by

$$\delta(E, E'\alpha^2) = \begin{cases} 1 & \text{if} \quad E'\alpha^2 \leqslant E \\ 0 & \text{if} \quad E'\alpha^2 > E \end{cases} \tag{2}$$

and p is now given by

$$p(E, E') = \frac{1}{1-\alpha^2}\frac{dE}{E'}\,\delta(E, E'\alpha^2). \tag{3}$$

Let $N(E)dE$ be the number of neutrons of a given energy E present in the stationary state in the system and $M(E)dE$ the number of neutrons per sec. leaving the energy interval dE in consequence of an elastic collision. Then

$$M(E)dE = N(E)(v/\lambda)dE. \tag{4}$$

Hence we have for the stationary state

$$M(E)dE = Qp(E, E_0)dE + \int_E^{E_0} p(E, E')M(E')dE'dE. \tag{5}$$

In this expression $QpdE$ means the number of neutrons of

initial energy E_0 thrown by one collision into the energy interval dE at E and the integral gives the sum of the contributions of all the intervals between E_0 and E. By introducing new variables

$$Z=\ln(E_0/E) \tag{6}$$

and defining a new discontinuous factor

$$\delta(x-x';\,a)=\begin{cases}1 & \text{if} \quad x-x'\leqq a\\ 0 & \text{if} \quad x-x'>a,\end{cases} \tag{7}$$

we get for p

$$p(x,\,x')=\frac{1}{1-\alpha^2}\frac{1}{E_0}\exp(x')\delta(x-x';\,a)dx. \tag{8}$$

The condition that the state is stationary is now given by

$$M(x)=\varphi\frac{1}{1-\alpha^2}\delta(x,\,a)+\int_0^x\frac{1}{1-\alpha^2}\delta(x-x',\,a)M(x')dx'. \tag{9}$$

This integral equation is of a particular type, its second member is a convolution (Faltung); therefore, we may solve it by means of a Laplace transformation.

The Laplace transformation of a function is defined by

$$\int_0^\infty e^{-sx}F(x)dx=f(s), \tag{10}$$

where the real part of s is positive. If $F(x)$ is definite and integrable in every finite interval, the inverse transformation exists and f and F are connected by

$$F(x)=\frac{1}{2\pi i}\int_{a-i\infty}^{a+i\infty}e^{xs}f(s)ds. \tag{11}$$

Here, the integration path has to be chosen in such a manner as to enclose all the singularities of $f(s)$.

Applying the Laplace transformation to our integral equation we get

$$m(s)=\varphi\frac{1}{1-\alpha^2}\frac{1}{s}[1-e^{-as}]+\frac{1}{1-\alpha^2}\int_0^\infty dxe^{-sx}\int_0^x dx'\delta(x-x',\,a)M(x'), \tag{12}$$

whereas

$$m(s)=\int_0^\infty e^{-sx}M(x)dx\left|\frac{1}{s}[1-e^{-as}]\right.=\int_0^\infty dxe^{-sx}\delta(x,\,a)=\int_0^a dxe^{-sx}.$$

The last term of Eq. (12) will be simplified by making use of the theorem of composition of the Laplace transformation[1]

$$\int_0^\infty\exp(-s_0x)F_1(x)dx\int_0^\infty\exp(-s_0y)F_2(y)dy=\int_0^\infty\exp(-s_0t)\left\{\int_0^t F_1(t-\tau)F_2(\tau)d\tau\right\}, \tag{13}$$

which holds if

$$\int_0^\infty\exp(-s_0x)F_1(x)dx \quad\text{and}\quad \int_0^\infty\exp(-s_0x)F_2(x)dx$$

exist and are convergent for the same s.

Thus we get for the last term of Eq. (12)

$$\int_0^\infty e^{-sx}dx\int_0^x dx'\delta(x-x',\,a)M(x')=\int_0^\infty\exp(-sx')M(x')dx'\int_0^\infty e^{-sx}\delta(x;\,a)dx=m(s)\frac{1}{s}[1-e^{-as}]. \tag{14}$$

Now the transformed Eq. (12) runs thus

$$m(s)=\varphi\frac{1}{1-\alpha^2}\frac{1}{s}[1-e^{-as}]+\frac{1}{1-\alpha^2}m(s)\frac{1}{s}[1-e^{-as}], \tag{15}$$

whence

$$m(s)=\varphi\frac{1-e^{-as}}{(1-\alpha^2)s-(1-e^{-as})}. \tag{16}$$

By means of the inverse transformation we get for $M(x)$

$$M(x)=\frac{1}{2\pi i}\int_{a-i\infty}^{a+i\infty}e^{xs}m(s)ds=\varphi\frac{1}{2\pi i}\int_{a-i\infty}^{a+i\infty}e^{xs}ds\frac{1-e^{-as}}{(1-\alpha^2)s-(1-e^{-as})}. \tag{17}$$

Considering $m(s)$ we find that all the poles $s=s_n$ of $m(s)$ are of the first order; accordingly the residues of $m(s)$ at s_n are

$$c_n=\frac{1-\exp(-as_n)}{1-\alpha^2-a\exp(-as_n)} \tag{18}$$

and we get for $M(x)$

$$M(x)=\varphi\sum_{\text{all poles}}c_n\exp(s_nx). \tag{19}$$

The only pole for which s_n has a positive real part is situated at $s_n=1$. All the other poles of $m(s)$ lie to the left of the imaginary axis. In consequence thereof we get the following asymptotic expression for $M(x)$ for large x, if we replace x by $E=E_0e^{-x}$,

$$M(E)dE=\frac{dE}{E}\frac{1}{1-\alpha^2-\alpha^2\ln(1/\alpha^2)} \quad\text{if}\quad E\ll E_0. \tag{20}$$

For a small M, the other poles were determined too, and we found that all the other terms of the series are completely negligible for $x\sim 5$. Equation (20) is the same expression as that given by Placzek.[2]

[1] Cf., Doetsch, *Laplace Transformation*, p. 161.
[2] G. Placzek, Phys. Rev. **55**, 1130 (1939).

On the Forward Scattering of Neutrons by Paramagnetic Media

MARTIN D. WHITAKER AND WILLIAM C. BRIGHT
New York University, University Heights, New York
July 14, 1941

HALPERN and Johnson[1] have concluded that the magnetic interaction between slow neutrons and certain paramagnetic ions should result in an amount of scattering at small angles that is several times the nuclear scattering in this region. This conclusion was arrived at under the assumption that the magnetic moment of the neutron is

2 nuclear magnetons and that the neutrons are slow enough that their wave-lengths are of the order of atomic dimensions. They[2] have also suggested the possibility that the magnetic moment may be 6 units instead of 2 and that the spin would then be $\frac{3}{2}$ instead of $\frac{1}{2}$. It is contended that the substantiation of these values would practically resolve the discrepancy between theory and experiment in the case of the transmission of slow neutrons through magnetized iron. This larger magnetic moment would result in a scattering cross section of "approximately 100×10^{-24} cm²" in the case of the free manganese ion Mn^{++} for suitably slow neutrons. Van Vleck[3] has pointed out the desirability of using materials in work of this kind which have small coupling between the spins of the various atoms, since coupling of this kind increases the inelastic scattering. Following the suggestions of these authors we have made measurements on differential scattering of slow neutrons at small angles by the salts $MnSO_4$ and MnF_2.

Using an angular ring arrangement which enabled us to count only those neutrons scattered through an angle of $15°\pm10°$, we compared the scattering of the $MnSO_4$ and the MnF_2 samples with that of lead and carbon samples. The MnF_2 was dried in a vacuum oven at a temperature of 200°C for 6 hours. The $MnSO_4$ was first dried at 325°C and was later dried at 550°C for 24 hours when tests indicated that earlier results[4] were not valid because the $MnSO_4$ still contained some water of crystallization. We have, as yet, been unable to prepare a satisfactory sample of MnS.

We conclude from these measurements that any scattering, in addition to the expected nuclear scattering, in the forward angular region studied could not have been greater than equivalent to 5 units (10^{-24} cm²) of cross section in this region, and we believe it to be considerably smaller. Modifications in technique and apparatus are in progress which will reduce the limit of error.

Some indication of the neutron spectrum used is obtained from the fact that with the same howitzer used here the interference effects in quartz have been observed in addition to other interference results. This seems to indicate that a sufficient number of the neutrons are slow enough that there can be little objection on this ground.

On the basis of these results and the current ideas[1] concerning paramagnetic scattering of slow neutrons it seems impossible to accept the suggestion that the magnetic moment of the neutron may be 6 units. As a matter of fact the 5 units of scattering which has been set as the upper limit is only about 25 percent of that to be expected on the basis of a neutron moment of only 2 nuclear magnetons. We have no explanation of why this magnetic scattering does not show up in these experiments to the extent expected for the lower value of the magnetic moment, since it seems unlikely that the elastic form factor can differ so greatly from unity, in the angular region used, that the entire explanation can be placed here. $MnSO_4$ has been studied thoroughly and its susceptibility as measured under various conditions indicates that the spin coupling cannot be blamed.

Financial support of this work by a grant (to M.D.W.) from the Permanent Science Fund of the American Academy of Arts and Sciences is gratefully acknowledged.

[1] O. Halpern and M. H. Johnson, Phys. Rev. **55**, 898 (1939).
[2] O. Halpern and M. H. Johnson, Phys. Rev. **57**, 160 (1940).
[3] J. H. Van Vleck, Phys. Rev. **55**, 924 (1939).
[4] M. D. Whitaker and W. C. Bright, Phys. Rev. **57**, 1076 (1940).

The Abundances of Molecules in the Solar Reversing Layer

R. H. LYDDANE AND F. T. ROGERS, JR.*
The University of North Carolina, Chapel Hill, North Carolina,
AND
F. E. ROACH.* *The University of Arizona, Tucson, Arizona*
June 20, 1941

WE have recalculated, essentially by the earlier method of Roach,[1] the abundances in the sun's reversing layer of the molecules OH, CN, NH, CH and C_2. Under the assumption of thermodynamic equilibrium at some definite temperature, the observed intensities of many electronic-transition band lines for each kind of molecule were converted by means of the appropriate "curve of growth"[2] and of the appropriate molecular sum rules to Nf values: N is the number of molecules in a cm² column through the reversing layer, and f is the f number associated with the complete electronic transition.[3] Then, having found f by any suitable means, N was obtained directly.

The data and results are summarized in Table I. The observational data are the same as were used by Roach,[1] except that Blitzer's recent microphotometric data[4] on CN are used. The values of Nf (given in the table in logarithmic form) are determined for an effective temperature of 5000° in the usual manner. The f values for OH and CN are the experimental ones found by Oldenberg and Rieke[5] and by White,[6] respectively. The f values for NH, CH and C_2 have been calculated by the wave mechanics in the following manner: the ratios of f values for OH, NH and CH, and for CN and C_2, were calculated with the most reasonable standard wave functions—both *AO* and *MO* approximations were considered—and then the f's for NH, CH and C_2 were obtained from these ratios and the experimental f values for OH and CN.

In column 5 are the resulting logarithms (base 10) of the abundances of the several molecules, diminished by 14 so as to make them roughly comparable with the figures in column 6. In column 6 are the logarithms of the relative molecular abundances as calculated by Russell[7] from his (1934) atomic abundances.

TABLE I. *Data on electronic-transition lines.*

Mol.	Transition	$\log Nf$ $T=5000°$	f	$\log N-14$ $T=5000°$	$\log N_{rel}$ Russell
OH	$^2\Sigma^+\leftarrow{}^2\Pi$	13.83	3.0×10^{-4}	3.36	5.3
CN	$^2\Sigma^+\leftarrow{}^2\Sigma^+$	14.00	2.6×10^{-2}	1.59	2.3
NH	$^3\Pi\leftarrow{}^3\Sigma^-$	13.57	7.2×10^{-4}	2.71	4.0
CH	$^2\Delta\leftarrow{}^2\Pi$	14.04	4.5×10^{-4}	3.39	5.1
C_2	$^3\Pi_g\leftarrow{}^3\Pi_u$	13.65	2.4×10^{-2}	1.27	0.9

While it is not possible to draw highly precise conclusions from column 5 (because of the low precision of most of the individual observations of band line intensities), nevertheless it appears that the actual abundances of CN and C_2 are quite significantly less than the abundances of the hydrides—this is in general agreement with the results of Russell. This fact did not appear in the earlier calculations[1] simply because at that time the CN and C_2 f values were not known to be much larger than the hydrides' values.

* This work was begun while two of the authors (FER and FTR) were in residence (1939) at The Yerkes Observatory of The University of Chicago, Williams Bay, Wisconsin.

[1] F. E. Roach, Astrophys. J. **89**, 99 (1939).
[2] See, e.g., D. H. Menzel, Astrophys. J. **84**, 462 (1936).
[3] See, e.g., R. S. Mulliken, J. Chem. Phys. **7**, 14 (1939).
[4] L. Blitzer, Astrophys. J. **91**, 421 (1940).
[5] O. Oldenberg and F. F. Rieke, J. Chem. Phys. **6**, 439 (1938). See also R. S. Mulliken, J. Chem. Phys. **8**, 382 (1940).
[6] J. U. White, J. Chem. Phys. **8**, 79 (1940).
[7] H. N. Russell, Astrophys. J. **79**, 317 (1934).